



CSIC



UNIVERSITAS
Miguel
Hernández



INSTITUTO DE NEUROCIENCIAS

Consejo Superior de Investigaciones Científicas
Universidad Miguel Hernández
Instituto de Neurociencias

New insights into mechanisms controlling
the Schwann cell phenotype during
tumourigenesis and after injury

Presented by:
Clara Gomis Coloma

For the degree of Doctor in Neuroscience from the University Miguel
Hernández de Elche

Director:
Dr. Hugo Cabedo Martí

San Juan de Alicante, Spain
2014

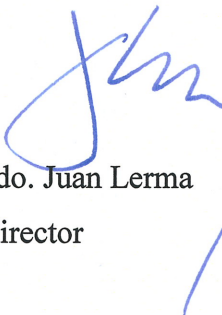
A QUIEN CORRESPONDA,

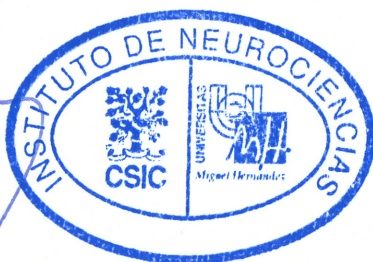
Prof. Juan Lerma Gómez, Director del Instituto de Neurociencias de Alicante, centro mixto de la Universidad Miguel Hernández (UMH) y la Agencia Estatal Consejo Superior de Investigaciones Científicas (CSIC)

CERTIFICA,

Que la Tesis Doctoral “New insights into mechanisms controlling the Schwann cell phenotype during tumourigenesis and after injury” ha sido realizada por Dña. Clara Gomis Coloma, Licenciada en Biología, bajo la dirección del Dr. Hugo Cabedo Martí, y da su conformidad para que se presente la tesis a la Comisión de Doctorado de la Universidad Miguel Hernández.

Para que así conste, y a los efectos oportunos, expide y firma el presente Certificado en San Juan de Alicante a 4 de septiembre de 2014


Fdo. Juan Lerma
Director



A QUIEN CORRESPONDA,

Dr. Hugo Cabedo Martí, Investigador Científico del Consejo Superior de Investigaciones Científicas, en el Instituto de Neurociencias de Alicante, centro mixto de la Universidad Miguel Hernández (UMH) y la Agencia Estatal Consejo Superior de Investigaciones Científicas (CSIC)

CERTIFICA,

Que Dña. Clara Gomis Coloma, Licenciada en Biología, ha realizado bajo su dirección el trabajo experimental que recoge en su Tesis Doctoral “New insights into mechanisms controlling the Schwann cell phenotype during tumourigenesis and after injury”.

Que ha revisado los contenidos científicos y los aspectos formales del trabajo y da su conformidad para que se presente la tesis a la Comisión de Doctorado de la Universidad Miguel Hernández.

Para que así conste, y a los efectos oportunos, expide y firma el presente Certificado en San Juan de Alicante a 1 de septiembre de 2014



Fdo. Hugo Cabedo Martí

Agradecimientos

Muchas personas han contribuido directa o indirectamente a que yo pudiera desempeñar el trabajo reflejado en esta tesis.

En primer lugar he de agradecer a Hugo Cabedo, por darme la oportunidad de trabajar en tu laboratorio, por tu continua guía y supervisión en el proyecto y por transmitirme tu entusiasmo por la ciencia.

En segundo lugar agradezco a mi maestro Jose, que ha estado durante estos años trabajando conmigo mano a mano en el proyecto. Por enseñarme tan bien tu gran sabiduría práctica en el labo. Y porque has hecho que las largas horas en el labo se pasaran de forma amena y agradable. Has sido un gran compañero y amigo.

También he de agradecer a mis demás compañeros del labo. A Mary, Manue, Mari Carmen, Vicky y Sergio por vuestra ayuda y apoyo a nivel de trabajo y a nivel personal.

Gracias a todas las personas del INA que me han ayudado amablemente en numerosas ocasiones para poder hacer determinados experimentos. A Cruz, a Eva Quintero, a Eduardo de Puelles and company, a Trini, y seguramente otros que no recuerdo ahora. Y también a los técnicos del INA cuyo trabajo me ha facilitado el mío. Gracias a Giovanna, Rosa, Sara y Trini.

I also would like to thank Kristjan Jessen and Rhona Mirsky, for giving me the great opportunity of working in your lab during six months. So little time and such a big learning experience. Thank you for your guidance and your teaching dedication. I must thank Daniel Wilton, as my second great teacher during this PhD. Thank you for your patience while teaching me as many techniques as I wanted to learn. And thank you for letting me be totally integrated in your project. Y también quiero darte las gracias a ti, Cristina, por tu ayuda y tus consejos.

A Rebeca y Annalu, por hacer la vida en el INA más agradable con nuestras charlas y comidas. A Ceci, por haberme ayudado tanto en mis inicios en Alicante y por haber sido tan buena compañera de piso.

A Jan, por tu gran ayuda en todos los sentidos durante estos años y por tu gran y crucial contribución en la escritura y ensamblaje de esta tesis.

A mi familia y amigos, por vuestro incesante apoyo.

Sinopsis

Las células de Schwann son altamente plásticas, siendo capaces de revertir su fenotipo a lo largo de las diferentes etapas de su desarrollo. De esta manera, pueden retornar desde un fenotipo mielinizante a un fenotipo de célula desdiferenciada y proliferativa. Esta propiedad es esencial para la adquisición de un fenotipo de reparación después de una lesión en el nervio, lo cual es fundamental para la regeneración nerviosa en el ratón. Sin embargo, esta plasticidad puede favorecer la proliferación descontrolada de las células de Schwann ante condiciones tumorigénicas. La sobreexpresión de la isoforma tipo III- β 3 de la NRG1 en los ratones *NSE-SMDF^{+/+}* provoca una hiperproliferación de las células de Schwann durante los primeros días del desarrollo del ratón, lo que conlleva la formación de nervios de tipo neurofibroma. Sin embargo, esta hiperproliferación es frenada después de P14, a pesar de que la señal mitogénica aun está presente. En la primera parte de esta tesis, demostramos que este freno en la hiperproliferación de las células de Schwann es debido a la activación del programa de Senescencia Inducida por Oncogenes (OIS), puesto que la expresión de *p19Arf* y *p16Ink4a*, dos mediadores clave de este programa, está activada en los nervios del ratón *NSE-SMDF^{+/+}*. Asimismo, también mostramos que el programa de OIS está activado en neurofibromas de pacientes de NF1. Además demostramos que el bloqueo de la vía p19Arf/p53 en los nervios de *NSE-SMDF^{+/+}* provoca la reanudación de la proliferación de las células de Schwann, lo que conlleva la formación de tumores malignos en el SNP. Al igual que en los neurofibromas, la activación del programa de OIS interviene en el freno de la proliferación de las células de Schwann durante la degeneración Waleriana después de una lesión nerviosa, previniendo con ello la posible formación de tumores.

La inducción y mantenimiento del fenotipo mielinizante en las células de Schwann está mediado por señales provenientes del axón que elevan el cAMP intracelular en las células de Schwann. En células de Schwann en cultivo, el incremento en los niveles de cAMP imita el contacto axonal y provoca la activación de la expresión de proteínas de la mielina y la inhibición de la expresión de c-Jun, un factor de transcripción que caracteriza la desdiferenciación y es crucial en el fenotipo de reparación de las células de Schwann en la degeneración Waleriana. En la segunda parte de esta tesis, demostramos que la represión de la expresión de c-Jun inducida por cAMP está mediada por la translocación de HDAC4 al núcleo, donde posiblemente interacciona con el promotor de *c-jun* y recluta a HDAC3 para inhibir su expresión. También mostramos datos preliminares que sugieren la implicación de receptores adrenérgicos de las células de Schwann en la transducción de las señales axonales que inducen la diferenciación de estas células.

Abstract

Schwann cells are highly plastic, having the ability to revert their phenotype through most of the different stages in their development. They can therefore shift from a myelinating phenotype back to a dedifferentiated and proliferative phenotype. This property is essential for Schwann cell acquisition of a repair phenotype after a nerve injury, which enables nerve regeneration in the mouse. However, this plasticity can facilitate an uncontrolled hyperproliferation of Schwann cells under tumourigenic conditions. The overexpression of NRG1 type III- β 3 in *NSE-SMDF^{+/+}* mice causes Schwann cell overproliferation during the first postnatal days, which leads to the formation of neurofibroma-like nerves in these mice. However, this overproliferation is halted after P14 even though the mitogenic signal still remains. In the first part of this thesis, we demonstrate that this halt in Schwann cell overproliferation is due to the activation of the Oncogenic Induced Senescence (OIS) program, as two key mediators of this program, *p16Ink4a* and *p19Arf*, are upregulated in the nerves of *NSE-SMDF^{+/+}* mice. We also show that the OIS program is activated in neurofibromas of NF1 patients. Additionally we demonstrate that the blockage of the p19Arf/p53 pathway in the nerves of *NSE-SMDF^{+/+}* mice causes Schwann cells to resume proliferation, leading to the formation of malignant tumours in the PNS. As well as in neurofibromas, the activation of OIS mediates Schwann cell proliferation arrest during Wallerian degeneration after a nerve injury, in order to prevent the putative formation of a tumour.

Induction and maintenance of the myelinating phenotype in Schwann cells is mediated through axonal signals that elevate the intracellular cAMP levels in Schwann cells. In cultured Schwann cells, elevation of cAMP mimics axonal contact and leads to the upregulation of myelin proteins and the downregulation of c-Jun, a transcription factor that characterizes dedifferentiation and is crucial for the repair phenotype of denervated Schwann cells in Wallerian degeneration. In the second part of this thesis, we demonstrate that the repression of c-Jun expression by cAMP is mediated through the translocation of HDAC4 to the nucleus, where it probably interacts with the promoter of c-Jun and recruits HDAC3 to repress the transcription. We also show preliminary data that suggests the involvement of Schwann cell adrenergic receptors in mediating the axonal signals that induce Schwann cell differentiation.



UNIVERSITAS

Miguel **INDEX**
Hernández

ABBREVIATIONS

INTRODUCTION

1. The development of the Schwann cell lineage.....	2
1.1 Schwann cells in nerve architecture.....	2
1.2 Schwann cell-axon domains in myelinated fibers.....	3
1.3 Myelin.....	4
1.4 Transitions in Schwann cell differentiation.....	6
1.5 Mechanisms of control in Schwann cell transitions.....	8
1.6 NRG1 in Schwann cell development and differentiation.....	9
1.7 Control of Schwann cell differentiation by cAMP.....	11
1.8 The role of Histone Deacetylases in Schwann cell differentiation.....	12
2. Schwann cell plasticity is pivotal for nerve repair	14
2.1 Post-injury Wallerian degeneration.....	14
2.2 The Bungner repair cell.....	14
2.3 The repair phenotype is controlled by the c-Jun transcription factor.....	15
2.4 Schwann cell proliferation after injury.....	16
3. Uncontrolled Schwann cell proliferation underlies PNS tumor development	17
3.1 Types of PNS tumours.....	17
3.2 Molecular mechanisms of neurofibroma development.....	18
4. The <i>NSE-SMDF</i>^(+/-) mouse	19

OBJECTIVES

General objectives.....	21
Specific objectives.....	21

MATERIALS AND METHODS

1. Mice.....	23
2. Tissue culture techniques.....	24
3. Transfection.....	26
4. Infection.....	27
5. β -Galactosidase Assay.....	28
6. Luciferase Assay.....	28
7. Immunofluorescence.....	30
8. Western Blot.....	33
9. Electron Microscopy.....	34
10. Real Time quantitative PCR (RT-qPCR).....	35
11. Chromatin Immunoprecipitation (ChIP) assay.....	37
12. In Vivo Nerve Injury.....	38

RESULTS

1. Control of Schwann cell proliferation in pathological conditions	40
1.1 Schwann cell proliferation is halted in neurofibromas from adult <i>NSE-SMDF^{+/+}</i> mutant mice.....	40
1.2 Proliferation of Schwann cells is restricted by the activation of the replicative senescence programme in the <i>NSE-SMDF^{+/+}</i> neurofibromas	41
1.3 Histone demethylase <i>Jmjd3</i> contributes to the activation of <i>Ink4a/Arf</i> in Schwann cells.	45
1.4 Oncogene Induced Senescence in human plexiform neurofibromas	47
1.5 Malignant transformation of the <i>NSE-SMDF^{+/+}</i> neurofibromas is associated with the loss of the senescence program.	48
1.6 The senescence program is activated in Schwann cells after injury	52
1.7 The activation of the senescence program after injury controls Schwann cell proliferation	54
2. Regulation of c-Jun expression in peripheral nerves	55
2.1 c-Jun expression in nerve explants	55
2.2 cAMP decreases c-Jun mRNA in cultured rat Schwann cells.....	56
2.3 c-Jun upregulation is cell autonomous	58
2.4 Signalling pathways controlling c-Jun upregulation.....	59
2.4.1 NRG1 accelerates c-Jun expression	59
2.4.2 JNK pathway mediates self-autonomous c-Jun expression after dbcAMP removal.....	59
2.4.3 NRG1 induces c-Jun temporal upregulation in dbcAMP differentiated Schwann cells.....	61
2.5 HDAC4 is involved in dbcAMP induced c-Jun downregulation.....	61
2.5.1 HDAC4 translocates to the nucleus in the developmental transition towards myelinated nerves.....	62
2.5.2 cAMP translocates HDAC4 into the nucleus of Schwann cells.....	63
2.5.3 MEF2 contributes to c-Jun expression in basal conditions <i>in vitro</i>	64
2.5.4 Loss of HDAC4 function (shRNA) prevents c-Jun downregulation by cAMP analogs.....	66
2.5.5 Gain of HDAC4 function leads to c-Jun downregulation.....	68
2.5.6 HDAC4 represses <i>c-jun</i> by recruiting HDAC3 through SMRT/NCoR1	70
2.6 The β -adrenergic receptors partially activate cell differentiation in cultured Schwann cells	74

DISCUSSION

Control of Schwann cell proliferation in pathological conditions.....	78
Regulation of c-Jun expression in peripheral nerves.....	83

CONCLUSIONS

BIBLIOGRAPHY

PUBLICATION

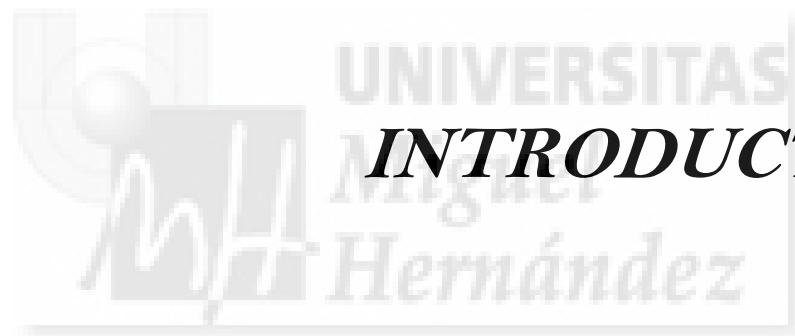
Abbreviations

Ab	Antibody
ABC	Active beta-Catenin
AKT	Protein Kinase B
ATP	Adenosin Triphosphate
AP1	Activator protein 1
BDNF	Brain-Derived Neurotrophic Factor
BFABP	Brain Fatty Acid-Binding Protein
BMP	Bone Morphogenetic Protein
CDK	Cyclin-Dependent Kinase
CGRP	Calcitonin gene-related peptide
CNTF	Ciliary Neurotrophic Factor
CREB	cAMP Response Element Binding Protein
cAMP	3',5'-cyclic Adenosine Monophosphate Cyclase
DNA	Deoxyribonucleic acid
DRG	Dorsal Root Ganglia
dbcAMP	Dibutyryl-cAMP
EGF-like	Epidermal Growth Factor like domain
ERK	Extracellular signal-Regulated Kinase
FABP7	Fatty Acid Binding Protein 7
FGF	Fibroblast Growth Factor
FSK	Forskolin
GAPDH	Glyceraldehyde-3-Phosphate Dehydrogenase
GDNF	Glial cell-Derived Neurotrophic Factor
GFAP	Glial fibrillary Acidic Protein
HA-tag	Human Influenza Hemagglutinin epitope tag
HAT	Histone Acetyltransferase
HDAC	Histone Deacetylase
HDFs	Human Dermal Fibroblasts
H3K27me3	Trimetilated lysine 27 on Histone H3
IGF	Insulin-like Growth Factor
IgG	Immunoglobulin G
JMJD3	Histone Demethylase Jumonji D3
JNK	c-Jun N-terminal Kinase
KO	Knock-out
LHO	Loss of Heterozygosity
LIF	Leukemia Inhibitory Factor
Lv	Lentivirus
MAG	Myelin Associated Glycoprotein

MAPK	Mytogen Activated Protein Kinase
MBP	Myelin Basic Protein
MEFs	Murine Embryo Fibroblasts
MEF2	Myocyte Enhancer Factor 2
MEK	Mitogen-activated Protein Kinase Kinase
MPNST	Malignant Peripheral Nerve Sheath Tumor
mRNA	Messenger Ribonucleic Acid
NAB2	NGFI-A Binding Protein 2 (EGR1-Binding Protein 2)
NCAM	Neural Cell Adhesion Molecule
NFATc	Nuclear Factor of Activated T-cells
NF-κB	Nuclear Factor Kappa B
NF1	Neurofibromatosis type 1
NGF	Nerve Growth Factor
NRG	Neuregulin
NSE	Neuron Specific Enolase
NT-3	Neurotrophin-3
Oct-6	Octamer Transcription Factor 6
OIS	Oncogene-Induced Senescence
OPC	Oligodendrocyte Precursor Cell
P0	Myelin Protein Zero
PRC2	Polycomb Repressive Complex 2
PCR	Polymerase Chain Reaction
PDE	Phosphodiesterase
PDGF-BB	Platelet Derived Growth Factor BB
pH3	Serine-10-phosphorylated Histone 3
PI3K	Phosphatidylinositol 3-Kinase
PLC-γ	Phospholipase C- γ
PMP-22	Peripheral Myelin Protein 22
PNS	Peripheral Nervous System
PTEN	Phosphatase and Tensin homolog
P2	Myelin Protein 2
p75NTR	p75 Neurotrophic Factor Receptor
qPCR	Quantitative-real Time PCR
Rb	Retinoblastoma
RNA	Ribonucleic Acid
RTK	Receptor-type Tyrosine kinase
RT-PCR	Reverse Transcription PCR
SAPK	Stress-Activated Protein Kinase
SA-β-GAL	Senescence-associated beta-galactosidase
SEMA4F	Semaphorin-4F

SC	Schwann Cell
SCP	Schwann Cell Precursor
shRNA	Short Hairpin RNA
SIR2	Silent Information Regulator 2 Protein
SMDF	Sensory and Motor Neuron derived Factor
ChIP	Chromatin Immunoprecipitation
CNS	Central Nervous System
SC1	Schwann Cell Factor 1
SREBP	Sterol Regulatory Element Binding Protein
TG	Transgenic
TGF-β	Transforming Growth Factor Beta
TSA	Trichostatin A
WT	Wild type





UNIVERSITAS

INTRODUCTION

*Miguel
Hernández*

1. The development of the Schwann cell lineage

1.1 Schwann cells in nerve architecture

The two main cell types in the nervous system are the neurons, which are directly involved in processing and transmission of information, and the glial cells. Glial cells outnumber neurons and have many essential functions both in the development of the nervous system and in its normal function. The major glial types are astrocytes and oligodendrocytes in the central nervous system (CNS) (Arroyo & Scherer, 2000), and Schwann cells in the peripheral nervous system (PNS). Both oligodendrocytes and Schwann cells form one of the most highly specialized structures in the body, which is the myelin sheath. The myelin sheath consists of multiple layers of opposed glial membranes that enwrap the axon, providing electrical insulation and thereby facilitating the rapid conduction of action potentials. Whereas unmyelinated axons have conduction velocities of 0.5-10 m/s, myelinated axons can conduct with velocities up to 150 m/s (Jessen, 2004). Besides increasing impulse speed, the insulating role of the myelin sheath also allows for the conservation of energy and space. In order to achieve the same conduction velocity, an unmyelinated axon should be 40 times larger in caliber and should consume 5000 times more energy than a myelinated axon (Garbay *et al*, 2000). Besides forming the myelin sheaths, Schwann cells provide trophic support to the axons.

Schwann cells ensheath all axons in the PNS and can be subdivided into myelinating and non-myelinating Schwann cells. In an adult nerve, axons with a diameter over 1 μm are surrounded by myelin, forming the so-called myelinated fibers. In contrast, smaller caliber axons are found in groups associated with non-myelinating Schwann cells, forming the Remak bundles (Jessen & Mirsky, 2005). Nerves may contain one or, more commonly, both types of fibers. The nerve fibers are grouped together, supported by an extracellular connective matrix called the endoneurium, forming a nerve fascicle. Together with the axon-Schwann cell units, each fascicle contains endoneurial fibroblasts and a few mast cells that are embedded in the extracellular matrix. Large nerves contain several fascicles, each one surrounded by the perineurium, which is a protective sheath formed by concentric layers of flat perineurial cells. The fascicles are bundled together with vessels and fatty tissue, surrounded by the outer-most protective layer, called the epineurium (Fig. 11).

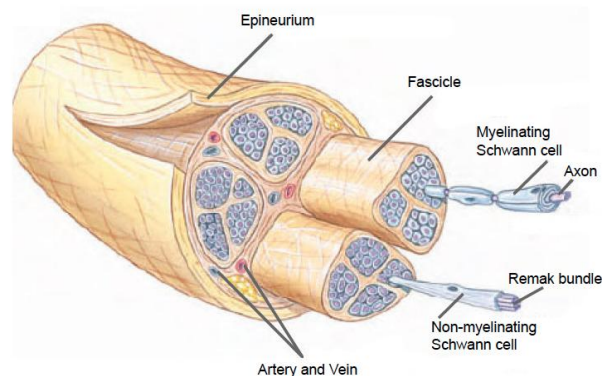


Figure 11.- Nerve architecture. The diagram represents the structure of a nerve that contains myelinated and non-myelinated axons. Myelinated axons and Remak bundles are immersed within the endoneurium and grouped in a fascicle. The epineurium surrounds the group of fascicles. Image taken from Biocyclopedia.com.

1.2 Schwann cell-axon domains in myelinated fibers

In a myelinated fiber, Schwann cells are aligned individually along the axonal length, forming Schwann cell-axon units. The Schwann cell membrane forms a defined number of wraps along a discrete axonal segment, and coats it with myelin sheaths that it produces. In the gap between two myelinating Schwann cells there is an uncoated site, about 1 μ m long, which is called the node of Ranvier (Salzer, 2003) (Fig. I2A).

Schwann cells possess radial polarity determined by two distinct cytoplasmic membranes. The outer membrane, called abaxonal membrane or outer mesaxon, is in contact with the basal lamina, a basement membrane secreted by the Schwann cell, and surrounds the whole Schwann cell-axon unit. In contrast, the inner membrane, called adaxonal membrane or inner mesaxon, is in contact with the axon membrane, called axolemma (Salzer, 2003; Scherer & Arroyo, 2002). Myelination establishes a series of distinct domains in the axolemma, called node, paranode, juxtaparanode and internode (Fig. I2A). The organization in these domains is essential for the saltatory conduction, which is the propagation of action potentials from one node of Ranvier to the next one, in myelinated fibers (Salzer, 2003). Moreover, the axonal cytoskeleton, organelle composition and rates of transport are differently organized along the axolemma domains (Sherman & Brophy, 2005).

In the nodes of Ranvier, the axon is exposed and communicates with the extracellular environment. However, the nodal gap is filled with interdigitating microvilli that project from the outer-most part of the Schwann cell and interact with the axolemma in the node. These microvilli send information for the correct node location and formation, and also connect the membranes of two adjacent Schwann cells through tight junctions. (Poliak & Peles, 2003). The high concentration of voltage gated sodium channels at the nodes facilitates the regeneration of action potentials. The arrival of a wave of positively charged sodium ions depolarizes the axonal membrane, which activates the voltage gated sodium channels, allowing the massive influx of more sodium ions into the axon and causing a new wave of depolarization, that is passively transmitted along the internodal segment, until it reaches the next node of Ranvier (Garbay *et al*, 2000).

At both sides of the node lay the paranodes, which are the sites at which the membranes of the Schwann cell and the axon are in closest apposition and form axo-glial junctions. These consist of septate-like junctions through which the axonal membrane interacts with cytoplasm-filled glial loops formed by the myelin sheath (Poliak & Peles, 2003; Salzer *et al*, 2008). The juxtaparanode is located in a short area beyond the innermost paranodal junction. In this region there is a high concentration of delayed potassium rectifier channels with the function of restoring the resting potential of the axon membrane after the electrical impulse (Poliak & Peles, 2003).

The internode is the largest domain in myelinated fibers and it comprises the portion of the axon underlying the compact myelin sheath. Along the internode, the Schwann cell membrane is separated from the axolemma by a periaxonal space of 15 nm. Nevertheless, both membranes interact with each other via cell-surface proteins, ionic changes in the extracellular space and non-synaptic release of neurotransmitters, growth factors and specialized axon-glial signalling molecules (Salzer *et al*, 2008). Studies on neuron-glial communication in non-synaptic regions provide increasing evidence for a possible influence of neuronal electrical activity on the myelination process during development in both PNS and CNS. (Fields & Stevens-Graham, 2002).

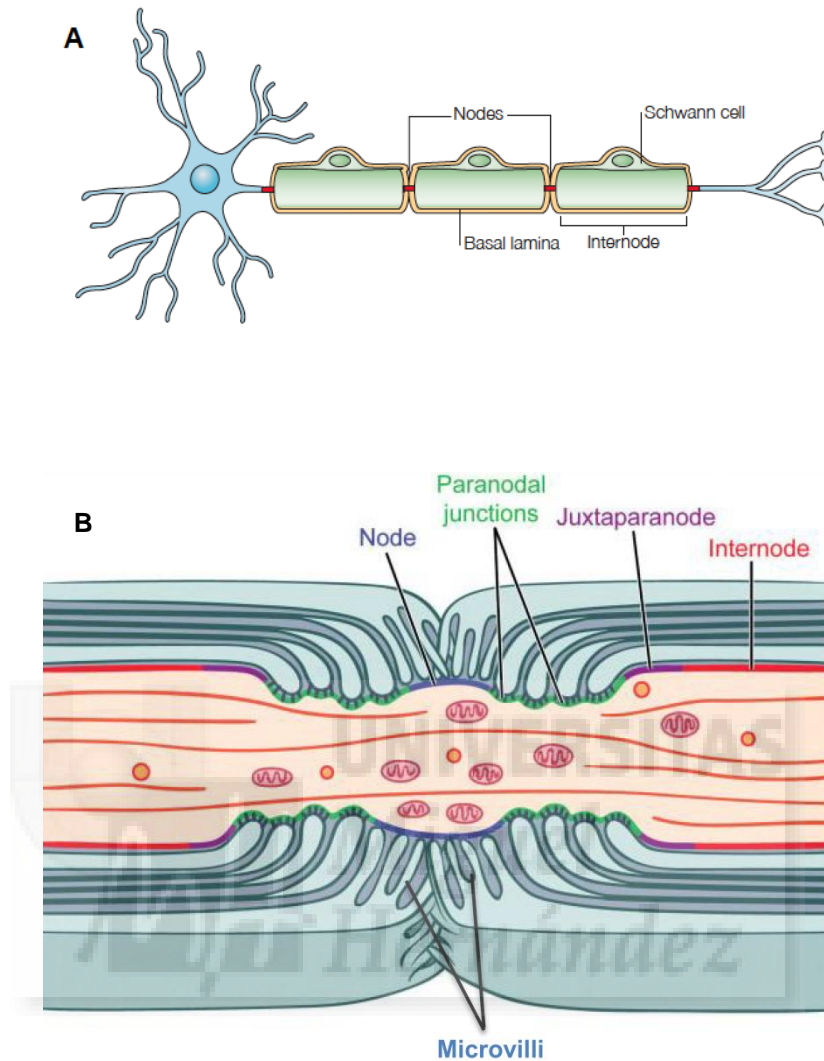


Figure 12.- Axon-Schwann cell domains in myelinated fibers. (A) Diagram representing the general structure of a myelinated fiber. Schwann cells are lined up individually along the axonal length. The gaps between adjacent Schwann cells are the nodes. The basal lamina covers every Schwann cell-axon unit. (Poliak & Peles, 2003). **(B)** Diagram representing the specialized domains in the axolemma centered in the Node of Ranvier (Salzer *et al*, 2008).

1.3 Myelin

Structure

To achieve an efficient and rapid electrical conduction, the axon needs to be insulated by large amounts of non-conducting material, keeping the aqueous, cytoplasmic material and extracellular space as far as possible from the axolemma. Schwann cells solve this problem by producing multiple layers of highly lipid-rich plasma membrane whose compaction excludes cytoplasmic and extracellular material. The myelin sheath consists of multiple wraps of compacted Schwann cell membrane around a discrete portion of the axon (Garbay *et al*, 2000). The number of lamellae is proportional to the axonal diameter, thus the larger the caliber of the axon is, the thicker the surrounding myelin sheath will be (Smith *et al*, 1982). In electron microscope images, the myelin sheath displays major dense lines that correspond to the fusion of cytoplasmic surfaces of the

membrane, and intraperiod lines that correspond to the close apposition between exoplasmic surfaces of the membrane (Garbay *et al*, 2000; Scherer & Arroyo, 2002) (Fig. 13).

The myelin sheath has a region with non-compacted structures and a much larger domain composed of compacted membranes (Scherer & Arroyo, 2002). For communication between the inner and outer cytoplasmic compartments of the myelinating Schwann cell, there exist channels called Schmidt-Lanterman Incisures that spiral through the myelin sheaths. They link apposed membranes of the same cell through tight junctions, adherens junctions and gap junctions, which permit the diffusion of small molecules across the non-compacted regions (Salzer, 2003).

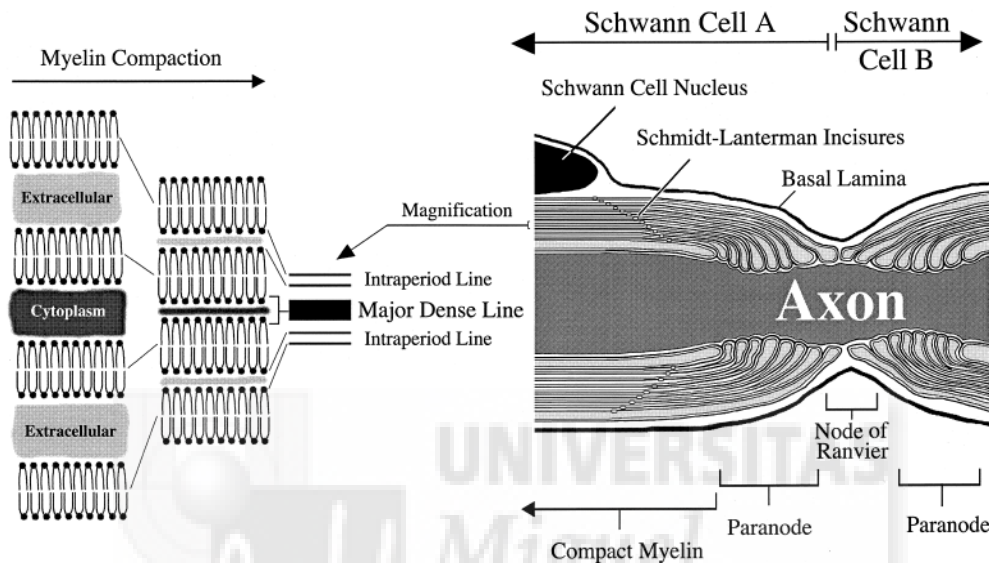


Figure 13.- Schematic representation of a myelinated axon (longitudinal section). The left part shows an enlargement of the compact myelin region, illustrating the formation of the major dense line and the intra-period lines (Garbay *et al*, 2000)

Composition

In comparison with other cellular membranes, myelin has a very high lipid-to-protein ratio: 70-80% lipids and 20-30% proteins. Cholesterol accounts for 20-30% of the total lipid content and is proposed to have a role in stabilization and compaction of the multiple lamellae. Myelin also contains a large proportion of monogalactosphingolipids (cerebrosides and sulfatides) and saturated long-chain fatty acids (Garbay *et al*, 2000).

The myelin sheath in the PNS is enriched in glycoproteins, which cover at least 60% of the total protein content, and basic proteins, which represent 20-30% of the total protein content (Garbay *et al*, 2000). Four membrane glycoproteins are abundant in myelin: Protein-zero (P0), peripheral myelin protein 22 (PMP-22), periaxin and myelin-associated glycoprotein (MAG). Two of these, P0 and PMP-22, are components of the compact myelin domain and play an important role as membrane adhesion molecules and also maintaining the very tight compaction of the myelin structure. MAG is found in periaxonal Schwann cell membranes, in Schmidt-Lanterman incisures, in lateral loops, and in the inner and outer mesaxons, having an adhesive role as well as a signalling role in axon-glia interaction. Unlike P0, PMP-22 and MAG, periaxin is not an integral membrane protein but is localized at the plasma membrane of Schwann cells (Quarles, 2002).

Basic proteins in myelin are represented by two classes: Myelin basic proteins (MBP), which participate in the compaction of the myelin sheath, and Protein P2, which functions as a lipid carrier, contributing in the assembly and maintenance of myelin (Garbay *et al*, 2000)

1.4 Transitions in Schwann cell differentiation

Schwann cells originate in the neural crest and follow a differentiation process that has three important transitions, of which the first two take place in the embryonic stage. The first transition is from neural crest cells to Schwann cell precursors. In the second transition, Schwann cell precursors give rise to immature Schwann cells. The third transition occurs postnatally and consist of the formation of mature myelinating and non-myelinating Schwann cells.

Neural crest cells emerge at the dorsal-most part of the neural tube, delaminate and migrate to different locations in the embryo. Depending on the local environment, these cells become fate restricted, giving rise to neural cells of the PNS, smooth muscle cells in the heart, melanocytes in the skin, craniofacial bones, cartilage and connective tissue (Le Douarin & Dupin, 2003). Gliogenesis takes place at embryonic day E12/13 in mouse (E14-15 in rat) when Schwann cell precursors (SCPs) arise from migrating neural crest cells. The transition from neural crest cells to SCPs is marked by the expression of brain fatty acid-binding protein (BFABP), myelin protein zero (P0), desert hedgehog, connexin 29 and cadherin 19. SCPs are found in the newly formed embryonic nerves, which are tightly packed structures without any extracellular matrix, connective tissue or blood vessels. SCPs extend large sheet-like processes connecting themselves to each other, and surround large groups of axons. At this stage neurons depend on SCPs for survival, but also SCPs need to be in contact with axons for their survival as they depend on the juxtacrine signal provided by neuregulin-1 type III in the axon (Jessen *et al*, 1994).

At E13-15 in mice (E15-E17 in rat), peripheral nerves reach their target areas and establish the first synaptic connections (Wolpowitz *et al*, 2000). In this period SCPs differentiate, giving rise to endoneurial fibroblasts and immature Schwann cells. The latter express S100 β , GFAP and the glycolipid antigen O4. Also at this stage, the cytoarchitecture of the nerves changes completely, as they start to develop an endoneurial space with connective tissue, blood vessels, endoneurial fibroblasts and “axon-Schwann cell families”, formed by immature Schwann cells surrounding small bundles of axons of different calibers (Wanner *et al*, 2006) (Fig. 14).

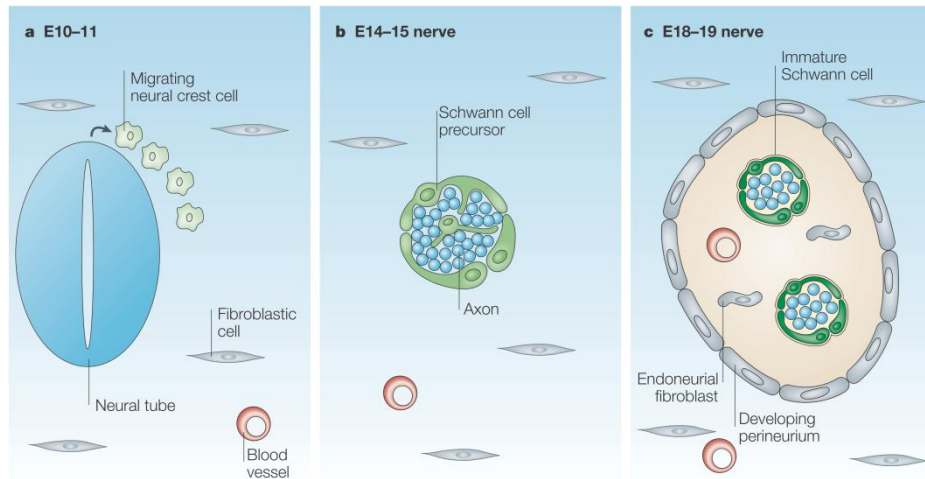


Figure 14.- Cell and tissue relationships at key stages of Schwann cell development in rodents.

(A) Migrating crest cells move through immature connective tissue before the time of nerve formation. (B) SCPs are tightly associated with axons and are found in early nerves that are still compact and do not yet contain blood vessels or connective tissue. (C) Immature schwann cells are found in nerves that have acquired the basic tissue relationships of adult nerves. The developing perineurium defines the endoneurial space that now contains axon-Schwann cell units, blood vessels, endoneurial fibroblasts and extracellular matrix (Jessen & Mirsky, 2005).

Before birth, immature Schwann cells send cytoplasmic processes into groups of axons. At this stage, large diameter axons ($>1\mu\text{m}$) undergo the radial sorting process, in which immature Schwann cells enwrap individual axons and establish a 1:1 relationship with them. Also, a large number of small axons that will not be myelinated (10-15% unmyelinated axons in rodents) are radially sorted by the same process (Sharghi-Namini *et al*, 2006). Before radial sorting, axon and Schwann cell numbers need to be matched, which is achieved by controlled Schwann cell proliferation and apoptosis (Woodhoo & Sommer, 2008). The radial sorting process leads to the promyelinating stage, in which the Schwann cell forms one and a half wraps around the axon. During this time, the Schwann cell also undergoes a substantial lateral elongation along the axon and secretes a basal lamina at the abaxonal surface of the Schwann cell-axon unit. The formation of the basal lamina promotes Schwann cell differentiation (Owens & Bunge, 1989). Small diameter axons become grouped in bundles, each one surrounded by one immature Schwann cell. At this stage, immature Schwann cells give rise to myelinating and non-myelinating Schwann cells, depending on the type of axon they are associated with (Fig. I5).

At the onset of myelination there is a strong upregulation of molecules that are associated with myelin formation such as Krox-20, MAG and PMP-22. At the same time there is a downregulation of molecules that are characteristic of the immature phenotype, including L1, NCAM and the p75 neurotrophin receptor. Non-myelinating Schwann cells continue to express these last proteins and in addition they express $\alpha 1\beta 1$ integrin and galactocerebroside (Mirsky *et al*, 2008).

In contrast to Schwann cell precursors, immature and mature Schwann cells can survive in the absence of axons, since they secrete survival factors such as IGF, NT-3 and PDGF-BB, that can act in an autocrine way (Jessen & Mirsky, 2005; Woodhoo & Sommer, 2008).

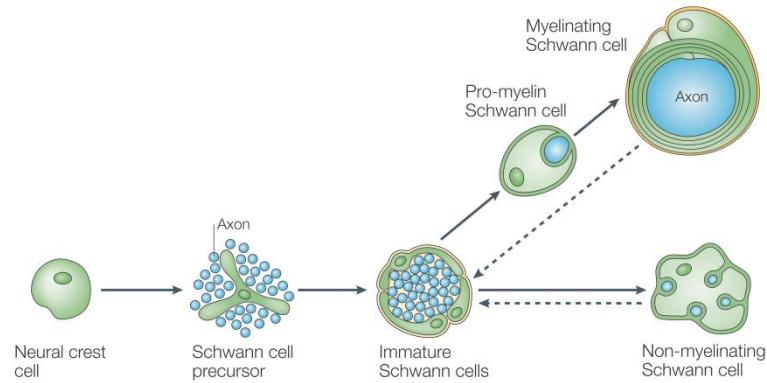


Figure 15.- The Schwann cell lineage. Schematic illustration of the main cell types and developmental transitions involved in Schwann cell development. Dashed arrows indicate the reversibility of the final, largely postnatal transition during which mature myelinating and non myelinating cells are generated. (Jessen & Mirsky, 2005)

1.5 Mechanisms of control in Schwann cell transitions

How neural crest cells are specified into peripheral glia is not known. Factors that suppress gliogenesis, such as bone morphogenic proteins (BMPs) 2 and 4, and factors that suppress neurogenesis, such as NRG1 and Notch-1, are believed to have a role in inducing the glial development. Sox-10 is the only gene known to be essential for the generation of the glial lineage, but it does not seem to initiate gliogenesis because is expressed in neural crest cells as well as in peripheral glia. Sox-10 induces expression of the neuregulin receptor ErbB3, fatty acid binding protein 7 (Fabp7) and myelin protein zero (P0) (Jessen & Mirsky, 2005).

Differentiation of SCPs depends on axonal signals such as NRG1 and Notch-1. NRG1 is sufficient for activation of SCP-immature Schwann cell transition in culture (Leimeroth *et al*, 2002). Notch-1 is involved in timing Schwann cell generation (Woodhoo *et al*, 2009).

The transition from promyelinating, proliferative Schwann cells to myelinating Schwann cells is controlled by the transcription factors Oct-6, Brn-2, Sox-10 and Krox-20 (Mirsky & Jessen, 1999). Oct-6 and Brn-2 are crucial for timing this transition. One of their major targets is Krox-20, which is essential for initiating myelination as well as for the maintenance of the myelinating phenotype afterwards (Birchmeier & Nave, 2008). The Sox-10 transcription factor is required for Schwann cell specification from the neural crest early in development. As it is expressed during all stages in Schwann cell development, Sox-10 also upregulates the expression of Oct-6 and Krox-20 at the onset of myelination (P1). This regulatory feed-back circuit has multiple inputs and provides a fine temporal control of the targeted networks. (Pereira *et al*, 2012)

The activation of Oct-6 expression at the onset of myelination is induced by various axonal signals that include Neuregulin1 type III. In contrast with Krox-20 expression, which remains active in myelinating Schwann cells, the expression of Oct-6 disappears as the transition towards the myelinating phenotype is completed. Oct-6 expression is also repressed when Schwann cells are cultured, but it becomes upregulated again when cAMP levels are elevated in these cells. Protein kinase A (PKA) is one of the main targets activated by cAMP, and it regulates several transcription factors, including Cre binding protein (CREBP) and NFkB. It is known that NFkB activates Oct-6 at a posttranscriptional level.

Schwann cell differentiation depends on several growth factors such as neuregulin, platelet-derived growth factor (PDGF) and insulin-like growth factor-I (IGF-I). Their receptors are receptor-type tyrosine kinases (RTKs) and activate two essential pathways. One of them is the mitogen-activated protein kinase (MAPK) pathway, which classically consists of RAS-RAF-MEK-ERK. The other one is the phosphatidylinositol-3-kinase (PI3K) pathway, which activates PKA. All three growth factors neuregulin, PDGF and IGF-I, activate both pathways but at different levels, which determines their differential effects in Schwann cell differentiation (Ogata *et al*, 2004).

An important aspect of myelination is the coordination of the expression of myelin genes with the expression of genes involved in lipid synthesis, since the formation of multiple layers of high cholesterol containing-myelin sheaths requires a huge amount of lipid being synthesized. Krox-20 activates the expression of major myelin proteins, such as P0, MBP, PMP-22, Connexin 32 and MAG, and also of the genes involved in lipid synthesis. Sox10 also controls many of these genes. Other important transcription factors that regulate gene expression involved in cholesterol and fatty acid biosynthesis are the sterol-regulatory element binding proteins (SREBPs) (Pereira *et al*, 2012).

Besides its crucial function in activating genes involved in myelination, Krox-20 also inhibits the expression of a number of genes involved in proliferation, maintenance of immature Schwann cell state and repair, such as L1 and c-Jun. There is a mutually antagonistic relationship between Krox-20 and c-Jun, which is important in controlling the Schwann cell transition from a myelinating phenotype towards a non-myelinating, repair phenotype after a nerve injury (Svaren & Meijer, 2008)

1.6 NRG1 in Schwann cell development and differentiation

Neuregulins (NRGs) are a family of growth and differentiating factors that share an epidermal growth factor-like domain (Clarke *et al*, 1998). Four different *nrg* genes have been identified. The best characterized is *nrg1*, being one of the largest mammalian genes. The expression of this gene gives rise to at least 15 different isoforms via transcription from different promoters and alternative splicing forms. All NRG1 type I, II and III isoforms contain an epidermal growth factor (EGF)-like domain that is necessary for the activation of ErbB receptors in the Schwann cell membrane (Holmes *et al*, 1992). They differ on their N'-terminal domain, which consist on an Ig-like domain in the case of NRG type I and II, and a cystein-rich domain (CRD) in NRG type III. NRG1 types I and II release their ectodomain (by proteolytic cleavage) to act as a paracrine signal. In contrast, in NRG 1 type III the EGF domain is exposed to act in a juxtacrine manner (Falls, 2003) (Fig. I6).

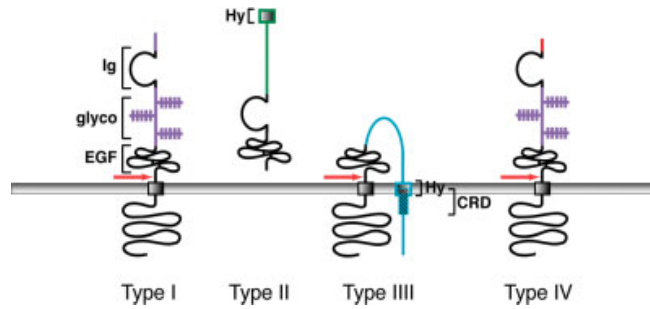


Figure 16.- Major isoforms of NRG1. From the *nrg1* gene, four different types of isoforms are produced. Common to all isoforms is an EGF-like domain. Other sequences present are an Ig-like domain, a domain rich in potential glycosylation sites (glyco) and a cysteine rich domain (CRD). Red arrows indicate cleavage sites. Sequences specific to only one of the four isoforms are shown in color. (Birchmeier & Nave, 2008)

The two NRG1 type III isoforms, $\beta 1$ and $\beta 3$, are strongly expressed in sensory and motor neurons. NRG1 type III- $\beta 1$ is necessary for the survival of Schwann cell precursors in embryonic development. In later stages, NRG1 type III- $\beta 1$ bound to the axonal membrane has been shown to be essential for the initiation and regulation of myelination in the PNS. Mice lacking the expression of NRG1 type III- $\beta 1$ fail to initiate myelination, and overexpression of this isoform leads to hypermyelination, which indicates that the thickness of the myelin sheath is determined by the amount of axonal NRG type III- $\beta 1$ (Birchmeier & Nave, 2008; Michailov *et al*, 2004; Taveggia *et al*, 2005).

NRG1 signal is transmitted via heterodimers of ErbB2/ErbB3 receptors. The physical interaction between NRG1 and ErbB3 activates the tyrosine kinase activity of ErbB2, which recruits Src homology 2 domain-containing signal-transducing proteins (Burden & Yarden, 1997). These include PI3-kinase (phosphatidylinositol 3-kinase), MAPKs (mitogen-activated protein kinases) and phospholipase C- γ .

PI3-kinase catalyzes the formation of PIP3 (phosphatidylinositol trisphosphate) from PIP2 (phosphatidylinositol diphosphate), activating the proto-oncogene AKT in the process. In experiments done using DRG-Schwann cell co-cultures, it was found that the PI3-kinase pathway, through its downstream effector AKT, is essential for the axon-contact dependent proliferation, survival and differentiation of Schwann cells, constituting a crucial pathway to initiate myelination (Maurel & Salzer, 2000). AKT is a serine-threonine kinase that phosphorylates and activates among others cAMP response element binding protein (CREB) (Du & Montminy, 1998), which is involved in myelin differentiation (Arthur-Farraj *et al*, 2011), and NF- κ B, which induces expression of pro-survival genes. AKT is also involved in cholesterol biosynthesis as it regulates the expression of SREBP proteins. (Porstmann *et al*, 2005).

MAPK signalling comprises four cascades: extracellular related kinases 1 and 2 (ERK1 and 2), ERK 5, c-Jun N-terminal kinases (JNK), and p38. In experiments using knock out animals, it was found that neuregulin induced activation of ERK1/2 is crucially required for survival of SCP and also for the progression towards the myelination phenotype of committed Schwann cells (Newbern *et al*, 2011).

Phospholipase C- γ (PLC- γ) triggers an increase of intracellular Ca^{2+} in Schwann cells, leading to the dephosphorylation of NFATc proteins through the activation of the phosphatase calcineurin. This facilitates NFATc translocation to the nucleus to become assembled into NFAT transcription complexes. These NFAT-containing complexes cooperate with Sox-10 to activate the expression of Krox-20 in the promyelinating stage and to activate the expression of myelin proteins such as P0 in the myelination stage (Kao *et al*, 2009).

1.7 Control of Schwann cell differentiation by cAMP

Maintenance of the myelination phenotype in Schwann cells requires constant contact with the axon. Any interruption of this interaction leads to reversion of Schwann cells towards an immature-like phenotype, with altered morphology, protein expression and functions. Although the precise axonal signals that mediate the maintenance of the myelinating Schwann cell phenotype are still unknown, various studies demonstrate the implication of intracellular cyclic adenosin monophosphate (cAMP) as a second messenger in the Schwann cell for the transduction of these axonal signals [reviewed in (Glenn & Talbot, 2013b)].

One major transducer of cAMP signaling is Protein Kinase A (PKA), a multimer composed by four subunits: two catalytic and two regulatory. Elevation of intracellular cAMP levels promotes the release of the two catalytic subunits from the regulatory subunits, which become activated and phosphorylate their protein substrates in specific serine/threonine residues.

After a nerve injury, the levels of cAMP in the Schwann cells in the distal stump decrease to 10% in three days and remain very low during the degeneration process. Only after the newly arrived axons become in contact with the Schwann cells and remyelination has taken place, cAMP intracellular levels increase again (Poduslo *et al*, 1995). It has been suggested that both an increased phosphodiesterase (PDE) activity and a decreased adenylyl cyclase activity are responsible for the declining cAMP levels in Schwann cells after injury (Walikonis & Poduslo, 1998).

In cultured Schwann cells, cAMP elevation can mimic at least partially the presence of the axon, promoting differentiation and myelination. Incubation with agents that elevate intracellular cAMP enhances the expression of myelin-associated proteins, including galactocerebroside (Gal-C), E-cadherin, periaxin, Oct-6, Sox-10, Krox-20, P0, nuclear factor N-kB and myelin basic protein (MBP). Furthermore, elevation of cAMP downregulates the expression of proteins that are present in immature Schwann cells but inhibited in myelinating Schwann cells. These include the low affinity neurotrophin factor p75^{NTR}, neural-cell adhesion molecule, N-cadherin, glial fibrillary acidic protein, growth associated protein 42, Sox-2 and c-Jun (Morgan *et al*, 1991).

Besides being involved in promotion of myelination, cAMP, at lower doses, has an important proliferative role in cultured Schwann cells. In fact, it is an indispensable co-mitogen for various growth factors, such as platelet-derived growth factor (PDGF), basic fibroblast growth factor (bFGF), insulin-like growth factor (IGF) and Reg-1. It has been shown that cAMP induced proliferation is mediated by cyclin D1, whose expression is activated by the combination of cAMP with growth factors during the G phase of the Schwann cell cycle (Kim *et al*, 2001; Rahmatullah *et al*, 1998).

Mitogenesis induced by NRG1 type III in Schwann cell cultures is greatly enhanced by elevating intracellular cAMP levels. The combination of both factors accelerates the initiation of

the S phase in the cell cycle. It has been proposed that this is due to the sustained activation of MEK-ERK and AKT pathways induced by the synergic interaction between cAMP and neuregulin in Schwann cells (Monje *et al*, 2006). In addition, it has been shown that both cAMP and NRG1 type III are necessary to induce a strong expression of the myelination markers P0 and Krox-20 in cultured Schwann cells. The levels of cAMP are determinant for the outcome of NRG1 signalling in the cells. Low levels of cAMP promote Schwann cell proliferation whereas high levels promote Schwann cell differentiation (Arthur-Farraj *et al*, 2011).

1.8 The role of Histone Deacetylases in Schwann cell differentiation

In recent years the involvement of epigenetic mechanisms in the control of Schwann cell differentiation and myelination has become a very active research area. Histone Deacetylases (HDACs) have epigenetic functions, based on chromatin remodeling by removal of acetyl groups in histone tails (de Ruijter *et al*, 2003) (Fig. I7). However, they regulate transcription using non-epigenetic mechanisms as well, since they can also deacetylate transcription factors, modulating their activity (Yao & Yang, 2011).

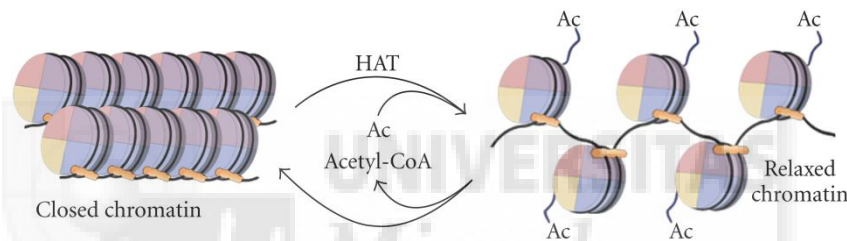


Figure I7.- Histone acetylation and deacetylation. Histone acetylation is regulated by the addition of acetyl-coA via the opposing actions of histone acetyltransferases (HATs) and histone deacetylases (HDACs) in lysine residues on core histones. Removal of acetyl groups by HDACs leads to a condensed, transcriptionally repressive chromatin conformation (Rodd *et al*, 2012).

There are two known protein families with HDAC activity: the SIR2 family of NAD⁺-dependent HDACs and the classical HDAC family. The latter is subdivided in two different phylogenetic classes: Class I HDACs comprise HDAC 1, 2, 3 and 8. Class II HDACs consist on HDAC 4, 5, 6, 7, 9 and 10 (Fig. I8). At variance with class I HDACs, which are exclusively found in the nucleus, class IIa HDACs shuttle from nucleus to cytoplasm in response to certain cellular signals (de Ruijter *et al*, 2003). HDACs do not bind to DNA directly but through interaction with protein complexes that contain DNA-binding proteins. For many years it was thought that all HDACs possess enzymatic histone deacetylase activity, but this idea was revoked by studies showing that the enzymatic activity associated with class II HDACs is due to the interaction with SMRT/N-CoR-HDAC3 complexes (Fischle *et al*, 2002).

HDAC1 and 2 have an essential role in survival of Schwann cells and in the regulation of the myelination program. Depletion in Schwann cells of both HDAC1 and HDAC2 has a dramatic effect as it leads to myelination failure and massive apoptosis, which results in the death of the mice about P17 (Jacob *et al*, 2011a).

HDAC2 promotes the transcription of genes involved in the myelination program, such as Sox-10, whose expression is induced by HDAC2 through deacetylating the p65 subunit in NF-κB, which then binds Sox-10 promoter and activates its transcription (Chen *et al*, 2011). HDAC2 is also

involved in Sox-10 dependent transcription of *Fabp7*, *P0* and *Krox-20*. In addition, both HDAC1 and 2 mediate *Krox20/Nab2* induced repression of the three inhibitors of myelination *Id2*, *Id4* and *Rad*. *Krox-20* associates with *Nab2* to repress transcription of the target genes through recruitment of the NuRD complex containing HDAC1 and HDAC2 (Jacob *et al*, 2011a).

HDAC1 promotes survival of Schwann cells during the first postnatal days through the repression of active beta-catenin (ABC), which is a downstream effector of the Wnt pathway. After P5, at the initiation of myelination, Sox-10 activates ABC, which has been shown to be essential in myelination timing (Jacob *et al*, 2011a).

Despite the different functions of HDAC1 and 2, with the more pro-survival effect of HDAC1 and the more pro-myelinating effect of HDAC2, the loss of one is compensated by the upregulation of the other, which takes over its role. Therefore, when Schwann cells are depleted for HDAC1 or HDAC2, their development is completely normal (Chen *et al*, 2011; Jacob *et al*, 2011a; Jacob *et al*, 2011b; Jacob *et al*, 2014).

HDACs could also be mediating cell cycle exit prior to myelination. In response to nerve growth factor induction, Schwann cell factor 1 (SC1), which is a p75 neurotrophin receptor interacting protein, translocates to the nucleus, binds to cyclin E promoter and recruits HDAC1, HDAC2 and HDAC3 to repress cyclin E transcription. This results in the arrest of proliferation (Jacob *et al*, 2011b).

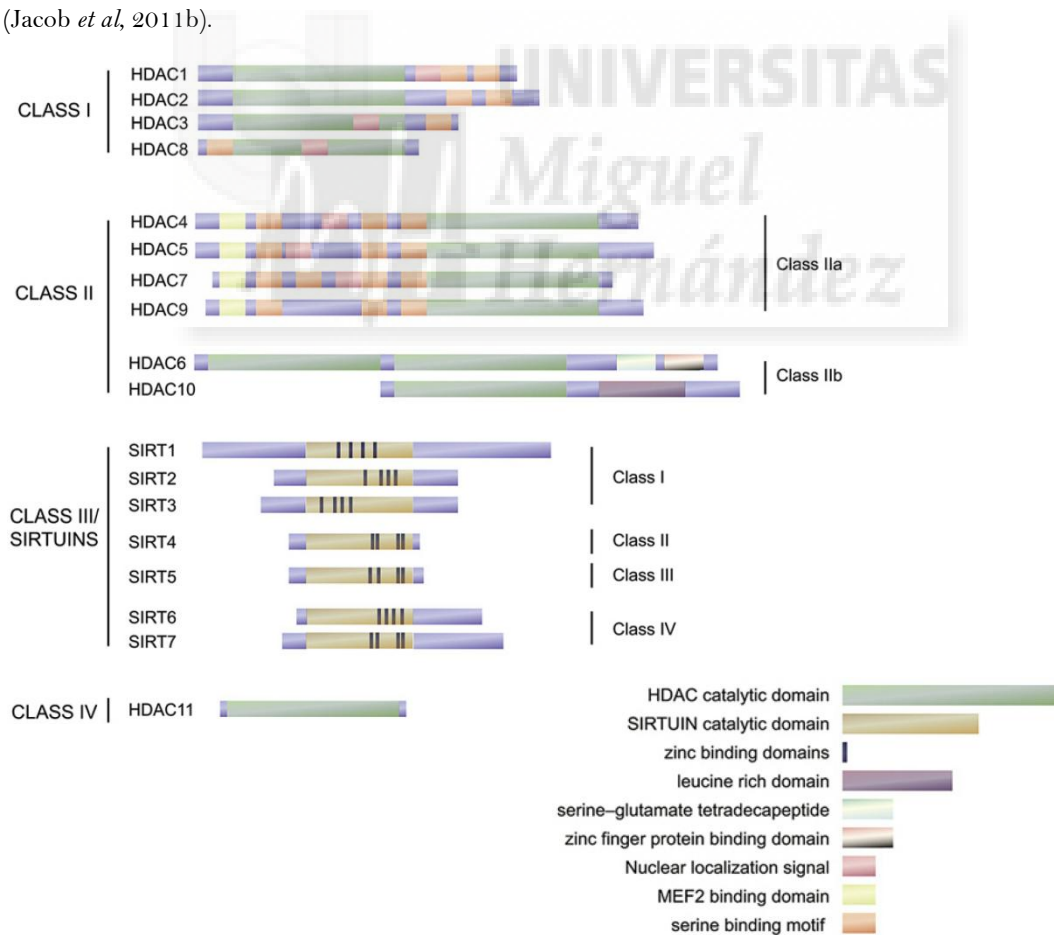


Figure 18.- Human HDACs superfamily. HDACs are grouped into four different classes according to the sequence similarity and homology to yeast proteins. Specific domains present in different members of each HDAC subfamily are presented in the illustrating cartoon (Barneda-Zahonero & Parra, 2012).

2. Schwann cell plasticity is pivotal for nerve repair

2.1 Post-injury Wallerian degeneration

Whereas in the CNS axons cannot regenerate upon an injury, peripheral nerves have the ability to regenerate after nerve damage sustained by crushing or transection. This is due to the combination of the activation of an intrinsic growth program in the neurons within the dorsal root ganglia (DRGs) and the formation of an appropriate environment in the distal stump that permits axon growth. The changes that occur in the distal stump after an injury are collectively referred to as Wallerian degeneration and consist of a number of events including axon death, blood-borne macrophage invasion, myelin clearance and Schwann cell transdifferentiation and proliferation. These processes permit the subsequent re-myelination of the axons and reinnervation of the target tissues, achieving functional recovery of the nerve within four or five weeks after transection (in rodents) [Reviewed in (Chen *et al.*, 2007)].

2.2 The Bungner repair cell

After injury, upon loss of axonal contact, both myelinating and non-myelinating Schwann cells experience a change of molecular expression that brings them back to a phenotypic state resembling that of the immature Schwann cell state. This includes the downregulation of genes involved in myelin formation such as MAG, P0, MBP and periaxin, and the upregulation of genes that characterize immature Schwann cells, such as L1, NCAM, p75^{NTR} and GFAP. However, denervated Schwann cells do not dedifferentiate to their immature state, since they possess properties not shared with immature Schwann cells (Jessen & Mirsky, 2008). Examples of this are the upregulation of N-cadherin and integrin $\alpha1\beta1$, and the downregulation of lipid antigen O4 (which is expressed both in immature and mature Schwann cells). Thus, on one hand denervated Schwann cells dedifferentiate, turning down expression of myelin proteins, but on the other hand they activate the expression of genes involved in the stimulation of axon growth, neuronal survival and macrophage recruitment. Additionally, they are able to adopt new functions, which will be subsequently explained. Recently, Arthur-Farraj and colleagues proposed that these changes occurring in Schwann cells upon nerve injury correspond with a transdifferentiation transition. They gave these newly found repair Schwann cells the name of “Bungner cells”, because they form the Bungner bands in the regenerating nerve (Arthur-Farraj *et al.*, 2012).

Bungner bands are regeneration tracks that provide a permissive substrate for the outgrowth of axons coming from the proximal stump as well as a structural guidance that directs them to re-innervate their correct targets. They are originated by denervated Schwann cells (Bungner cells) that proliferate and organize into a line of cells within their basal lamina, forming a structure of cellular columns that define basal laminar tubes (Vargas & Barres, 2007).

Bungner cells release a number of different chemokines and cytokines after injury, some of which are responsible for macrophage recruitment from the circulation into the degenerating nerve by 3 days post-axotomy (Shamash *et al.*, 2002). Bungner cells also acquire a new phagocytic activity that, together with the invading macrophages, is responsible for the myelin breakdown as well as for the clearance of its debris (Schafer *et al.*, 1996). The elimination of myelin debris is a very important function since neurite outgrowth is inhibited by molecules present in the myelin, constituting one of the major obstacles for CNS regeneration (Filbin, 2003).

A wide range of neurotrophic factors such as NGF, BDNF, GDNF, CNTF, LIF, IGF, FGF and osteonectin, together with their corresponding receptors, are expressed by Bungner cells, fibroblasts and macrophages in the distal stump. These factors play an essential role in promoting axonal growth and survival (Terenghi, 1999). In addition, recent studies are revealing new roles of these neurotrophic factors in nerve regeneration, such as promotion of re-myelination by BDNF and regulation of Schwann cell proliferation and re-differentiation by FGF. The post-injury upregulation of neurotrophic molecules and its receptors returns to basal levels once re-myelination of the regenerated nerve is completed [reviewed in (Chen *et al*, 2007)].

2.3 The repair phenotype is controlled by the c-Jun transcription factor

As previously described, the phenotypic transition from myelinating and Remak Schwann cells towards Bungner repair cells is essential for Wallerian degeneration and the posterior nerve regeneration. This transdifferentiation is a consequence of the huge plasticity that characterizes Schwann cells (Jessen & Mirsky, 2005). After a nerve injury, one of the early genes activated in the distal stump is the transcription factor c-Jun (Shy *et al*, 1996). This transcription factor has been shown to inhibit the myelinating phenotype of Schwann cells *in vitro* (Parkinson *et al*, 2008). More recently, Arthur-Farraj and colleagues used mice in which c-Jun was knocked out specifically in Schwann cells, to demonstrate that this transcription factor is responsible for the characteristic features in gene expression, function and structure of the repair Bungner cell (Arthur-Farraj *et al*, 2012).

c-Jun belongs to an extensive group of proteins which together are called AP-1. This comprises members of the Jun (c-Jun, JunB and JunD) and Fos family of proteins (c-Fos, FosB, Fra-1 and Fra-2). Jun proteins can form homodimers as well as heterodimers together with other Jun or Fos members to constitute transcriptionally active complexes. The members of the AP-1 transcription factor family have a high degree of homology in their sequence. All of them belong to the bZIP group of DNA binding transcription factors, which is characterized by a structure that contains a highly charged basic DNA binding domain followed by an amphipathic dimerization domain called the Leucine zipper domain (Mechta-Grigoriou *et al*, 2001).

Among the Jun protein family, c-Jun is the predominant isoform expressed in Schwann cells, being also the only one whose expression is modulated by forskolin, which is an adenylyl cyclase activator. In nerve development, the levels of c-Jun decrease at P5 and remain low in the mature myelinated nerve unless a nerve injury occurs. After a nerve lesion (either by transection or crushing damage), c-Jun expression is activated rapidly in the distal stump while the expression of myelin proteins decrease dramatically. In a crushed nerve, 12 days after the lesion, coinciding with the return of regenerating axons into the distal stump, c-Jun expression begins to fall while the expression of myelin proteins becomes activated again. (Shy *et al*, 1996).

In the nervous system, changes in the expression of c-Jun both at the transcriptional and posttranscriptional level occur under a number of conditions. One important posttranslational modification that regulates the activity of c-Jun is the Ser-63 and Ser-73 phosphorylation on the N-terminal transactivation domain. This phosphorylation is catalyzed by the c-Jun N-terminal kinases JNK1, JNK2 and JNK3 (also known as stress-activated protein kinases or SAPKs). JNKs, which belong to the group of mitogen-activated protein kinases (MAPKs), are mediators of stress-

response mechanisms such as proliferation, growth arrest and apoptosis. JNK docks to c-Jun and forms a relatively stable interaction. MAPK 7 phosphorylates and activates JNK, which leads to the phosphorylation of c-Jun. Phosphorylated c-Jun is a transcriptional activator of AP-1 promoters, which are promoters containing AP-1 sites, such as the c-Jun promoter itself. However, the phosphorylation of c-Jun is required for some but not all its functions. [reviewed in (Raivich & Behrens, 2006)].

It has been shown that the upregulation of c-Jun in Schwann cells in the distal stump after a nerve injury is essential for the repair functions that these cells display during Wallerian degeneration. The roles of c-Jun in Schwann cells in Wallerian degeneration have been studied in lesioned mice with c-Jun-depleted Schwann cells. These experiments showed that c-Jun controls the upregulation of genes for trophic support, such as BDNF and GDNF, as well as the downregulation of myelin genes such as P0, MBP and E-cadherin. Furthermore, c-Jun was also found to be essential for the proper formation of the bands of Bungner. In addition, reduced survival of sensory neurons and motoneurons was described in these KO mice, as well as a failure in target reinnervation. Altogether, this resulted in a failed functional recovery of these mice (Arthur-Farrar *et al*, 2012; Fontana *et al*, 2012).

2.4 Schwann cell proliferation after injury

After a transection of the nerve, Schwann cells lose their myelinating phenotype and start to proliferate. There is a peak of proliferation between day three and day eight posttransection, after which mitotic activity sharply declines (Stoll & Muller, 1999). A second proliferation peak takes place when the regenerating axons grow into the denervated distal stump (Pellegrino & Spencer, 1985). The neurotrophic factors FGF-2 (basic fibroblast growth factor-2) and GDNF (glial-cell-line-derived neurotrophic factor) are upregulated after nerve injury and have been suggested to promote Schwann cell proliferation and migration (Hoke *et al*, 2003; Jungnickel *et al*, 2006).

The mechanisms involved in Schwann cell proliferation during development and after injury are not identical. For instance, cyclin D1 is not essential for immature Schwann cell proliferation during development, since the loss of cyclin D1 can be compensated by other D-type cyclins. However, after injury, cyclin D1 translocates from the cytoplasm to the nucleus and is crucially involved in Schwann cell proliferation (Atanasoski *et al*, 2001; Kim *et al*, 2000).

Growth arrest of Schwann cells constitutes a prerequisite to initiate myelination in development and after injury. Exit from the cell cycle in Schwann cells depends on members of both Kip/Cip and Ink family of CDK inhibitors. p21, a member of Kip/Cip family of CDK inhibitors, has an inhibitory effect on Schwann cell proliferation. p21 exerts this inhibition both in development, when it becomes located in the cytoplasm of Schwann cells at about P7, as well as after injury, when it translocates to the nucleus of denervated Schwann cells. Also p16Ink4, a member of the Ink family of CDK inhibitors, was demonstrated to have a role in repressing Schwann cell proliferation during development and post-injury, although the effects post-injury are less prominent than those from p21 (Atanasoski *et al*, 2006). The nuclear protein Ski is also crucially involved in the regulation of Schwann cell growth arrest in development and after injury. Ski represses the TGF- β signaling pathway, a pathway that induces Schwann cell proliferation and inhibits myelination. Myelinating Schwann cells express Ski and, after injury, it becomes

downregulated when Schwann cell proliferation takes place. Subsequent Schwann cell growth arrest and myelination requires upregulation of Ski, which also induces the expression of p21 (Atanasoski *et al*, 2004).

3. Uncontrolled Schwann cell proliferation underlies PNS tumor development

3.1 Types of PNS tumours

Three different types of tumours can arise in the PNS: neurofibromas, schwannomas and malignant peripheral nerve sheath tumours (MPNSTs). Many of these tumors are associated with a group of genetic disorders named neurofibromatosis type 1 (NF1), neurofibromatosis type 2 (NF2) and schwannomatosis.

Schwannomatosis is a rare disease, characterized by the presence of multiple schwannomas throughout the PNS, with the exception of the vestibular organ. Schwannomas consists of benign tumours that arise from differentiated Schwann cells, remain encapsulated by an epineurium layer and grow eccentric to the underlying nerve. Schwann cells are the only cell type within these tumours. The formation of schwannomas is mainly sporadic, although there are cases of autosomal-dominant transmission. The aberrant proliferation of Schwann cells is due to mutations in tumour suppressor genes. It is often found that schwannomas have mutations that affect both NF2 and SMARCB1, a tumour suppressor gene located on chromosome 22, close to the NF2 gene (Koontz *et al*, 2013).

Neurofibromatosis type 2 is a dominantly inherited disorder with an incidence of 1:25.000, caused by mutations in the NF2 gene, which encodes for a cell-membrane protein named merlin. NF2 is characterized by the development of schwannomas, meningiomas and ependymomas, but the majority of affected patients present bilateral schwannomas in the superior vestibular branch of the eighth cranial nerve. This causes symptoms such as hearing loss, tinnitus or imbalance (Evans, 2009).

Neurofibromatosis type 1 is a dominantly inherited genetic disease, constituting the most common monogenetic disorder in humans with an incidence of 1:3.500. Patients are born with an heterozygous inactivation of the NF1 gene, which encodes for a protein named neurofibromin. This predisposes them to develop the illness. The main clinical manifestation consists of the development of benign peripheral nerve tumours, termed neurofibromas. Neurofibromas are mixed tumours composed of Schwann cells, perineural cells, fibroblasts and mast cells. There are two different types of neurofibromas: dermatofibromas and plexiform neurofibromas. Dermatofibromas are encapsulated masses that develop in the dermis or subcutaneously, and are rather harmless although they can be quite disfiguring. Plexiform neurofibromas are diffuse tumours that develop near the nerve roots and commonly entail clinical threats such as nerve dysfunctions and chronic pain. Ten percent of plexiform neurofibromas eventually progress into malignancy, giving rise to malignant peripheral nerve sheath tumours (MPNSTs), which are very aggressive and almost incurable.

Neurofibromas display an altered structure and composition compared to normal healthy nerves. There is a large increase in Schwann cell and fibroblast numbers as well as in collagen deposition. They also show extensive mast cell infiltration, and its perineurium is disorganized (Fig. I9).

Besides the formation of neurofibromas, neurofibromatosis is characterized by a number of clinical manifestations such as the presence of café au lait macules, Lisch nodules, optic gliomas, neoplasias of the haematopoietic system and learning disabilities (Cichowski & Jacks, 2001; McClatchey, 2007; Parrinello & Lloyd, 2009).

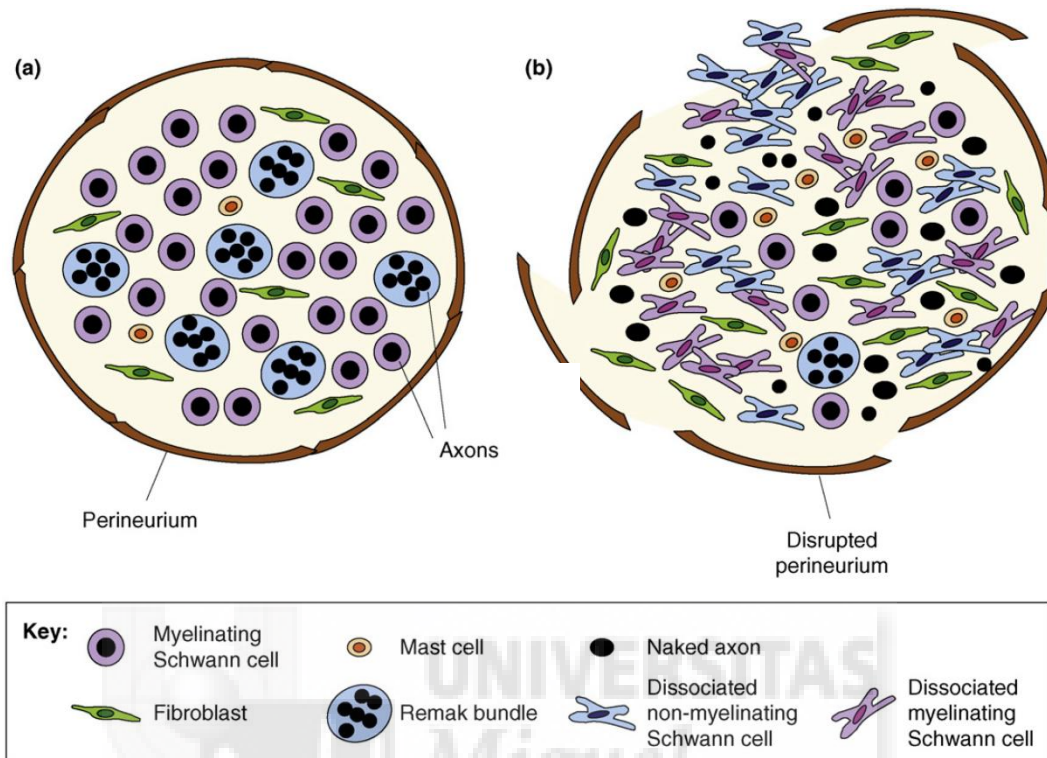


Figure 19.- Structure of normal nerves and neurofibromas. Diagram showing a cross-section of (A) a normal nerve fascicle and (B) the aberrant structure of nerve fascicle in neurofibromas (Parrinello and Lloyd, 2009).

3.2 Molecular mechanisms of neurofibroma development

Neurofibromas originate when Schwann cells undergo loss of heterozygosity (LHO) at the NF1 locus, due to somatic mutations in the inherited wild type allele. This results in the complete loss of neurofibromin in these cells. Neurofibromin is a large cytoplasmatic protein that shares a region of homology with the catalytic domains of the mammalian p120RasGAP protein. GAP or GTPase-activating proteins act by inhibiting small G proteins such as Ras. Neurofibromin functions as a tumour suppressor inactivating the RAS pathway by converting the active GTP-bound Ras form to the inactive Ras-GDP form (Martin *et al*, 1990).

Various groups have developed several NF1 mouse models in order to identify the origin of neurofibroma development among the Schwann cell lineage. Recent studies indicate that the LHO occurs at the embryonic E12-13 stage, among late Schwann cell precursors and early immature Schwann cells (Joseph *et al*, 2008; Wu *et al*, 2008; Zheng *et al*, 2008). In fact, the timing of neurofibromin inactivation seems to be a key point that determines neurofibroma formation.

Schwann cell precursors that experience a LHO, becoming *Nf1*^{-/-}, at first differentiate normally into myelinating and non myelinating Schwann cells, exhibiting only a subtle segregation defect as the Remak bundles present slightly more non-segregated axons. However, eventually, the Remak bundles become disrupted, and non-myelinating Schwann cells dissociate from the axons and proliferate, leading to neurofibroma formation. It has been shown that the

dissociation from the axons is due to the downregulation of a transmembrane protein expressed in the Schwann cells, called semaphoring 4F (Sema4F). This is caused by the overactivation of the RAS-RAF-ERK pathway (Parrinello *et al*, 2008).

It has been proposed that the *Nf1*^(+/-) microenvironment plays an essential role for neurofibroma formation and specifically the massive infiltration of *Nf1*^(+/-) mast cells could be crucial. The segregation of inflammatory cytokines by these cells may maintain the RAS pathway in an activated state, leading to low Sema4f expression, and also may promote proliferation of the Schwann cells that have lost axonal contact (Zhu *et al*, 2002).

4. The *NSE-SMDF*^(+/-) mouse

As aforementioned, there are two NRG1 type III described isoforms, NRG1 type III- β 1 and NRG1 type III- β 3. The first one described was NRG1 type III- β 3 and received the name of Sensory and Motor neuron Derived Factor (SMDF) (Ho *et al*, 1995). Since all functional studies to assess the role of NRG1 type III in myelination had been conducted with the β 1a isoform, the role of NRG1 type III- β 3 was unknown. This is why, in my laboratory, Gomez-Sanchez and colleagues generated a transgenic mouse that overexpresses the human SMDF under the neuronal enolase (NSE) promoter, which starts to be expressed at E18.

Although the nerves of *NSE-SMDF*^(+/-) mice did not display alterations in the myelin thickness of individual myelinated axons, the structure of their Remak Bundles was highly altered. In addition, there was an overproliferation of non-myelinating Schwann cells which, in combination with increased collagen accumulation in the endoneural matrix, lead to the formation of enlarged nerves with traits very similar to the neurofibromas in NF1 patients. Importantly, the abnormal increase of Schwann cell proliferation in these mice was limited to the first postnatal days and did not persist after P14 (Gomez-Sanchez *et al*, 2009).



UNIVERSITAS

OBJECTIVES

*Miguel
Hernández*

General objectives

Schwann cells have a distinct property in contrast to many mammalian cells, which is their high plasticity. This peculiarity is fundamental for their repair role after a lesion in the nerve, enabling nerve regeneration. In this thesis we intend to contribute in clarifying the molecular mechanisms underlying Schwann cell phenotype shifts between myelination, dedifferentiation and proliferation in development, after a nerve injury and in conditions of tumoral growth.

Specific objectives

- 1.- Further characterize the *NSE-SMDF^{+/+}* mouse by trying to understand the molecular mechanisms involved in the halt of Schwann cell overproliferation in the nerves of these mice.
- 2.- Find the molecular mechanisms that regulate Schwann cell proliferation after injury.
- 3.- Unveil the molecular pathways that control c-Jun re-expression and the transition of Schwann cells towards a repair phenotype after nerve injury.





MATERIALS AND METHODS

1. Mice

All animal work was conducted according to EU guidelines and with protocols approved by the 'Comité de Bioética y Bioseguridad del Instituto de Neurociencias de Alicante UMH-CSIC'.

Transgenic lines

NSE-hSMDF mice

Transgenic mice expressing the human SMDF driven by the NSE promoter were generated previously (Gomez-Sanchez *et al*, 2009). These mice have been characterized extensively in the lab of Hugo Cabedo. The mice used in all the experiments in this thesis come from the NSE-hSMDF#1 line, with 24 copies of the transgene, in a C57BJ6 background.

p53 Knock out mice

p53^{+/-} were obtained from The Jackson Laboratory (Stock Number 008652) (Jacks *et al*, 1994). Their breed is C57BJ6. They were crossed with *NSE-hSMDF^{+/-}* mice to obtain *NSE-hSMDF^{+/-};p53^{+/-}* mice.

Ink4a/Arf Knock out mice

Ink4a/Arf^{+/-} were provided by Dr M. Serrano (CNIO) (Serrano *et al*, 1996). Their breed is C57BJ6.

Genotyping protocol

10X TAE (1 litre): Trizma base 48 g (Sigma), EDTA 7.44 g (Panreac), glacial acetic acid 11.4ml (JK.Baker), distilled H₂O.

DNA extraction: When the mice were around twenty days of age, a piece of tail was cut. Samples were digested using HotShot reagent (25mM NaOH, 0.2mM disodium EDTA, pH12) for 30min at 95°C. Samples were then vortexed, neutralized with 40mM Tris-HCl and centrifuged at 12.000g for 7min. We transferred 50µl of the supernatant to a new tube and measured the DNA concentration using a NanoDrop (Thermo Scientific).

PCR master mix components (per PCR reaction): 1µl of dNTPs 10mM (Sigma) , 0,125µl of GoTaq Flexi DNA Polymerase (5U/µl, Promega), 5µl of 5X Green GoTaq Flexi Buffer (Promega), 2 µl of MgCl₂ 25mM (Promega), 2µl of each primer (diluted at 10ng/µl in H₂O), and milliQ H₂O

PCR: Polymerase Chain Reactions were performed for each sample using 100ng of DNA from the above extraction in a total reaction volume of 25µl. PCR was performed in a Mastercycler personal thermocycler (Eppendorf) . Specific conditions were used for each primer set (see bellow). 10µl of the PCR product was subjected to electrophoresis in 1% agarose gels (low agarose, AppliChem) containing ethidium bromide, immersed in 1x Tris Acetate EDTA (TAE) buffer. Samples were run alongside 5µl of 1kb DNA ladder.

Primers and protocols

NSE-hSMDF mice:

Sense GAGTCTGCAGTCCTCGACCT

Antisense GATGGGGACAATGCAGATTT

3 min at 94°C, 35 cycles (30 sec. at 94°C, 50 sec. at 62°C, 1 min. at 72°C)

Band at 355 bp

p53 KO mice

Sense(A) TGGTTTGTGCGTCTTAGAGACAGT

Sense(B) CCAGCTCATTCCTCCCACTCA

Antisense AAGGATAGGTCGGCGGTTTCAT

1 min at 94°C, 35 cycles (30sec at 94°C, 30 sec. at 60°C, 30 sec. at 72°C)

WT band – 480 bp

HO band – 330 bp

HE bands – 480bp and 330bp

Ink4a/Arf KO mice

WT-allele

Sense ATGATGATGGGCAACGTTC

Antisense CAAATATCGCACGATGTC

KO-allele

Sense CTATCAGGACATAGCGTTGG

Antisense AGTGAGAGTTTGGGGACAGAG

3 min at 94°C, 30 cycles (30sec at 94°C, 30 sec. at 60°C, 1 min. at 72°C)

WT band – 236 pb

KO band - 723 bp

2. Tissue culture techniques

Media components

Schwann cell: DMEM GlutaMAX (4.5g/l glucose) (Invitrogen) supplemented with 100U/ml penicillin, 100U/ml streptomycin and 10% bovine fetal serum.

Schwannoma RT4D6 complete medium: DMEM GlutaMAX (4.5g/l glucose) (Invitrogen) supplemented with 100U/ml penicillin, 100U/ml streptomycin and 5% bovine fetal serum.

Schwann cell expansion medium: DMEM GlutaMAX was enhanced with the following: 3% bovine fetal serum, 5 µM forskolin (Sigma), 10ng/ml rNRG1 (R&D Systems), 100U/ml penicillin, 100U/ml streptomycin.

Schwann cell SATO medium: 1:1 mixture of DMEM and Ham's F12 medium (Invitrogen) was supplemented with 5 µg/ml insulin (Sigma), 5µg/ml transferrin (Sigma), 0.1mM putrescine (Sigma), 2x10⁻⁸M progesterone (Sigma) and 3x10⁻⁸M sodium selenite (Sigma) [Taken from (Bottenstein & Sato, 1979)].

Nerve explants medium: DMEM GlutaMAX supplemented with 5% horse serum, 100U/ml penicillin, 100U/ml streptomycin.

Preparation of dishes and coverslips

All the procedures were under sterile conditions. Petri dishes and flasks were coated with Poly-L-Lysine (PLL) 0.01% solution (Sigma) and left for at least 30 minutes in the incubator. Afterwards, the PLL was removed and the dishes were washed three times with distilled water before Schwann cell plating.

12mm² coverslips were introduced in 24-well plates, coated with one drop of PLL (~150 µl) and left for at least 1 hour in the incubator. The PLL was then removed and the coverslips washed three times with distilled water. Afterwards, they were left in the hood to dry. Subsequently, the coverslips were covered with a drop of laminin (~100 µl) and left in the incubator for at least 30 minutes. The laminin was removed immediately prior plating the Schwann cells.

Laminin was purchased from Sigma and diluted to 20µg/ml in DMEM.

Rat Schwann cell culture protocol

All animal work was conducted according to EU guidelines and with protocols approved by the 'Comité de Bioética y Bioseguridad del Instituto de Neurociencias de Alicante UMH-CSIC'.

We used P1-P4 Wistar rat pups. The nerve extraction and cleaning was done using binoculars. Each rat was placed upside down and the sciatic nerves were extracted from just before reaching the DRGs until the knee area. Afterwards the rat was turned upside up to extract the brachial plexus nerves from ribs to wrist. During the extraction and cleaning, the nerves were introduced in a 35mm cell culture dish containing 2 ml of cold Leibovitz's F-15 medium (Invitrogen) placed on ice. After having extracted all the sciatic and brachial plexus nerves from the pups, we proceeded to clean up the nerves. This consisted on removing the blood and connective tissue that could be attached to the nerves as well as removing as much of the epineurium layer as possible. Once all the nerves were clean, we placed them in a new 35mm² cell culture dish containing DMEM with 1mg/ml of collagenase A (Roche). Subsequently they were grinded in very little pieces using a scalpel and left in the incubator for 2 hours. In the meanwhile we prepared 35mm² PLL coated cell culture dishes (We used approximately one dish for every one and a half pup used). After the 2 hours of collagenase incubation, the nerve pieces were homogenized using a 1ml pipette. We used Complete medium to stop the digestion reaction and poured the homogenate through a 40µm Falcon Cell Strainer (Fisher Scientific). We then centrifuged the homogenate at 210 g for 10 minutes at room temperature and resuspended the pellet in Complete medium supplemented with 10 µM of cytosine-β-D-arabino-furanoside (AraC) (Sigma), an antimetabolic, to prevent fibroblast growth. The resuspended cells were then introduced in the PLL-coated 35mm² cell culture dishes. After 72 hours, we removed the medium, washed once with DMEM and added Expansion medium to promote Schwann cell growth. After approximately 4 days, the Schwann cells were confluent in the dish.

Nerve explants

Sciatic nerves from adult mice (about one month old) were extracted and cut in 5 mm long pieces. We then carefully cleaned the pieces and completely removed the epineurium layer. During these steps, the nerves were kept in 35mm² cell culture dishes containing cold Leibovitz's F-15 medium and placed on ice. The nerve fragments were subsequently transferred to a 24 well plate containing nerve explant medium (plus the indicated pharmacological reagent or DMSO as control). Three to four nerve fragments were introduced in each well. As a control of intact nerve, the same number of nerve fragments were transferred to an eppendorf to be snap frozen. The nerve explants were incubated during four days. ¼ of the medium was refreshed after the first two days. The nerve explants were then snap frozen and later homogenized in RIPA buffer for protein extraction (following the protocol explained below).

Schwannoma RT4D6

RT4D6-P2T rat Schwannoma cells were obtained from Professor Dies Meijer, from the Centre for Neuroregeneration at the University of Edinburgh. The cells were grown in non-coated flasks with Complete medium.

3. Transfection

Constructs

pEGFP-N1: was from Clontech laboratories.

phJMJD3: was obtained from Addgene pCMV-HA-JMJD3 (addgene n° 24167).

phHDAC4-GFP: was provided by Professor Claudio Brancolini, from the Department of Medical and Biological Sciences at the University of Udine (Paroni *et al*, 2004).

phHDAC4ΔC-GFP: was generated from HDAC4-GFP by digesting it with XcmI Restriction Enzyme. This enzyme cleaved HDAC4-GFP at two sites, which released the C-terminal domain of HDAC4. The two ends generated in the vector were subsequently polished by T4 polymerase, before re-ligating with T4 DNA ligase. Competent *E. coli* were transformed with the generated plasmid. The correct sequence of the construct was confirmed by sequencing.

phHDAC4-GFP 3S/A: was provided by Professor Claudio Brancolini (Paroni *et al*, 2007)

phHDAC4-GFP 3S/A D934N: was generated by site directed mutagenesis following the protocol described in QuikChange Site-Directed Mutagenesis Kit (Stratagene). The HDAC4-GFP 3S/A plasmid was amplified by PCR using the following primers: 5'- GTG TCA TCA GGC TTC AAT GCC GTG GAG GGC -3' (forward); 5'- GCC CTC CAC GGC ATT GAA GCC TGA TGA CAC -3'(reverse). The change of this base pair (in red) caused the substitution of one aspartic acid for asparagine. Competent *E. coli* were transformed with the generated plasmid. The correct sequence of the construct was confirmed by sequencing.

HDAC4 shRNA: was obtained from Addgene pENTR/U6 HDAC4 shRNA (addgene n° 32220).

GFP shRNA: was obtained from Addgene pENTR/pTER shEGFP (addgene n°17470).

Plasmid purification was performed with the NucleoBond Xtra Midi kit (Macherey-Nagel), following the instructions of the kit.

Schwann cell transfection protocol

In order to maximize the transfection efficiency, we used fresh cells, this is: P0 Schwann cells cultured in a 35mm cell culture dish and expanded there (with no passages), or P0 Schwann cells that had been trypsinized and seeded into wells or coverslips.

To transfect P0 Schwann cells in 35mm cell culture dishes, we added 4µg of plasmid DNA and 5µl of Lipofectamine 2000 (Life Technologies) per dish. In an eppendorf, 4µg of plasmid DNA was mixed with 100µl of DMEM by pipetting up and down. In a different eppendorf, 5µl of Lipofectamine was mixed with 100µl of DMEM. These solutions were left for ten minutes before mixing them both together pipetting up and down. The mixture was left in the hood for 20 or 30 minutes before adding it to the cells (the cells were in 2ml of Expansion medium and we removed 200µl of this medium before adding the 200µl of the Lipofectamine-plasmid DNA mix). Then the cells were left in the incubator for five and a half hours. After this time, we removed the medium, washed the cells with DMEM once and added 2ml of fresh Expansion medium. If we needed to incubate the cells in serum free medium (such as SATO medium), we gave them some time (at least one night) to recuperate from the transfection in Expansion medium before adding the medium of interest.

When we wanted to have Schwann cells in several wells or coverslips transfected with the same plasmid, the best way was by transfecting the cells in the 35mm cell culture dish. After the five and a half hours of transfection, the cells were trypsinized using 200-250µl of trypsin which was subsequently deactivated with 1ml of Complete medium. After centrifuging the cells for 10minutes at 210g, we resuspended the pellet in Expansion medium and counted the cells. In order to seed the cells in several wells of a 24 well plate, for them to be confluent by next day, we put 250.000 cells per well in 500µl of Expansion medium. In order to seed the cells in several 12mm² coverslips placed in a 24 well plate, for them to be confluent by next day, we put 100.000 cells per coverslip in a ~100µl drop and left it overnight (or at least for 4 hours) before topping them up.

When we wanted to transfect the cells with several different plasmids, we first trypsinized the 35mm petridish containing P0 SC and seeded them in wells or coverslips in a 24 well plate (in the way explained previously). In order to make the transfection on the next day we put 100.000 cells per coverslip or 250.000 cells per well. In the transfection, for each one of the wells we mixed 1µg of plasmid DNA with 50µl of DMEM and separately 3µl of Lipofectamine with 50µl of DMEM. After 10 minutes we mixed them and waited for 20 or 30 minutes before adding the 100µl of the mixture to each of the wells, containing 400µl of Expansion medium.

4. Infection

Constructs

Lv HDAC4 shRNA: was generated by the Gateway technology, following the protocol described in BLOK-iT Lentiviral RNAi Expression System (Invitrogen). As Entry Construct, we used pENTR/U6 HDAC4 shRNA (addgene n° 32220), and as Destination Construct, pLenti CMV GFP

DEST (addgene n° 19732). A recombination reaction was performed between these two constructs using the Gateway LR Clonase II (Invitrogen) before transformation of *E. coli* and selection with ampicillin. The resulting Expression construct was used (15µg) to co-transfect HEK293T cells seeded in a 10cm² cell culture dish, in combination with the packaging vectors pVSV-G (3 µg) and pCMVΔ8.9 (20 µg), using 50µl of Lipofectamine and following the protocol described in (Campeau *et al*, 2009). 48 hours after the co-transfection, the HEK293T medium was collected, filtered and aliquoted.

Lv GFP control: was generated in the same way as explained above, but as Entry Construct we used pENTR/U6 (addgene 17387), and as Destination Construct pLenti CMV GFP DEST (addgene 19732).

Protocol

We infected Schwann cells that were confluent in 35mm² cell culture dishes. The culture medium was replaced completely by the collected HEK293T medium containing the viral particles. Schwann cells were incubated with this medium overnight. Afterwards, the cells were washed once and Expansion medium was added. Seven days after infection, the cells were trypsinized, seeded onto coverslips and left in SATO medium during 24 hours, before fixing them and performing immunofluorescence stainings (whose protocol is explained below).

5. β-Galactosidase Assay

Schwann cells that had being through 9 to 11 passages and Schwann cells with no passages (or maximum 1 passage) were seeded in 12mm² coverslips (50.000 cells per coverslip) in a 24 well-plate. The day after, we performed a β-galactosidase assay using the Senescence beta-Galactosidase Staining Kit Cell (Cell Signalling), following the instructions of the kit. Briefly, the cells were first washed with PBS, fixed with the Fixative solution (from the kit) for 15 minutes, followed by two washes with PBS. Subsequently 200µl of Staining solution (from the kit) was added to each well and the cells were incubated overnight in an oven at 37°C. Approximately 15 hours after, we took the plate out of the oven and fixed the cells with NN-dimethylformamide (DMF). Images were obtained with a Eclipse TE 2000-S (Nikon) fluorescence microscope (using the transmission light mode).

6. Luciferase Assay

Constructs

***c-jun* prom WT-luciferase:** (addgene n°11979)

***c-jun* prom ΔMEF2-luciferase** (addgene n°11980)

***c-jun* prom ΔATF-luciferase** (addgene n° 11980)

***c-jun* prom ΔATF/ ΔMEF2-luciferase** (addgene n°11982)

pRSV40-βGal (pSV-β-Galactosidase Control Vector, Promega)

Protocol

Schwann cells in a 24 well-plate were co-transfected with each of the luciferase reporter *c-jun* prom constructs together with a β -galactosidase reporter construct under the SV40 constitutive promoter (pRSV40- β Gal). The co-transfected cells were always in duplicate. The day after transfection, Expansion medium was substituted by SATO medium in which the cells were incubated during 24 hours. Subsequently we performed the luciferase activity determination assay. For this we used the Luciferase Assay System kit (Promega). First the cells were lysed in the wells using the Lysis solution from the kit. 5 μ l of each lysate was introduced in polypropylene tubes (Sarstedt), containing 50 μ l of Luciferase Assay Reagent (from the kit) and mixed immediately prior measuring the luciferase activity in a Single Tube Luminometer (Titertek Berthold). In order to normalize the assay, we used the Beta-Glo Assay System (Promega) which permits measuring β -galactosidase activity in a bioluminescent assay that couples β -galactosidase activity to a luciferase reaction. We used 2 μ l of each cell lysate and mixed it with 50 μ l of Beta-Glo Reagent (from the kit). These mixtures were incubated at room temperature before measuring the luciferase/ β -galactosidase activity.

Analysis

For each lysate, luciferase net activity was given by dividing the Luciferase Assay Reagent activity value by the Beta-Glo Reagent activity value. The average luciferase activity of the duplicates was used to compare between the different conditions. In each experiment, luciferase net activity values were converted to percentages relative to the value obtained from the *c-jun* prom WT.

7. Immunofluorescence

Antibodies

Antibody	Reference	Company	Species	Dilution	
				Immuno	Western
β -Actin (clone AC-15)	A5441	Sigma	Mouse		1:4000
c-Jun	9165	Cell Signaling	Rabbit	1:200	1:500
erbB2 (29D8)	2165	Cell Signaling	Rabbit		1:500
ErbB-3 (C-17)	sc-285	Santa Cruz	Rabbit		1:1000
GAPDH	G9545	Sigma	Rabbit		1:10.000
GFP	Ab13970	Abcam	Chicken	1:3000	
HDAC4	H0163	Sigma	Mouse	1:200	1:500
phospho-Histone H3	H 0412	Sigma	Rabbit	1:200	
IgG-ChIP Grade	ab27478	Abcam	Rabbit		
Jmjd3	ab38113	Abcam	Rabbit	1:100	1:500
Ki-67	Ab15580	Abcam	Rabbit		
Krox-20 (Egr2)	PRB-236P	ATOM	Rabbit	1:100	
MAG	SC-166849	Santa Cruz	Mouse		1:1000
MAPK (Erk1/2) p44/42	9102S	Cell Signalling	Rabbit		1:1000
Phospho MAPK p44/42 (Tyr202/204)	9101	Cell Signaling	Rabbit		1:1000
p14_Arf (4C6/4)	2407	Cell Signalling	Mouse	1:100	
p16 (F-12)	sc-1661	Santa Cruz	Mouse	1:100	
p16 (M-156)	sc-1207	Santa Cruz	Rabbit	1:100	1:100
p19_Arf (5-C3-1)	sc-32748	Santa Cruz	Rat	1:100	1:100
P0	PZ00308	Aves Lab	Chicken		1:1000
S-100 β	S 2644	Sigma	Rabbit	1:400	
Trimethyl-Histone H3 (Lys 27)	07-449	Millipore	Rabbit		1:3000
α -Tubulin	ab4074	Abcam	Rabbit		1:2000
Anti-rabbit biotinylated	711-065-152	Jackson	Donkey	1:600	
cy2 streptavidin	PA42001	GE Healthcare		1:500	

Table 1. List of antibodies used.

Protocol for immunofluorescence staining of cells

Blocking solution: 1XPBS with 10% horse serum and 0,1% triton.

The cells needed to be in coverslips. To fix them, the medium was removed and the cells were incubated in 4% paraformaldehyde for 10 minutes at room temperature, and subsequently the cells were washed three or four times with 1XPBS. Afterwards we placed the coverslips in hand-made pedestals and incubated the cells during one hour with blocking solution (50 μ l per coverslip). The blocking solution was then substituted by 50 μ l of blocking solution containing the antibody of interest. The cells were incubated with the primary antibody at 4°C overnight. On the next day we removed the primary antibody, rinsed the coverslips multiple times immersing them in several 50ml Falcon tubes containing 1X PBS (we used 6 Falcon and did 6 immersions in each Falcon). The cells were subsequently incubated with the appropriate fluorescent secondary antibodies (AlexaFluor 594 anti-mouse, AlexaFluor 488 anti-rabbit and anti-chicken, AlexaFluor 555 anti-rat 1:1000; Invitrogen) for one hour at room temperature. Nuclei were counterstained with

bisbenzimidazole (Hoechst nuclear stain) diluted together with the secondary antibodies in blocking solution. After incubating for one hour at room temperature, we removed the secondary antibody, rinsed the coverslips in 1XPBS in the same way as before and mounted them on slides using a drop of Fluoromount-G mounting solution (Southern Biotech) for each coverslip. Images were obtained with a Eclipse TE 2000-S (Nikon) fluorescence microscope.

Analysis: In the experiments to see the nuclear translocation of HDAC4-GFP in Schwann cells, we obtained an average of 10 images in different zones in each coverslip. To analyze the images we used Metamorph Microscopy Automation and Image Analysis Software. For each transfected (green) cell we quantified the average fluorescence intensity in the regions of interest (ROI) in the nucleus and the cytoplasm (thus, we draw a circle in the nucleus and in the cytoplasm, and measured the average of intensity in both of them). We defined the localization of HDAC4 by the nucleo/cytoplasmic ratio of intensities. In the experiments to quantify the levels of nuclear c-Jun in Schwann cells, from each coverslip we obtained a number of non-overlapping images covering approximately the totality of the coverslip. For the analysis we used Metamorph Microscopy Automation and Image Analysis Software. To measure the intensity of nuclear c-Jun, for every transfected (green) cell we quantified the average anti c-Jun fluorescence intensity in the ROI in the nucleus and cytoplasm. We then subtracted the average intensity in the cytoplasm to the average intensity in the nucleus. This quantification was also performed in non-transfected cells in the same coverslip (same numbers as the number of transfected cells). In each experiment, the average nuclear c-Jun intensity in the totality of non-transfected cells quantified for each condition was normalized to one, and the average nuclear c-Jun intensity of the transfected cells was expressed as a fraction relative to the non-transfected cells.

Protocol for immunofluorescence staining of mice sciatic nerves and tumours

For sciatic nerve extraction, after sacrificing the mice with CO₂, they were placed upside down and both sciatic nerves were exposed and carefully removed, cutting them in the knee area and as close to the DRGs as possible.

The development of a malignant tumour in a mouse was suspected when observing clear neurological deficits in the behaviour of the mouse, usually limping, or upon observation of a protuberance that emerged commonly on the back in the neck area. In these cases we proceeded to the identification and extraction of the tumoral mass, after sacrificing the mouse by CO₂. If a clear protuberance was observed, we dissected the tumour located below that area. If the location of the tumour was not obvious, we carefully exposed the DRGs and nerve roots successively, starting from most anterior ones, until we localized the nerve root in which the tumour had developed. We then carefully extracted the tumoural mass.

After the extraction of sciatic nerves or tumours, the tissue was embedded them in OCT (TissueTek; Sakura) in little molds, straighten and frozen at -80°C. We then cut the blocks in a cryostat, either longitudinally or transversally in 10µm sections. To begin with the immunostaining, we fixed the sections with 4% paraformaldehyde during 10 minutes at room temperature. We then blocked the sections with blocking solution during at least one hour at room temperature, before adding the primary antibodies, which were diluted in blocking solution. After

an overnight incubation at 4°C, we removed the primary antibody solution and washed the slides with 1XPBS three times for five minutes. The sections were subsequently incubated with the appropriate fluorescent secondary antibodies diluted 1:1000 in blocking solution. Afterwards the sections were washed three times in 1X PBS during 5 minutes and one time in Hoescht diluted 1:1000 in 1XPBS, before mounting them in Fluoromount G. Images were obtained using a confocal ultraspectral microscope (Leica TCS SP2).

For Ki67 staining, after incubation with the primary rabbit anti-Ki67 antibody, sections were incubated with anti-rabbit biotinylated antibody for two hours, followed by one hour incubation with cy2 streptavidin.

Analysis: After immunofluorescence staining of mice nerve sections, we obtained 7 to 9 images of each nerve sample with the confocal microscope. We counted the number of cells immunopositive for a particular marker and divided it by the number of nuclei (stained with Hoestch).

Protocol for immunofluorescence staining of human tissues

Blocking solution: PBS1X plus 0,075% triton plus 10% horse serum.

PBS-t: PBS1X plus 0,075% triton.

All the procedures were performed according to the EU guidelines. Patients were diagnosed according to the accepted standard NF1 diagnostic criteria. They were informed about the study, and consent was obtained from all them. Neurofibromas were obtained from 6 patients after surgery. Adult human healthy peripheral nerves were obtained from diagnostic biopsies. In a paraffin microtome, the paraffin blocks containing the human tissues were cut in 10µm sections. The sections were then de-parafinated: firstly they were incubated in an oven at 62 degrees for 20 minutes, this was followed by two and a half hours in xylene (refreshing the xylene every 30 minutes). Sections were subsequently submitted to a serial incubation in ethanol 100-95-70% (seven minutes in each ethanol solution) and finally the slides were left in distilled water for seven more minutes. Afterwards the sections were submitted to antigen retrieval by using the citrate method: this consisted on boiling the slides while they were immersed in a sodium citrate solution composed by 450ml distilled water plus 50ml sodium citrate 0,1M pH6. For the boiling process, we used a microwave at 750 w where we heated the slides four times four minutes each time. We then slowly displaced the hot citrate solution with room temperature distilled water. After three washes with PBS-t (seven minutes each wash), the sections were incubated with blocking solution for one hour. Subsequently the primary antibody was added and left at 4°C for approximately 40 hours. After that time, the sections were washed six times in PBS-t (seven minutes each time). The secondary antibody was then added and left at room temperature for one hour. The sections were subsequently washed with PBS-t two times (seven minutes each time), followed by an incubation during 10 minutes in PBS-t plus Hoescht and two more washes with PBS-t. The slides were then mounted using fluoromount. Images were obtained using a confocal ultraspectral microscope (Leica TCS SP2).

8. Western Blot

Buffers composition

Protease and phosphatase inhibitors concentrated cocktail (x40): One Complete Mini tablet (Roche) and one PhosphoSTOP tablet (Roche) diluted in 500µl of milliQ water.

RIPA buffer plus inhibitors: PBS pH 7.4, 0.1% SDS, 1% Nonidet P-40, 0.5% sodiumdeoxycolate, 5mM EGTA, 1:40 protease and phosphatase inhibitors concentrated (x40) cocktail.

Laemmli sample buffer (5x): 60mM Tris-HCl pH 6.8, 2% SDS, 10% glycerol, 5% 2-βmercaptoethanol, 0.01% bromophenol blue.

Acrilamide resolving gel buffer (7.5% acrilamide): 375mM Tris-HCl pH 8.8, 7.5% acrilamide solution (30%acrilamide, 0.8% bis-acrilamide) (Sigma), 0.1% SDS, 1:50 of ammonium persulfate solution 10% (in water), 1:500 of TEMED (Sigma).

Acrilamide stacking gel buffer: 130mM Tris-HCl pH 6.8, 4% acrilamide solution (30%acrilamide, 0.8% bis-acrilamide), 0.1% SDS, 1:50 of ammonium persulfate solution 10% (in water), 1:500 of TEMED.

Running buffer: 25mM Tris-base, 192mM glycine, 1% SDS.

Transfer buffer: 25mM Tris-base, 192mM glycine.

TBS buffer (pH 7.6): 20mM Tris-base, 137mM NaCl.

TBS-t: TBS, 1% Tween 20 (Sigma).

Blocking solution: TBS, 5% powder skimmed milk.

Protein extraction

From mice tissue

For the extraction of protein from mice sciatic nerves or tumours, after dissection the tissue was rapidly frozen at -80°C. To start with the protein extraction we first grinded the tissue in the desired volume of RIPA buffer (~100µl) using a glass tissue homogenizer (1ml capacity, GPE Scientific Limited), this was done at 4°C. The homogenate was transferred to a new tube and then sonicated (10 minutes of 30sec ON and 30sec OFF) at High Power in a Bioruptor (Diagenode) and centrifuged at 12.000g at 4°C during 15 minutes. The supernatant was then transferred to a new tube and the protein concentration was measured using the BCA method, following the instructions of the kit (Pierce).

From cells

In order to extract protein from cultured cells, we trypsinized them and kept the cell pellets frozen at -80°C. On the day that we wanted to do the Western Blot, the cell pellets were resuspended in RIPA buffer and the protein was extracted following the protocol described above.

SDS-PAGE and Immunoblotting

The protein samples were mixed with Laemmli sample buffer, boiled at 95°C during 5 minutes and loaded in an acrilamide gel. The electrophoresis was run at 140 V in running buffer, letting the protein samples migrate and separate according to size. Proteins were then transferred from the gel to a Protran nitrocellulose membrane (Whatman) during 2 hours at 4°C in transfer buffer. Subsequently the membrane was blocked in blocking solution during one hour at room

temperature in a shaker. Afterwards the membrane was incubated overnight at 4°C with blocking solution containing the indicated primary antibody. The next day, the membrane was washed three times (ten minutes each time) with TBS-t in a shaker. The secondary antibodies, which were conjugated with horseradish peroxidase (Sigma), were diluted 1:2000 in blocking solution and added to the membrane. After one hour incubation at room temperature, the membrane was washed again three times with TBS-t. Finally, the membrane was incubated with ECL plus (Amersham), during 5 minutes in darkness. The membrane was then exposed using a Bioimager (Fujifilm).

9. Electron Microscopy

For ultra-structural images of sciatic nerves and malignant tumours, the mice were profoundly anesthetized by intraperitoneal injection of 40 mg/kg ketamine and 30 mg/kg xylazine and then intracardially perfused with 2% paraformaldehyde, 2.5% glutaraldehyde, and 0.1 M phosphate buffer (pH7.4). Tissues were dissected and immersed in the same fixative solution at 4°C overnight. They were then washed 4 times in PBS (30 min. each time) and post-fixed in 2% osmium tetroxide for 2 hours. After 4 more washes with PBS (15 min. each), the samples were dehydrated in graded ethanol series (50-70-95-100%, 10 min. each), then immersed in propylene acid, and finally embedded in epoxyresin (Durcupan). Semi-thin sections were cut with a glass knife at 1–3 µm and stained with toluidine blue to check the quality of the tissue before the EM studies. For EM, ultrathin sections (70–90 nm) were cut on an ultramicrotome (Reichert Ultracut E; Leica) and collected on 200-mesh nickel grids. Staining was performed on drops of 1% aqueous uranyl acetate, followed by Reynolds's lead citrate. Ultra-structural analyses were performed in a Philips TECNAI 12 electron microscope.

10. Real Time quantitative PCR (RT-qPCR)

Primer sequences

Primer	Accession		Sequence (5' → 3')
c-Jun	NM_010591	Sense	TGGGCACATCACCCTACAC
		Antisense	AGTTGCTGAGGTTGGCGTA
cyclinD1	NM_007631.2	Sense	AACTCCTCTCCTGCTACCG
		Antisense	CAGGAACAGATTGAAGCCC
GAPDH	GU214026.1	Sense	TGCACCACCAACTGCTTAGC
		Antisense	GGCATGGACTGTGGTCATGAG
HDAC4	NM_207225.1	Sense	GCCATCTGTGATGCTTCTGA
		Antisense	ATTGGCATTGGGTCTCTGAT
MEF2-A	NM_001014035.1	Sense	AAAAGCAGGAACAAGAAAG
		Antisense	GTGCAAACAGTTATGTGTG
MEF2-B	NM_001017507.1	Sense	AAAAATCCAGATCTCACGC
		Antisense	AACTCGTAAGCTTTCTTCATC
MEF2-C	NM_001170537.1	Sense	AAAAAGATTGAGATCACGAGG
		Antisense	CATAAGCCTTCTTCATCAGTC
MEF2-D	NM_030860.2	Sense	ATCATTGGAACAATGCCAG
		Antisense	GCTGGTAATCTGTGTTGTAG
JMJD3	NM_001017426	Sense	CTCTGGAACCTTCATGCCGG
		Antisense	CTTAGCCCCATAGTTCCGTTTG
SREBP2	AF374267	Sense	AAGTCTGGCGTTCTGAGGAA
		Antisense	CCAGGAAGGTGAGGACACAT
18S	NR_003278	Sense	CGGCTACCACATCCAAGGAA
		Antisense	GCTGGAATTACCGCGGCT
p16Ink4a	NM_001040654	Sense	TACCCCGATTCAGGTGAT
		Antisense	TTGAGCAGAAGAGCTGCTACGT
p19Arf	NM_009877	Sense	GCCGCACCGGAATCCT
		Antisense	TTGAGCAGAAGAGCTGCTACGT
p19Arf (Chip)	p19_Arf promoter	Sense	GACCGTGAAGCCGACCCCTTCAGC
		Antisense	GGGGTCGCTTTCCCTTCGG
p16Ink4a (Chip)	p16_Ink4b promoter	Sense	GATGGAGCCCGACTACAGAAG
		Antisense	CTGTTTCAACGCCAGCTCTC
p14Arf	NM-000077	Sense	CCCTCGTGCTGATGCTACTG
		Antisense	CATCATGACCTGGTCTTCTAGGAA
Human p16Ink4a	NM_000077	Sense	GGGGGCACCAGAGGCAGT
		Antisense	GGTTGTGGCGGGGCAGTT

Table 2. Overview of all primers used for the experiments.

RNA Extraction

From mice tissue:

Sciatic nerves or tumours were extracted from the mice and rapidly frozen at -80°C . To start with the RNA extraction, we first grinded the tissue in $200\mu\text{l}$ of TRIzol Reagent (Life Technologies) using glass tissue homogenizers (1ml capacity, GPE Scientific Limited) previously sterilized with chloroform. Afterwards $50\mu\text{l}$ of isoamyl chloroform was added to each sample. We then vortexed them during 30 seconds and left them sit at room temperature for 5 minutes. Afterwards, the samples were centrifuged at $12000g$ at 4°C for 15 minutes. The top clear phase that appeared was collected in a new tube. We then added 0,53 parts of absolute ethanol and finger-mixed it. The samples were then poured into RNA extraction columns (PureLink RNA Mini Kit, Ambion). For the RNA purification we followed the kit manufacturer instructions, eventually eluting the RNA in $32\mu\text{l}$ of RNase free water.

From cells:

We trypsinized the cells and pelleted them centrifuging at $210g$ at 4°C for 10 minutes. After taking out the supernatant, we quickly froze the cell pellet at -80°C . For the RNA extraction, we added $200\mu\text{l}$ of TRIzol Reagent to the cell pellet and homogenized it pipetting up and down. Afterwards we added $50\mu\text{l}$ of chloroform isoamyl alcohol and followed the same protocol as previously explained for the RNA extraction from sciatic nerves.

cDNA Synthesis

First the purified RNA was digested with RNase Free DNase I (Fermentas) to get rid of genomic DNA. For this purpose we measured the RNA concentration in a Nanodrop. For each $1\mu\text{g}$ of RNA, $1\mu\text{l}$ of DNase I was needed. We used $3,5\mu\text{l}$ of Dnase I and $3,5\mu\text{l}$ of MgCl_2 plus-DNase buffer (Fermentas) and mixed it with the purified RNA, obtaining a final volume of $28\mu\text{l}$ (RNase free water was added if needed to equalize the total RNA quantity in all the samples). The Dnase I digestion took place at 37°C for 30 minutes. Afterwards, in order to inactivate the DNase I, we added $3,5\mu\text{l}$ of EDTA $25\mu\text{M}$ (Applichem) and placed the tubes at 65°C for 10 minutes.

From each purified and digested RNA sample, we used $10\mu\text{l}$ for cDNA synthesis and $10\mu\text{l}$ to obtain a negative control of the retrotranscription reaction. We first added $1\mu\text{l}$ of Random Primers (Invitrogen) and $1\mu\text{l}$ of dNTPs 10mM (Sigma) to each tube containing $10\mu\text{l}$ of RNA. We mixed it and incubated it at 65°C for 5 minutes, placing it on ice immediately after. We left it for approximately 5 minutes to cool off in the ice and then we added $2\mu\text{l}$ of DTT (Invitrogen), $2\mu\text{l}$ of 5x First Strand Buffer (Invitrogen) and $1\mu\text{l}$ of RnaseOUT Recombinant Ribonuclease Inhibitor (Invitrogen). We mixed it and incubated it for 3 minutes at room temperature. We then added $1\mu\text{l}$ of SuperScript II Reverse Transcriptase (Invitrogen) and $2\mu\text{l}$ of 5x First Strand Buffer (Invitrogen). For the negative control samples, $3\mu\text{l}$ of 5x First Strand Buffer was added instead of the Reverse Transcriptase. We mixed it and left it for 10 minutes at room temperature. Afterwards the samples were incubated at 42°C for one hour, followed by 15 minutes at 70°C . The cDNA obtained was ready to be used for Real Time qPCR.

Real Time qPCR Protocol

We used the Applied Biosystems 7500 Real Time PCR System and Platinum SYBR_Green qPCR SupermixUDG (Invitrogen). To avoid genomic amplification, PCR primers were designed to fall into separate exons flanking a large intron when possible. Reactions were performed in duplicates of three different dilutions, and threshold cycle values were normalized to the housekeeping genes (ribosomal 18S if we used cDNA from sciatic nerves, and GAPDH if the cDNA was obtained from cultured Schwann cells). The qPCR conditions were: 5 min at 50°C, 5 min at 94°C, 40 cycles (30sec at 95°C, 32 sec. at 60°C, 32 sec. at 72°C), melting curve.

The specificity of the products was determined by melting curve analysis and gel electrophoresis. The ratio of the expression of each gene relative to the housekeeping was calculated by using the 2^{-CT} formula ($2^{-(\text{gene CT} - \text{housekeeping CT})}$).

11. Chromatin Immunoprecipitation (ChIP) assay**Buffer Components**

Buffer A: 150mM NaCl, 10% glycerol, 0,3% triton, 50mM Tris-HCl pH8, protease and phosphatase inhibitors

Low salt buffer: 0,1%SDS, 1% Triton, 2mM EDTA, 20mM Tris-HCl pH 8.1, 150mM NaCl, phosphatase and protease inhibitors.

High salt buffer: 500mM NaCl, 0,1%SDS, 1% Triton, 2mM EDTA, 20mM Tris pH 8.1, 150mM NaCl, phosphatase and protease inhibitors.

LiCl buffer: 0,25M LiCl, 1% IGEPAL, 1% sodium deoxycholate, 1mM EDTA, 10mM Tris pH8.1, phosphatase and protease inhibitors.

TE buffer: 10 μ M TrisHCl, 1mM EDTA pH 8.

Elution buffer: 1%SDS, 0.1M NaHCO₃, 200 mM NaCl.

ChIP protocol

Sciatic nerves from seven P20 wild type and seven P20 transgenic mice were extracted, after sacrificing the animals with CO₂. While extracting the nerves from all the animals, they were placed in two 35mm cell culture dishes with 1% PFA in PBS. The nerves were then chopped with a scalpel in very little pieces and placed in a 2ml tubes containing 1% PFA. They were subsequently left in rotation for 25 minutes at room temperature. We then centrifuged them for 3 minutes at 1000g and discarded the supernatant. We added PBS1X and centrifuged again at 1000g for 3 minutes. The samples were resuspended in 1.2 ml of buffer A. Chromatin was then clarified by centrifugation at 21.000g for 30 min at 4°C. We collected the supernatant and quantified the protein using the BCA method (Pierce). We saved an aliquot containing 30 μ g of protein and labeled it as input. We also used an aliquot with 10 μ g for phenol/chloroform extraction to check the DNA shearing in an agarose gel. At this point, all samples could be frozen at -80°C.

The volume corresponding to 300 μ g of protein was incubated with the indicated antibody (and a non specific IgG of the same species for the negative control). For the amount of antibody, we followed the suggested protocol for IP in the antibody information sheet (~2 μ g). The mixture was left overnight at 4°C in rotation to form immunocomplexes. We then proceeded to prepare the

Sepharose protein A slurry: Sepharose protein A resin (Cl-4B GE Healthcare) was resuspended in distilled water (200 μ l H₂O/ mg powder). The powder was left to sink to the bottom by gravity or light centrifugation (<500g). The H₂O was changed the three times. In the last change, the pellet was resuspended in H₂O containing 0,5mg/ml of bovine albumine (Sigma) and 0,2mg /ml of DNA from sonicated herring sperm (Sigma). The powder was left to sink again and the volume was adjusted in order to have 70% of the total volume of the slurry occupied by the powder. This Sepharose protein A slurry was kept at 4°C. We added 40 μ l of this Sepharose slurry to each immunocomplex. They were then incubated for an hour at 4°C in rotation, centrifuged at 500g for 3min at 4°C, and washed two times with 1ml of Low Salt Buffer at 4°C. Subsequently they were washed once with 1ml of High Salt Buffer and then washed three times with 1ml of LiCl buffer, at 4°C, followed by two washes with 1ml TE buffer. Chromatin from immunocomplexes and input was eluted with 300 ml of Elution buffer and incubated at 65°C for 6 h (to break the DNA-protein complexes). DNA was purified using a column purification kit (GE healthcare) and submitted to SYBR green Real Time qPCR with the indicated primers.

12. In Vivo Nerve Injury

All the procedures were performed following the European Union guidelines. For nerve transection experiments, twenty days old C57BL/6J mice were anaesthetized deeply with 2.5% isoflurane and the sciatic nerve was exposed. After exposition, the sciatic nerve was sutured with surgical 8-0 nylon monofilament (Ethicon) and cut in the sciatic notch. In one group of mice, instead of cut, the nerves were crushed with forceps twice during 15 seconds. Muscle and skin wounds were sutured and mice were left to recover in a heated box. Mice were then provided with analgesia by intraperitoneal injection of saline (0.9mg/ml NaCl) containing buprenorphine (0.05mg/kg). 4, 12 or 24 days after surgery, transected and contra lateral nerves were collected and processed for immunofluorescence staining (following the protocol described above).



RESULTS

1. Control of Schwann cell proliferation in pathological conditions

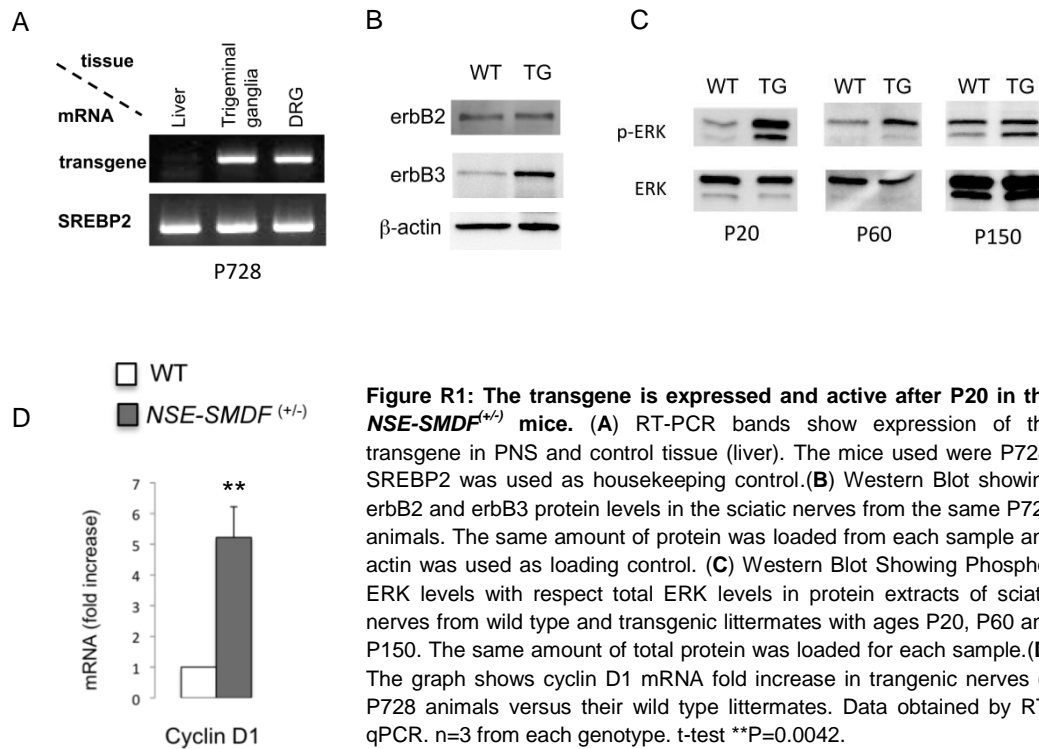
1.1 Schwann cell proliferation is halted in neurofibromas from adult *NSE-SMDF*^{+/+} mutant mice

Previously, our laboratory generated and partially characterized a transgenic mouse that over-expresses the SMDF neuregulin isoform in axons (Gomez-Sanchez *et al*, 2009). The nerves as well as the dorsal root ganglia of these mice are abnormally enlarged. Gomez-Sanchez and colleagues demonstrated that there is an overproliferation of Schwann cells in early postnatal stages in these mice, which gives rise to the formation of enlarged nerves with features very similar to the plexiform neurofibromas from human that are affected with Neurofibromatosis type I (NF1). Strikingly, the overproliferation of Schwann cells in these transgenic mice stops around the age of P14. From this moment on, the difference in cell numbers between wild type and transgenic mice remains stable, being 3 fold bigger in the transgenic nerves.

We first thought that the expression of the NSE-SMDF transgene might decrease in the mice with time. To check the expression of the transgene, we performed RT-PCR, with specific primers, of sciatic nerve and control tissue. Figure R1A shows that the transgene is still expressed in the PNS of two year old transgenic mice, ruling out this possibility. Secondly, there could be less expression of the NRG1 receptors, erbB2 and erbB3, in the transgenic mice, compensating for the increase of NRG1. However, in the Western Blot data, shown in figure R1B, we can observe that the levels of these receptors were not decreased in the transgenic mouse. Furthermore, the levels of erbB3 receptor were increased. In order to study the functionality of the signalling pathways activated by the transgene, we decided to explore the activation/phosphorylation status of the ERK pathway, which mediates Schwann cell proliferation in response to neuregulin 1 (Birchmeier & Nave, 2008). Figure R1C shows that the active, phosphorylated form of ERK is increased in the transgenic animals.

It has been described that neuregulin induced proliferation of breast cancer cells is dependent on the activation of *cyclin D1* gene expression (Yang *et al*, 2008). Cyclin D1 also mediates proliferation of Schwann cells *in vitro* in response to NRG1 (Kim *et al*, 2000). Moreover, *in vivo* data shows that, after an injury in the nerve, there is an increase of Cyclin D1 in the mature Schwann cells, which in association with its catalytic partners CDK4 and CDK6 is fundamental for the regulation of the G1/S transition that leads to proliferation (Atanasoski *et al*, 2001). We therefore wondered if the halt in the proliferation in the *NSE-SMDF*^{+/+} nerves was due to the downregulation of cyclin D1, but an RT-qPCR with tissue of transgenic sciatic nerves ruled out this possibility, since the expression levels of *cyclinD1* in the mutant nerves are, in contrast to our prediction, actually increased by 5 fold with respect to their wild type littermates (Figure R1D).

Taken together, these data show that there is a sudden halt in the proliferation of the Schwann cells in the nerves of the transgenic *NSE-SMDF*^{+/+} mice, and occurs even though the mitogenic stimulus persists.



1.2 Proliferation of Schwann cells is restricted by the activation of the replicative senescence programme in the *NSE-SMDF*^(+/+) neurofibromas

The introduction of mutated variants of the *HRas* gene into mammalian cell lines can transform them into tumoral cells. However, their introduction into normal primary mammalian cell cultures induces a stop in proliferation after a few cycles, due to the activation of a protection mechanism against oncogenic insult, called OIS (Oncogene Induced Senescence) (Serrano *et al*, 1997). This causes them to enter into cell cycle arrest and adopt a number of phenotypic features characteristic of senescent-like cells. The OIS program is induced by activation of the RAS-RAF-ERK pathway. As we have shown previously, ERK is activated in the nerves of the mutant mice, even though proliferation has halted. Furthermore, there is compelling evidence, resulting from many different studies, that associates the benign nature of tumours with the abundance of senescent cells within them (Collado *et al*, 2007). Briefly, senescent cells have been found in prostate benign tumours in mice lacking the tumour suppressor PTEN (Chen *et al*, 2005), and in human, the presence of senescent cells has been detected in benign lesions in the skin with a mutated oncogene BRAF (Michaloglou *et al*, 2005). In the light of these data, we decided to explore the possibility of OIS program activation in the Schwann cells of the neurofibromas developed by *NSE-SMDF*^(+/+) transgenic mice.

We first observed that after serial cultivation of primary rat Schwann cells, the cells stopped proliferating and acquired a very characteristic phenotype. They became larger, flat and amorphous. This sort of phenotype has been described in previous studies for cells undergoing replicative senescence (Serrano *et al*, 1997). A biomarker that has been commonly used to detect senescent cells is the induction of endogenous SA- β -GAL activity in their lysosomes (Debacq-

Chainiaux *et al*, 2009; Dimri *et al*, 1995). In these cells, SA- β -GAL activity increases so much that it can be detected at a suboptimal pH 6 (Kurz *et al*, 2000), which is the pH imposed to the cells in the SA- β -GAL determination assay that we used to compare “old” cultured rat Schwann cells (8 passages or more) with “young” cultured Schwann cells (1 or 2 passages). Using this assay, senescent cells are easily detected because they acquire a characteristic blue colour. In figure R2 we can observe that there was a clear difference in the number of senescent positive cells (blue cells) between “young” and “old” Schwann cells. Having counted 500 cells for each type of Schwann cells, 73% of the old ones were positive in contrast with 35% positive among the young ones. The morphological data together with the results obtained in the SA- β -GAL assay suggested that Schwann cells in culture can become senescent.

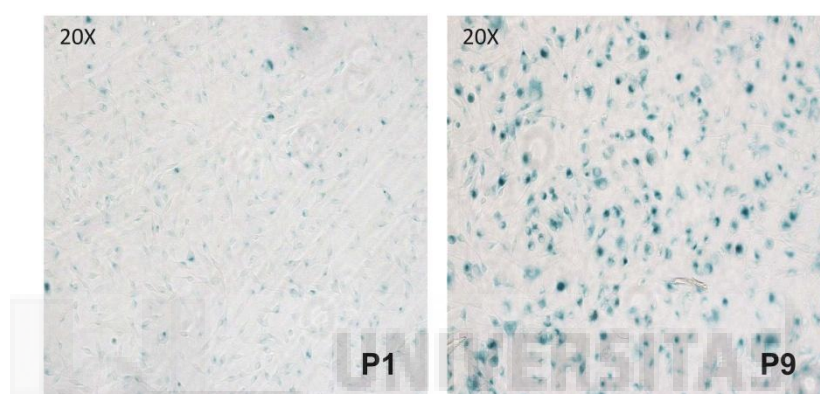
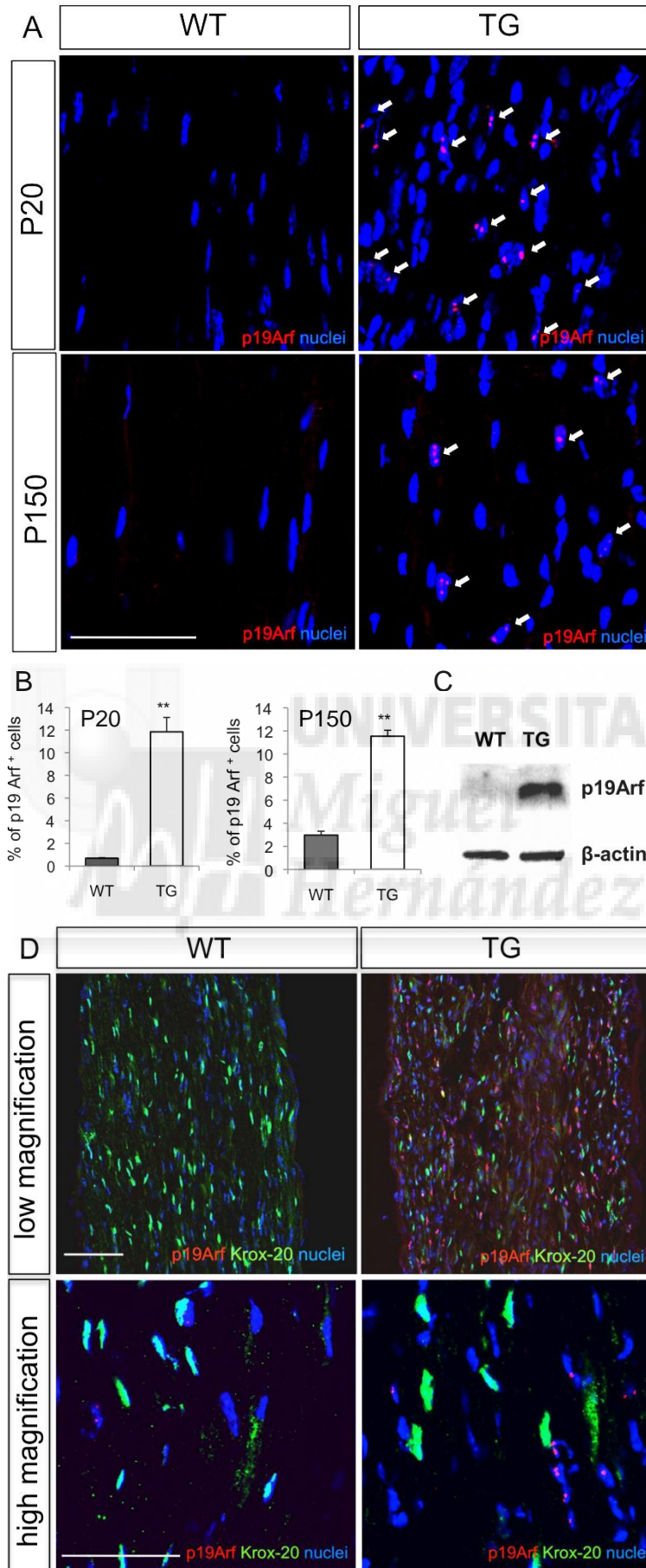


Figure R2: Schwann cells in culture reach cellular senescence after several passages. Representative image of β -galactosidase staining (blue) in P1 and P9 cultured rat Schwann cells. n=3.

The high lipid content of myelin in the peripheral nerves makes them difficult to stain with the SA- β -GAL assay. However, it is well established that the OIS program is mainly mediated through the p19Arf/p53 and p16Ink4/Rb pathways (Gorgoulis & Halazonetis). As an indicator of senescence, we decided to compare the abundance of p16Ink4 and p19Arf proteins in the neurofibroma-like nerves of the transgenic *NSE-SMDF^{+/+}* mice and their wild type littermates. We found no p19Arf staining in longitudinally sectioned nerves of wild type animals in contrast to a clear nucleolar staining for p19Arf in many of the cells in the transgenic nerves. This was the case in both P20 and in P150 mice, showing a maintained expression of p19Arf in the transgenic nerves as opposed to the wild type nerves (Fig. R3A and B). This result was confirmed by Western Blotting, which showed a clear band corresponding to p19Arf in transgenic nerves and not in wild type (Fig. 3C). Interestingly, the Schwann cells positive for p19Arf were the non-myelinating ones, as shown by the lack of co-localization with Krox-20 staining (Figure R3D). Regarding p16Ink4, we found a clear nuclear staining in the transgenic nerves, which was not present in their wild type littermates (Figure R3E). We observed that p19Arf and p16Ink4 co-localized in the same cells, which was unsurprising as the transcripts of these two proteins are encoded in the same locus in the genome, the *Ink4a/Arf* locus. However, in some cells we did not find co-localization of p19Arf with p16Ink4. The probable reason for this is the downregulation of *p19Arf* by p53 through a previously described negative feedback-regulating loop that does not affect the synthesis of p16Ink4 (Gil and Peters, 2006).



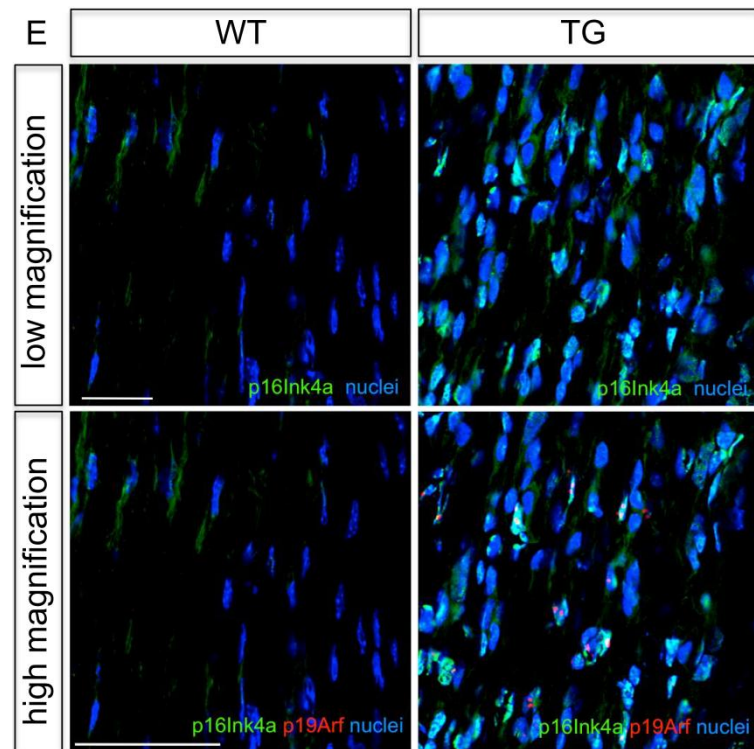


Figure R3: *Ink4a/Arf* locus products are expressed in the neurofibromas of *NSE-SMDF^{+/-}* mice.

(A and B) Longitudinal sections of transgenic and wild type nerves (P20 and P150) were incubated with anti-p19Arf antibody and Hoescht. A clear nucleolar labelling (red) was observed in many of the neurofibroma cells, t-test $**P < 0.001$. $n=3$ from each genotype. (C) Western Blot from protein extracts of wild type and transgenic sciatic nerves incubated with anti-p19Arf antibody. β -actin was used as loading control. $n=2$. (D) Co-immunostaining with anti-Krox-20 and anti-p19Arf antibodies shows the practically absence of co-localization between Krox-20 and p19Arf. (E) The immunostaining with anti-p16Ink4 antibody shows upregulation of p16Ink4 in the transgenic nerves. Co-staining with anti-p16Ink4 and anti-p19Arf antibodies shows a high degree of co-localization between p16Ink4 and p19Arf. Scale bars = 50 μ m. $n=3$.

In order to study the temporal expression pattern of *p16Ink4a* and *p19Arf* in the mutant mice, we extracted RNA from sciatic nerves of wild type and *NSE-SMDF^{+/-}* transgenic mice of different ages and assayed the levels of transcription by performing RT-qPCR with specific primers. As we can see in the graphs in figure R4, the expression of *p19Arf* and *p16Ink4a* was increased in the mutant mice from P20 to P750.

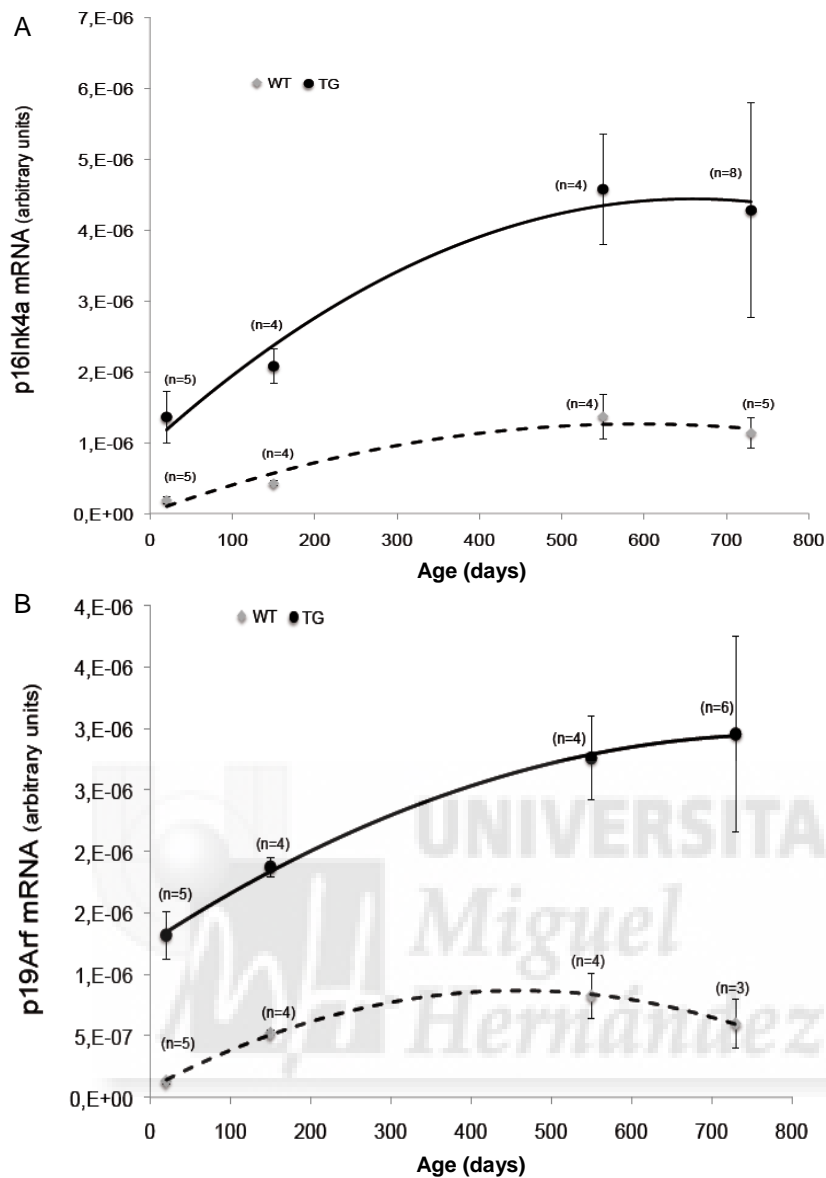


Figure R4: Expression of *p16Ink4a* and *p19Arf* is upregulated in the PNS during the whole life of *NSE-SMDF^{+/+}* mice. (A) The graph shows the levels of *p16Ink4a* transcript, from RNA extracted from *NSE-SMDF^{+/+}* mice of different ages and their wild type littermates. Measured by RT-qPCR. (B) Expression levels of *p19Arf* messenger RNA from transgenic mice of different ages and their wild type littermates. Measured by RT-qPCR. Results are normalized against 18S. Data are given as mean SE. Three or more animals were used per condition. (n = number of mice). t-test $P \leq 0.005$ in all the experiments.

1.3 Histone demethylase *Jmjd3* contributes to the activation of *Ink4a/Arf* in Schwann cells.

It has been demonstrated that in actively growing human fibroblasts, the *Ink4a/Arf* locus is silenced by trimethylation in lysine 27 of histone 3 (H3K27me3) at the promoters. This is done by the EZH2 enzymatic subunit of the Polycomb PRC2 complex (Wysocka and Swigut, 2007). *Jmjd3* is a histone demethylase that counteracts the repression of PRC2 by de-methylating H3k27me3. It has been described that upon activation of oncogenic RAS, epigenetic control by *Jmjd3* permits the expression of the *Ink4a/Arf* locus in mouse primary fibroblasts. It was therefore interesting to explore whether *Jmjd3* could be mediating the transcriptional activation of the *Ink4a/Arf* locus in the nerves of the *NSE-SMDF^{+/+}* transgenic mice. For this purpose, several approaches were

employed. First, the expression levels of *Jmjd3* in the nerves were studied by immunofluorescence. Frozen, longitudinal samples of transgenic and wild type littermates were stained with an anti-*Jmjd3* polyclonal antibody (see methods) and compared. In figure R5A, we observe a clear nuclear staining of *Jmjd3* in many cells in the transgenic nerve, which is almost non-existent in the nerve from a wild type littermate. To study the expression of *Jmjd3* at the mRNA level, RT-qPCR was performed as described in methods, using as a template cDNA synthesized from the mRNA of transgenic and wild type mice. The graph in figure R5B shows a 3-fold increase of the *Jmjd3* mRNA levels in the transgenic versus the wild type nerves. In order to make sure that this change occurs specifically for this demethylase, we measured the mRNA levels of *Utx*. *Utx* is a demethylase that contains the Jumonji C domain and has been shown to demethylate H3K27me2/3 as well (Hubner and Spector, 2010). In figure R5B we can see that *Utx* expression was unchanged in sciatic nerves from transgenic mice.

In order to test if *Jmjd3* plays a role in the activation of the *Ink4a/Arf* locus in the transgenic mice, we explored the methylation status of chromatin in the promoters of the *Ink4a/Arf* locus by the Chromatin immunoprecipitation assay (ChIP). Briefly, an anti-H3K27me3 antibody was used to immunoprecipitate the crosslinked DNA-protein complexes of sciatic nerves from wild type and transgenic mice. A non-specific IgG antibody (ChIP grade) was used as a negative control. By RT-qPCR with specific primers for the *p16Ink4a* and *p19Arf* promoters, we measured the relative amount of DNA pulled down by the anti-H3K27me3 antibody. The graphs in figure R5C show that there was a substantial decrease of H3K27me3 in both *p19Arf* and *p16Ink4a* promoters in the transgenic nerves. The specificity of the assay was confirmed as there was no change when a non-specific IgG was used to immunoprecipitate. Because it is well established that *Jmjd3* activates the expression of genes by de-methylating H3K27me3 in their promoters, this result suggests that *Jmjd3* is involved in the induction of *p19Arf* and *p16Ink4a* expression in the neurofibroma-like nerves of the *NSE-SMDF^{V+/+}* transgenic mice.

We then wanted to find out whether an increase of *Jmjd3* might induce *p19Arf* expression. In order to enforce the expression of *Jmjd3*, we co-transfected cultured rat Schwann cells with a plasmid encoding *Jmjd3* under the CMV promoter and with a reporter plasmid encoding *pEGFP*. After 48 hours in SATO medium the cells were fixed and stained for p19Arf. About 40% of the cells expressing *Jmjd3* and GFP were positive for p19Arf, whereas less than 3% of the non-transfected cells were p19Arf positive (Figure R5D). This result reinforces the idea that *Jmjd3* is involved in the induction of *p19Arf* expression in Schwann cells.

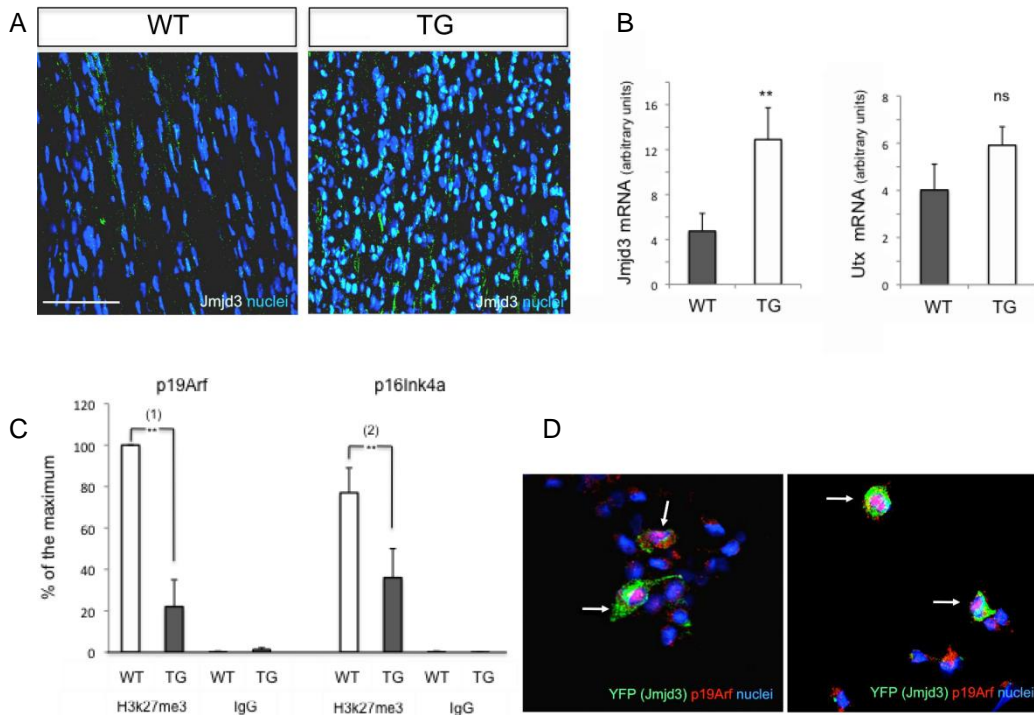


Figure R5: Chromatin modification by the Jmjd3 demethylase contributes to the activation of the *Ink4a/Arf* locus in neurofibromas of *NSE-SMDF^{+/+}* mice. (A) Longitudinal sections of P20 *NSE-SMDF^{+/+}* and wild type sciatic nerves were incubated with anti-Jmjd3 antibody (green) and nuclei counterstained with Hoechst (blue). Many cells in the transgenic nerve were positive for Jmjd3. n = 3. Scale bar = 50 μ m. (B) The graph shows *Jmjd3* transcript levels from RNA extracted from P20 transgenic and wild type littermates. Results were normalized against 18S ribosomal RNA. mRNA for *Jmjd3* was increased by 2.74-fold in transgenic nerves. The increase was specific for *Jmjd3*, as the messenger RNA levels of *Utx*, a demethylase of the same family, remained unchanged. Results are given as mean SE. n = 8 for *Jmjd3*, and n = 3 for *Utx*. t-test**P= 0.025. (C) ChIP shows that there is less H3K27me3 bound to the promoters of *p19Arf* and *p16Ink4a* in transgenic nerves than in their wild type littermates. Sciatic nerves from seven mice were crosslinked and immunoprecipitated with anti-H3K27me3 antibody or a non-specific IgG. Quantitative PCR was performed with specific primers for promoter regions in the *Ink4a/Arf* locus. Results were normalized against the maximum amount of immunoprecipitated promoter and expressed as a percentage. Data are given as mean SE. Three independent experiments were performed (n = 3); Paired t-test; (1) P= 0.01; (2) P= 0.03. (D) Enforced expression of *Jmjd3* up-regulates *p19Arf* in Schwann cells. Rat Schwann cells were co-transfected with *pCMV-Jmjd3* and *pEGFP* (as reporter). About 40% of the *pCMV-Jmjd3* expressing cells (green) were p19Arf positive (red), whereas this gene was expressed in 3% of non-transfected cells. (n = 3).

1.4 Oncogene Induced Senescence in human plexiform neurofibromas

NF1 patients can develop either dermatofibromas, which are benign tumours that grow on or around superficial nerves, or plexiform neurofibromas, which develop in the nerve roots. Approximately 10% of these plexiform neurofibromas eventually experience a malignant progression, giving rise to Malignant Peripheral Nerve Sheath Tumours (MPNST). These are very aggressive, highly metastatic and almost incurable (Cichowski *et al*, 1999; McClatchey, 2007).

In order to determine whether the OIS program is also activated in the human neurofibromas, we collected samples of paraffin embedded sections from six different NF1 associated human plexiform neurofibromas (see methods). We stained the sections with antibodies against p14Arf, which is the human homolog of p19Arf, and p16Ink4, comparing them to a staining of a healthy human nerve sample. In figure R6 we can observe that there is a high expression of both p14Arf and p16Ink4 in the NF1 plexiform neurofibroma shown, in contrast to

the lack of nuclear p14Arf and the low presence of nuclear p16Ink4 in the healthy nerve. Activation of p14Arf and p16Ink4 expression was seen in all six plexiform neurofibromas. This suggests that, like in neurofibroma-like nerves of the *NSE-SMDF^{+/-}* transgenic mice, the OIS program is activated in human plexiform neurofibromas to prevent the tumour progression towards malignancy.

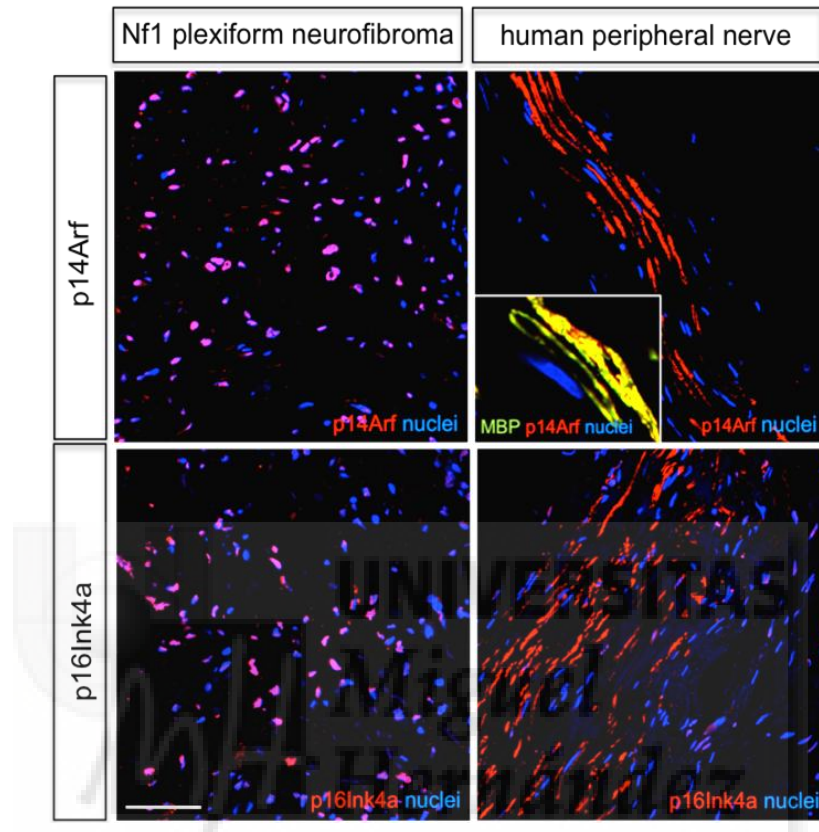


Figure R6: *Ink4a/Arf* locus products are expressed in human plexiform neurofibromas. Human NF1 plexiform neurofibromas express *p14Arf* (the human homologue for *p19Arf*), whereas it is barely detectable in the nuclei of Schwann cells of nerves obtained from biopsies of healthy subjects. *p16Ink4a* is also abundantly expressed in human plexiform neurofibromas but it can be detected (although less frequently) in the Schwann cell nuclei of normal nerves. We did notice non-nuclear staining for p16Ink4 and p14Arf in healthy human nerves, which co-localizes with MBP (inset). This is probably due to nonspecific binding of the antibodies to the lipid rich myelin in the formalin fixed paraffin embedded tissues. Scale bar = 50 μ m.

1.5 Malignant transformation of the *NSE-SMDF^{+/-}* neurofibromas is associated with the loss of the senescence program.

Despite having enlarged nerves throughout the PNS, most of the *NSE-SMDF^{+/-}* transgenic mice display a normal phenotype, behavior and life expectancy. Nevertheless, approximately 15% of these transgenic mice started to show symptoms of neurological alterations, usually motor deficits, from around eight months of age. These alterations correlated with the appearance of local tumours growing in nerve roots or in dorsal root ganglia. In these tumours, the proliferation of Schwann cells is resumed, as indicated by the abundance of pH3-stained cells, in contrast to the absence of pH3 staining in the neurofibroma-like nerves from the same animals (figure R7A).

In recent studies, it was demonstrated that the inactivation of senescence mediators in benign tumours of transgenic mice expressing the oncogenic RAS leads to the malignant progression of

the tumour (Sarkisian *et al*, 2007). It was therefore important to analyze the expression of the two key senescence mediators, *p19Arf* and *p16Ink4a*, within these malignant tumours found in *NSE-SMDF^{+/+}* mice. For this purpose, we obtained RNA from the carefully extracted tumours and performed RT-qPCR to determine *p16Ink4a* and *p19Arf* transcript levels. In this way we measured the expression levels of *p19Arf* and *p16Ink4a* in a total number of 10 malignant tumours. The graphs in R7B show the mRNA levels of *p16Ink4a* and *p19Arf* of each individual tumour, plotted together with the mRNA levels for these transcripts in the neurofibroma-like nerves of transgenic *NSE-SMDF^{+/+}* mice and in wild type nerves. As we can observe, there is a clear decrease in the expression of *p19Arf* in most of the malignant tumours (seven out of ten) compared to the levels in the neurofibroma-like nerves. However, the level of *p16Ink4a* does not decrease, but exhibits a higher variability in its expression.

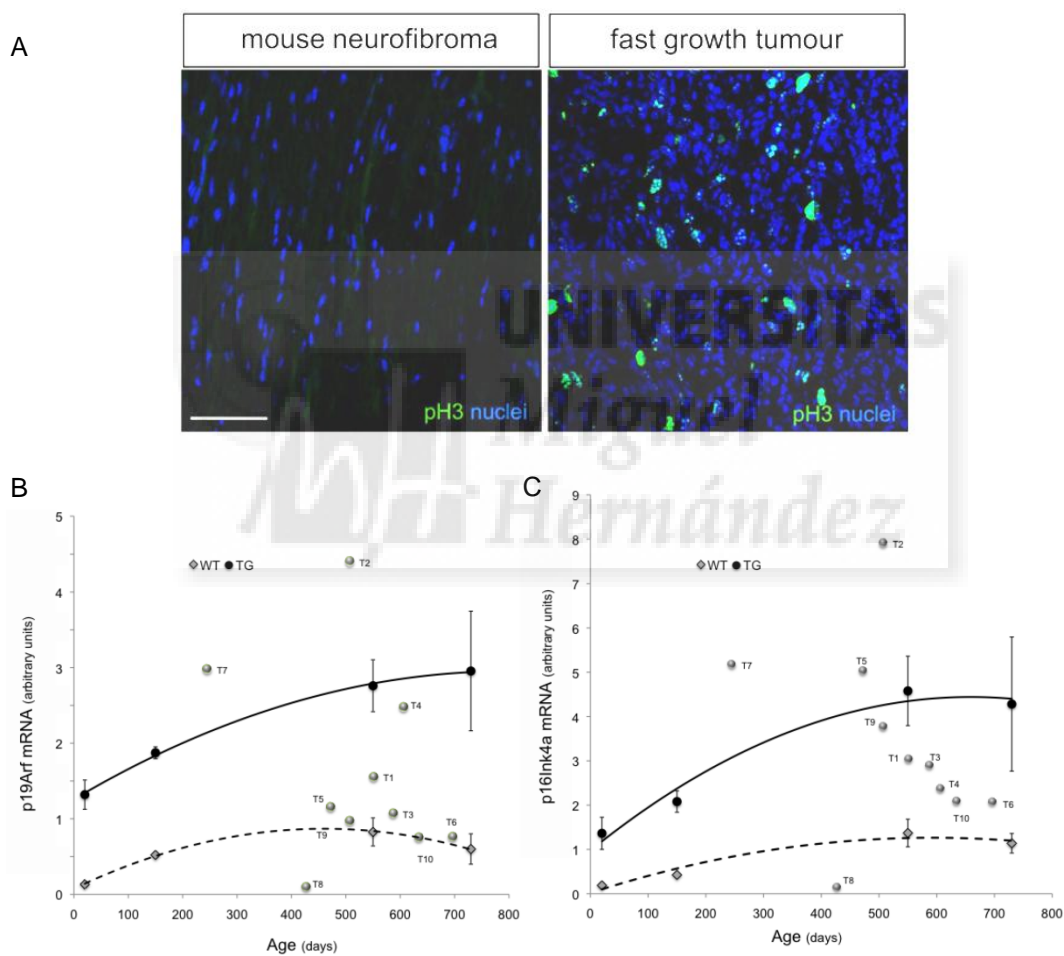


Figure R7: Loss of the senescence programme induces malignant transformation of neurofibromas in *NSE-SMDF^{+/+}* mice. (A) Sections of *NSE-SMDF^{+/+}* fast growing tumours and neurofibroma-like nerves were incubated with anti-pH3 antibody (green) and nuclei counterstained with Hoechst (blue). As shown, many cells were positive for pH3 in the tumours but not in the neurofibromas. Scale bar = 50 μm. n=3. (B) Total RNA was obtained from 10 fast-growing tumours developed by the *NSE-SMDF^{+/+}* mice and the messenger RNA for *p19Arf* quantified by RT-qPCR. Results were normalized against 18S ribosomal RNA. *p19Arf* messenger RNA was plotted against the levels in sciatic nerves of wild-type and transgenic mice. As shown, in seven of these tumours *p19Arf* messenger RNA was downregulated to the levels of wild type nerves. (C) In contrast, there was a high variability in expression levels of *p16Ink4a* messenger RNA in the tumours, without a clear downregulation.

These data suggest that there is a loss of the senescence program, mediated mainly by a blockage in the expression of *p19Arf*, leading to the malignant transformation of the tumours. In previous studies, genetic manipulations to block the senescence program, for instance by having only one *p53* allele in mice that also lack a tumour suppressor gene, such as PTEN, induced the malignant progression of the tumours (Chen *et al*, 2005). We decided to use a similar approach by crossing *NSE-SMDF^{+/-}* mice with *p53^{+/-}* mice. Figure R8A shows a Kaplan-Meier curve obtained by plotting the percentage of survival versus age for wild type, *p53^{+/-}*, *NSE-SMDF^{+/-}* and double heterozygous *p53^{+/-} NSE-SMDF^{+/-}* mice (approximately 30 mice for each genotype; see legend to figure R8A). We can observe that the survival rates for *p53^{+/-}* and *NSE-SMDF^{+/-}* mice are rather similar and reduced in comparison to the survival of wild type mice. Strikingly, we found that eliminating a single copy of *p53* in the *NSE-SMDF^{+/-}* mice increases the incidence of malignant tumour formation up to 100% of cases. Furthermore, it also decreases the average age at which the tumour starts to develop. Most highly proliferative tumours in these double mutants grew within the nerve roots or in the dorsal root ganglia, but some of them developed from the sciatic nerves. An example of this is illustrated in figure R8B, which shows a portion of a neurofibroma-like sciatic nerve in a double heterozygote *p53^{+/-} NSE-SMDF^{+/-}* mouse, and a malignant tumour that has originated from it. Looking at the pH3 staining we can see the lack of proliferation in the neurofibroma-like nerve, in contrast to the highly proliferative rate in the malignant tumour. To study the morphology of these malignant tumours in a more detailed manner, we processed some of the tumours so they could be analyzed by transmission electron microscopy. These malignant tumours showed huge deposits of collagen and dissociated Schwann cells in the extracellular matrix (Figure R8C), presenting a similar morphology to the MPNSTs that develop in human NF1 patients (Cichowski *et al*, 1999).

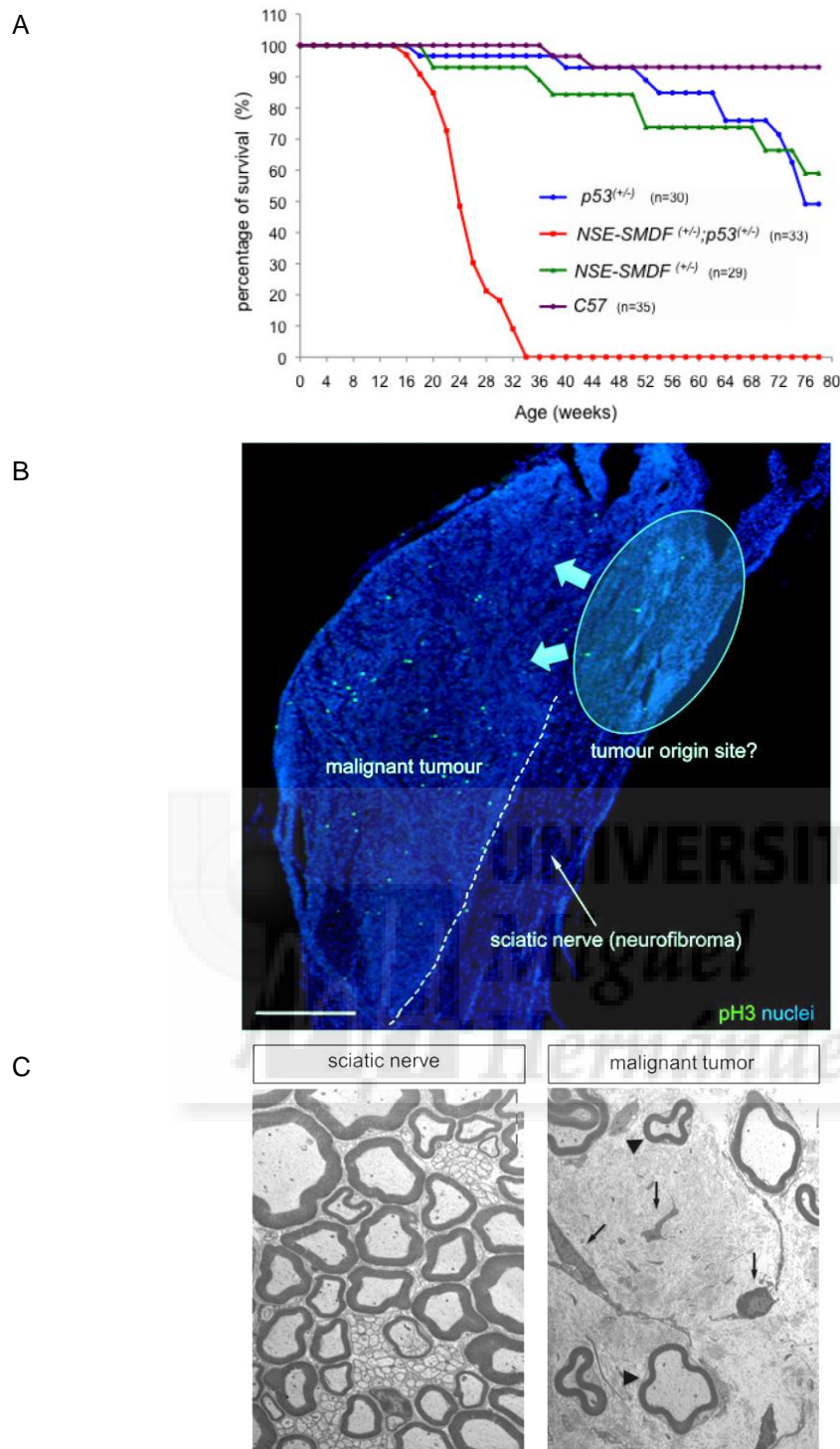


Figure R8: Loss of p19Arf/p53 pathway function induces malignant transformation of the neurofibromas developed by *NSE-SMDF*^{+/-} mice. (A) Elimination of a single copy of *p53* (*NSE-SMDF*^{+/-}; *p53*^{+/-} double heterozygotes) dramatically increases the incidence (up to 100%) of malignancies and decreases the age of malignant tumour formation. Kaplan-Meier survival plots are shown. The exact number of animals per genotype is indicated in the graph. (B) Low magnification field of a highly proliferative tumour developed by the *NSE-SMDF*^{+/-}; *p53*^{+/-} mice. The origin of the malignant tumour can be identified as a localized region of the neurofibroma with increased proliferation rate. Sections of the tissue were incubated with anti-pH3 antibody (green) and nuclei counterstained with Hoechst (blue). Scale bar = 600 μ m. (C) Transmission electron microscopy images from a malignant tumour developed by a *NSE-SMDF*^{+/-} mice (right) and from the sciatic nerve of a wild type littermate (left). Malignant tumours developed by the double mutants show dramatically increased collagen-rich extracellular matrix with dissociated Schwann cells (arrows), intermingled with normally myelinated axons (arrowheads). Similar findings were obtained in two different tumours. Scale bar = 5 μ m.

1.6 The senescence program is activated in Schwann cells after injury

After a nerve lesion due to crushing or transection, the Schwann cells in the distal stump dedifferentiate and proliferate, upregulate the expression of genes that stimulate axonal growth, neuronal survival and macrophage recruitment, activate mechanisms for myelin break-down and change their shape to form the bands of Bungner. All this creates an optimal environment for the regrowth of the axons towards the target tissue, eventually allowing the regeneration of the nerve (Parkinson *et al*, 2008). In injured nerves, Schwann cells in the distal stump have a proliferation peak between 4 and 8 days post lesion, after which proliferation decreases and Schwann cells remain in a dedifferentiated but non-proliferative status until the arrival of the regrowing axons from the proximal stump. This is even the case in a transected nerve in which the regrowth of the proximal axon is prevented by increasing the distance between the proximal and the distal stump. In this situation, it has been shown that the Schwann cells remain dedifferentiated and non-proliferating up to at least two months after injury (Scherer *et al*, 1994). The reason for this decrease in the rate of proliferation is unknown. It could be due to a washing off of mitogenic signals and/or the involvement of an active mechanism that prevents proliferation. Considering the similarity between the halt in proliferation after injury and the halt in proliferation in the neurofibromas of the transgenic *NSE-SMDF^{+/+}* mice, it was interesting to explore whether the senescence program also plays a role after injury. For this purpose we performed surgery on C57BL/6J wild type mice, transecting the sciatic nerve and making sure that the growing axons could not reach the distal stump. We then extracted the distal part of the sciatic nerve at 4, 12 and 24 days after the lesion. The staining of these nerve fragments compared to uncut nerves is shown in figure R9A. We can observe that some cells have a clear nucleolar p19Arf staining in the cut nerves in contrast to the absence of p19Arf staining in the uncut nerves. This is visible already 4 days after the lesion, and remains so 12 and 24 days after lesion. The labelling of p19Arf suggests that the senescence program is activated after injury. Interestingly, *Jmjd3* seems to be abundantly expressed in all three stages in cut nerves compared to the uncut nerves (Figure R9B). This staining suggests that, as in neurofibroma-like nerves, *Jmjd3* is probably involved in the activation of the senescence program in injured nerves. pH3 staining shows the proliferating cells and, as has been previously observed by others in injured nerves (Scherer *et al*, 1994), it decreases overtime being completely extinct 24 days after the lesion.

One of the unique features of Schwann cells in comparison with most mamalian cells is their great plasticity, having the ability to switch between differentiation states. Taking this plasticity into account it might be possible that Schwann cells are able to turn off the senescence program under specific circumstances, such as when they become in contact with a re-growing axon. To explore this hypothesis, nerves of C57BL/6J wild type mice were crushed. When the nerve is crushed, axotomy occurs but the epineurium remains intact, which facilitates the regrowth of the regenerating axons into the distal stump. By means of immunofluorescence we checked the expression of p19Arf in the nerves 12 and 24 days after crushing. As we can observe in figure R9C, at the stage of 12 days after the lesion there were a few p19Arf positive cells in the distal stump. However, 24 days after the lesion, coinciding with the re-entry of the proximal axons, we found no p19Arf staining (fig. R9D). This suggests that the senescence program becomes inactivated when the regenerating axons make contact with the Schwann cells in the distal stump. However, we

cannot rule out the possibility that senescent cells could be removed by fagocytosis during the regeneration process.

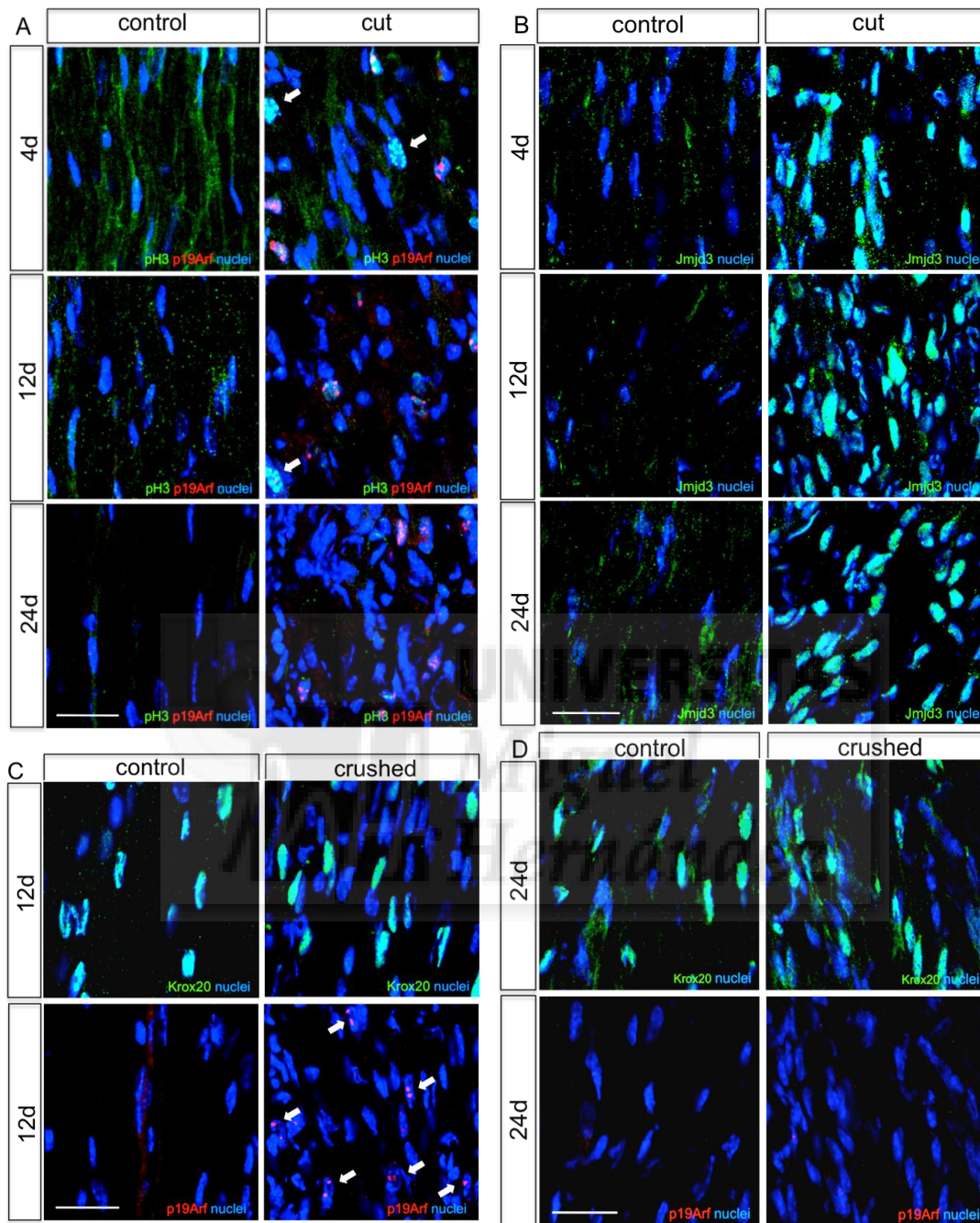


Figure R9: Nerve injury induces the expression of the *Ink4a/Arf* locus in Schwann cells. (A) After complete sciatic nerve transection, expression of p19Arf (arrows) is induced in the distal stump. Expression of this protein is maintained up to 24 days post-injury. (B) Jmjd3 is also upregulated in the distal stump after cut. (C) p19Arf expression is also induced in crushed (but not transected) nerves. At 12 days post-crush, regrowing axons trigger the re-expression of Krox-20. Despite this, p19Arf can be detected in Schwann cells. (D) By Day 24 post-crush levels of p19Arf were found to be reduced to those present in non-injured nerves. Longitudinal sections of the distal stump of transected or crushed sciatic nerves and the contralateral non-injured nerves from adult wild type mice were incubated with the indicated antibodies and nuclei counterstained with Hoechst. Three or more animals were used per condition. A representative image is shown. Scale bars = 50 μ m

1.7 The activation of the senescence program after injury controls Schwann cell proliferation

We next wanted to see if turning off the senescence program might affect the proliferation rate of Schwann cells after injury. To this aim, in collaboration with other members of my lab, nerve transections were performed in the sciatic nerves of *Ink4a/Arf*^{-/-} mice and the distal stumps were immuno-stained using an antibody against Ki-67 as a proliferation marker. Four days after nerve transection, Schwann cell proliferation was the same in both wild type and *Ink4a/Arf*^{-/-} mice. However, it became significantly increased in *Ink4a/Arf*^{-/-} at the stage of 12 days after injury (Figure R10A). A similar result was obtained for the *p53*^{-/-} mice. However, in this case, the proliferation rate was already increased 4 days after injury (Figure 10B). These results suggest that the senescence program is activated in Schwann cells after an injury in order to prevent Schwann cell hyperproliferation.

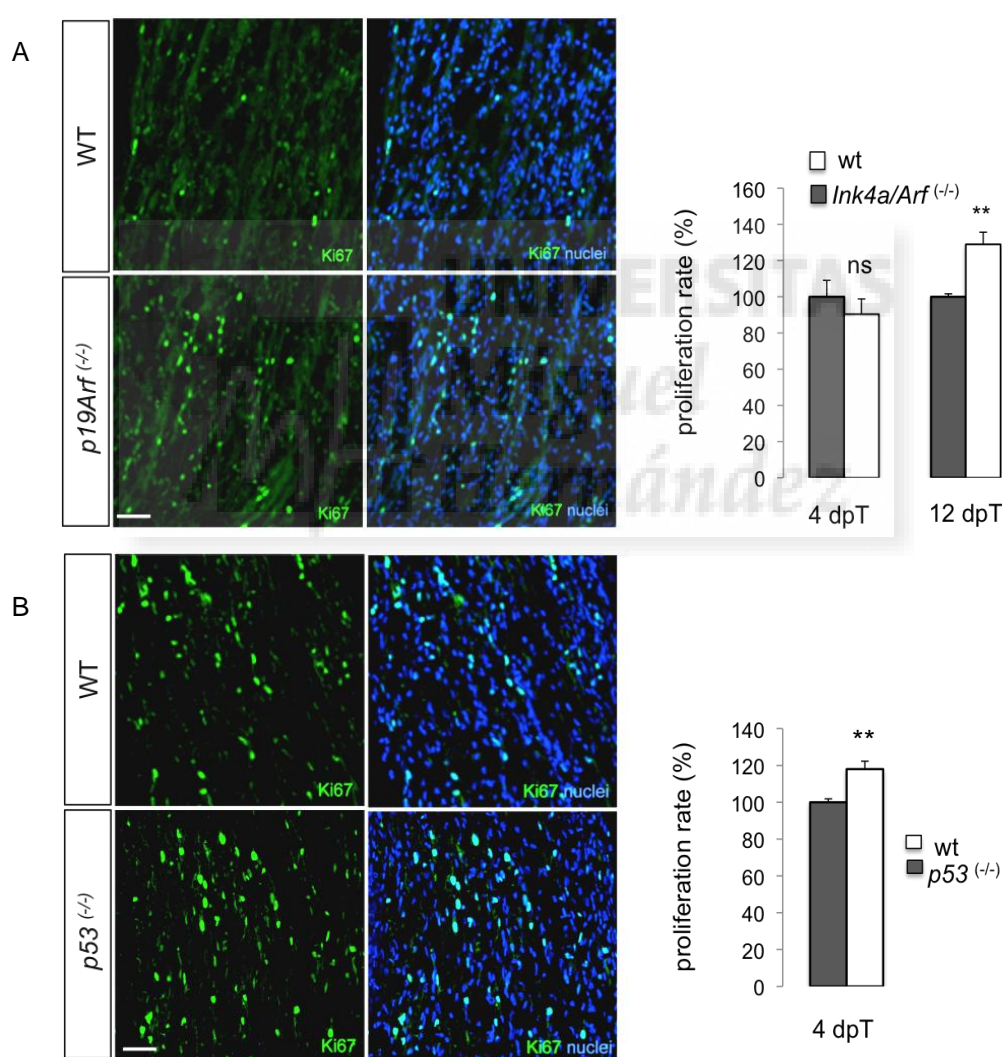


Figure R10: *Ink4a/Arf* locus contributes to proliferation arrest in injured nerves. (A) Cell proliferation is increased in the injured nerves of *Ink4a/Arf*^{-/-} mice. The number of Ki-67-positive cells was counted in the distal stumps of *Ink4a/Arf*^{-/-} and wild type littermates. Proliferation rate was calculated by dividing the number of Ki-67-positive cells by the total nuclei. As shown, the density of proliferating cells was significantly increased in the *Ink4a/Arf*^{-/-} mice. n = 3; t-test**P = 0.016. (B) Proliferation rate was also increased in the injured nerves of *p53*^{-/-} mice. n = 3; t-test **P = 0.012

2. Regulation of c-Jun expression in peripheral nerves

2.1 c-Jun expression in nerve explants

The transcription factor c-Jun is expressed by immature Schwann cells and is downregulated as myelination proceeds. Interestingly, it has been demonstrated that c-Jun inhibits Schwann cell myelination *in vitro* (Parkinson *et al*, 2008) as well as *in vivo* (Arthur-Farraj *et al*, 2012). During the course of our experiments we observed a strong upregulation of c-Jun in the neurofibroma-like nerves of the *NSE-SMDF^{+/+}* mice as well as in human plexiform neurofibromas (data not shown). These data suggest that deregulation of c-Jun expression could underlie the development of PNS tumors. In spite of the central role of c-Jun in Schwann cells development, the regulation of its expression in glial cells is largely unknown. We therefore decided to explore how c-Jun expression is regulated in the PNS.

c-Jun is dramatically upregulated after nerve injury and has been proposed to be a key component of the regeneration process that occurs in the distal stump. It controls crucial functions of denervated Schwann cells, such as the formation of regeneration tracks (or Bungner bands), their support for neuronal survival, promotion of axon regrowth and myelin clearance (Arthur-Farraj *et al*, 2012). *In vitro*, it is possible to reproduce many of the biological processes that take place in the distal stump of injured nerves by performing nerve explants (Jung *et al*, 2011; Lee *et al*, 2009). Indeed there is a fast upregulation of c-Jun expression in these nerve explants, as well as a later downregulation of myelin proteins. Therefore we decided to use this approach as a more accessible way to explore the mechanisms that regulate c-Jun expression in injured nerves.

Sciatic nerves from adult C57B/J mice were removed and cut in 5 mm long pieces. The epineurial layer was carefully removed and explants were left in DMEM with 5% horse serum during four days, mimicking post-injury axonal loss of contact. After this time, we homogenized the tissue from these explants and extracted and quantified the total protein content. We then checked the protein levels of c-Jun and of the myelination markers P0, Krox-20 and MAG by Western Blot. As shown in figure R11A, after four days, there was a clear upregulation of c-Jun compared to a non-injured nerve, which is a piece of the same nerve that was rapidly frozen after being removed. This is in accordance with what has been previously described (Shin *et al*, 2013). In contrast, the expression of Schwann cell differentiation markers, such as MAG, was notably downregulated with respect to the non-injured nerve. The same results were obtained with a different set of myelination markers, Krox-20 and P0 (Fig. R11B).

It has been shown that in adult nerves, the loss of axon-glia contact after injury produces a downregulation of cAMP levels in Schwann cells. This drop in cAMP is probably the consequence of a decrease in the adenyl cyclase activity combined with an increase in the phosphodiesterase (PDE) activity (Poduslo *et al*, 1995; Walikonis & Poduslo, 1998). In order to learn whether the decrease in intracellular cAMP is the ultimate cause in the upregulation of c-Jun, we treated some explants with dibutyryl adenosine 3',5'-cyclic monophosphate (dbcAMP), a non-hydrolysable analog of cAMP. As shown in Fig R11A, dbcAMP was able to maintain the expression levels of c-Jun low, similar to that of the non-injured nerve. Interestingly, the downregulation of the myelin protein MAG was prevented by dbcAMP as well, suggesting that high intracellular levels of cAMP are necessary to maintain low c-Jun levels and a myelinating Schwann cell phenotype in the adult normal nerve. As previously mentioned, the drop of cAMP levels is in part consequence of an

increase in the phosphodiesterase (PDE) activity. Since PDE4, a low K_m cAMP-specific phosphodiesterase, predominantly contributes to this activity in the injured nerve (Walikonis & Poduslo, 1998), we incubated the nerve explants with rolipram, a specific PDE4 inhibitor. As shown in figure R11A, PDE4 inhibition did not prevent the upregulation of c-Jun in nerve explants. Then we decided to stimulate adenylyl cyclase activity, which, as previously mentioned, plays a role in the modulation of intracellular cAMP levels. To this aim, we incubated the explants with forskolin, a plant derived compound that binds and activates adenylyl cyclase (Wagh *et al*, 2012). As shown in figure R11A, forskolin efficiently prevented c-Jun upregulation and maintained Schwann cells in a differentiated status in nerve explants during at least four days. Taken together, our data suggest that, after loss of axonal contact, c-Jun is upregulated in Schwann cells mainly by a decrease in the activity of the adenylyl cyclase.

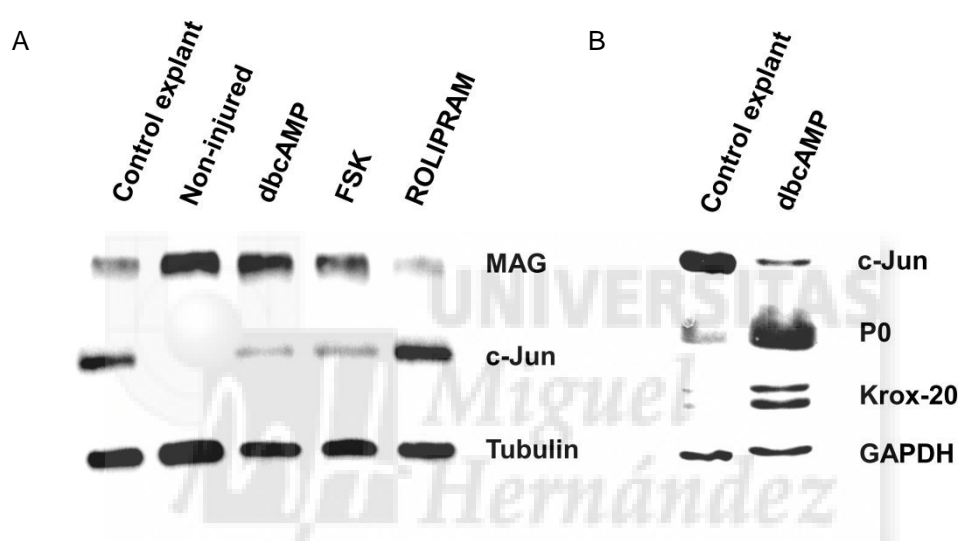


Figure R11: De-differentiation is delayed in sciatic explants incubated with forskolin or dbcAMP. (A) Western blot from sciatic explants obtained from adult (about 3 months old) wild type mice. Three explants per condition in each assay, incubated during 4 days in DMEM plus 5% horse serum plus the corresponding treatment: DMSO (as control), dbcAMP 1mM, FSK 50 μ M, Rolipram 50 μ M. "Non-injured" stands for explants snap frozen without any incubation time. The same amount of protein was loaded from each of the samples. Incubation with anti-MAG and anti-c-Jun antibodies. Tubulin was used as loading control. n=3. A representative WB is shown. (B) The same experiment was performed only with dbcAMP 1mM and DMSO incubation. The same amount of protein was loaded from each of the samples. Incubation with anti-c-Jun, anti-P0 and anti-Krox-20 antibodies. GAPDH was used as loading control.

2.2 cAMP decreases c-Jun mRNA in cultured rat Schwann cells

When Schwann cells are cultured, they adopt the Bungner repair cell-like phenotype that characterizes denervated Schwann cells (Arthur-Farrar *et al*, 2012). As a consequence, c-Jun levels are normally high in cultured Schwann cells (Monuki *et al*, 1989). This is upon incubation with expansion medium, SATO medium and even DMEM alone. In cultured Schwann cells, elevation of intracellular cAMP mimics axonal contact and drives differentiation towards a myelinating phenotype (Morgan *et al*, 1991; Parkinson *et al*, 2008). In concordance with this data we observed that c-Jun protein levels decrease dramatically after applying dbcAMP to cultured Schwann cells. Figure R12A shows the detection of c-Jun by Western Blot, using total protein extracts from cultured rat Schwann cells that had been incubated in SATO with dbcAMP 1mM for 24 hours.

Since we previously observed that dbcAMP is able to maintain low c-Jun levels in nerve explants, we reasoned that cultured Schwann cells could be a good model to study the regulation of c-Jun expression in PNS.

We then decided to check if the decrease in c-Jun protein in cultured Schwann cells upon dbcAMP incubation is caused by a decrease of c-Jun mRNA levels. For this purpose, we incubated cultured rat Schwann cells with dbcAMP 1mM for 24 and 48 hours, then harvested the cells, extracted their total RNA and synthesized cDNA from it. We used this cDNA as a template for RT-qPCR using specific primers for c-Jun and for GAPDH (as housekeeping gene). As is shown in figures R12B and R12C, there is a huge drop in c-Jun mRNA levels in Schwann cells incubated with dbcAMP during 24 and 48 hours. This indicates that the decrease of c-Jun protein levels is due to a reduction of its mRNA levels. There can be two factors involved in the decrease of mRNA levels: transcriptional repression and decrease of mRNA stability. Later in this section we will show some results that suggest that cAMP specifically inhibits c-Jun transcription.

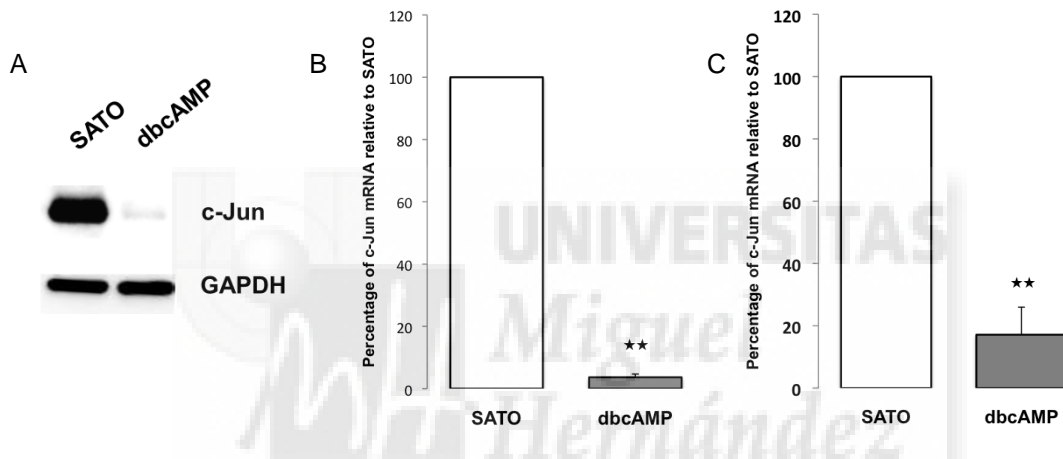


Figure R12: dbcAMP inhibits c-Jun expression at the messenger RNA level. (A) Western Blot using protein extracts from cultured Schwann cells incubated during 24h in SATO vs SATO plus dbcAMP. Incubation with anti-c-Jun antibody and anti-GAPDH as loading control. (B and C) The graphs show the levels of c-Jun messenger RNA in Schwann cells incubated with dbcAMP 1mM during 24h (B) and 48h (C), expressed in percentages relative to the transcription levels in Schwann cells incubated in SATO medium. Measurements done by RT-qPCR. 24h t-test $**P < 0,001$ n=3; 48h t-test $**P < 0,001$ n=3.

2.3 c-Jun upregulation is cell autonomous

To model c-Jun induction in the injured nerve, we treated cultured rat Schwann cells with 1mM dbcAMP for 48h. As has been previously shown, in this condition c-Jun expression is notably downregulated and Schwann cells remain in a differentiated-like phenotype (Monuki *et al*, 1989; Morgan *et al*, 1991; Shy *et al*, 1996). We then removed the dbcAMP, leaving the cells in SATO medium and harvest them at different time points, lysed them and determined c-Jun expression by Western Blot. As shown in figure R13A, c-Jun expression was already upregulated at 2 hours, increased further at 5 hours and was almost maximal at 10h post dbcAMP removal. To learn if c-Jun upregulation depends on some of the components of the SATO medium, such as insulin, we repeated the same experiment in DMEM with no additives. As shown in figure R13B, a similar result was obtained, ruling out the possibility that c-Jun upregulation could be stimulated by the SATO medium.

Schwann cells secrete factors, such as GDNF and NRG1, that could theoretically activate intracellular signaling pathways and stimulate c-Jun upregulation (Jessen & Mirsky, 1999; Xu *et al*, 2013). To discard this possibility in our setting, we repeated the experiment refreshing the DMEM every 30 minutes during a total of 10 hours. In this way any potential secreted factor would be washed out. The cells were then harvested and c-Jun expression levels checked by Western Blot. Interestingly, the profile of c-Jun upregulation was not changed by avoiding the accumulation of secreted factors in the incubation medium (Figure R13C). Furthermore, c-Jun upregulation was insensitive to lapatinib, a dual Erb1/Erb2 receptor tyrosine kinase inhibitor, which discards c-Jun induction by neuregulin juxtacrine signalling (Kumler *et al*, 2014) (figure R13D). Together, our data suggest that c-Jun upregulation after cAMP removal in Schwann cells is cell-autonomous.

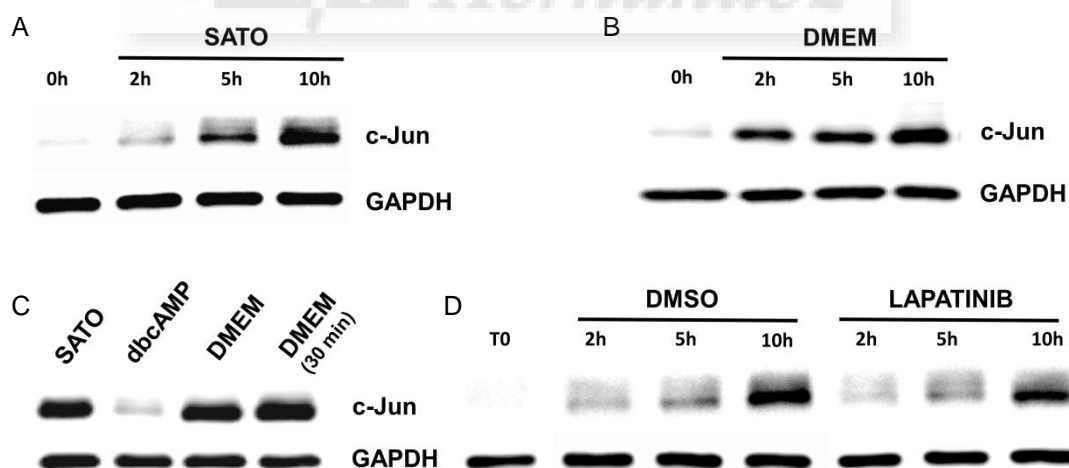


Figure R13: c-Jun re-expression after removal of dbcAMP is cell-autonomous. (A) Western Blot from Schwann cells incubated in SATO during 2, 5 and 10 hours after a 48h incubation with dbcAMP. (B) Western Blot from Schwann cells incubated in DMEM during 2, 5 and 10 hours after a 48h incubation with dbcAMP. (C) Western Blot from Schwann cells incubated with dcAMP during 48 h, followed by 10h in SATO alone, 10h in dbcAMP, 10 hours in DMEM alone, and 10 hours in DMEM replacing the medium every 30 minutes. (D) Western Blot from Schwann cells treated with dbcAMP for 48h and then, after dbcAMP removal, treated with lapatinib or DMSO (control). Cells were collected at different timepoints. T0 stands for cells treated only with dbcAMP for 48h. The same amount of total protein was loaded from each sample. GAPDH was used as loading control. Each experiment was repeated at least 3 times. Representative WBs are shown.

2.4 Signalling pathways controlling c-Jun upregulation

2.4.1 NRG1 accelerates c-Jun expression

We have observed that in *NSE-SMDF^{+/+}* transgenic mice there is a notable increase in expression of c-Jun in peripheral nerves (data not shown). Also it has been shown that exposure of DRG-Schwann cell cultures to high concentrations of NRG1 increases c-Jun expression levels in the Schwann cells (Parkinson *et al*, 2008). In light of these data, we decided to explore whether NRG1 affects the kinetics of c-Jun expression in cultured Schwann cells from the moment they are released from the inhibitory effect of dbcAMP. For this purpose we incubated the cells with 1mM dbcAMP during 48 hours and then removed the dbcAMP and incubated the cells with SATO medium or with SATO plus recombinant NRG1 (rNRG1). In figure R14, we can see the c-Jun protein levels in Schwann cells incubated with SATO alone or SATO plus rNRG at 2 and 5 hours after dbcAMP withdrawal. As previously shown in the cells incubated with SATO alone, two hours after dbcAMP withdrawal, c-Jun was already upregulated and the expression levels became higher five hours after. When rNRG1 (10ng/ml) was added at the same time as we released the cells from dbcAMP, there was a premature increase of c-Jun expression that led to a temporary peak in c-Jun expression levels after two hours. However, after this peak, the levels of c-Jun expression decreased and became similar to the c-Jun levels in the cells incubated in SATO alone. This result suggests that rNRG1 increases c-Jun expression in a temporal way. The effects of NRG1 towards enhancing c-Jun expression seem to be mediated through the JNK pathway, since the addition of SP600125, a selective inhibitor of JNK1 and JNK2 (Bennett *et al*, 2001), in combination with rNRG1 prevented the upregulation of c-Jun (Fig. R14).

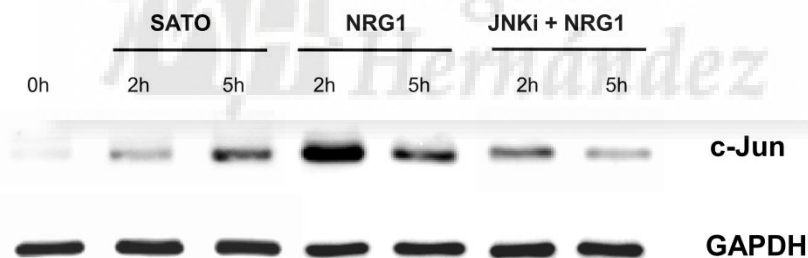


Figure R14: c-Jun induction after dbcAMP withdrawal is accelerated upon NRG1 addition. Western Blot using protein extracts from cultured Schwann cells that were incubated in 1mM dbcAMP for 48 hours and, after dbcAMP removal, incubated with SATO containing NRG1 (10ng/ml), NRG1 plus SP600125 (JNKi, 30 μ M) or SATO alone (as control). The cells were collected just before dbcAMP removal (0h) and 2 and 5 hours later. Incubation with anti-c-Jun and anti-GAPDH (for loading control) antibodies. The same amount of protein was loaded from each sample. n=3. A representative WB is shown.

2.4.2 JNK pathway mediates self-autonomous c-Jun expression after dbcAMP removal

We then decided to check which signaling pathways are involved in the Schwann cell autonomous c-Jun upregulation. To this aim we used inhibitors for different pathways that are activated in Schwann cells by NRG1 signalling (Birchmeier & Nave, 2008). After 48 hours of dbcAMP 1mM incubation, cells were incubated in SATO medium with different pharmacological inhibitors. We used the ERK1/2 inhibitor U126 (10 μ M), the PI-3 kinase inhibitor LY294002 (20 μ M), and the JNK inhibitor SP600125 (30 μ M). We collected the cells just before dbcAMP withdrawal and at different time points after addition of the inhibitor. As control we used Schwann

cells incubated only with SATO after dbcAMP withdrawal. After harvesting the cells, we extracted the total protein content and checked the c-Jun protein levels by Western Blot. As we can observe in figure R15, U126 did not prevent c-Jun expression, but the JNK inhibitor SP600125 prevented c-Jun upregulation (figure R15).

The *c-jun* promoter contains AP-1 binding sites and it is well established that c-Jun binds to them and positively regulates its own transcription, giving rise to a positive feedback loop (Angel *et al*, 1988). It has also been suggested that phosphorylation of c-Jun by JNK increases the capacity of c-Jun in enhancing *c-jun* transcriptional activation by de-repression of the promoter (Weiss *et al*, 2003). Together with our data, a model emerges in which, when cAMP levels decrease, *c-jun* promoter becomes de-repressed and the few c-Jun molecules existing in the cell, phosphorylated by JNK, bind to the promoter and activate *c-jun* transcription, which is low in the beginning, but as more c-Jun molecules are synthesized, transcription increases due to the positive feedback loop..

We also observed that the widely used inhibitor of the PI3K pathway, LY294002, was also able to block c-Jun upregulation. This was unexpected, as it has been shown by others (Maurel & Salzer, 2000; Ogata *et al*, 2004) that the activation of the PI3K has a positive effect in Schwann cell differentiation and myelin formation (see discussion).



Figure R15: Inhibition of JNK prevents c-Jun upregulation after dbcAMP removal. Western Blot showing c-Jun induction in Schwann cells incubated with 1mM dbcAMP for 48 hours (T0) and, after dbcAMP removal, treated with different pharmacological inhibitors. DMSO was used as control. Cells were collected at different timepoints from the addition of the inhibitor. Under treatment with U126, the induction of c-Jun was not altered, but both treatment with LY (PI-3 kinase inhibitor) and with SP600125 (JNK inhibitor) prevented c-Jun induction. The same amount of total protein was loaded from each sample. GAPDH was used as loading control. n=3. A representative WB is shown.

2.4.3 NRG1 induces c-Jun temporal upregulation in dbcAMP differentiated Schwann cells

We wanted to know if the c-Jun upregulation induced by NRG1 was prevented by elevation of intracellular cAMP. After 48h of incubation in 1mM dbcAMP, we added rNRG1 (10 ng/ml) to Schwann cells, and maintained dbcAMP in the incubation medium. We collected the cells after 2, 5 and 10 hours and then extracted the protein and performed a Western Blot using anti-c-Jun antibody. As shown in figure R16, when rNRG1 was added in combination with dbcAMP to these cells, there was an initial upregulation of c-Jun during the two first hours, but 10 hours later, c-Jun was completely downregulated by dbcAMP.

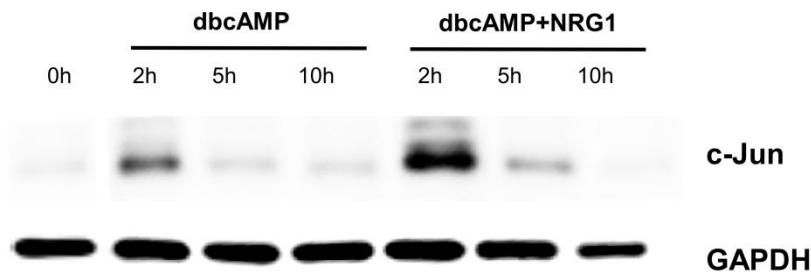


Figure R16: dbcAMP overcomes NRG1 dependent c-Jun induction in cultured Schwann cells. Western Blot showing c-Jun expression in cultured rat Schwann cells treated with 1mM dbcAMP alone or dbcAMP plus NRG1, previously incubated in SATO with 1mM dbcAMP during 48h (T=0h). Cells collected at different timepoints. The same amount of total protein was loaded from each sample. GAPDH was used as loading control. n=3. A representative WB is shown.

2.5 HDAC4 is involved in dbcAMP induced c-Jun downregulation

At this point we wanted to address the question of how elevated levels of cAMP in the Schwann cell downregulate the expression of c-Jun. Vascular smooth muscle cells (VSMCs) are, like Schwann cells, derived from the neural crest, and adopt an activated status after injury that allows them to proliferate, migrate and secrete growth factors. The activated phenotype is pivotal for vascular repair and as soon as this is terminated, VSMCs return to the differentiated phenotype (Owens *et al*, 2004). Interestingly, the activated phenotype is associated with c-Jun upregulation. The expression of c-Jun in these cells is controlled by Histone Deacetylase type 4 (HDAC4), which inhibits the transcriptional activity of Myocyte Enhancer Factor 2 (MEF2) at the *c-jun* promoter (Du *et al*, 2008; Gordon *et al*, 2009). HDAC4 belongs to the class II HDACs family of histone deacetylases, which in contrast to the other HDACs families, have no deacetylase activity. Whereas class I and class III HDACs are expressed ubiquitously in most cell types, the expression of class II HDACs is highly restricted. In addition, class I HDACs are localized only in the cell nucleus while class IIa HDACs shuttle in and out of the nucleus and their cellular distribution depends on their interaction with other proteins (Fischle *et al*, 2002). Interestingly, the shuttling of HDAC4 between the nucleus and the cytoplasm is regulated by the levels of cAMP through the Protein Kinase A (PKA) pathway (Gordon *et al*, 2009).

The absence of intrinsic deacetylase enzymatic activity in HDAC4 is the consequence of the substitution of a tyrosine residue in the catalytic pocket by a histidine, at position 976 in the human protein (Haberland *et al*, 2009). Despite this, HDAC4 has a strong repressing activity on

some transcription factors, such as MEF2 (Lu *et al*, 2000) RUNX2 (Vega *et al*, 2004) and FOX (Mihaylova *et al*, 2011). It has also been shown that HDAC4 interacts with SMRT/N-CoR-HDAC3 complexes via its C-terminal domain (612-1084). In this way HDAC4 becomes part of a protein complex that can recruit the deacetylase activity of the HDAC3, a type I deacetylase, to different promoters.

2.5.1 HDAC4 translocates to the nucleus in the developmental transition towards myelinated nerves

c-Jun is highly expressed in immature Schwann cells. However, around P5, at the start of myelination, c-Jun expression decreases and remains low in the mature intact nerve (Parkinson *et al*, 2008). In light of these data, we were interested to see whether the subcellular location of HDAC4 changes along with the transition from immature un-myelinated nerves in P1 mice to fully myelinated nerves in P20 mice. For this purpose, we extracted sciatic nerves from C57BL/6J wild type mice of different ages: P1, P5, P11 and P20. After embedding the nerves in OCT, they were frozen at -80 °C and subsequently cut in 10 µm sections in a cryostat. The sections were then fixed with paraformaldehyde and immunostained with anti-HDAC4 and anti-c-Jun antibodies. Images of the stained sections were obtained with an inverted confocal microscope. In addition, we used some of the sciatic nerves to look at their structure with toluidine blue staining. In figure R17, the fluorescence immunostaining showed that HDAC4 appears to be localized in the cytoplasm of the Schwann cells at early postnatal stages. However, once the nerve starts to become myelinated, HDAC4 is concentrated in the nuclei of the cells as it co-localizes with the Hoescht staining (not shown). We can see the difference especially in the transition from P5, in which HDAC4 shows a typical cytoplasmic staining and c-Jun nuclear staining is rather high, towards P11, in which HDAC4 staining becomes nuclear and c-Jun staining is decreased. The toluidine blue staining shows the myelination state in each developmental stage.

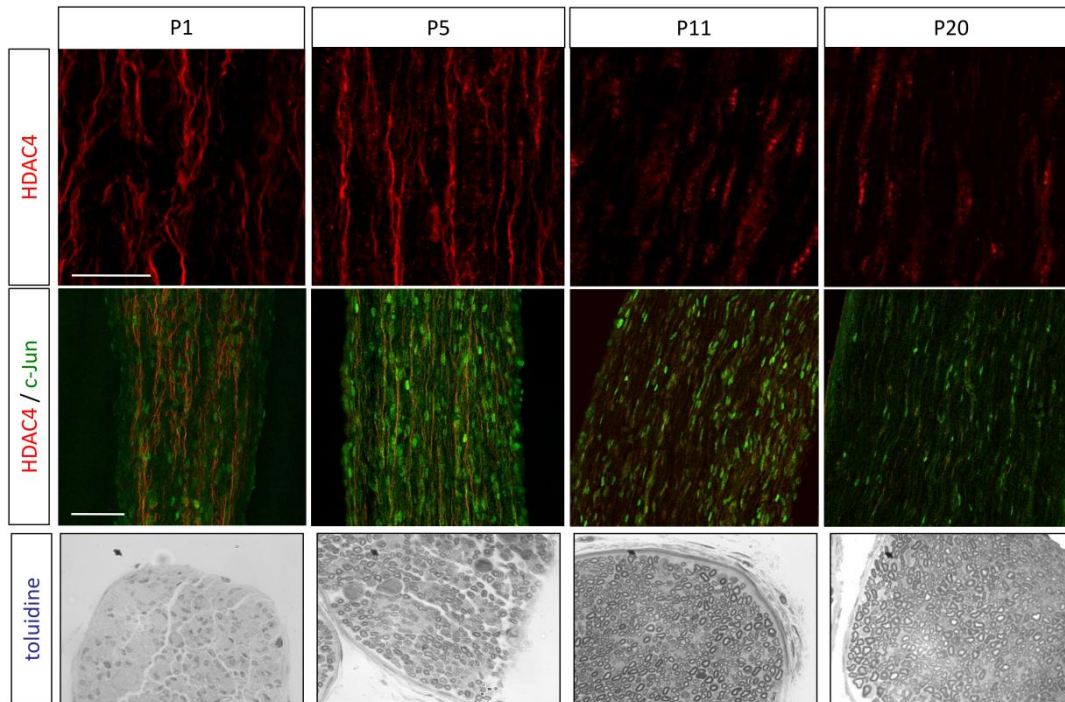


Figure R17: HDAC4 translocates to Schwann cell nuclei during PNS development. The first two rows show confocal images from sciatic nerve sections extracted from wild type mice at P1, P5, P11 and P20. Cryostat sections were stained with anti-HDAC4 and anti-c-Jun antibodies. HDAC4 labelling gave a typical Schwann cell cytoplasmic staining in P1 and P5 whereas it was concentrated in dots in the nuclei in P11 and P20 mice. c-Jun nuclear staining gradually decreases from P5 to P20. Scale bars = 50 μ m. The third row shows toluidine staining of resin embedded nerves. At P1 myelinating fibers are inexistent, afterwards axon sorting and myelination start, and the process is completed by P20.

2.5.2 cAMP translocates HDAC4 into the nucleus of Schwann cells

In order to analyze whether cAMP levels also modulate the cellular distribution of HDAC4 in cultured Schwann cells, we used a plasmid encoding the human full-length HDAC4 with a GFP-tag (HDAC4-GFP) under a CMV constitutive promoter, kindly provided by Professor Claudio Brancolini, from the Department of Medical and Biological Sciences at the University of Udine (Paroni *et al*, 2004). This plasmid was used to transfect cultured rat Schwann cells. We then incubated the transfected cells with SATO or with SATO plus 1mM dbcAMP during 4h, after which the cells were fixed and immunostained with an anti-GFP antibody. As we can see in figure R18A, in Schwann cells with SATO medium the fluorescence of HDAC4-GFP was clearly excluded from the nucleus and remained mainly confined to the cytoplasm. In contrast, after a 4h incubation with 1mM dbcAMP, most of the cells showed HDAC4-GFP in the nucleus, although in most of them fluorescence remained visible in the cytoplasm as well. To objectively determine the translocation of HDAC4-GFP, we quantified the average fluorescence intensity in the regions of interest (ROI) in the nucleus and the cytoplasm for each cell, and defined the localization of HDAC4-GFP by the nucleo/cytoplasmic ratio of intensities (see methods). As shown in figure R18B, dbcAMP produced a marked nuclear localization of HDAC4-GFP. This observation is quite relevant, since the function of HDAC4 is markedly regulated by agents that control its subcellular localization (Li *et al*, 2012; Wang & Yang, 2001). By favouring the shift of HDAC4 to the nucleus, cAMP may facilitate the access of HDAC4 to its targets, such as the *c-jun* promoter, for transcriptional control.

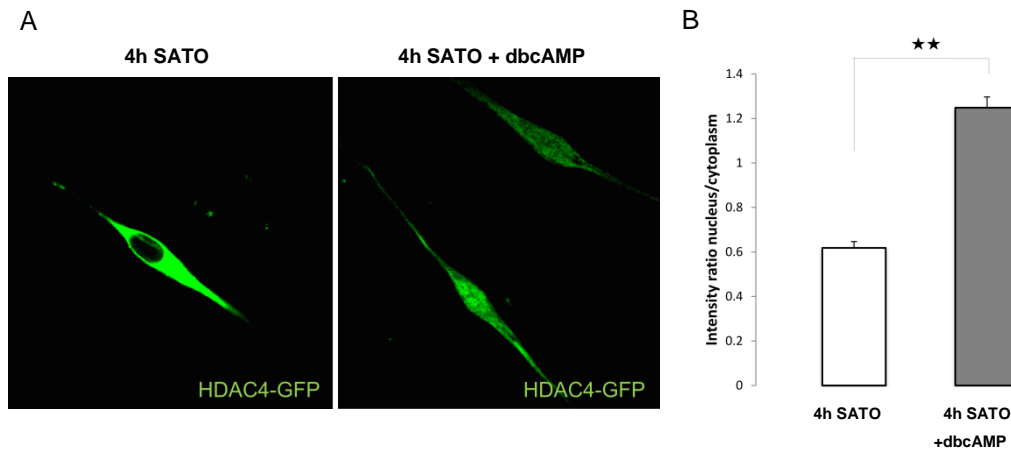


Figure R18: cAMP elevation translocates HDAC4 to the nucleus. (A) Schwann cells transfected with the HDAC4-GFP construct were incubated for 24h in SATO and subsequently during 4h in SATO with 1mM dbcAMP or SATO alone. The cells were then fixed and immunostained with anti-GFP antibody. Nuclei were labelled with Hoestch (not shown in the images). In SATO, GFP staining excludes the nucleus whereas in dbcAMP the distribution is more uniform. (B) The graph shows the nuclear intensity of c-Jun staining in the transfected HDAC4-GFP cells. The values are expressed as ratio between intensity of staining in the nucleus versus cytoplasm. Schwann cells incubated in SATO show more intensity of the signal in the cytoplasm, whereas in Schwann cells incubated with dbcAMP the nucleus is more stained than the cytoplasm. t-test **P= 0.0078; A minimum of 200 cells were analyzed for each condition in 3 different experiments.

2.5.3 MEF2 contributes to c-Jun expression in basal conditions *in vitro*

Studies performed in vascular smooth muscle cells show that the nuclear translocation of HDAC4 upon elevation of cAMP levels contributes to *c-jun* repression by interaction with MEF2 (Gordon *et al*, 2009). HDAC4 has been shown to physically interact with MEF2D and to function as a co-repressor in other cell types too (Fitzsimons *et al*, 2013; Kozhemyakina *et al*, 2009; Li *et al*, 2012; Lu *et al*, 2000). In light of these data, we first wanted to determine the expression of *Mef2* in Schwann cells and compare the expression levels of the different *Mef2* isoforms (*a*, *b*, *c* and *d*). For this we performed RT-qPCR with cDNA synthesized from RNA extracts obtained from cultured rat Schwann cells. As shown in figure R19A, we detected *Mef2a*, *c* and *d*. However we could not detect *Mef2b*. Taking in account that the amplicons were designed to be similar in size, the Ct can be used as a measure of the abundance of each transcript. Our data suggests that *Mef2d* is probably the most abundant *Mef2*, followed by *Mef2a*, in cultured Schwann cells. In the case of mouse sciatic nerves, we detected the expression of *Mef2a* and *Mef2d*, of which *Mef2a* was more abundant. When we compared nerves from P3 and P20 wild type mice, we could observe that both the expression of *Mef2a* and *Mef2d* decreases in the transition from immature nerves to fully myelinated nerves (Figure R19B).

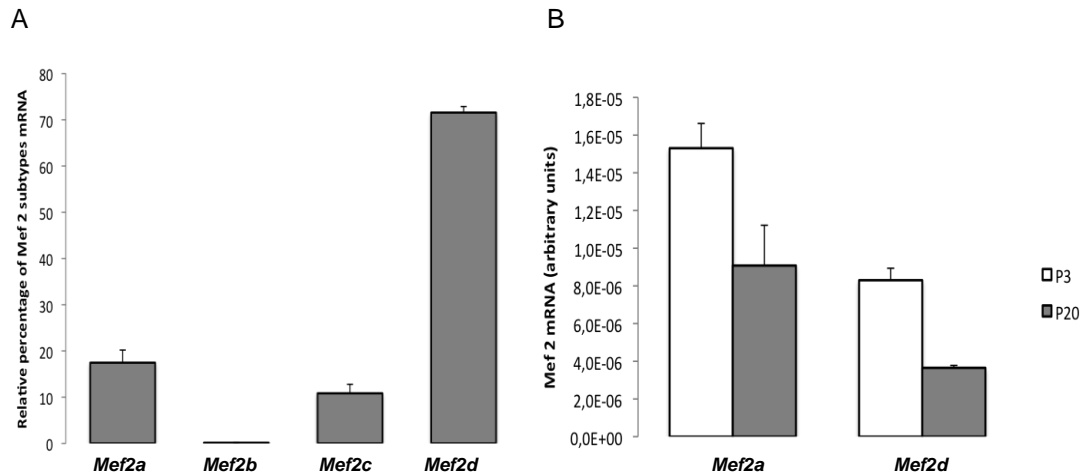


Figure R19: *Mef2* is expressed in Schwann cells. (A) The graph shows the proportion (in percentages) of messenger RNA of each of the four *Mef2* isoforms in cultured rat Schwann cells (100% would be the sum of all of them together), measured by RT-qPCR. GAPDH was used as housekeeping. The error bars correspond to experimental standard deviation, n=1. (B) Transcript expression of *Mef2a* and *Mef2d* in absolute values, measured by RT-qPCR. The cDNA used was synthesized with RNA extracted from sciatic nerves from P3 and P20 wild type mice. The error bars correspond to experimental standard deviation. n=1.

We next decided to explore whether MEF2 could regulate the transcription of the *c-jun* promoter in Schwann cells as well as it does in VSMCs. It has been shown that a fragment of 375 nucleotides around the ATG is able to reproduce many of the properties of the *c-jun* promoter (Clarke *et al*, 1998). This fragment harbors different consensus sequences for the binding of distinct transcription factors. One of these sequences is a binding site, at position -59, for the MEF2 family members, including MEF2-A, -B, -C and -D. Interestingly there is also an AP-1 binding site at position -72, which can bind to CREB, AP-1 (c-Jun/c-Fos) and ATF proteins (Clarke *et al*, 1998; Han *et al*, 1992) (Fig. 20A). In order to discriminate the extent to which these two elements in the *c-jun* promoter are involved in the regulation of *c-jun* in cultured rat Schwann cells, we performed luciferase reporter gene assays. We used pGL3-luciferase vectors that contained positions -225 to +150 of the mouse *c-jun* promoter and had point mutations at different sites within the promoter (Clarke *et al*, 1998). The first construct had the intact *c-jun* promoter sequence (labeled as *c-jun* prom WT) (addgene n°11979); the second construct had two point mutations in the MEF2 binding site (*c-jun* prom Δ MEF2) (addgene n°11980); the third had four point mutations in the ATF binding site (*c-jun* prom Δ ATF) (addgene n° 11980); the fourth construct had both ATF and MEF2 binding sites mutated (*c-jun* prom Δ ATF/ Δ MEF2) (addgene n°11982). We wanted to know the contribution of the MEF2- and ATF-binding sites to the basal transcription levels of *c-jun* upon a 24h incubation with SATO medium. For this purpose, cultured Schwann cells were transfected with the different luc-*c-jun* promoter constructs: *c-jun* prom WT, *c-jun* prom Δ MEF2, *c-jun* prom Δ ATF and *c-jun* prom Δ ATF/ Δ MEF2. In each well, Schwann cells were co-transfected with one of these constructs, and a β -galactosidase reporter construct containing the constitutively active CV40 promoter, in order to normalize for transfection efficiency. Twenty-four hours after transfection, the cells were incubated in SATO during 24 h. Subsequently, we lysed the cells and performed the assay for determination of the luciferase and β -galactosidase activity (see methods).

As we can see in figure R20B, mutations in the MEF2 binding site repressed transcription by about 50%, whereas having a mutated ATF site did not affect the basal transcription levels. This suggests that basal transcription of *c-jun* in cultured Schwann cells depends partially on MEF2 transcriptional activity.

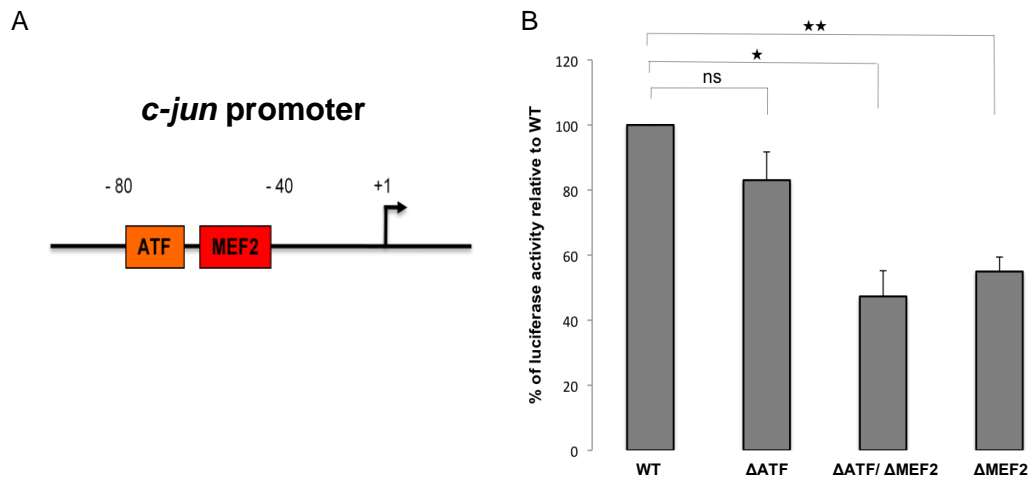


Figure R20: Mutation in MEF2 binding site reduces expression of luciferase-*c-jun* promoter construct.

(A) Schematic representation of ATF and MEF2 positions in *c-jun* promoter. (B) Luciferase activity detected in Schwann cells transfected with the different luc-*c-jun* promoter constructs: *c-jun* prom WT (no mutations), *c-jun* prom ΔMEF2 (construct with mutated MEF2 site) *c-jun* prom ΔATF (construct with mutated ATF binding site), and *c-jun* prom ΔATF/ ΔMEF2 (construct with both mutations). Luciferase signal was recorded after incubation in SATO for 24h. Values expressed in percentage of luciferase activity relative to *c-jun* prom WT. t-test ns P=0,12, *P=0,018,**P<0,001. n=4. In all cases the cells were co-transfected with a β-galactosidase reporter construct containing the constitutively active CV40 promoter to correct for transfection efficiency.

2.5.4 Loss of HDAC4 function (shRNA) prevents c-Jun downregulation by cAMP analogs

In light of the previous results, we wanted to learn if the decrease of c-Jun expression caused by elevation of intracellular cAMP levels in Schwann cells is mediated by HDAC4. In order to study this, we used several approaches based on loss of function and gain of function experiments. First, we decided to analyze if the repressive effect of dbcAMP on c-Jun expression is maintained when HDAC4 levels in the Schwann cells are decreased. In other laboratories, HDAC4 protein levels have been efficiently knocked down by RNA interference (Kao *et al*, 2003). We therefore decided to use iRNA short hairpin constructs to downregulate HDAC4 expression in cultured Schwann cells. For this aim we obtained a plasmid encoding a short hairpin designed against HDAC4 (pENTR/U6 HDAC4 shRNA, addgene n° 32220) (Mihaylova *et al*, 2011) and generated a lentivirus assembled with the Gateway technology (see methods). We also generated a lentivirus harbouring a pENTR/U6 empty-vector, assembled in the same way, to use as a control. In both cases, the destination vector included GFP under the CMV promoter. Cultured rat Schwann cells were then infected with a lentivirus encoding the short hairpin designed against HDAC4 or with the empty-vector control. We waited a total of 7 days from the infection day to ensure optimal expression of the construct. At this point, we incubated the infected cells during 24 hours with 1mM dbcAMP in SATO. Subsequently, the cells were harvested and the total protein content was extracted for Western Blotting using anti c-Jun antibody. We wanted to compare the effect of 24h dbcAMP incubation in the shHDAC4 infected cells with the cells infected with the control. We could still observe a strong inhibition of c-Jun by dbcAMP, although the shHDAC4 exerted a

small but consistent effect, partially blocking the inhibition of c-Jun expression (Figure R21A). To explain why we have only a partial effect, we must first take into account the limited rate of infection of the Schwann cells, which is about 30%. Another aspect to be aware of is the fact that dbcAMP enhances the expression of HDAC4 in Schwann cells (as we can observe in figure R21C) which could partially mask the effect of the short hairpin. Finally there could also be some compensatory effect by other class II HDACs, since their MEF2 binding site is a 17 aminoacid motif which is conserved in all of them (Parra & Verdin, 2010)

Due to the mentioned limitations that could mask a stronger effect of shHDAC4 in the expression of c-Jun in Schwann cells, other members of my lab tested shHDAC4 in the RT4-D6P2T rat schwannoma cell line. This cell line displays features that resemble those of normal myelinating Schwann cells, such as the expression of myelin proteins (Hai *et al*, 2002). Transfection efficiency in these cells is very high, unlike the transfection/infection efficiency in Schwann cells, so at least in this regard the effects of shHDAC4 should be more emphasized using RT4D6 cells. Two days after transfection with shHDAC4 or with a shGFP (as control), the cells were incubated with dbcAMP during 24 hours and then harvested for Western Blotting. In this case we could clearly see that dbcAMP failed in downregulating the expression of c-Jun in the shHDAC4 transfected cells (Figure R21B). The downregulation of HDAC4 was also very clear in these cells, as we practically see no band for HDAC4.

To get a better appreciation of the expression of c-Jun in the cells infected with the shHDAC4 lentivirus, 7 days after infection, we seeded the infected Schwann cells onto properly coated coverslips. We incubated for 24h with SATO or SATO plus 1mM dbcAMP, fixed and finally immunostained the cells with antibodies against c-Jun and GFP. In figure R21D, we can observe that the nuclear c-Jun staining is generally low in Schwann cells incubated with dbcAMP, although it is important to point out that there are still some c-Jun expressing cells. Importantly, even though not all shHDAC4 infected cells showed an increased nuclear c-Jun staining, we could observe that there was a much higher frequency of cells with intense c-Jun staining in the shHDAC4 infected than in the control infected ones. To quantify c-Jun, we determined the ROI in the nucleus of Schwann cells immunolabelled with the anti-c-Jun antibody. The background was subtracted from the labelling of the cytoplasm (see methods). As shown in the graph in figure R21E, in Schwann cells infected with the shHDAC4 lentivirus the average levels of c-Jun were increased by more than two fold.

Together, our results suggest that the downregulation of c-Jun by cAMP is in part mediated by HDAC4.

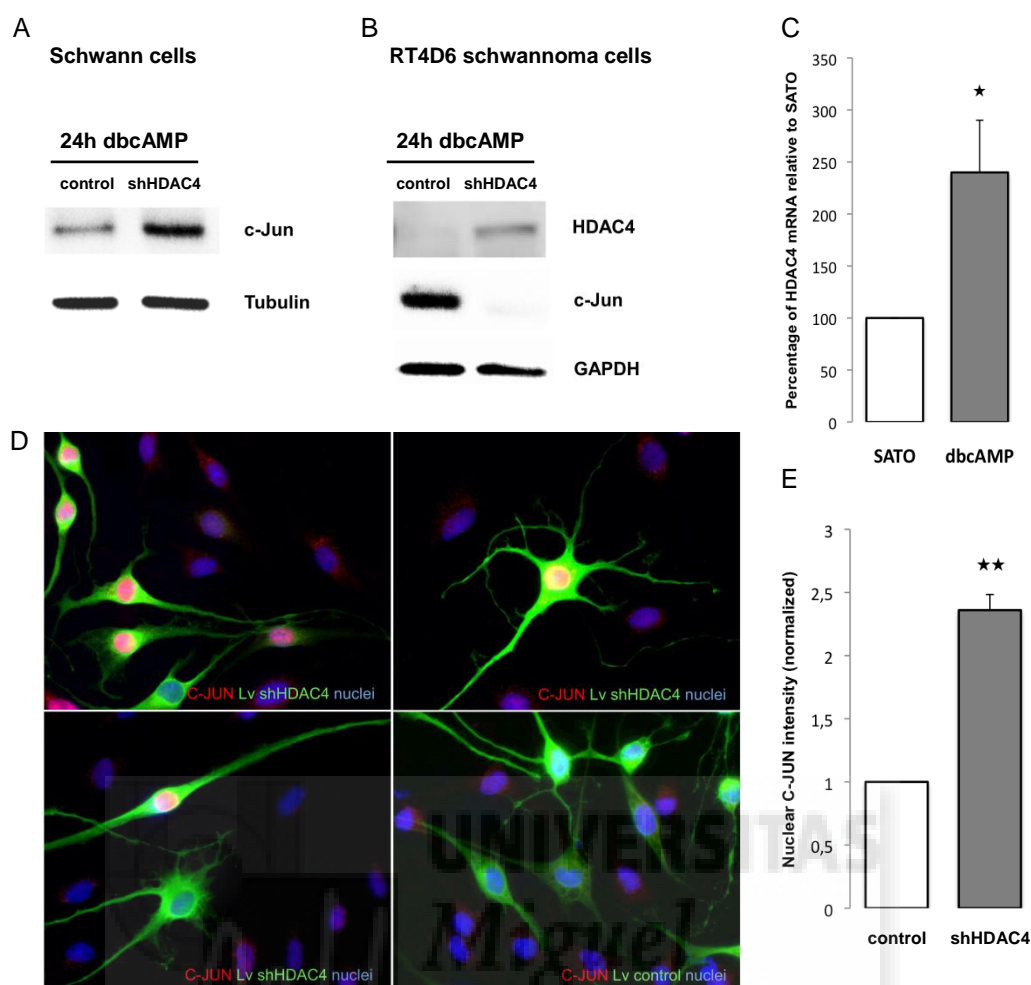


Figure R21: Loss of HDAC4 function (shRNA) prevents c-Jun downregulation by cAMP analogs.

(A) Western Blot from Schwann cells infected with shHDAC4-GFP lentivirus or empty-vector-GFP lentivirus as control. 7 days after infection, the cells were incubated with 1mM dbcAMP for 24 hours. The same amount of total protein was loaded from each sample. Tubulin was used as loading control. $n=4$. A representative WB is shown. (B) Western Blot with anti-c-Jun and anti-HDAC4 antibodies. Protein extracts from RT4D6 cells transfected with shHDAC4 or shYFP (control plasmid). The second day after transfection, the cells were incubated with 1mM dbcAMP for 24 hours. The same amount of protein was loaded from each sample. GAPDH was used as loading control. $n=3$. A representative WB is shown. (C) dbcAMP enhances HDAC4 expression: Levels of HDAC4 transcript expression in Schwann cells incubated with 1mM dbcAMP for 24h. Values expressed as percentage relative to the transcription levels in cells incubated in SATO. Measured by RT-qPCR. $t\text{-test}^*P=0,02$ $n=3$. (D) Immunostaining of cultured rat Schwann cells infected with shHDAC4-GFP lentivirus. 7 days after infection, the cells were incubated with dbcAMP for 24 hours and then fixed and stained against c-Jun and GFP. (E) 361 cells infected with shHDAC4 lentivirus and 450 cells infected with shYFP lentivirus (control) were analyzed from 3 different experiments. $t\text{-test}^{**}P<0,001$.

2.5.5 Gain of HDAC4 function leads to c-Jun downregulation

The function of class II HDACs is highly regulated through cellular compartmentalization. HDAC4 possesses a nuclear localization signal (NLS) in residues 244 to 279 (close to the N-terminus) and a nuclear export signal in the C-terminus (see figure R22A) (Wang *et al*). In addition, HDAC4 has a 14-3-3 binding region which is essential for cytoplasmic retention after nuclear export. The binding to 14-3-3 proteins is mediated by phosphorylation of residues Ser246, Ser467 and Ser632 in the human HDAC4 (Grozinger & Schreiber, 2000; Nishino *et al*, 2008). In line with our previous findings, we next asked ourselves whether an increase in the expression of

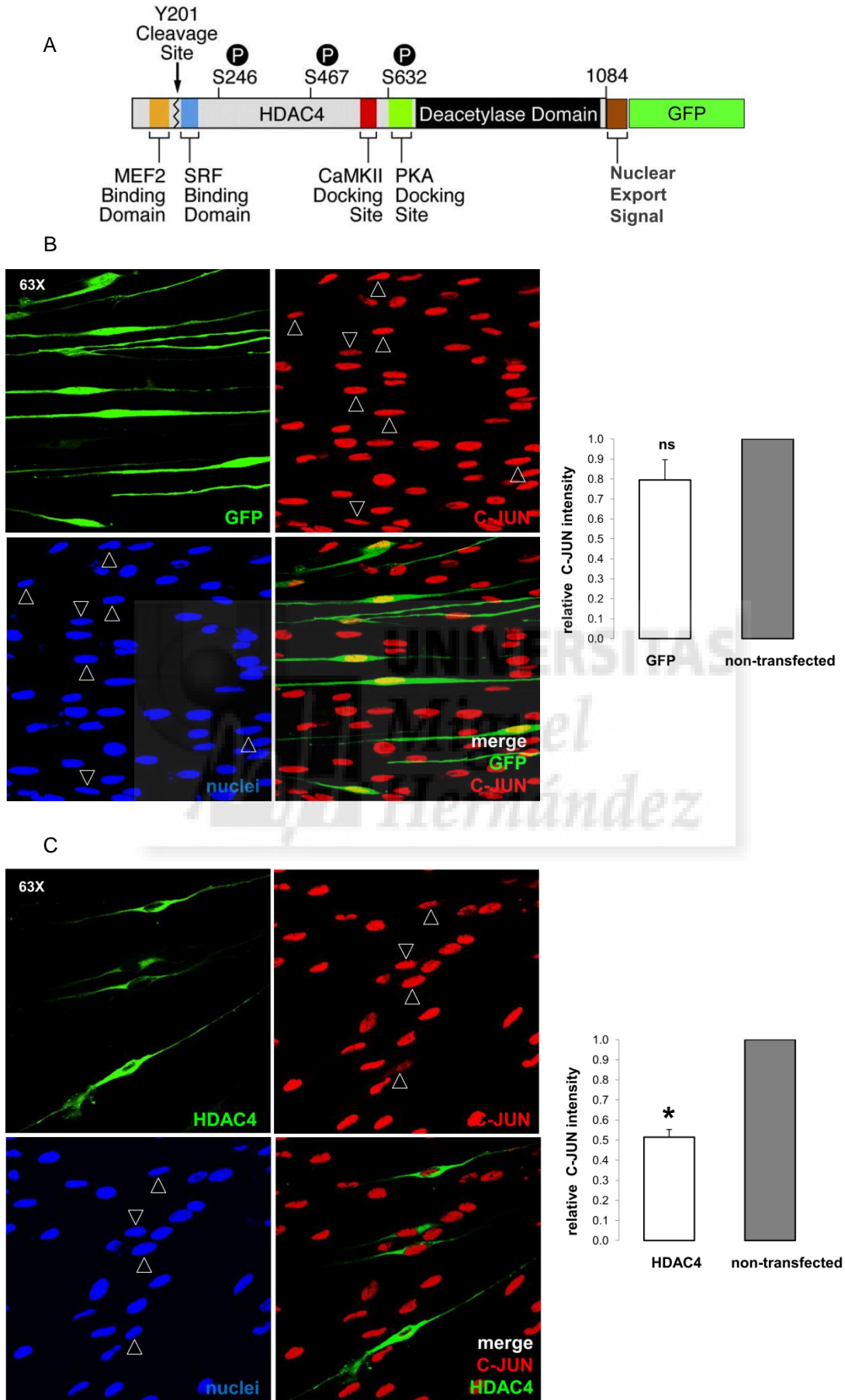
HDAC4 could inhibit c-Jun expression under normal culture conditions. As we have already mentioned, c-Jun expression is normally high in cultured Schwann cells. We decided to use SATO medium in order to minimize artifact effects caused by growth factors or compounds present in serum. Cultured rat Schwann cells were transfected with a plasmid encoding a GFP-tagged full-length HDAC4 under a CMV promoter. As a negative control, we used Schwann cells transfected with a plasmid encoding GFP under the same promoter. The transfected cells were left for 24h in SATO medium. We then fixed and stained them against c-Jun and GFP. As is shown in figure R22C, c-Jun staining intensity in the nucleus of most of HDAC4-GFP transfected cells was similar to the non-transfected cells. However, in some cells, c-Jun staining intensity was clearly lower than in non-transfected cells. This condition coincided with a tendency of having a strong GFP signal, a less bipolar morphology and having an enlarged nucleus. To have an objective measurement we quantified the intensity of the staining for c-Jun with the help of the MetaMorph analysis software (see methods). As a control we used GFP transfected Schwann cells. As shown in the graph in figure 22C, HDAC4-GFP transfected Schwann cells showed a decrease of c-Jun expression when compared with the GFP transfected cells.

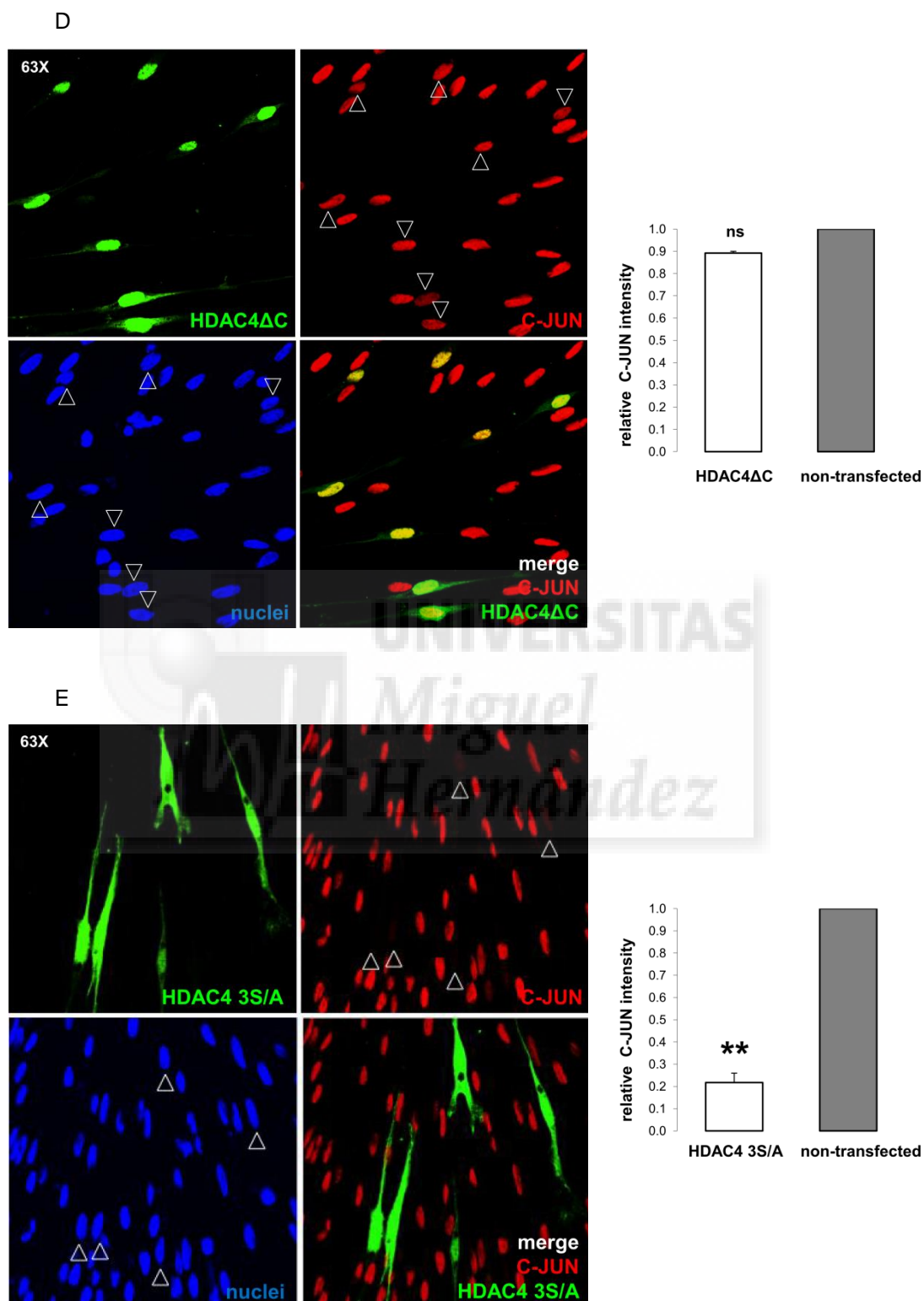
As aforementioned, HDAC4 regulates c-Jun expression in VMSCs by blocking the transcriptional activity of MEF2. To explore whether this is the case for Schwann cells as well, we generated a truncated form of HDAC4-GFP lacking the C-terminal domain (HDAC4 Δ C-GFP). This mutant lacks the NES and so gets accumulated in the nucleus, but, as shown in similar constructs by others (Backs *et al*, 2011), it retains the capacity to block the MEF2 transcriptional activity (see methods). As expected, this construct was localized mainly in the nucleus (Fig22D), where it can easily interact with MEF2 and other transcription factors. Surprisingly, we observed that the levels of c-Jun in these cells were not changed when compared to GFP transfected Schwann cells. In fact, c-Jun expression levels were clearly higher than in full length HDAC4-GFP transfected cells. This result suggests that the slightly negative effect caused by the full length HDAC4-GFP on c-Jun expression is mediated by the C-terminal domain and not by the repression of the transcriptional activity of MEF2. Thus we decided to use a construct that is able to spontaneously localize in the nucleus, but retains the C-terminal domain. As previously mentioned, the phosphorylation of serines S246, S467 and S632 promotes the retention of HDAC4 in the cytoplasm. Indeed, it has been shown that the mutation of these serines to non-phosphorylatable residues (HDAC4 3S/A) induces the nuclear localization of the construct. Therefore we decided to transfect this mutated form of HDAC4 tagged with GFP (HDAC4-GFP 3S/A) into Schwann cells and observe c-Jun expression by immunofluorescence. As shown in figure R22E, in most of the cells transfected with HDAC4-GFP 3S/A, c-Jun practically disappeared (see quantification in fig. R22E), supporting a role for the C-terminal domain of HDAC4 in the regulation of c-Jun expression in Schwann cells. This result was puzzling, as there is no known transcription factor binding site present in the C-terminal domain. Furthermore, HDAC4 has no deacetylase activity.

2.5.6 HDAC4 represses *c-jun* by recruiting HDAC3 through SMRT/NCoR1

Although initially it was found deacetylase activity associated to HDAC4 immunoprecipitates, later it was demonstrated that HDAC4 does not have intrinsic enzymatic activity. In fact, it was elegantly shown that the deacetylase activity found could be attributed to the contamination of the immunoprecipitates with HDAC3 (Fischle *et al*, 2002). The same authors demonstrated that HDAC4 interacts with HDAC3 through the NCoR1/SMRT co-repressor complex. Therefore, the *c-Jun*-repressing function of HDAC4 might require the involvement of HDAC3 for histone deacetylation. In order to test this hypothesis, we introduced a point mutation (D934N) in the HDAC4-GFP 3S/A construct (see methods), which has been shown to be sufficient to disrupt the interaction of HDAC4 with the NCoR1/SMRT/HDAC3 complex (Fischle *et al*, 2002). We transfected cultured rat Schwann cells with this construct, or with the original HDAC4-GFP 3S/A, to see whether the strong repressive effect of this construct towards *c-Jun* is lost when interaction with HDAC3 is prevented. After a 24h incubation in SATO medium, we fixed and stained the cells with GFP and *c-Jun* antibodies. Interestingly, we observed that *c-Jun* repression was partially blocked in the cells transfected with the HDAC4-3S/A that contained the D934N single point mutation to prevent HDAC3 recruitment (Figure R22F). This result demonstrates that *c-jun* repression by HDAC4 is probably mediated by the deacetylase activity of HDAC3.

Finally, we decided to perform a simple experiment to further test the involvement of the deacetylase activity of HDAC3 in *c-jun* repression by HDAC4. For this purpose we used trichostatin A (TSA), a widely used deacetylase inhibitor (Sanchez del Pino *et al*, 1994). After incubating Schwann cells with dbcAMP for 48h, we added TSA in the presence of dbcAMP, and collected the cells two or five hours later. We then extracted the total protein content and checked the levels of *c-Jun* by Western Blot. In figure R23A we can clearly see that TSA reverts dbcAMP induced *c-Jun* downregulation. This sustains that the deacetylase activity indeed mediates the ability of cAMP to downregulate *c-Jun*. In support of this view, we also observed that when the intact *c-jun* promoter-luciferase reporter construct (*c-jun* prom WT) was transfected into Schwann cells, where it remains mainly as an episome, the cotransfection with HDAC4-GFP 3SA produced no decrease in the luciferase activity (see figure R23B and discussion).





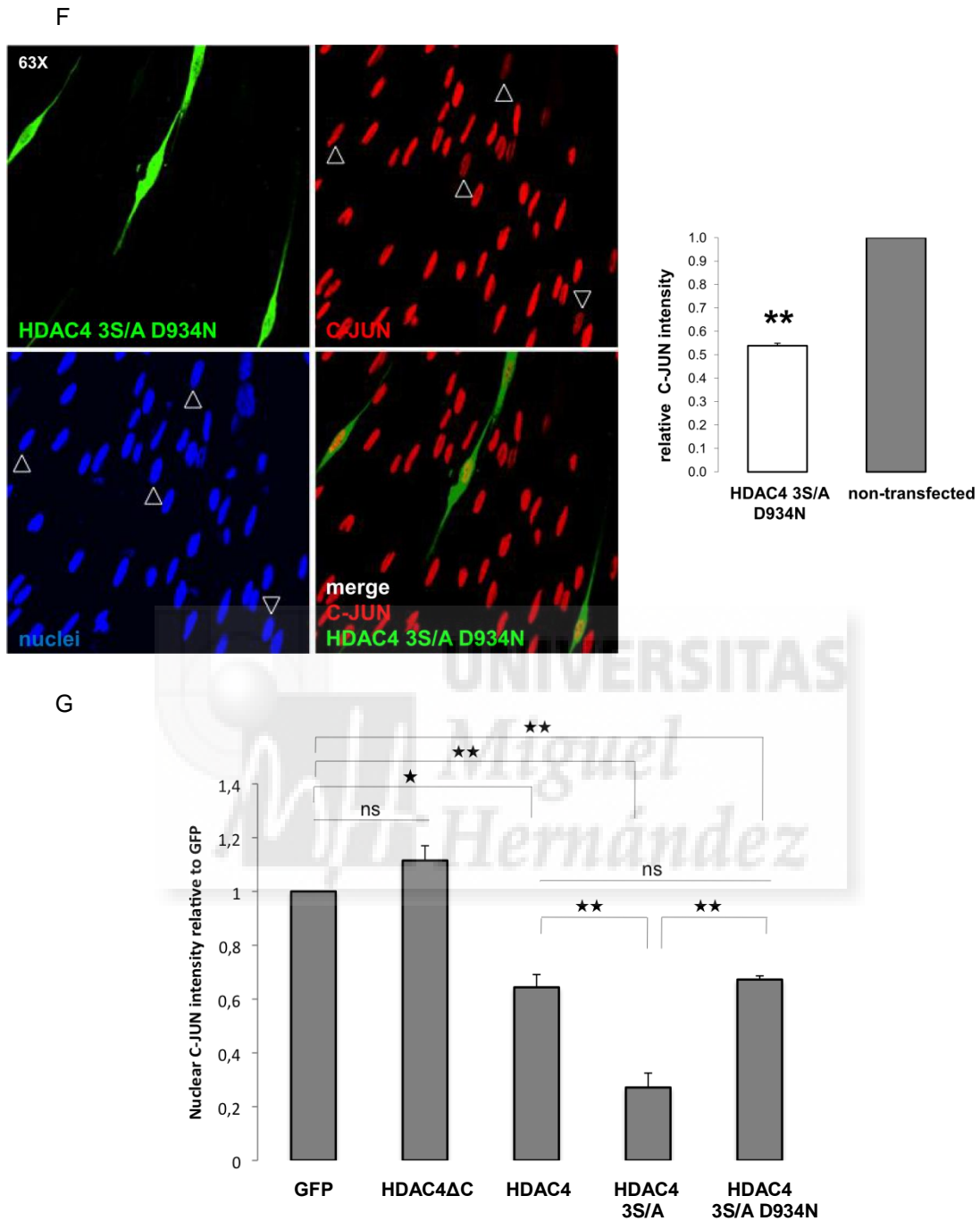


Figure R22: Gain of HDAC4 function leads to c-Jun downregulation. (A) Diagram showing the different domains of HDAC4. We include here the position of GFP in the GFP tagged-HDAC4 encoded in the vector. Cultured rat Schwann cells were transfected with the different HDAC4-GFP constructs, they were left in SATO for 24 hours, fixed and stained with anti-GFP and anti-c-Jun antibodies. Nuclei were labelled with Hoestch. Arrowheads show c-Jun nuclear staining in transfected cells. The graphs show the intensity of c-Jun nuclear staining in the transfected cells relative to the non-transfected cells from the same coverslips. A minimum of 300 transfected and 300 non-transfected cells were analyzed for each condition (B) Cells transfected with a GFP-encoding plasmid (control). t-test ns $P=0,12$. (C) Cells transfected with the intact, full HDAC4-GFP. t-test $*P=0,0498$. (D) Cells transfected with HDAC4ΔC-GFP. t-test ns $P=0,54$. (E) Cells transfected with HDAC4-GFP 3S/A. The transfected cells have practically no c-Jun staining. t-test $**P=0,0056$. (F) When interaction with HDAC3 is prevented, HDAC4-GFP 3S/A D934N is unable to inhibit c-Jun expression. t-test $**P<0,001$. (G) the graph shows a recopilation of the nuclear c-Jun intensity in the cells transfected with the different HDAC4-GFP constructs normalized with the GFP transfected cells.

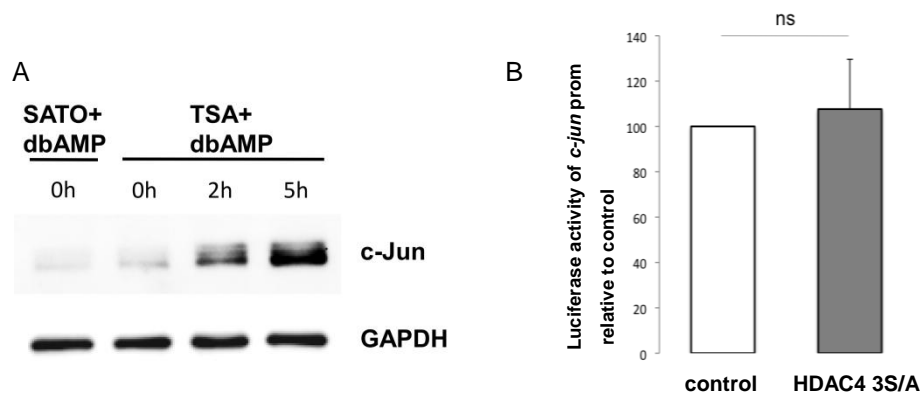


Figure R23: HDAC3 interaction is indispensable for c-Jun repression by HDAC4. (A) TSA treatment prevents dbcAMP induced c-Jun downregulation. Western Blot showing c-Jun expression in Schwann cells treated with TSA plus 1mM dbcAMP after different timepoints. The cells had been previously incubated with dbcAMP in SATO for 48h (T=0h). Cells collected at different timepoints. The same amount of total protein was loaded from each sample. GAPDH was used as loading control. n=3. A representative WB is shown. (B) HDAC4 does not suppress expression of the luciferase-*c-jun* promoter construct. Luciferase activity detected in Schwann cells co-transfected with the luciferase-*c-jun* prom WT construct in combination with HDAC4-GFP 3S/A, after 24h incubation in SATO. The cells were co-transfected with a β -galactosidase reporter construct containing the constitutively active CV40 promoter to correct for transfection efficiency. Values expressed in percentage of luciferase signal relative to the control (Schwann cells co-transfected with the luciferase-*c-jun* prom WT construct in combination with GFP). n=4. t-test: ns P=0,74.

2.6 The β -adrenergic receptors partially activate cell differentiation in cultured Schwann cells

The mechanism that controls cAMP levels in Schwann cells in the nerves is currently unknown. In this regard, Monk and colleagues made an important contribution when they found that the orphan adhesion G-protein-coupled receptor Gpr126, which is expressed in Schwann cells, is required to initiate myelination in zebrafish and mice (Monk *et al*, 2009; Monk *et al*, 2011). Their results indicated that Gpr126 functions by elevating intracellular cAMP levels at the onset of myelination. However, a recent study demonstrated that this receptor is essential for initiating myelination but not for the subsequent maintenance of myelin (Glenn & Talbot, 2013a). Glenn and colleagues could overcome the block at the promyelinating stage in Gpr126 mutants with a pulse of forskolin. These results indicate that the transition from promyelinating to myelinating phenotype requires an axonal signal that is recognized by Gpr126 receptor in Schwann cells. However, after initiation of myelination, there may be other axonal signals, recognized by other receptors within Schwann cells, which maintain the myelinating phenotype through the maintenance of high intracellular cAMP levels. Recently, there has been increasing evidence showing that axonal activity mediates myelination in both CNS and PNS (Fields & Stevens-Graham, 2002). Glial cells express receptors for several neurotransmitters (Magnaghi *et al*, 2009; Uggenti *et al*, 2014). There has been increasing evidence showing that neurotransmitters are involved in axon-glia cross-talk (Fields & Stevens-Graham, 2002; Uggenti *et al*, 2014). cAMP levels depend on G-protein coupled receptors and several neurotransmitters exist that can activate these type of receptors. We therefore decided to screen putative candidates that might activate cAMP and therefore maintain the Schwann cell in a differentiated myelinating state. We selected molecules that fulfill four requirements: They should bind to G-protein coupled receptors, be known to stimulate adenylate cyclase, be released along the axon and their receptors should be expressed in Schwann cells. The investigated molecules included carbachol, isoproterenol,

glutamate and CGRP. In addition, we decided to explore the effect of KCl as well, as it is released in the Nodes of Ranvier during axonal depolarization.

Carbacol is a muscarinic receptor agonist. Schwann cells express several muscarinic Ach receptors and it has been described that Ach can be released along cholinergic axons (Corsetti *et al*, 2012; Uggenti *et al*, 2014). Muscarinic receptors subtypes M2 and M4 couple to G proteins and modulate adenylate cyclase (Uchiyama & Chess-Williams, 2004)

The presence of CGRP receptors has been described in Schwann cells (Vause & Durham, 2010). CGRP is a potent stimulator of adenylate cyclase activity in Schwann cells (Cheng *et al*, 1995). It has been observed that noxious heat stimulation induces axonal release of CGRP in sciatic explants *in vitro* (Sauer *et al*, 2001).

Isoproterenol is a β_1 - and β_2 - adrenoreceptor agonist (Crompton, 2006). It has been described that adrenalin and noradrenalin are secreted by sympathetic neurons from varicosities along the axon (Teschemacher, 2005). Adrenergic receptors stimulate cAMP production in myocytes (Harvey & Hell, 2013). The expression of β_1 and β_3 adrenergic receptors has been detected in Schwann cells (Limberg *et al*, 2010).

It has been reported that glutamate is released by axons in the gray matter and by unmyelinated axons in the white matter (Ziskin *et al*, 2007). NMDA glutamate receptors are expressed in oligodendrocyte precursor cells (OPCs) and its stimulation *in vitro* promotes myelination (Li *et al*, 2013). The metabotropic glutamate receptors are G-protein receptors that are divided in three groups: I, II and III. Group II and III function by modulating cAMP levels (Willard & Koochekpour, 2013).

In order to explore the function of these candidates in Schwann cell myelination, we incubated rat cultured Schwann cells in the presence of each compound in SATO medium containing rolipram. Rolipram was added as it is an inhibitor of phosphodiesterase 4 (PDE4), which, as aforementioned, contributes predominantly to the degradation of cAMP. In this way, rolipram could prevent the putative masking effect that cAMP degradation could have in the repression of c-Jun expression. After 24h incubation we harvested the cells for Western Blotting. In this first screening with all candidates we only checked the levels of c-Jun, using it as differentiation marker. Among the different compounds, the only one that seemed to downregulate c-Jun, at least partially, was isoproterenol (Figure R24A). We next wanted to confirm this effect by incubating Schwann cells with different isoproterenol dosages ranging from 10 μ M to 10nM during a longer period of time, 72h. Comparing cells incubated with isoproterenol versus dbcAMP and SATO, we saw that isoproterenol had a very consistent effect of downregulating c-Jun at concentrations of 1 μ M and 10 μ M (Figure R24B). At these dosages, isoproterenol also promoted an upregulation of the myelination marker MAG. Comparing with the cells incubated with dbcAMP, these effects are very limited. Nevertheless, these results suggest that activation of β -adrenergic receptors in Schwann cells by catecholamines released along the axons may contribute to the maintenance of its differentiated phenotype in the adult nerve.

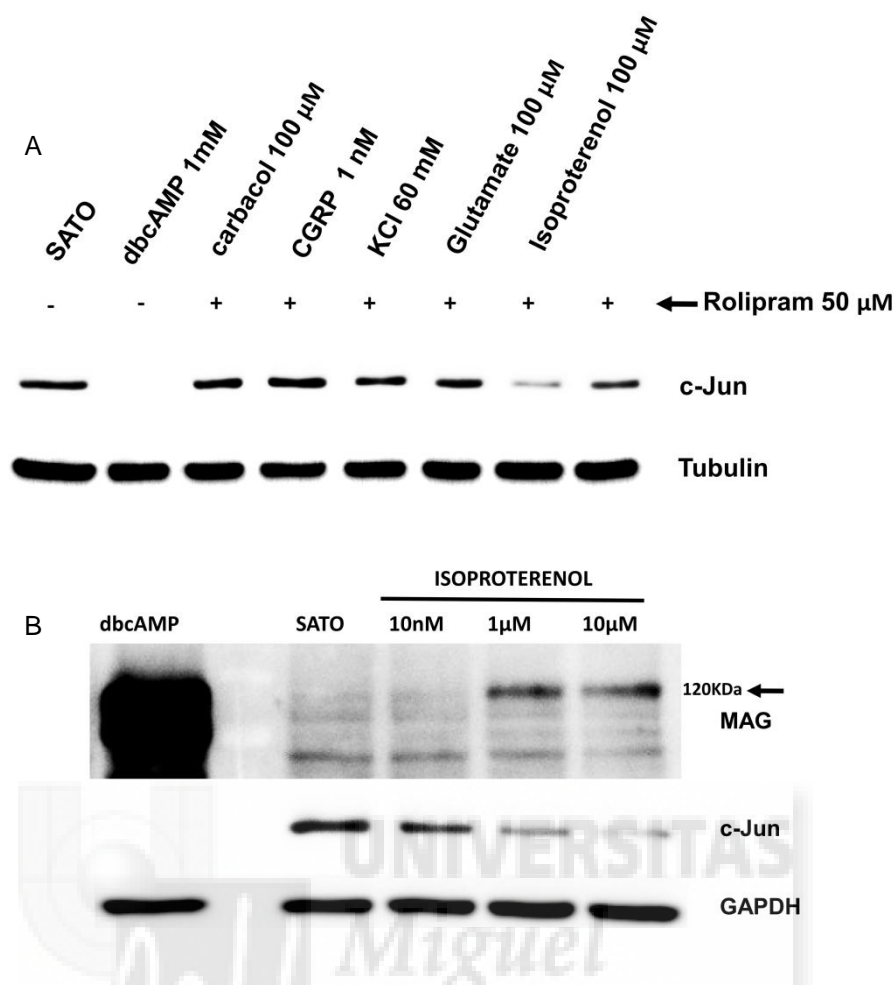


Figure R24: Incubation with isoproterenol lowers down c-Jun levels and higher up MAG levels in Schwann cells. (A) Western Blot showing c-Jun and MAG expression in cultured Schwann cells incubated with different molecules in SATO during 72h. Rolipram was added together with each of the molecules, but not in the cells incubated in SATO alone and in the cells incubated with dbcAMP. The molecules names and concentrations are indicated in the figure. The only one that gave a slight lower expression of c-Jun was isoproterenol (n=3). (B) Western Blot from Schwann cells incubated during 72 hours in SATO medium with dbcAMP and isoproterenol at 10nM, 1μM and 10μM. In the cells incubated with isoproterenol at 1μM and 10μM, there is a band at 120KDa that corresponds to MAG and the c-Jun band is much fainter than in the cells incubated with SATO. The same amount of total protein was loaded in every sample. We used anti-MAG as differentiation marker, anti-c-Jun as differentiation marker and anti-GAPDH as a loading control (n=5). A representative image is shown.



UNIVERSITAS

Miguel

Hernández

DISCUSSION

Control of Schwann cell proliferation in pathological conditions

In the postnatal period of nerve development, Schwann cell numbers need to be matched with axonal length for a correct myelination and thus conduction velocity of the axon (Sherman & Brophy, 2005). This is achieved by controlling Schwann cell survival and proliferation rates. Proliferation is regulated by axonal signals, and among them, NRG1 has been shown to be the major axonal mitogen. NRG1 supports Schwann cell survival as well (Jessen & Mirsky, 2005). NRG1 type III is probably the most important neuregulin isoform in the PNS since is strongly expressed in the motor and sensory neurons that project to the periphery. NRG1 type III is subdivided in two isoforms: NRG III β 1a and NRG III β 3. To study the physiological function of NRG III β 3, also called SMDF, our lab previously generated a transgenic mouse that overexpresses the human SMDF under the neuronal enolase (NSE) promoter. *NSE-SMDF*^(+/+) mice are characterized by nerve enlargement due to the hyperproliferation of non-myelinating Schwann cells during the first postnatal days (Gomez-Sanchez *et al.*, 2009).

Strikingly, Schwann cell hyperproliferation is halted in *NSE-SMDF*^(+/+) mice by the age of P14, giving rise to nerves that largely resemble the neurofibromas developed in neurofibromatosis type 1 (NF1). Interestingly, the benign nature of the neurofibromas in NF1 patients is also due to a limited growth in spite of persistence of tumourigenic stimulus (Carroll & Ratner, 2008; Harrisingh *et al.*, 2004; McClatchey, 2007). Given that NRG1 induced mitogenic stimuli continues to be received and transduced by Schwann cells in *NSE-SMDF*^(+/+) neurofibroma-like nerves, we reasoned that a mechanism for cell growth control may be activated.

Our results show that the Schwann cell growth in the *NSE-SMDF*^(+/+) neurofibroma-like nerves is eventually repressed via activation of the Oncogene-Induced Senescence program. The process of cellular senescence was first described by Hayflick and Moorhead in a seminal study (Hayflick & Moorhead, 1961). They observed that human fibroblasts entered in an irreversible state of growth arrest after serial cultivation. They also observed that, in contrast, cancer cells could not enter in this steady state. Hayflick and Moorhead hypothesized that this could be the cellular mechanism behind organismal aging. Years later, Serrano and colleagues demonstrated that the introduction of the RAS oncogene in fibroblast primary cultures leads to the activation of a mechanism that prevents the tumoral transformation of the cells, the so-called Oncogene-Induced Senescence (OIS) (Serrano *et al.*, 1997). They also found that the activation of OIS is mediated by the expression of the genes in the *Ink4a/Arf* locus. Nowadays cellular senescence is considered a stress response in the cell triggered by three different mechanisms, which are telomere shortening, accumulation of unrepaired DNA and chromosomal damage, and the activation of the *Ink4a/Arf* locus. Importantly, these mechanisms are also involved in protection against cancer. (Collado *et al.*, 2007).

While it has been demonstrated that p16Ink4 and p19Arf become accumulated in murine embryo fibroblasts (MEFs) and eventually lead to cellular senescence (Palmero *et al.*, 1998), it has been proposed that Schwann cells become immortalized, never reaching a state of replicative senescence (Mathon *et al.*, 2001). Although, in the same study, *p19Arf* and *p16Ink4a* became upregulated in these Schwann cells, the authors suggested that the cells could be insensitive to the effects of these genes in cell growth arrest. In contrast with these results, we found that most of our cultured Schwann cells do stop proliferating after eight to ten cell passages. Furthermore,

their morphology changes and their β -D-galactosidase activity is increased. These are all clear indications that Schwann cells eventually become senescent. Nevertheless, we also observed that few cultures continued proliferating after ten passages. Although we have limited clues to the cause of this effect, it could be possible that in the initial steps of the culture there is a selection of a spontaneous immortalizing mutation that potentially blocks the senescence program. However, because most of the Schwann cell cultures stop proliferating and have notably increased β -D-galactosidase activity, we concluded that Schwann cells, as most of the other cell types, can activate the senescence program.

The *Arf/Ink4a* locus, located at the chromosome 9p21, contains two overlapping genes, *p16Ink4a* and *p14/p19Arf*, that are regulated by distinct promoters and encode for two key tumor suppressors, the p16Ink4 and the p19Arf (p14Arf in human) proteins. After transcription and splicing, *p16Ink4a* and *p14/p19Arf* have a different 1st exon but share a common 2nd and 3rd exon. In spite of this, the two proteins are encoded with different reading frames (Arf: Alternative reading frame) and therefore they do not have any amino acid homology and are involved in different pathways (Gil & Peters, 2006) (Fig. D1). p16Ink4 recruits the cyclin-dependent kinases CDK4 and CDK6, preventing their binding to D-type cyclins. In this way, it inhibits the phosphorylation of retinoblastoma (Rb) family members by CDK4/6. This prevents the binding of E2F transcription factors to their target promoters to regulate the expression of essential cell cycle genes (Gil & Peters, 2006) (Fig. D2). Therefore, p16Ink4 leads to an imposed G1 cell cycle arrest, even in the presence of high levels of cyclin D1, as this will not be able to bind to CDK4 and CDK6. This could be the case in *NSE-SMDF^{+/-}* peripheral nerves, as they overexpress cyclin D1 (probably as a consequence of the overactivation of the ERK pathway) but also overexpress *p16Ink4a*, thus limiting the effects of the former. p19Arf protein stabilizes p53 tumour suppressor by inactivating the Mdmf2, an E3 ubiquitin ligase that degrades p53.

Using high throughput gene expression analysis by microarrays, other members of my lab found other genes involved in the establishment of replicative senescence that are upregulated in *NSE-SMDF^{+/-}* neurofibroma-like nerves (Gomez-Sanchez et al. Brain 2013). Among them, they found the upregulation of *p15Ink4b*, which is located next to the *Ink4a/Arf* locus (Gil and Peters, 2006), as well as a slight upregulation of *p53*. Another senescence gene that was remarkably upregulated is *Wnt16*, a gene that is overexpressed and secreted from cells undergoing Oncogene-Induced Senescence, both *in vitro* and *in vivo* in the murine model of KRasV12-induced senescence (Binet et al., 2009). These results suggest that a combination of independent mechanisms contribute to the establishment of the OIS program in Schwann cells in the neurofibroma-like nerves of *NSE-SMDF^{+/-}* mice.

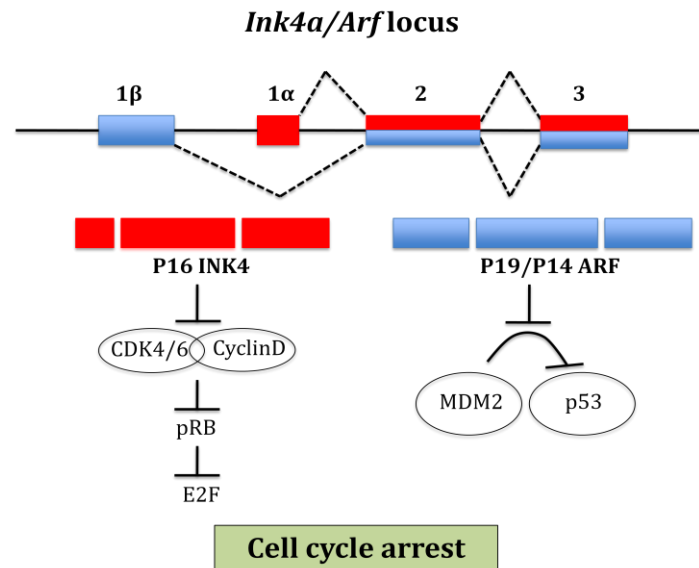


Figure D1: The *Ink4a/Arf* locus. The two products of *Ink4a/Arf* locus have a unique first exon but share a common second and third exons, in alternate reading frames. Both products lead to cell cycle arrest through different pathways. p16Ink4 inhibits the transcription of genes controlled by E2F transcription factors by blocking retinoblastoma protein de-phosphorylation. p19Arf stabilizes p53 by preventing its MDM2-mediated degradation. Adapted from Sharpless, 2005.

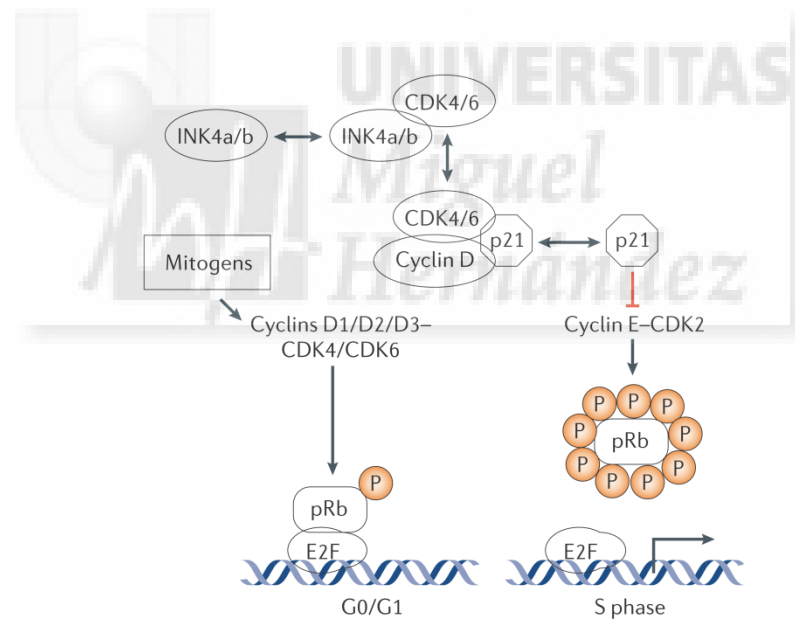


Figure D2: Effect of INK4 proteins on G1-S progression. Exit from quiescence and initiation of DNA synthesis requires the activation of cyclin D-dependent kinases CDK4 and CDK6 and the activation of cyclin E-CDK2, which through phosphorylating members of the retinoblastoma protein (pRb) family, activate the transcription of genes under the control of E2F transcription factors. INK4 proteins dissociate the assembly of cyclinD-CDK complexes by sequestering CDK4 and CDK6. This enables p21 to interact and inhibit CyclinE-CDK2, which leads to G1-phase cell-cycle arrest. (Gil & Peters, 2006).

Interestingly, OIS seems to be a general mechanism to avoid PNS tumour growth because, as in the *NSE-SMDF^{+/+}* mice, we found that the OIS program is activated in the plexiform neurofibromas developed by NF1 patients. This is in line with a study that showed, in human fibroblasts, the accumulation of p53 and phosphorylated Rb in response of hyperactivated RAS signalling due to the absence of NF1 (Courtois-Cox *et al*, 2006). The observation of tumour cell

senescence has been reported in humans before as well. The presence of senescence markers has been detected in melanomas (Michaloglou *et al*, 2005), in prostate intraepithelial neoplasias (Alimonti *et al*, 2010) and in colon adenomas (Kuilman *et al*, 2008).

Evolution favored the co-localization of *p16Ink4a* and *p14/p19Arf* in the same locus in the genome with the likely advantage of being regulated in block by the same chromatin-remodelling events. Because the expression of these two genes leads to p16Ink4-pRb and Arf-p53 triggered cell cycle arrest, the locus needs to be tightly regulated. Such control is achieved, at least partially, by the Polycomb Group of proteins (PcG) which participate in the PRC1 and PRC2 protein complexes. It has been demonstrated that the Bmi1-containing Polycomb-Repressive Complex I (PRC1) has a crucial role in the epigenetic silencing of the *Ink4a/Arf* locus. This has been done in studies in which Bmi-1 expression was turned on and off in MEFs (Jacobs *et al*, 1999). In a more recent work it was demonstrated that the binding of Bmi1-PRC1 to the locus is dependent on the trimethylation of histone H3 in Lys 27 (H3K27me3) done by a second complex, PRC2, which contains the histone methyltransferase EZH2 (Bracken *et al*, 2007). Later it was demonstrated that the activation of the *Ink4a/Arf* expression by the oncogenic RAS is mediated by the reversal of the PcG repression. This de-repression is achieved in MEFs both by the downregulation of the methyltransferase EZH2 and the activation of a specific demethylase called Jumonji D3 (Jmjd3) (Agger *et al*, 2009; Barradas *et al*, 2009).

The elevated levels of Jmjd3 in the neurofibroma-like nerves of the *NSE-SMDF^(+/-)* mice are an indication that this demethylase could contribute to the expression of *p16Ink4* and *p19Arf*. The decrease of H3K27me3 in the promoters of both *p16Ink4a* and *p19Arf* that we observed in the ChIP assay, suggests that the Jmjd3 expressed in the nerves is functional and has an active role in the de-repression of the locus. The role of Jmjd3 in the regulation of *Ink4a/Arf* in Schwann cells was further confirmed by transfection with a plasmid encoding *Jmjd3*, which was able to upregulate p19Arf expression in the cells. However, even though we could detect a clear increase of p19Arf, we did not see any difference in the levels of p16Ink4a, suggesting that in cultured rat Schwann cells, Jmjd3 might be necessary but not sufficient to de-repress the *p16Ink4a* gene expression. This is in line with previous studies showing that OIS induced growth arrest in MEFs cultures is dependant of *p19Arf* and not of *p16Ink4a* (Sharpless *et al*, 2004). Interestingly, in contrast with the results obtained in rodents, in human dermal fibroblasts (HDFs) Jmjd3 seems to activate *p16Ink4a* but not *p14Arf*. Barradas and colleagues showed that upon RAS signaling, only the promoter of *p16Ink4a* has a decrease of H3K27me3 in HDFs. They also showed that after transfecting HDF with HA-tagged *Jmjd3* constructs, the expression of *p16Ink4a* was increased and the expression of *p14Arf* was not affected. (Barradas *et al*, 2009). However, this *in vitro* data is inconsistent with our results obtained from mice and human tissues, since we detected expression of both *p19/p14Arf* and *p16Ink4a* in the neurofibroma-like nerves from *NSE-SMDF^(+/-)* mice as well as in human plexiform neurofibromas. In addition, we found a decrease of H3K27me3 in the promoter of both genes in the mice. Moreover, other *in vitro* studies show that, in contrast to MEFs, in other murine cell types such as lymphocytes, macrophages and astrocytes, cell growth arrest is predominantly dependant of *p16Ink4a* rather than of *p19Arf* (Sharpless, 2005). These inconsistencies between the *in vivo* and the *in vitro* data suggest that there are limitations when

inducing growth arrest in cultured cells, probably due to the culturing process. This could explain why p16Ink4 did not get upregulated in cultured Schwann cells transfected with *Jmjd3*, while *p19Arf* became upregulated. Taken together, these data suggest that histone de-methylation by *Jmjd3* induces the expression of one or both gene products encoded in the *Ink4a/Arf* locus, contributing to the establishment of the OIS program.

10% of NF1 human plexiform neurofibromas progress into malignancy (McClatchey, 2007). Interestingly, a similar percentage of the *NSE-SMDF^{+/+}* mice develop malignant tumours in nerve roots or in dorsal root ganglia. The abundance of pH3 positive cells in these malignant tumours indicates that their development results from the re-entry of Schwann cells into the cell cycle. We observed that the expression of *p19Arf* was blocked in most of these malignant tumours. In line with this result, it has been shown that components of the *Ink4a/Arf* locus are deleted in various human tumours, including melanoma, pancreatic adenocarcinoma, glioblastoma, certain leukemias and bladder carcinoma (Sherr & DePinho, 2000). However, in contrast with *NSE-SMDF^{+/+}* mice, most of these human tumours feature somatic loss of *p16Ink4a*, by point mutations or small deletions [reviewed in (Sharpless, 2005)], whereas somatic loss of *p14Arf* is less common, having been reported only in cases of colon cancer (Esteller *et al*, 2001). There could be two explanations for the selectivity of *p19Arf* in *NSE-SMDF^{+/+}* mice malignant tumours. First, *p19Arf* could represent a hot spot for mutations and so be preferentially hit by spontaneous mutations over *p16Ink4a*. A second explanation is that the loss of *p19Arf*, and not of *p16Ink4a*, could cause the Schwann cell cycle to resume. The second explanation would imply that *p19Arf*, and not *p16Ink4a*, could have a predominant role in the senescence-induced growth control in mice. This explanation is in accordance with a previous report showing that MEFs derived from *p19Arf* null mice experienced oncogenic transformation, whereas MEFs derived from *p16Ink4a* null mice did not (Sharpless *et al*, 2004). Although the OIS-induced responses of cultured mouse cells do not necessarily correspond with the mechanisms activated *in vivo*, the dramatic effect caused by the loss of one copy of *p53* in the double heterozygotes *p53^{+/-} NSE-SMDF^{+/+}*, which display malignant tumour formation in 100% of the cases, supports the crucial role of p19Arf-p53 in the maintenance of growth arrest in Schwann cells.

In addition to tumorigenesis, Schwann cells re-enter the cell cycle during the process of Wallerian degeneration, caused by nerve-injury. Denervated Schwann cells start proliferating and acquire a repair phenotype that depends on the expression of c-Jun (Arthur-Farraj *et al*, 2012). It has been described that in chronically denervated distal nerve stumps, proliferation of Schwann cells reaches a peak between 4-8 days post-injury, falls steeply during the second week and remains very low during months in the absence of regrowing axons (Hall, 1999; Scherer *et al*, 1994). This halted proliferation may be a consequence of the removal of locally produced or blood transported mitogens (such as soluble NRG1 gene products), but it could also be due to an active protection mechanism to prevent uncontrolled Schwann cell proliferation if the axons cannot reach the distal stump. In support of the latter hypothesis, we saw that *p19Arf* expression is rapidly induced after injury, suggesting that the senescence program has a role in preventing an overproliferation of denervated Schwann cells in the distal stump. *p19Arf* induction could be due to the activation of *Jmjd3* expression, whose levels were also increased in denervated Schwann cells.

The AP-1 family member c-Jun has a key role in many of the phenotypical changes that occur in denervated Schwann cells. AP-1 transcription factors bind to TPA-responsive element (TRE), a sequence that is found in many promoters. Three putative distal TRE sites have been indentified in the *p19Arf* promoter and it has been demonstrated that c-Jun-FRA-1 heterodimers bind to these sequences, activating the promoter and contributing to *p19Arf*-induced growth arrest (Ameyar-Zazoua *et al*, 2005). Also the promoter of *Jmjd3* contains two TRE sites and it has been shown that c-Jun containing-AP1 dimers activate *Jmjd3* expression in response of oncogenic stimulation (Lin *et al*, 2012). Although these data suggest that c-Jun could be involved in the activation of the senescence program in denervated, proliferative Schwann cells, experiments to address this question have not been performed yet.

In the crush injury experiments we observed that, as soon as re-inervation was achieved, marked by upregulation of Krox-20, *p19Arf* expression disappeared completely. Cellular senescence is characterized by a permanent and largely irreversible cell cycle arrest. However, it has been demonstrated that, under certain circumstances, senescent cells can be shifted into quiescent cells, which are characterized by stable but reversible growth arrest (Serrano, 2010). The axonal contact could therefore trigger some type of signal that reverts the senescence phenotype, which would be another example of the great plasticity that characterizes Schwann cells. Additionally, senescent Schwann cells could be eliminated by phagocytosis, which is an event that has been described to occur to senescent cells in tumours during the process of tumour regression (Xue *et al*, 2007). More experiments are necessary to distinguish between these two possibilities.

The increase in Schwann cell proliferation after sciatic nerve transection in *Ink4a/Arf^{-/-}* and *p53^{-/-}* mice (Fig R11), indicates that the activation of the senescence program in denervated Schwann cells contributes to proliferation arrest. While the effect on cell proliferation could already be observed 4 days post injury in *p53^{-/-}* mice, in *Ink4a/Arf^{-/-}* mice we could not observe changes in proliferation rates until up to 7 days after nerve transection. Because p19Arf functions by stabilizing p53, in *Ink4a/Arf^{-/-}* mice there might be still some active p53 molecules that inhibit proliferation. This could explain that the increased proliferation is observed earlier in *p53^{-/-}* animals in contrast with *Ink4a/Arf^{-/-}*. In summary, these results suggest that the senescence program is activated in Schwann cells after an injury, in order to prevent undesired Schwann cell over-proliferation in the distal stumps of the injured nerves.

Besides constituting a protective mechanism against overproliferation, activation of the senescence program in denervated Schwann cells could also contribute to the process of myelin clearance during Wallerian degeneration, since senescent cells often upregulate and secrete inflammatory cytokines to attract macrophages to the area (Xue *et al*, 2007).

Regulation of c-Jun expression in peripheral nerves

The transcription factor c-Jun is expressed in immature Schwann cells during postnatal development. In the adult nerve, c-Jun is expressed at very low levels, mainly by the non-myelinating Schwann cells of the Remak bundles. After a nerve injury, it is strongly re-expressed by denervated Schwann cells. c-Jun promotes dedifferentiation, inhibits myelination and plays a crucial role in the repair phenotype that Schwann cells display after injury (Arthur-Farraj *et al*,

2012; Parkinson *et al*, 2008).

To study how the expression of c-Jun is controlled after injury, we used explants of sciatic nerves. It has been shown that in nerve explants Schwann cells recapitulate the dedifferentiation process that they experience after a nerve injury (Shin *et al*, 2013). It is well established that elevation of cAMP in cultured Schwann cells mimics axonal contact, induces c-Jun downregulation and promotes differentiation (Jessen & Mirsky, 2005). Interestingly, it has been shown that there is a dramatic decrease in the intracellular levels of cAMP in Schwann cells after nerve injury. This suggests that the loss of the myelination program in the injured nerve could be the consequence of a loss in the capacity to maintain the levels of cAMP by Schwann cells. In this line, we observed that adding dbcAMP, which is a non-hydrolysable cAMP analog, prevented the upregulation of c-Jun and also prevented the downregulation of myelin proteins in sciatic nerve explants (Fig R12). Therefore, cAMP mimics axonal contact also in this system. Walikonis and Poduslo proposed that the decrease of cAMP levels after a nerve injury is due both to an increased cAMP hydrolysis by phosphodiesterase (PDE) activity and a decreased adenylyl cyclase activity (Walikonis & Poduslo, 1998). We observed that the sole induction of the endogenous adenylyl cyclase activity by forskolin inhibited c-Jun upregulation and MAG downregulation. Furthermore, the incubation with the PDE4 inhibitor rolipram alone did not have any effects in preventing dedifferentiation. This result indicates that the decrease of cAMP synthesis is the most determining factor to maintain cAMP levels in the nerve explant, although this does not rule out that an increase in phosphodiesterase activity could contribute in this system as well.

Together, these data suggest that cAMP activates a mechanism that represses c-Jun expression, increases c-Jun downregulation or both. To distinguish between these possibilities, we measured the levels of mRNA for c-Jun in Schwann cells treated with dbcAMP. As shown in figure R13, the mRNA levels for c-Jun are dramatically decreased, suggesting that cAMP blocks c-Jun biosynthesis. Although this does not rule out an effect on protein stability, the extremely short half life of c-Jun of about 30 minutes (Kayahara *et al*, 2005), suggests that a further increment in protein degradation velocity would not contribute significantly to the effects of cAMP on c-Jun.

When cAMP is removed, c-Jun becomes rapidly upregulated. Our results indicate that this upregulation is cell autonomous, as it happened even when the cells were incubated in DMEM alone. Moreover, when the incubation medium was changed frequently to avoid the accumulation of secreted factors, c-Jun expression remained unaltered. Altogether, our data suggests that cAMP activates a break that blocks c-Jun expression which, when removed, allows the expression of c-Jun in a cell autonomously way.

Our results suggest that JNK pathway is crucially involved in c-Jun upregulation upon dbcAMP removal. It has been shown that there are several AP1 binding sites within the promoter of *c-jun* and that phosphorylated c-Jun binds and efficiently activates its own transcription. Therefore JNK could participate in *c-jun* induction by phosphorylating c-Jun. Besides, JNK can modulate the activity of other transcription factors such as other Jun, Fos or ATF family members (Besirli *et al*, 2005), and these could also contribute in c-Jun upregulation. Surprisingly, we observed that the inhibition of PI3K-AKT pathway also prevented c-Jun induction, which might seem contradictory since this pathway has long been associated with promotion of differentiation and myelination in Schwann cells. However, PI3K-AKT also plays a crucial role in axon-contact

induced Schwann cell proliferation and survival (Maurel & Salzer, 2000). The effects of PI3K-AKT in c-Jun regulation could be mediated by cAMP response element-binding protein (CREB), since PI3K-AKT can activate CREB by phosphorylation (Kay *et al*, 2013), and it has been described that phosphorylated CREB binds the *c-jun* promoter and activates its transcription (Clarke *et al*, 1998).

In a previous study, Monje and colleagues showed that exogenous addition of growth factors such as PDGF, IGF, FGF, including neuregulin and FBS, do not have any effect on c-Jun expression (Monje *et al*, 2010). In contrast, we observed that the exogenous addition of recombinant neuregulin 1 (rNRG1) to cultured Schwann cells accelerates c-Jun induction after dbcAMP removal. However, rNRG1 only increases c-Jun levels temporarily, and after five hours c-Jun levels are similar whether rNRG1 is present or not. This supports the idea that c-Jun induction is basically dependent on cAMP reduction and does not depend of growth factors, even when these factors can modulate the speed at which c-Jun is re-expressed by Schwann cells. This temporal effect of rNRG1 could also explain the apparent discrepancies between our results and those of Monje *et al*, who determined the effects of growth factors on c-Jun levels at 3 days after cAMP withdrawal.

In Schwann cells, axonal neuregulin induces the activation of the PI3-kinase pathway and its downstream effectors AKT and PKC, as well as the MAP kinases ERK and JNK. As is the case in the cell autonomous upregulation of c-Jun, we observed that the inhibition of JNK blocks the effects of rNRG1. Monje and colleagues recently showed that, in the presence of elevated cAMP levels, neuregulin fails to induce c-Jun expression, regardless of the concentration used (Monje *et al*, 2010). In contrast, we observed that addition of rNRG1 in the presence of dbcAMP leads to a rapid, but temporal, enhancement of c-Jun expression (Fig R16). The only transient rise of c-Jun expression is probably due to NRG1 signaling no longer being able to compensate the repressive effects of cAMP on c-Jun expression after a few hours. The temporal effect of NRG1 could again reconcile our data with those of Monje *et al*, as their studies on c-Jun expression in Schwann cells are performed after a 3 day incubation with rNRG1 under cAMP stimulation.

To try to understand how c-Jun might be regulated in Schwann cells, we explored the literature, looking for examples of c-Jun regulation in other cell types. We found that vascular smooth muscle cells (VSMCs) have extremely low rates of proliferation, but that, like in Schwann cells, this can be induced by injury or insult to the vessel wall. Pathological loss of quiescence is triggered by the release of mitogens from platelets and VSMCs, which activate signalling pathways that stimulate the expression of cell-cycle genes. The inactivation of negative signals that normally repress VSMC proliferation is also required. Interestingly, cAMP is the best characterized inhibitor of VSMC proliferation, implicated in maintaining VSMCs quiescent and promoting healing after vessel injury. Elevated cAMP levels inhibit VSMC proliferation *in vitro* and *in vivo* after vascular injury, ultimately leading to a reduction in intima formation. In these cells, it has been shown that activation of PKA by increased intracellular cAMP levels, leads to nuclear accumulation of HDAC4, a specific class II histone deacetylase (Du *et al*, 2008). Interestingly, it has been demonstrated that HDAC4 is involved in the regulation of c-Jun expression associated with a proliferative phenotype in response to vascular injury in VSMCs (Gordon *et al*, 2009). The inhibition of c-Jun expression is achieved by blocking the transcriptional activity of MEF2 (Fig. D3). The fact that cAMP regulates c-Jun expression through HDAC4 in

VSMCs, and that Schwann cells and VSMC share a common origin in the neural crest cells (Woodhoo & Sommer, 2008), led us to explore the role of HDAC4 in *c-Jun* regulation by cAMP in Schwann cells.

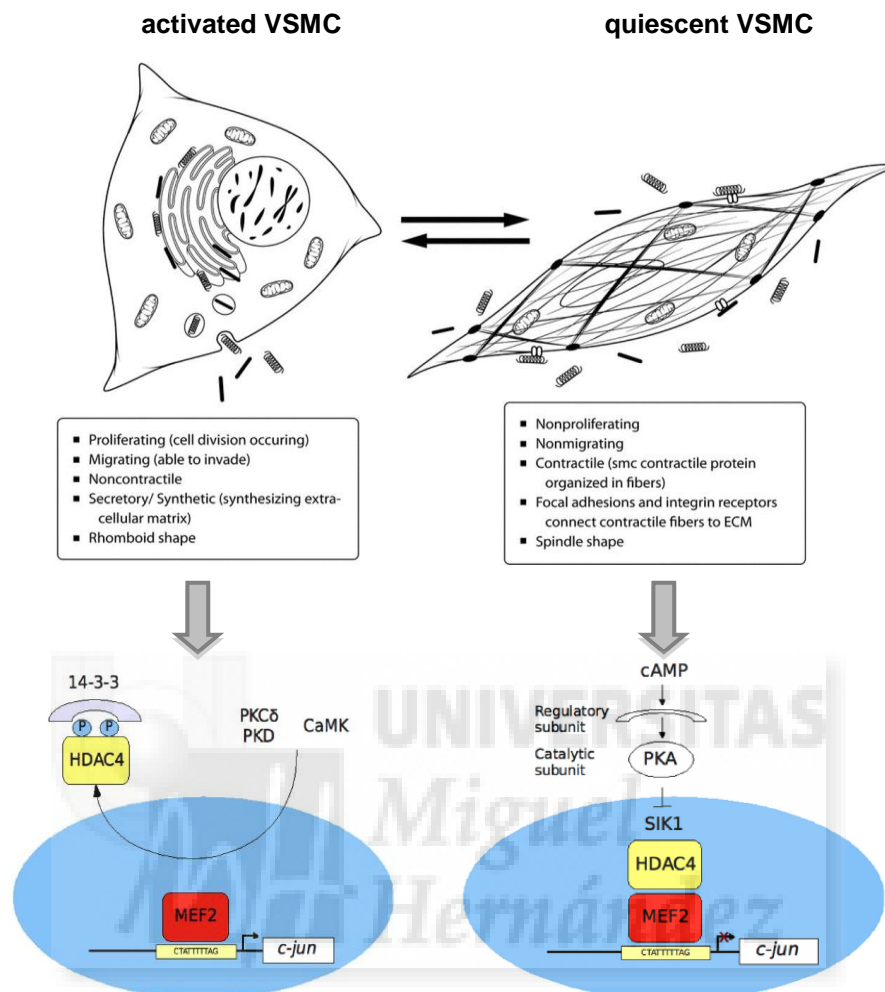


Figure D3: *c-Jun* regulation in quiescent and activated VSMCs. In quiescent conditions, *c-jun* expression is repressed by the HDAC4-MEF2 complex, promoted by PKA inhibition of SIK1. In activated, proliferative VSMCs *c-jun* expression is derepressed by CaMK induced nuclear export of HDAC4. Adapted from Gordon *et al*, 2009.

We found it very interesting that in early postnatal nerves, prior to nerve myelination, HDAC4 seemed to be localized predominantly in the Schwann cell cytoplasm, coinciding with high levels of *c-Jun* expression. This contrasted with the clearly nuclear localization of HDAC4 in mature, myelinated nerves, in which *c-Jun* expression is very low. Therefore, the axonal signals that induce differentiation and myelination in Schwann cells, including *c-Jun* downregulation, could also provoke the translocation of HDAC4 to the nucleus, which could be involved in the regulation of genes that play a role in the maintenance of myelination. Corroborating this idea, we observed that transfected HDAC4-GFP has a cytoplasmic distribution in cultured Schwann cells under basal conditions, clearly excluding the nucleus. In contrast, the addition of dbcAMP translocated HDAC4-GFP to the nucleus (Fig. R19). This is very significant, as the modulation of HDAC4 activity is largely achieved by controlling its subcellular localization (Parra & Verdin, 2010).

In order to explore the mechanisms by which HDAC4 could regulate the expression of *c-Jun* in Schwann cells, we first speculated that MEF2 could mediate the capacity of HDAC4 to block *c-*

Jun expression in Schwann cells, as it does in VSMCs. The myocyte family of enhancer factors 2 (MEF2A to -D) are involved in the regulation of muscle differentiation, neuronal survival and T-cell activation. MEF2A, -C and -D have been shown to physically interact with the class II histone deacetylases HDAC4 and HDAC5 in several types of cells. In addition, it has been shown that MEF2 interacts with the *c-jun* promoter and is involved in regulating its expression. In quiescent VSMCs, HDAC4 binds to MEF2 and acts as a corepressor, which leads to the downregulation of *c-jun*. This repression is largely abolished during conditions of cell growth, when HDAC4 is expelled from the nuclear compartment into the cytoplasm (Gordon *et al*, 2009; Lu *et al*, 2000). The four MEF2 factors share a high homology in the N'-terminal domain, which mediates DNA-binding affinity and interaction with transcription cofactors. The more divergent C'-terminal domain mediates transcription activation (Lu *et al*, 2000). We found that in sciatic nerves the more abundant isoforms are MEF2A and MEF2D, and their expression decreases during development as the nerve becomes myelinated.

MEF2 regulates the *c-jun* promoter by binding to a region in the promoter at -59, named the MEF2 binding site (Clarke *et al*, 1998). In addition to being regulated by MEF2, the *c-jun* promoter is also regulated by a series of transcription factors, which include CREB, AP1 dimers and ATF proteins. These transcription factors bind to the same region at -72, which is called the ATF binding site. As we mentioned before, c-Jun expression is high in cultured Schwann cells. Using a luciferase assay system with *c-jun* promoter constructs carrying mutations in ATF and MEF2 binding sites, we saw that the ATF binding site is not required for the transcription of *c-jun* in cultured Schwann cells under basal conditions. In contrast, the transcription is partially dependent on the MEF2 binding site, as it decreases by half when this site is mutated. Probably the reason why transcription partially occurs in the absence of the MEF2 binding site is because there are other important sites for *c-jun* induction apart from the ATF and MEF2 binding sites. It is important to emphasize that in this luciferase assay system, luc-*c-jun* promoter constructs remain mostly episomal in the cell nucleus and do not form the adequate physiological association with histones to fold into nucleosomes. Therefore, the transcriptional activation or repression that we see in this system depends only on regulation by transcription factors and does not take into account the effects of histone regulation.

The results showing HDAC4 translocation under cAMP elevated levels in Schwann cells, and the putative implication of MEF2 on *c-jun* expression based on the luciferase assays, prompted us to perform loss of function experiments of HDAC4 in Schwann cells. As is shown in Fig R22, when HDAC4 expression was decreased by infecting Schwann cells with a lentivirus encoding a shRNA for this protein, the capacity of cAMP to downregulate c-Jun was decreased. It is important to point out that although the shHDAC4 lentivirus led to a significant increase of c-Jun, it was not able to completely eliminate the capacity of cAMP to downregulate c-Jun. The partial effects reported can be explained by several non-mutually exclusive mechanisms. Firstly, we usually obtained infection efficiencies of about 30%, therefore the downregulation of c-Jun by cAMP in uninfected cells could partially mask the results in the Western Blots. This problem was overcome by looking at c-Jun levels in each infected cell with immunofluorescence. Secondly, we found an unexpected upregulation of HDAC4 by cAMP, both at the protein and at the mRNA level, which might prevent the shHDAC4 from blocking efficiently the HDAC4 expression. The

upregulation of HDAC4 by cAMP has never been reported before, but is interesting because, by promoting HDAC4 transcription, the cAMP signaling cascade could enhance the HDAC4-mediated cAMP effects. Finally, other class II histone deacetylases such as HDAC5 could compensate the effects that HDAC4 loss could have in c-Jun regulation. HDAC5 presents 70% of similarity with HDAC4 and also interacts physically with MEF2A, -C and -D in several type cells (Lu *et al*, 2000). Both HDAC4 and 5 can interact with SMRT/N-CoR repressor complex, and in muscle differentiation they both exert co-repression of MEF2 (Fischle *et al*, 2002). To consolidate our results we performed the shHDAC4 experiments in RT4D6 Schwannoma cell line, which, in contrast with Schwann cells, can be very efficiently transfected. dbcAMP induced c-Jun repression was largely blocked by shHDAC4 in these cells, supporting the view that HDAC4 has an active role in cAMP induced repression of c-Jun in Schwann cells.

After studying the HDAC4 loss of function, we decided to explore the effects of enhancing the function of this protein. As previously mentioned, c-Jun is highly expressed in cultured Schwann cells under basal conditions. In such conditions, an increase of the total levels of HDAC4 in Schwann cells by transfection with GFP-tagged HDAC4 resulted in a partial repression of c-Jun. The distribution of HDAC4-GFP in these cells seemed predominantly cytoplasmic. HDAC4 contains a nuclear localization signal (NLS) and a nuclear export signal (NES) that facilitates a continuous switch between nucleus and cytoplasm. Cellular compartmentalization is essential for the regulation of HDAC4 function and is achieved by interaction with specific factors (Wang & Yang, 2001). The nuclear exclusion of the HDAC4-GFP is mainly due to phosphorylation by Ca²⁺/calmodulin-dependent kinase II (CaMKII). The cytosolic anchor protein 14-3-3 binds to the phosphorylated HDAC4 and retains it in the cytoplasm. This mechanism has been described in proliferating VSMC (Nishino *et al*, 2008). The limited c-Jun repressive effect driven by HDAC4-GFP could be due to a preferential accumulation in the cytoplasm, reducing accessibility of HDAC4 to its targets and therefore preventing it from fully accomplishing its function. To enforce the nuclear accumulation of HDAC4, we deleted the C'-terminal domain of HDAC4 but maintained the MEF2 binding site, which is located in the very N'-terminal part of HDAC4 (Lu *et al*, 2000). As we expected, there was a strong nuclear accumulation when the C-terminal domain was deleted in the HDAC4 Δ C-GFP construct, since NES was absent and therefore CRM1 mediated nuclear export was prevented. Surprisingly, even though the MEF2 interacting site was intact in this construct, it did not exert any suppressive effect on c-Jun expression. The partial c-Jun downregulation achieved by HDAC4-GFP was lost in HDAC4 Δ C-GFP. This made us think that there is a region in the C-terminal domain that is fundamental for the repression of c-Jun by HDAC4. This was confirmed as transfection with HDAC4 3S/A, a mutant that cannot be phosphorylated by CamKII and thus cannot be retained in the cytoplasm, reduced c-Jun levels in a dramatic way. Although the cellular distribution of this construct was less confined to the nucleus than that of HDAC4 Δ C-GFP due to the presence of NES, which allows nuclear exportation, the effects on c-Jun expression were notable, strongly supporting the idea that HDAC4 plays an important role in cAMP induced c-Jun repression in Schwann cells.

As aforementioned, HDAC4 has no deacetylase activity, and most of its effects are mediated by the capacity of its N'-terminal domain to bind and block the activity of some transcription

factors such as Mef2 and Runx2 (Yao & Yang, 2011). When HDAC4 was first isolated, it was believed to have a strong deacetylase activity (Wang *et al*, 1999). Later it was elegantly shown that the deacetylase activity attributed to HDAC4 was the consequence of the capacity of HDAC4 to interact with HDAC3, which is a type I HDAC, through the SMRT/NcoR co-repressor complex (Fischle *et al*, 2002). When we modified HDAC4 3SA by introducing one single point mutation reported to interrupt HDAC3 interaction, the repressive effect of HDAC4 3SA on c-Jun was abolished. This result strongly suggests the requirement of histone deacetylase activity provided by HDAC3 for the HDAC4-dependent repression of c-Jun.

Interestingly this result could explain two of our observations. Firstly, we found that TSA, a widely used deacetylase inhibitor, reverted the cAMP-induced c-Jun repression, suggesting that deacetylase activity is indeed involved in the capacity of cAMP to downregulate c-Jun expression in Schwann cells. Secondly, in luciferase assays, the transfection with HDAC4 3S/A did not have any repressive effect on the transcription of the luc-*c-jun* promoter construct, which, as aforementioned, is episomal and therefore not influenced by histone regulation mechanisms.

Based on these results, we propose a model in which axonal induced cAMP signaling in Schwann cells leads to the nuclear translocation of HDAC4. Once in the nucleus, HDAC4 interacts in a yet undefined way with the promoter of *c-jun* and recruits the SMRT-CoR-HDAC3 complex, which, through histone deacetylase activity, represses *c-jun* transcription. The recruitment of HDAC4 to the *c-jun* promoter could be mediated by the interaction with MEF2 (Gordon *et al*, 2009), although this remains to be demonstrated and therefore open to speculation.

As aforementioned, it has long been suggested that a cAMP-dependent intracellular signal in Schwann cells mediates the axonal signals that drive the process of myelination. It has been demonstrated that the orphan Gpr126 receptor intervenes in the initiation of myelination. However, this receptor is not required for the maintenance of myelinating phenotype (Glenn & Talbot, 2013a; Monk *et al*, 2009; Monk *et al*, 2011). On the other hand, there is increasing evidence that indicates that the myelination-inducing signals depend on axonal activity (Fields & Stevens-Graham, 2002). Adrenergic receptors are G-protein coupled receptors that stimulate cAMP synthesis in different cell types. Their ligands, adrenalin and noradrenalin, are released along the axon in sympathetic neurons. Incubation of Schwann cells with isoproterenol, a β_1 - and β_2 -adrenoreceptor agonist, led to a partial but consistent induction of MAG, a positive marker of myelination, and to the repression of c-Jun, a negative myelination marker. Involvement of β -adrenoreceptors in cAMP signaling in Schwann cells has been reported before by Monje and colleagues. They showed that isoproterenol promotes PKA activity and synergistically enhances neuregulin-stimulated proliferation, ErbB2-ErbB3 activation and MEK-ERK/PI3K-AKT signaling (Monje *et al*, 2008). Furthermore, treatment of VSMCs with isoproterenol causes nuclear translocation of HDAC4 and repression of MEF2-driven transcriptional activity of *c-jun* (Gordon *et al*, 2009). Our results, although preliminary, suggest that adrenalin and/or noradrenalin released along the axonal length could participate in myelination induction or maintenance by interacting with β -adrenergic receptors in the Schwann cell membrane. The partial effect that we observed could mean that myelination is driven by a combination of receptors in Schwann cells, which could be differentially activated depending on the type of fiber they myelinate.



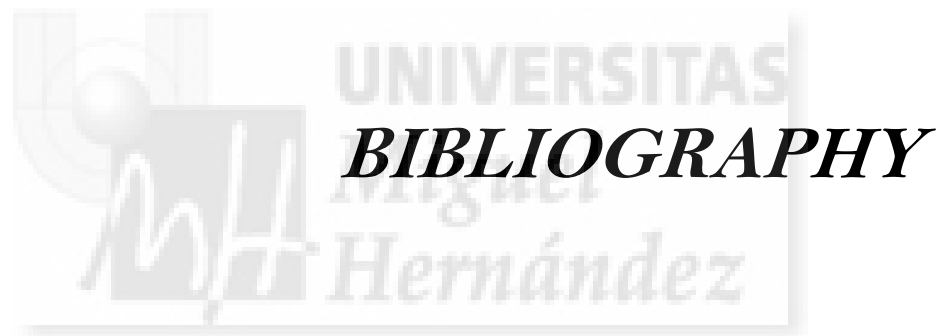
CONCLUSIONS

Las principales conclusiones que se pueden extraer de los resultados presentados en esta tesis son las siguientes:

1. La hiperproliferación de las células de Schwann inducida por la sobreexpresión de la NRG1 tipo III- β 3 en los ratones transgénicos *NSE-SMDF^{+/+}* es frenada mediante la activación del programa de OIS, consecuencia de la expresión del locus *Ink4a/Arf*.
2. La expresión de *p19Arf* and *p16Ink4a* en los nervios del ratón *NSE-SMDF^{+/+}* es activada, al menos en parte, por desmetilación de H3k27m3 en las regiones promotoras, mediada por Jmjd3.
3. La expresión de *p14Arf* y *p16Ink4a* sugiere que el programa de OIS bloquea también la proliferación en los neurofibromas plexiformes de los pacientes con NF1
4. El bloqueo de la vía p19Arf/p53 promueve la transformación maligna de los neurofibromas de los ratones *NSE-SMDF^{+/+}*.
5. La expresión del locus *Ink4a/Arf* contribuye al bloqueo de la proliferación de las células de Schwann tras las lesiones de los nervios periféricos.
6. La bajada en los niveles de AMPc media la desdiferenciación de las células de Schwann en los explantes de nervios.
7. La HDAC4 se transloca al núcleo en las células de Schwann en cultivo, en respuesta a la elevación de AMPc y también *in vivo* coincidiendo con el proceso de mielinización.
8. Una vez en el núcleo, la HDAC4 reprime la expresión de c-Jun reclutando la actividad deacetilasa de HDAC3 a través del complejo NCoR1/SMRT.
9. La activación de los receptores β -adrenérgicos activa parcialmente el programa de diferenciación de las células de Schwann en cultivo.

The main conclusions that can be drawn from the results presented in this thesis are the following:

1. The Schwann cell overproliferation induced by neuronal overexpression of NRG1 type III- β 3 in NSE-SMDF^(+/-) transgenic mice is halted through the activation of the OIS program, as a consequence of the upregulation of the *Ink4a/Arf* locus.
2. The expression of *p19Arf* and *p16Ink4a* in the nerves of NSE-SMDF^(+/-) transgenic mice is activated at least in part through H3k27m3 de-methylation by Jmjd3 in their promoters.
3. The upregulation of *p14Arf* and *p16Ink4a* suggests that the OIS program also blocks the proliferation in plexiform neurofibromas from NF1 patients.
4. The blockage of p19Arf/p53 pathway leads to the malignant transformation of neurofibromas from NSE-SMDF^(+/-) mice.
5. The expression of *Ink4a/Arf* locus contributes to the Schwann cell growth arrest after a peripheral nerve lesion.
6. The decrease in intracellular cAMP levels mediates Schwann cell de-differentiation in nerve explants.
7. HDAC4 translocates to the nucleus in cultured Schwann cells in response to cAMP elevation and also *in vivo* coinciding with the myelination process.
8. Once in the nucleus, HDAC4 represses *c-jun* expression by recruiting the deacetylase activity of HDAC3 through the NCoR1/SMRT complex.
9. The activation of β -adrenoreceptors partially induces the differentiation program in cultured Schwann cells.



- Agger K, Cloos PA, Rudkjaer L, Williams K, Andersen G, Christensen J, Helin K (2009) The H3K27me3 demethylase JMJD3 contributes to the activation of the INK4A-ARF locus in response to oncogene- and stress-induced senescence. *Genes Dev* **23**: 1171-1176
- Alimonti A, Nardella C, Chen Z, Clohessy JG, Carracedo A, Trotman LC, Cheng K, Varmeh S, Kozma SC, Thomas G, Rosivatz E, Woscholski R, Cognetti F, Scher HI, Pandolfi PP (2010) A novel type of cellular senescence that can be enhanced in mouse models and human tumor xenografts to suppress prostate tumorigenesis. *The Journal of clinical investigation* **120**: 681-693
- Ameyar-Zazoua M, Wisniewska MB, Bakiri L, Wagner EF, Yaniv M, Weitzman JB (2005) AP-1 dimers regulate transcription of the p14/p19ARF tumor suppressor gene. *Oncogene* **24**: 2298-2306
- Angel P, Hattori K, Smeal T, Karin M (1988) The jun proto-oncogene is positively autoregulated by its product, Jun/AP-1. *Cell* **55**: 875-885
- Arroyo EJ, Scherer SS (2000) On the molecular architecture of myelinated fibers. *Histochemistry and cell biology* **113**: 1-18
- Arthur-Farraj P, Wanek K, Hantke J, Davis CM, Jayakar A, Parkinson DB, Mirsky R, Jessen KR (2011) Mouse schwann cells need both NRG1 and cyclic AMP to myelinate. *Glia* **59**: 720-733
- Arthur-Farraj PJ, Latouche M, Wilton DK, Quintes S, Chabrol E, Banerjee A, Woodhoo A, Jenkins B, Rahman M, Turmaine M, Wicher GK, Mitter R, Greensmith L, Behrens A, Raivich G, Mirsky R, Jessen KR (2012) c-Jun reprograms Schwann cells of injured nerves to generate a repair cell essential for regeneration. *Neuron* **75**: 633-647
- Atanasoski S, Boller D, De Ventura L, Koegel H, Boentert M, Young P, Werner S, Suter U (2006) Cell cycle inhibitors p21 and p16 are required for the regulation of Schwann cell proliferation. *Glia* **53**: 147-157
- Atanasoski S, Notterpek L, Lee HY, Castagner F, Young P, Ehrenguber MU, Meijer D, Sommer L, Stavnez E, Colmenares C, Suter U (2004) The protooncogene Ski controls Schwann cell proliferation and myelination. *Neuron* **43**: 499-511
- Atanasoski S, Shumas S, Dickson C, Scherer SS, Suter U (2001) Differential cyclin D1 requirements of proliferating Schwann cells during development and after injury. *Mol Cell Neurosci* **18**: 581-592
- Backs J, Worst BC, Lehmann LH, Patrick DM, Jebessa Z, Kreusser MM, Sun Q, Chen L, Heft C, Katus HA, Olson EN (2011) Selective repression of MEF2 activity by PKA-dependent proteolysis of HDAC4. *J Cell Biol* **195**: 403-415
- Barradas M, Anderton E, Acosta JC, Li S, Banito A, Rodriguez-Niedenfuhr M, Maertens G, Banck M, Zhou MM, Walsh MJ, Peters G, Gil J (2009) Histone demethylase JMJD3 contributes to epigenetic control of INK4a/ARF by oncogenic RAS. *Genes Dev* **23**: 1177-1182
- Bennett BL, Sasaki DT, Murray BW, O'Leary EC, Sakata ST, Xu W, Leisten JC, Motiwala A, Pierce S, Satoh Y, Bhagwat SS, Manning AM, Anderson DW (2001) SP600125, an anthrapyrazolone inhibitor of Jun N-terminal kinase. *Proceedings of the National Academy of Sciences of the United States of America* **98**: 13681-13686
- Besirli CG, Wagner EF, Johnson EM, Jr. (2005) The limited role of NH2-terminal c-Jun phosphorylation in neuronal apoptosis: identification of the nuclear pore complex as a potential target of the JNK pathway. *J Cell Biol* **170**: 401-411
- Birchmeier C, Nave KA (2008) Neuregulin-1, a key axonal signal that drives Schwann cell growth and differentiation. *Glia* **56**: 1491-1497
- Bottenstein JE, Sato GH (1979) Growth of a rat neuroblastoma cell line in serum-free supplemented medium. *Proceedings of the National Academy of Sciences of the United States of America* **76**: 514-517

- Bracken AP, Kleine-Kohlbrecher D, Dietrich N, Pasini D, Gargiulo G, Beekman C, Theilgaard-Monch K, Minucci S, Porse BT, Marine JC, Hansen KH, Helin K (2007) The Polycomb group proteins bind throughout the INK4A-ARF locus and are disassociated in senescent cells. *Genes Dev* **21**: 525-530
- Burden S, Yarden Y (1997) Neuregulins and their receptors: a versatile signaling module in organogenesis and oncogenesis. *Neuron* **18**: 847-855
- Campeau E, Ruhl VE, Rodier F, Smith CL, Rahmberg BL, Fuss JO, Campisi J, Yaswen P, Cooper PK, Kaufman PD (2009) A versatile viral system for expression and depletion of proteins in mammalian cells. *PLoS one* **4**: e6529
- Carroll SL, Ratner N (2008) How does the Schwann cell lineage form tumors in NF1? *Glia* **56**: 1590-1605
- Chen Y, Wang H, Yoon SO, Xu X, Hottiger MO, Svaren J, Nave KA, Kim HA, Olson EN, Lu QR (2011) HDAC-mediated deacetylation of NF-kappaB is critical for Schwann cell myelination. *Nature neuroscience* **14**: 437-441
- Chen Z, Trotman LC, Shaffer D, Lin HK, Dotan ZA, Niki M, Koutcher JA, Scher HI, Ludwig T, Gerald W, Cordon-Cardo C, Pandolfi PP (2005) Crucial role of p53-dependent cellular senescence in suppression of Pten-deficient tumorigenesis. *Nature* **436**: 725-730
- Chen ZL, Yu WM, Strickland S (2007) Peripheral regeneration. *Annual review of neuroscience* **30**: 209-233
- Cheng L, Khan M, Mudge AW (1995) Calcitonin gene-related peptide promotes Schwann cell proliferation. *J Cell Biol* **129**: 789-796
- Cichowski K, Jacks T (2001) NF1 tumor suppressor gene function: narrowing the GAP. *Cell* **104**: 593-604
- Cichowski K, Shih TS, Schmitt E, Santiago S, Reilly K, McLaughlin ME, Bronson RT, Jacks T (1999) Mouse models of tumor development in neurofibromatosis type 1. *Science* **286**: 2172-2176
- Clarke N, Arenzana N, Hai T, Minden A, Prywes R (1998) Epidermal growth factor induction of the c-jun promoter by a Rac pathway. *Mol Cell Biol* **18**: 1065-1073
- Collado M, Blasco MA, Serrano M (2007) Cellular senescence in cancer and aging. *Cell* **130**: 223-233
- Corsetti V, Mozzetta C, Biagioni S, Augusti Tocco G, Tata AM (2012) The mechanisms and possible sites of acetylcholine release during chick primary sensory neuron differentiation. *Life sciences* **91**: 783-788
- Courtois-Cox S, Genter Williams SM, Reczek EE, Johnson BW, McGillicuddy LT, Johannessen CM, Hollstein PE, MacCollin M, Cichowski K (2006) A negative feedback signaling network underlies oncogene-induced senescence. *Cancer Cell* **10**: 459-472
- Crompton G (2006) A brief history of inhaled asthma therapy over the last fifty years. *Primary care respiratory journal: journal of the General Practice Airways Group* **15**: 326-331
- de Ruijter AJ, van Gennip AH, Caron HN, Kemp S, van Kuilenburg AB (2003) Histone deacetylases (HDACs): characterization of the classical HDAC family. *Biochem J* **370**: 737-749
- Debacq-Chainiaux F, Erusalimsky JD, Campisi J, Toussaint O (2009) Protocols to detect senescence-associated beta-galactosidase (SA-beta-gal) activity, a biomarker of senescent cells in culture and in vivo. *Nature protocols* **4**: 1798-1806

- Dimri GP, Lee X, Basile G, Acosta M, Scott G, Roskelley C, Medrano EE, Linskens M, Rubelj I, Pereira-Smith O, *et al.* (1995) A biomarker that identifies senescent human cells in culture and in aging skin in vivo. *Proceedings of the National Academy of Sciences of the United States of America* **92**: 9363-9367
- Du K, Montminy M (1998) CREB is a regulatory target for the protein kinase Akt/PKB. *The Journal of biological chemistry* **273**: 32377-32379
- Du M, Perry RL, Nowacki NB, Gordon JW, Salma J, Zhao J, Aziz A, Chan J, Siu KW, McDermott JC (2008) Protein kinase A represses skeletal myogenesis by targeting myocyte enhancer factor 2D. *Mol Cell Biol* **28**: 2952-2970
- Duarte-Araujo M, Timoteo MA, Correia-de-Sa P (2004) Adenosine activating A(2A)-receptors coupled to adenylate cyclase/cyclic AMP pathway downregulates nicotinic autoreceptor function at the rat myenteric nerve terminals. *Neurochemistry international* **45**: 641-651
- Esteller M, Cordon-Cardo C, Corn PG, Meltzer SJ, Pohar KS, Watkins DN, Capella G, Peinado MA, Matias-Guiu X, Prat J, Baylin SB, Herman JG (2001) p14ARF silencing by promoter hypermethylation mediates abnormal intracellular localization of MDM2. *Cancer research* **61**: 2816-2821
- Evans DG (2009) Neurofibromatosis type 2 (NF2): a clinical and molecular review. *Orphanet journal of rare diseases* **4**: 16
- Falls DL (2003) Neuregulins: functions, forms, and signaling strategies. *Experimental cell research* **284**: 14-30
- Fields RD, Stevens-Graham B (2002) New insights into neuron-glia communication. *Science* **298**: 556-562
- Filbin MT (2003) Myelin-associated inhibitors of axonal regeneration in the adult mammalian CNS. *Nat Rev Neurosci* **4**: 703-713
- Fischle W, Dequiedt F, Hendzel MJ, Guenther MG, Lazar MA, Voelter W, Verdin E (2002) Enzymatic activity associated with class II HDACs is dependent on a multiprotein complex containing HDAC3 and SMRT/N-CoR. *Mol Cell* **9**: 45-57
- Fitzsimons HL, Schwartz S, Given FM, Scott MJ (2013) The histone deacetylase HDAC4 regulates long-term memory in *Drosophila*. *PLoS one* **8**: e83903
- Fontana X, Hristova M, Da Costa C, Patodia S, Thei L, Makwana M, Spencer-Dene B, Latouche M, Mirsky R, Jessen KR, Klein R, Raivich G, Behrens A (2012) c-Jun in Schwann cells promotes axonal regeneration and motoneuron survival via paracrine signaling. *J Cell Biol* **198**: 127-141
- Garbay B, Heape AM, Sargueil F, Cassagne C (2000) Myelin synthesis in the peripheral nervous system. *Progress in neurobiology* **61**: 267-304
- Gil J, Peters G (2006) Regulation of the INK4b-ARF-INK4a tumour suppressor locus: all for one or one for all. *Nature reviews Molecular cell biology* **7**: 667-677
- Glenn TD, Talbot WS (2013a) Analysis of Gpr126 function defines distinct mechanisms controlling the initiation and maturation of myelin. *Development* **140**: 3167-3175
- Glenn TD, Talbot WS (2013b) Signals regulating myelination in peripheral nerves and the Schwann cell response to injury. *Current opinion in neurobiology* **23**: 1041-1048
- Gomez-Sanchez JA, Lopez de Armentia M, Lujan R, Kessar N, Richardson WD, Cabedo H (2009) Sustained axon-glia signaling induces Schwann cell hyperproliferation, Remak bundle myelination, and tumorigenesis. *J Neurosci* **29**: 11304-11315

- Gordon JW, Pagiatakis C, Salma J, Du M, Andreucci JJ, Zhao J, Hou G, Perry RL, Dan Q, Courtman D, Bendeck MP, McDermott JC (2009) Protein kinase A-regulated assembly of a MEF2 HDAC4 repressor complex controls c-Jun expression in vascular smooth muscle cells. *The Journal of biological chemistry* **284**: 19027-19042
- Gorgoulis VG, Halazonetis TD Oncogene-induced senescence: the bright and dark side of the response. *Curr Opin Cell Biol* **22**: 816-827
- Grozinger CM, Schreiber SL (2000) Regulation of histone deacetylase 4 and 5 and transcriptional activity by 14-3-3-dependent cellular localization. *Proceedings of the National Academy of Sciences of the United States of America* **97**: 7835-7840
- Haberland M, Montgomery RL, Olson EN (2009) The many roles of histone deacetylases in development and physiology: implications for disease and therapy. *Nature reviews Genetics* **10**: 32-42
- Hai M, Muja N, DeVries GH, Quarles RH, Patel PI (2002) Comparative analysis of Schwann cell lines as model systems for myelin gene transcription studies. *J Neurosci Res* **69**: 497-508
- Hall SM (1999) The biology of chronically denervated Schwann cells. *Annals of the New York Academy of Sciences* **883**: 215-233
- Han TH, Lamph WW, Prywes R (1992) Mapping of epidermal growth factor-, serum-, and phorbol ester-responsive sequence elements in the c-jun promoter. *Mol Cell Biol* **12**: 4472-4477
- Harrisingh MC, Perez-Nadales E, Parkinson DB, Malcolm DS, Mudge AW, Lloyd AC (2004) The Ras/Raf/ERK signalling pathway drives Schwann cell dedifferentiation. *EMBO J* **23**: 3061-3071
- Harvey RD, Hell JW (2013) CaV1.2 signaling complexes in the heart. *Journal of molecular and cellular cardiology* **58**: 143-152
- Hayflick L, Moorhead PS (1961) The serial cultivation of human diploid cell strains. *Experimental cell research* **25**: 585-621
- Ho WH, Armanini MP, Nuijens A, Phillips HS, Osheroff PL (1995) Sensory and motor neuron-derived factor. A novel heregulin variant highly expressed in sensory and motor neurons. *The Journal of biological chemistry* **270**: 26722
- Hoke A, Ho T, Crawford TO, LeBel C, Hilt D, Griffin JW (2003) Glial cell line-derived neurotrophic factor alters axon schwann cell units and promotes myelination in unmyelinated nerve fibers. *J Neurosci* **23**: 561-567
- Holmes WE, Sliwkowski MX, Akita RW, Henzel WJ, Lee J, Park JW, Yansura D, Abadi N, Raab H, Lewis GD, *et al.* (1992) Identification of heregulin, a specific activator of p185erbB2. *Science* **256**: 1205-1210
- Jacks T, Remington L, Williams BO, Schmitt EM, Halachmi S, Bronson RT, Weinberg RA (1994) Tumor spectrum analysis in p53-mutant mice. *Current biology : CB* **4**: 1-7
- Jacob C, Christen CN, Pereira JA, Somandin C, Baggiolini A, Lotscher P, Ozcelik M, Tricaud N, Meijer D, Yamaguchi T, Matthias P, Suter U (2011a) HDAC1 and HDAC2 control the transcriptional program of myelination and the survival of Schwann cells. *Nature neuroscience* **14**: 429-436
- Jacob C, Lebrun-Julien F, Suter U (2011b) How histone deacetylases control myelination. *Molecular neurobiology* **44**: 303-312
- Jacob C, Lotscher P, Engler S, Baggiolini A, Varum Tavares S, Brugger V, John N, Buchmann-Moller S, Snider PL, Conway SJ, Yamaguchi T, Matthias P, Sommer L, Mantei N, Suter U (2014) HDAC1 and HDAC2 Control the Specification of Neural Crest Cells into Peripheral Glia. *J Neurosci* **34**: 6112-6122

- Jacobs JJ, Kieboom K, Marino S, DePinho RA, van Lohuizen M (1999) The oncogene and Polycomb-group gene *bmi-1* regulates cell proliferation and senescence through the *ink4a* locus. *Nature* **397**: 164-168
- Jessen KR (2004) Glial cells. *The international journal of biochemistry & cell biology* **36**: 1861-1867
- Jessen KR, Brennan A, Morgan L, Mirsky R, Kent A, Hashimoto Y, Gavrilocic J (1994) The Schwann cell precursor and its fate: a study of cell death and differentiation during gliogenesis in rat embryonic nerves. *Neuron* **12**: 509-527
- Jessen KR, Mirsky R (1999) Why do Schwann cells survive in the absence of axons? *Annals of the New York Academy of Sciences* **883**: 109-115
- Jessen KR, Mirsky R (2005) The origin and development of glial cells in peripheral nerves. *Nat Rev Neurosci* **6**: 671-682
- Jessen KR, Mirsky R (2008) Negative regulation of myelination: relevance for development, injury, and demyelinating disease. *Glia* **56**: 1552-1565
- Joseph NM, Mosher JT, Buchstaller J, Snider P, McKeever PE, Lim M, Conway SJ, Parada LF, Zhu Y, Morrison SJ (2008) The loss of *Nf1* transiently promotes self-renewal but not tumorigenesis by neural crest stem cells. *Cancer Cell* **13**: 129-140
- Jung J, Cai W, Lee HK, Pellegatta M, Shin YK, Jang SY, Suh DJ, Wrabetz L, Feltri ML, Park HT (2011) Actin polymerization is essential for myelin sheath fragmentation during Wallerian degeneration. *J Neurosci* **31**: 2009-2015
- Jungnickel J, Haase K, Konitzer J, Timmer M, Grothe C (2006) Faster nerve regeneration after sciatic nerve injury in mice over-expressing basic fibroblast growth factor. *Journal of neurobiology* **66**: 940-948
- Kao GD, McKenna WG, Guenther MG, Muschel RJ, Lazar MA, Yen TJ (2003) Histone deacetylase 4 interacts with 53BP1 to mediate the DNA damage response. *J Cell Biol* **160**: 1017-1027
- Kao SC, Wu H, Xie J, Chang CP, Ranish JA, Graef IA, Crabtree GR (2009) Calcineurin/NFAT signaling is required for neuregulin-regulated Schwann cell differentiation. *Science* **323**: 651-654
- Kay JC, Xia CM, Liu M, Shen S, Yu SJ, Chung C, Qiao LY (2013) Endogenous PI3K/Akt and NMDAR act independently in the regulation of CREB activity in lumbosacral spinal cord in cystitis. *Experimental neurology* **250**: 366-375
- Kayahara M, Wang X, Tournier C (2005) Selective regulation of *c-jun* gene expression by mitogen-activated protein kinases via the 12-*o*-tetradecanoylphorbol-13-acetate- responsive element and myocyte enhancer factor 2 binding sites. *Mol Cell Biol* **25**: 3784-3792
- Kim HA, Pomeroy SL, Whoriskey W, Pawlitzky I, Benowitz LI, Sicinski P, Stiles CD, Roberts TM (2000) A developmentally regulated switch directs regenerative growth of Schwann cells through cyclin D1. *Neuron* **26**: 405-416
- Kim HA, Ratner N, Roberts TM, Stiles CD (2001) Schwann cell proliferative responses to cAMP and *Nf1* are mediated by cyclin D1. *J Neurosci* **21**: 1110-1116
- Koontz NA, Wiens AL, Agarwal A, Hingtgen CM, Emerson RE, Mosier KM (2013) Schwannomatosis: the overlooked neurofibromatosis? *AJR American journal of roentgenology* **200**: W646-653
- Kozhemyakina E, Cohen T, Yao TP, Lassar AB (2009) Parathyroid hormone-related peptide represses chondrocyte hypertrophy through a protein phosphatase 2A/histone deacetylase 4/MEF2 pathway. *Mol Cell Biol* **29**: 5751-5762

Kuilman T, Michaloglou C, Vredeveld LC, Douma S, van Doorn R, Desmet CJ, Aarden LA, Mooi WJ, Peeper DS (2008) Oncogene-induced senescence relayed by an interleukin-dependent inflammatory network. *Cell* **133**: 1019-1031

Kumler I, Tuxen MK, Nielsen DL (2014) A systematic review of dual targeting in HER2-positive breast cancer. *Cancer treatment reviews* **40**: 259-270

Kurz DJ, Decary S, Hong Y, Erusalimsky JD (2000) Senescence-associated (beta)-galactosidase reflects an increase in lysosomal mass during replicative ageing of human endothelial cells. *Journal of cell science* **113** (Pt **20**): 3613-3622

Le Douarin NM, Dupin E (2003) Multipotentiality of the neural crest. *Current opinion in genetics & development* **13**: 529-536

Lee HK, Shin YK, Jung J, Seo SY, Baek SY, Park HT (2009) Proteasome inhibition suppresses Schwann cell dedifferentiation in vitro and in vivo. *Glia* **57**: 1825-1834

Leimeroth R, Lobsiger C, Lussi A, Taylor V, Suter U, Sommer L (2002) Membrane-bound neuregulin1 type III actively promotes Schwann cell differentiation of multipotent Progenitor cells. *Developmental biology* **246**: 245-258

Li C, Xiao L, Liu X, Yang W, Shen W, Hu C, Yang G, He C (2013) A functional role of NMDA receptor in regulating the differentiation of oligodendrocyte precursor cells and remyelination. *Glia* **61**: 732-749

Li J, Chen J, Ricupero CL, Hart RP, Schwartz MS, Kusnecov A, Herrup K (2012) Nuclear accumulation of HDAC4 in ATM deficiency promotes neurodegeneration in ataxia telangiectasia. *Nature medicine* **18**: 783-790

Limberg BJ, Andersson KE, Aura Kullmann F, Burmer G, de Groat WC, Rosenbaum JS (2010) beta-Adrenergic receptor subtype expression in myocyte and non-myocyte cells in human female bladder. *Cell and tissue research* **342**: 295-306

Lin TY, Cheng YC, Yang HC, Lin WC, Wang CC, Lai PL, Shieh SY (2012) Loss of the candidate tumor suppressor BTG3 triggers acute cellular senescence via the ERK-JMJD3-p16(INK4a) signaling axis. *Oncogene* **31**: 3287-3297

Lu J, McKinsey TA, Nicol RL, Olson EN (2000) Signal-dependent activation of the MEF2 transcription factor by dissociation from histone deacetylases. *Proceedings of the National Academy of Sciences of the United States of America* **97**: 4070-4075

Magnaghi V, Procacci P, Tata AM (2009) Chapter 15: Novel pharmacological approaches to Schwann cells as neuroprotective agents for peripheral nerve regeneration. *International review of neurobiology* **87**: 295-315

Martin GA, Viskochil D, Bollag G, McCabe PC, Crosier WJ, Haubruck H, Conroy L, Clark R, O'Connell P, Cawthon RM, *et al.* (1990) The GAP-related domain of the neurofibromatosis type 1 gene product interacts with ras p21. *Cell* **63**: 843-849

Mathon NF, Malcolm DS, Harrisingh MC, Cheng L, Lloyd AC (2001) Lack of replicative senescence in normal rodent glia. *Science* **291**: 872-875

Maurel P, Salzer JL (2000) Axonal regulation of Schwann cell proliferation and survival and the initial events of myelination requires PI 3-kinase activity. *J Neurosci* **20**: 4635-4645

McClatchey AI (2007) Neurofibromatosis. *Annu Rev Pathol* **2**: 191-216

Mechta-Grigoriou F, Gerald D, Yaniv M (2001) The mammalian Jun proteins: redundancy and specificity. *Oncogene* **20**: 2378-2389

- Michailov GV, Sereda MW, Brinkmann BG, Fischer TM, Haug B, Birchmeier C, Role L, Lai C, Schwab MH, Nave KA (2004) Axonal neuregulin-1 regulates myelin sheath thickness. *Science* **304**: 700-703
- Michaloglou C, Vredevelde LC, Soengas MS, Denoyelle C, Kuilman T, van der Horst CM, Majoor DM, Shay JW, Mooi WJ, Peeper DS (2005) BRAFE600-associated senescence-like cell cycle arrest of human naevi. *Nature* **436**: 720-724
- Mihaylova MM, Vasquez DS, Ravnskjaer K, Denechaud PD, Yu RT, Alvarez JG, Downes M, Evans RM, Montminy M, Shaw RJ (2011) Class IIa histone deacetylases are hormone-activated regulators of FOXO and mammalian glucose homeostasis. *Cell* **145**: 607-621
- Mirsky R, Jessen KR (1999) The neurobiology of Schwann cells. *Brain Pathol* **9**: 293-311
- Mirsky R, Woodhoo A, Parkinson DB, Arthur-Farraj P, Bhaskaran A, Jessen KR (2008) Novel signals controlling embryonic Schwann cell development, myelination and dedifferentiation. *Journal of the peripheral nervous system : JPNS* **13**: 122-135
- Monje PV, Athauda G, Wood PM (2008) Protein kinase A-mediated gating of neuregulin-dependent ErbB2-ErbB3 activation underlies the synergistic action of cAMP on Schwann cell proliferation. *The Journal of biological chemistry* **283**: 34087-34100
- Monje PV, Bartlett Bunge M, Wood PM (2006) Cyclic AMP synergistically enhances neuregulin-dependent ERK and Akt activation and cell cycle progression in Schwann cells. *Glia* **53**: 649-659
- Monje PV, Soto J, Bacallao K, Wood PM (2010) Schwann cell dedifferentiation is independent of mitogenic signaling and uncoupled to proliferation: role of cAMP and JNK in the maintenance of the differentiated state. *The Journal of biological chemistry* **285**: 31024-31036
- Monk KR, Naylor SG, Glenn TD, Mercurio S, Perlin JR, Dominguez C, Moens CB, Talbot WS (2009) A G protein-coupled receptor is essential for Schwann cells to initiate myelination. *Science* **325**: 1402-1405
- Monk KR, Oshima K, Jors S, Heller S, Talbot WS (2011) Gpr126 is essential for peripheral nerve development and myelination in mammals. *Development* **138**: 2673-2680
- Monuki ES, Weinmaster G, Kuhn R, Lemke G (1989) SCIP: a glial POU domain gene regulated by cyclic AMP. *Neuron* **3**: 783-793
- Morgan L, Jessen KR, Mirsky R (1991) The effects of cAMP on differentiation of cultured Schwann cells: progression from an early phenotype (04+) to a myelin phenotype (P0+, GFAP-, N-CAM-, NGF-receptor-) depends on growth inhibition. *J Cell Biol* **112**: 457-467
- Newbern JM, Li X, Shoemaker SE, Zhou J, Zhong J, Wu Y, Bonder D, Hollenback S, Coppola G, Geschwind DH, Landreth GE, Snider WD (2011) Specific functions for ERK/MAPK signaling during PNS development. *Neuron* **69**: 91-105
- Nishino TG, Miyazaki M, Hoshino H, Miwa Y, Horinouchi S, Yoshida M (2008) 14-3-3 regulates the nuclear import of class IIa histone deacetylases. *Biochemical and biophysical research communications* **377**: 852-856
- Ogata T, Iijima S, Hoshikawa S, Miura T, Yamamoto S, Oda H, Nakamura K, Tanaka S (2004) Opposing extracellular signal-regulated kinase and Akt pathways control Schwann cell myelination. *J Neurosci* **24**: 6724-6732
- Owens GC, Bunge RP (1989) Evidence for an early role for myelin-associated glycoprotein in the process of myelination. *Glia* **2**: 119-128
- Owens GK, Kumar MS, Wamhoff BR (2004) Molecular regulation of vascular smooth muscle cell differentiation in development and disease. *Physiological reviews* **84**: 767-801

- Palmero I, Pantoja C, Serrano M (1998) p19ARF links the tumour suppressor p53 to Ras. *Nature* **395**: 125-126
- Parkinson DB, Bhaskaran A, Arthur-Farraj P, Noon LA, Woodhoo A, Lloyd AC, Feltri ML, Wrabetz L, Behrens A, Mirsky R, Jessen KR (2008) c-Jun is a negative regulator of myelination. *J Cell Biol* **181**: 625-637
- Paroni G, Fontanini A, Cernotta N, Foti C, Gupta MP, Yang XJ, Fasino D, Brancolini C (2007) Dephosphorylation and caspase processing generate distinct nuclear pools of histone deacetylase 4. *Mol Cell Biol* **27**: 6718-6732
- Paroni G, Mizzau M, Henderson C, Del Sal G, Schneider C, Brancolini C (2004) Caspase-dependent regulation of histone deacetylase 4 nuclear-cytoplasmic shuttling promotes apoptosis. *Mol Biol Cell* **15**: 2804-2818
- Parra M, Verdin E (2010) Regulatory signal transduction pathways for class IIa histone deacetylases. *Current opinion in pharmacology* **10**: 454-460
- Parrinello S, Lloyd AC (2009) Neurofibroma development in NF1—insights into tumour initiation. *Trends Cell Biol* **19**: 395-403
- Parrinello S, Noon LA, Harrisingh MC, Wingfield Digby P, Rosenberg LH, Cremona CA, Echave P, Flanagan AM, Parada LF, Lloyd AC (2008) NF1 loss disrupts Schwann cell-axonal interactions: a novel role for semaphorin 4F. *Genes Dev* **22**: 3335-3348
- Pellegrino RG, Spencer PS (1985) Schwann cell mitosis in response to regenerating peripheral axons in vivo. *Brain research* **341**: 16-25
- Pereira JA, Lebrun-Julien F, Suter U (2012) Molecular mechanisms regulating myelination in the peripheral nervous system. *Trends in neurosciences* **35**: 123-134
- Poduslo JF, Walikonis RS, Domec MC, Berg CT, Holtz-Heppelmann CJ (1995) The second messenger, cyclic AMP, is not sufficient for myelin gene induction in the peripheral nervous system. *Journal of neurochemistry* **65**: 149-159
- Poliak S, Peles E (2003) The local differentiation of myelinated axons at nodes of Ranvier. *Nat Rev Neurosci* **4**: 968-980
- Porstmann T, Griffiths B, Chung YL, Delpuech O, Griffiths JR, Downward J, Schulze A (2005) PKB/Akt induces transcription of enzymes involved in cholesterol and fatty acid biosynthesis via activation of SREBP. *Oncogene* **24**: 6465-6481
- Quarles RH (2002) Myelin sheaths: glycoproteins involved in their formation, maintenance and degeneration. *Cellular and molecular life sciences: CMLS* **59**: 1851-1871
- Rahmatullah M, Schroering A, Rothblum K, Stahl RC, Urban B, Carey DJ (1998) Synergistic regulation of Schwann cell proliferation by heregulin and forskolin. *Mol Cell Biol* **18**: 6245-6252
- Raivich G, Behrens A (2006) Role of the AP-1 transcription factor c-Jun in developing, adult and injured brain. *Progress in neurobiology* **78**: 347-363
- Rodd AL, Ververis K, Karagiannis TC (2012) Current and Emerging Therapeutics for Cutaneous T-Cell Lymphoma: Histone Deacetylase Inhibitors. *Lymphoma* **2012**: 10
- Salzer JL (2003) Polarized domains of myelinated axons. *Neuron* **40**: 297-318
- Salzer JL, Brophy PJ, Peles E (2008) Molecular domains of myelinated axons in the peripheral nervous system. *Glia* **56**: 1532-1540
- Sanchez del Pino MM, Lopez-Rodas G, Sendra R, Tordera V (1994) Properties of the yeast nuclear histone deacetylase. *Biochem J* **303** (Pt 3): 723-729

- Sarkisian CJ, Keister BA, Stairs DB, Boxer RB, Moody SE, Chodosh LA (2007) Dose-dependent oncogene-induced senescence in vivo and its evasion during mammary tumorigenesis. *Nature cell biology* **9**: 493-505
- Sauer SK, Reeh PW, Bove GM (2001) Noxious heat-induced CGRP release from rat sciatic nerve axons in vitro. *The European journal of neuroscience* **14**: 1203-1208
- Schafer M, Fruttiger M, Montag D, Schachner M, Martini R (1996) Disruption of the gene for the myelin-associated glycoprotein improves axonal regrowth along myelin in C57BL/Wlds mice. *Neuron* **16**: 1107-1113
- Scherer SS, Arroyo EJ (2002) Recent progress on the molecular organization of myelinated axons. *Journal of the peripheral nervous system : JPNS* **7**: 1-12
- Scherer SS, Wang DY, Kuhn R, Lemke G, Wrabetz L, Kamholz J (1994) Axons regulate Schwann cell expression of the POU transcription factor SCIP. *J Neurosci* **14**: 1930-1942
- Serrano M (2010) Shifting senescence into quiescence by turning up p53. *Cell cycle* **9**: 4256-4257
- Serrano M, Lee H, Chin L, Cordon-Cardo C, Beach D, DePinho RA (1996) Role of the INK4a locus in tumor suppression and cell mortality. *Cell* **85**: 27-37
- Serrano M, Lin AW, McCurrach ME, Beach D, Lowe SW (1997) Oncogenic ras provokes premature cell senescence associated with accumulation of p53 and p16INK4a. *Cell* **88**: 593-602
- Shamash S, Reichert F, Rotshenker S (2002) The cytokine network of Wallerian degeneration: tumor necrosis factor-alpha, interleukin-1alpha, and interleukin-1beta. *J Neurosci* **22**: 3052-3060
- Sharghi-Namini S, Turmaine M, Meier C, Sahni V, Umehara F, Jessen KR, Mirsky R (2006) The structural and functional integrity of peripheral nerves depends on the glial-derived signal desert hedgehog. *J Neurosci* **26**: 6364-6376
- Sharpless NE (2005) INK4a/ARF: a multifunctional tumor suppressor locus. *Mutation research* **576**: 22-38
- Sharpless NE, Ramsey MR, Balasubramanian P, Castrillon DH, DePinho RA (2004) The differential impact of p16(INK4a) or p19(ARF) deficiency on cell growth and tumorigenesis. *Oncogene* **23**: 379-385
- Sherman DL, Brophy PJ (2005) Mechanisms of axon ensheathment and myelin growth. *Nat Rev Neurosci* **6**: 683-690
- Sherr CJ, DePinho RA (2000) Cellular senescence: mitotic clock or culture shock? *Cell* **102**: 407-410
- Shin YK, Jang SY, Park JY, Park SY, Lee HJ, Suh DJ, Park HT (2013) The Neuregulin-Rac-MKK7 pathway regulates antagonistic c-jun/Krox20 expression in Schwann cell dedifferentiation. *Glia* **61**: 892-904
- Shy ME, Shi Y, Wrabetz L, Kamholz J, Scherer SS (1996) Axon-Schwann cell interactions regulate the expression of c-jun in Schwann cells. *J Neurosci Res* **43**: 511-525
- Smith KJ, Blakemore WF, Murray JA, Patterson RC (1982) Internodal myelin volume and axon surface area. A relationship determining myelin thickness? *Journal of the neurological sciences* **55**: 231-246
- Stoll G, Muller HW (1999) Nerve injury, axonal degeneration and neural regeneration: basic insights. *Brain Pathol* **9**: 313-325
- Svaren J, Meijer D (2008) The molecular machinery of myelin gene transcription in Schwann cells. *Glia* **56**: 1541-1551

- Taveggia C, Zanazzi G, Petrylak A, Yano H, Rosenbluth J, Einheber S, Xu X, Esper RM, Loeb JA, Shrager P, Chao MV, Falls DL, Role L, Salzer JL (2005) Neuregulin-1 type III determines the ensheathment fate of axons. *Neuron* **47**: 681-694
- Terenghi G (1999) Peripheral nerve regeneration and neurotrophic factors. *Journal of anatomy* **194** (Pt 1): 1-14
- Teschemacher AG (2005) Real-time measurements of noradrenaline release in periphery and central nervous system. *Autonomic neuroscience : basic & clinical* **117**: 1-8
- Uchiyama T, Chess-Williams R (2004) Muscarinic receptor subtypes of the bladder and gastrointestinal tract. *Journal of smooth muscle research = Nihon Heikatsukin Gakkai kikanishi* **40**: 237-247
- Ugenti C, Egle De Stefano M, Costantino M, Loreti S, Pisano A, Avallone B, Talora C, Magnaghi V, Maria Tata A (2014) M2 muscarinic receptor activation regulates schwann cell differentiation and myelin organization. *Dev Neurobiol*
- Vargas ME, Barres BA (2007) Why is Wallerian degeneration in the CNS so slow? *Annual review of neuroscience* **30**: 153-179
- Vause CV, Durham PL (2010) Calcitonin gene-related peptide differentially regulates gene and protein expression in trigeminal glia cells: findings from array analysis. *Neuroscience letters* **473**: 163-167
- Vega RB, Matsuda K, Oh J, Barbosa AC, Yang X, Meadows E, McAnally J, Pomajzl C, Shelton JM, Richardson JA, Karsenty G, Olson EN (2004) Histone deacetylase 4 controls chondrocyte hypertrophy during skeletogenesis. *Cell* **119**: 555-566
- Wagh VD, Patil PN, Surana SJ, Wagh KV (2012) Forskolin: upcoming antiglaucoma molecule. *Journal of postgraduate medicine* **58**: 199-202
- Walikonis RS, Poduslo JF (1998) Activity of cyclic AMP phosphodiesterases and adenylyl cyclase in peripheral nerve after crush and permanent transection injuries. *The Journal of biological chemistry* **273**: 9070-9077
- Wang AH, Bertos NR, Vezmar M, Pelletier N, Crosato M, Heng HH, Th'ng J, Han J, Yang XJ (1999) HDAC4, a human histone deacetylase related to yeast HDA1, is a transcriptional corepressor. *Mol Cell Biol* **19**: 7816-7827
- Wang AH, Kruhlik MJ, Wu J, Bertos NR, Vezmar M, Posner BI, Bazett-Jones DP, Yang XJ (2000) Regulation of histone deacetylase 4 by binding of 14-3-3 proteins. *Mol Cell Biol* **20**: 6904-6912
- Wang AH, Yang XJ (2001) Histone deacetylase 4 possesses intrinsic nuclear import and export signals. *Mol Cell Biol* **21**: 5992-6005
- Wanner IB, Mahoney J, Jessen KR, Wood PM, Bates M, Bunge MB (2006) Invariant mantling of growth cones by Schwann cell precursors characterize growing peripheral nerve fronts. *Glia* **54**: 424-438
- Weiss C, Schneider S, Wagner EF, Zhang X, Seto E, Bohmann D (2003) JNK phosphorylation relieves HDAC3-dependent suppression of the transcriptional activity of c-Jun. *EMBO J* **22**: 3686-3695
- Willard SS, Koochekpour S (2013) Glutamate, glutamate receptors, and downstream signaling pathways. *International journal of biological sciences* **9**: 948-959
- Wolpowitz D, Mason TB, Dietrich P, Mendelsohn M, Talmage DA, Role LW (2000) Cysteine-rich domain isoforms of the neuregulin-1 gene are required for maintenance of peripheral synapses. *Neuron* **25**: 79-91

- Woodhoo A, Alonso MB, Droggiti A, Turmaine M, D'Antonio M, Parkinson DB, Wilton DK, Al-Shawi R, Simons P, Shen J, Guillemot F, Radtke F, Meijer D, Feltri ML, Wrabetz L, Mirsky R, Jessen KR (2009) Notch controls embryonic Schwann cell differentiation, postnatal myelination and adult plasticity. *Nature neuroscience* **12**: 839-847
- Woodhoo A, Sommer L (2008) Development of the Schwann cell lineage: from the neural crest to the myelinated nerve. *Glia* **56**: 1481-1490
- Wu J, Williams JP, Rizvi TA, Kordich JJ, Witte D, Meijer D, Stemmer-Rachamimov AO, Cancelas JA, Ratner N (2008) Plexiform and dermal neurofibromas and pigmentation are caused by Nf1 loss in desert hedgehog-expressing cells. *Cancer Cell* **13**: 105-116
- Xu P, Rosen KM, Hedstrom K, Rey O, Guha S, Hart C, Corfas G (2013) Nerve injury induces glial cell line-derived neurotrophic factor (GDNF) expression in Schwann cells through purinergic signaling and the PKC-PKD pathway. *Glia* **61**: 1029-1040
- Xue W, Zender L, Miething C, Dickins RA, Hernando E, Krizhanovsky V, Cordon-Cardo C, Lowe SW (2007) Senescence and tumour clearance is triggered by p53 restoration in murine liver carcinomas. *Nature* **445**: 656-660
- Yang C, Klein EA, Assoian RK, Kazanietz MG (2008) Heregulin beta1 promotes breast cancer cell proliferation through Rac/ERK-dependent induction of cyclin D1 and p21Cip1. *Biochem J* **410**: 167-175
- Yao YL, Yang WM (2011) Beyond histone and deacetylase: an overview of cytoplasmic histone deacetylases and their nonhistone substrates. *Journal of biomedicine & biotechnology* **2011**: 146493
- Zheng H, Chang L, Patel N, Yang J, Lowe L, Burns DK, Zhu Y (2008) Induction of abnormal proliferation by nonmyelinating schwann cells triggers neurofibroma formation. *Cancer Cell* **13**: 117-128
- Zhu Y, Ghosh P, Charnay P, Burns DK, Parada LF (2002) Neurofibromas in NF1: Schwann cell origin and role of tumor environment. *Science* **296**: 920-922
- Ziskin JL, Nishiyama A, Rubio M, Fukaya M, Bergles DE (2007) Vesicular release of glutamate from unmyelinated axons in white matter. *Nature neuroscience* **10**: 321-330



Epigenetic induction of the *Ink4a/Arf* locus prevents Schwann cell overproliferation during nerve regeneration and after tumorigenic challenge

Jose Antonio Gomez-Sanchez,^{1,2,*} Clara Gomis-Coloma,^{1,2,*} Cruz Morenilla-Palao,¹ Gloria Peiro,² Eduard Serra,³ Manuel Serrano⁴ and Hugo Cabedo^{1,2}

1 Instituto de Neurociencias de Alicante UMH-CSIC, San Juan de Alicante 03550, Spain

2 Fundación para el Fomento de la Investigación Sanitaria y Biomédica de la Comunidad Valenciana (FISABIO), Hospital General Universitario de Alicante, Alicante 03010, Spain

3 Institut de Medicina Predictiva i Personalitzada del Càncer (IMPPC), Barcelona 08916, Spain

4 Grupo Supresión Tumoral, Centro Nacional de Investigaciones Oncológicas (CNIO), Madrid 28029, Spain

*These authors contributed equally to this work.

Correspondence to: Hugo Cabedo,
Instituto de Neurociencias de Alicante UMH-CSIC,
San Juan de Alicante 03550, Spain
E-mail: hugo.cabedo@umh.es

The number of Schwann cells is fitted to axonal length in peripheral nerves. This relationship is lost when tumorigenic stimuli induce uncontrolled Schwann cell proliferation, generating tumours such as neurofibromas and schwannomas. Schwann cells also re-enter the cell cycle following nerve injury during the process of Wallerian degeneration. In both cases proliferation is finally arrested. We show that in neurofibroma, the induction of Jmjd3 (jumonji domain containing 3, histone lysine demethylase) removes trimethyl groups on lysine-27 of histone-H3 and epigenetically activates the *Ink4a/Arf*-locus, forcing Schwann cells towards replicative senescence. Remarkably, blocking this mechanism allows unrestricted proliferation, inducing malignant transformation of neurofibromas. Interestingly, our data suggest that in injured nerves, Schwann cells epigenetically activate the same locus to switch off proliferation and enter the senescence programme. Indeed, when this pathway is genetically blocked, Schwann cells fail to drop out of the cell cycle and continue to proliferate. We postulate that the *Ink4a/Arf*-locus is expressed as part of a physiological response that prevents uncontrolled proliferation of the de-differentiated Schwann cell generated during nerve regeneration, a response that is also activated to avoid overproliferation after tumorigenic stimuli in the peripheral nervous system.

Keywords: cellular biology; nerve injury; nerve regeneration; Schwann cells; neuroscience

Introduction

The plasticity of the Schwann cell lineage contributes to the successful regeneration of peripheral nerves. After injury, axotomized

myelinating Schwann cells de-differentiate and proliferate, generating an environment that stimulates the growth of axons from the proximal stump and helps to direct them back towards target tissues. It has been suggested that this process depends on

expression of the AP-1 transcription factor c-Jun (Guertin *et al.*, 2005; Jessen and Mirsky, 2008; Parkinson *et al.*, 2008). Re-entry of growing axons into the distal segment induces Schwann cell differentiation and remyelination, eventually leading to successful nerve repair. However, if for some reason the axons cannot reach the distal stump, the Schwann cells will remain in a de-differentiated but non-proliferative state (Scherer *et al.*, 1994; Shy *et al.*, 1996).

Schwann cell de-differentiation and proliferation are also hallmarks of PNS tumours (Carroll and Ratner, 2008). In type I neurofibromatosis (produced by mutations in *Nf1* gene) loss of function mutations chronically activate the RAS/RAF/ERK pathway contributing to uncontrolled Schwann cell proliferation and tumour development (Harrisingh *et al.*, 2004; McClatchey, 2007; Parrinello and Lloyd, 2009). We have recently shown that the neuronal over-expression of a specific isoform of neuregulin (type III- β 3, also known as SMDF) activates the ERK pathway and induces Schwann cell hyperproliferation and neurofibroma development (Gomez-Sanchez *et al.*, 2009). The benign nature of neurofibromas is probably due to the eventual cessation of proliferation. This occurs for no obvious reason and despite the persistence of the tumorigenic stimulus. Here we show that, in these benign tumours, Schwann cell proliferation is limited by the activation of the oncogene-induced senescence programme, a fail-safe mechanism that prevents uncontrolled growth after pathological activation of oncogenes that signal through the RAS/RAF/ERK pathway (Collado and Serrano, 2010). As happens with other non-malignant tumours (Agger *et al.*, 2009; Agherbi *et al.*, 2009; Barradas *et al.*, 2009), neurofibroma oncogene induced senescence is promoted by the epigenetic induction of the *Ink4a/Arf* locus mediated by the histone H3 demethylase *Jmjd3*, which through the p19Arf/p53 and p16Ink4a/Rb pathways, blocks Schwann cell proliferation. We also show that expression of this locus and the demethylase *Jmjd3* is induced in the distal stump of injured nerves. Interestingly loss of function of this signalling pathway (in the *Ink4a/Arf*^{-/-} or *p53*^{-/-} mice) provokes an increased cell proliferation rate after nerve injury, suggesting that, akin to neurofibromas, the epigenetic induction of the *Ink4a/Arf* locus prevents uncontrolled Schwann cell proliferation in distal nerve segments when axon regeneration is delayed or precluded.

Materials and methods

Antibodies

The antibodies and primers are listed in Table 1.

Plasmids

pCMV-Jmjd3 was obtained from K. Helin (Agger *et al.*, 2007) (Addgene plasmid 24167). pEYFP was from Clontech.

Animal studies

All animal work was conducted according to EU guidelines and with protocols approved by the 'Comité de Bioética y Bioseguridad del

Instituto de Neurociencias de Alicante UMH-CSIC' (<http://in.umh.es/>). The generation of the *NSE-SMDF* transgenic mice is described elsewhere (Gomez-Sanchez *et al.*, 2009). M. Serrano (CNIO) provided *Ink4a/Arf* and *p53* knock-out mice. For nerve transection experiments, mice were anaesthetized deeply with isoflurane (2.5%) and the sciatic nerve exposed, sutured with surgical 8–0 nylon monofilament (Ethicon) and then cut 2 mm proximal to the suture. In one group of mice, nerves were crushed with forceps instead of cut. The wound was sutured in layers, and the mice provided with analgesia by intraperitoneal injection of saline (0.9 mg/ml NaCl) containing buprenorphine (0.05 mg/kg). Four, 12 or 24 days after surgery, transected and contralateral nerves were collected and processed for immunofluorescence. To avoid suffering animals were anaesthetized before euthanasia.

Human tissues

All the procedures were performed according to the EU guidelines and approved by the hospital ethics committee. Patients were diagnosed according to the accepted standard NF1 diagnostic criteria. They were informed about the study, and consent was obtained from all. Neurofibromas were obtained from seven patients after surgery. Samples from six tumours were sectioned, deparaffinized and submitted to antigen retrieval by using the citrate method. Samples were prepared for immunofluorescence, as described below, and incubated with the indicated antibodies. One neurofibroma was used to obtain RNA. Healthy adult human peripheral nerves were obtained from diagnostic biopsies and submitted to the same protocol described for the tumours.

Cell cultures

Schwann cells were cultured from sciatic nerves of neonatal rats as described previously by Brockes *et al.* (1979). All the procedures were performed following EU and institutional guidelines. Cell cultures were expanded in Dulbecco's modified Eagle medium supplemented with 3% foetal bovine serum, 5 μ M forskolin and 50 nM GST-Nrg1. Where indicated, cells were transfected with plasmid DNA using NanoJuice[®] transfection reagent (Merck) following the manufacturer's recommendations.

Messenger RNA detection and quantification by quantitative reverse transcription polymerase chain reaction

To detect and quantify gene expression, animals were euthanized, the sciatic nerve was dissected, and total RNA isolated using PureLink[™] Micro-To-Midi[™] kit according to the instructions of the manufacturer (Invitrogen). Genomic DNA was removed by incubation with RNase free DNase I (Fermentas), and RNA was primed with random hexamers and retrotranscribed to complementary DNA with SuperScript[™] II reverse transcriptase (Invitrogen). Control reactions were performed omitting reverse transcriptase. Quantitative real-time PCR was performed using the Applied Biosystems 7500 Real Time PCR System and Platinum[®] SYBR[®] Green qPCR SuperMix-UDG (Invitrogen). To avoid genomic amplification, PCR primers were designed to fall into separate exons flanking a large intron when possible. Reactions were performed in duplicates of three different dilutions, and threshold cycle values were normalized to the housekeeping gene 18S. The specificity of the products was determined by melting curve analysis and gel electrophoresis. The ratio of the relative expression for each gene to 18S was calculated by using the $2^{-\Delta\Delta CT}$ formula.

Table 1 Antibodies and primer sequences

Antibody	Reference	Company	Species	Dilution	
				Immunofluorescence	Western
β-Actin (clone AC-15)	A5441	Sigma	Mouse		1:4000
c-Jun	9165	Cell Signaling	Rabbit	1:200	1:500
erbB2 (29D8)	2165	Cell Signaling	Rabbit		1:500
erbB3 (C-17)	sc-285	Santa Cruz	Rabbit	1:500	1:1000
GFP	ab13970	Abcam	Chicken	1:3000	
Phospho-Histone H3	H0412	Sigma	Rabbit	1:200	
IgG-ChIP Grade	ab27478	Abcam	Rabbit		
Jmjd3	ab38113	Abcam	Rabbit	1:100	
Krox-20 (Egr2)	PRB-236P	ATOM	Rabbit	1:100	
MAPK (Erk1/2) p44/42	9102S	Cell Signaling	Rabbit		1:1000
Phospho MAPK p44/42 (Tyr202/204)	9101	Cell Signaling	Rabbit		1:1000
p14_Arf (4C6/4)	2407	Cell Signaling	Mouse	1:100	
p16 (F-12)	sc-1661	Santa Cruz	Mouse	1:100	
p19_Arf (5-C3-1)	sc-32748	Santa Cruz	Rat	1:100	1:100
S-100β	S 2644	Sigma	Rabbit	1:400	
Trimethyl-Histone H3 (Lys 27)	07-449	Millipore	Rabbit		1:3000
α-Tubulin	ab4074	Abcam	Rabbit		1:2000
Tuj1 (β-III-Tubulin)	MMS435P	Covance	Mouse	1:500	
Ki-67	Ab15580	Abcam	Rabbit	1:100	
Anti-rabbit biotinylated	711-065	Jackson	Donkey	1:600	
cy2 streptavidin	PA42001	GE Healthcare		1:500	
Primer sequences					
Primer	GenBank accession number		Sequence (5'–3')		
p19Arf	NM_009877	Sense	GCCGCACCCGAATCCT		
		Antisense	TTGAGCAGAAGAGCTGCTACGT		
p16Ink4a	NM_009877	Sense	ATGATGATGGGCAACGTTT		
		Antisense	CAAATATCGCACGATGTC		
Neo R1	NM_009877	Sense	CTATCAGGACATAGCGTTGG		
R1	NM_009877	Antisense	AGTGAGAGTTTGGGGACAGAG		
Cyclin D1	NM_007631	Sense	AACTTCCTCTCTGCTACCG		
		Antisense	GGGCTTCAATCTGTTCTCTG		
p19Arf (ChIP)	p19Arf promoter	Sense	GACCGTGAAGCCGACCCCTTCAGC		
		Antisense	GGGGTCGCTTTCCCTTCGG		
p16Ink4a (ChIP)	p16Ink4b promoter	Sense	GATGGAGCCCGGACTACAGAAG		
		Antisense	CTGTTTCAACGCCAGCTCTC		
JMJD3	NM_001017426	Sense	CTCTGGAACCTTCATGCCGG		
		Antisense	CTTAGCCCCATAGTCCGTTTG		
SREBP2	AF374267	Sense	AAGTCTGGCGTTCTGAGGAA		
		Antisense	CCAGGAAGGTGAGGACACAT		
NSE-hSMDF	–	Sense	GAGTCTGCAGTCTCGACCT		
		Antisense	GATGGGGACAATGCAGATTT		
p53	M13874	p53r_1B3	AAGGATAGGTGGCGGTTTCAT		
		p53f_12B7	TGGTTTGTGCGTCTTAGAGACAGT		
		pPNTf_2B5	CCAGCTCATTCTCCCACTCA		
18S	NR_003278	Sense	CGGCTACCACATCCAAGGAA		
		Antisense	GCTGGAATTACCGCGCT		
p14Arf	NM_000077	Sense	CCCTCGTGTGATGCTACTG		
		Antisense	CATCATGACCTGGTCTTAGGAA		
human p16Ink4a	NM_000077	Sense	GGGGGCACCAAGGAGGAGT		
		Antisense	GGTTGTGGCGGGGAGT		
human GAPDH	NM_014364	Sense	GGAAGGTGAAGGTCCGAGTCA		
		Antisense	GTCATTGATGGCAACAATATCCA		

Immunofluorescence and electron microscopy studies

For immunofluorescence, mice were sacrificed and sciatic nerves dissected, embedded in O.C.T. (TissueTek) and frozen on dry ice. Longitudinal or transverse nerve sections (10 µm) were fixed in 4% paraformaldehyde, blocked for 1 h in 10% horse serum and 0.1% TritonTM X-100 in PBS. Primary antibodies were diluted in blocking solution and incubated overnight at 4°C (human tissues were incubated for 36 h at 4°C). Sections were then washed with PBS, and detection was performed applying the appropriate fluorescent secondary antibodies (Alexa Fluor[®] 594 anti-mouse, Alexa Fluor[®] 488 anti-rabbit and anti-chicken, Alexa Fluor[®] 555 anti-rat 1:1000; Invitrogen) for 1 h. Nuclei were counterstained with bisbenzimidazole (Hoechst nuclear stain) in PBS. Samples were mounted in FluoromountTM G (Southern Biotechnology Associates). Anti-Krox 20 immunofluorescence was performed as described by Le *et al.* (2005). Images were obtained using a confocal ultraspectral microscope (Leica TCS SP2). For ultra structural images of the malignant tumours, symptomatic mice were anaesthetized by intraperitoneal injection of 40 mg/kg ketamine and 30 mg/kg xylazine and then intracardially perfused with 2% paraformaldehyde, 2.5% glutaraldehyde, and 0.1 M phosphate buffer, pH 7.4. Tissues were dissected and immersed in the same fixative solution at 4°C overnight, washed in phosphate buffer, post-fixed in 1% osmium tetroxide, dehydrated in graded ethanol series, and embedded in epoxyresin (Durcupan). Semi-thin sections were cut with a glass knife at 1–3 µm and stained with toluidine blue to check the quality of the tissue before the electron microscopy studies. For electron microscopy, ultrathin sections (70–90 nm) were cut on an ultramicrotome (Reichert Ultracut E; Leica) and collected on 200-mesh nickel grids. Staining was performed on drops of 1% aqueous uranyl acetate, followed by Reynolds's lead citrate. Ultrastructural analyses were performed in a Philips TECNAI 12 electron microscope.

Sodium dodecyl sulphate polyacrylamide gel electrophoresis and immunoblotting

Nerves or cultured Schwann cells were homogenized at 4°C in radioimmunoprecipitation assay buffer (PBS, 1% Nonidet P-40, 1% sodium deoxycholate, 0.1% SDS, and 5 mM EGTA) containing protease inhibitors (Complete MINI tablets; Roche) and, where necessary, phosphatase inhibitors (Phospho STOP tablets, Roche). Protein concentrations were determined by the bicinchoninic acid method (Pierce). Total protein (10–50 µg) of was subjected to SDS-PAGE and blotted onto Protran nitrocellulose membrane (Whatman). Membranes were blocked and incubated overnight at 4°C with the indicated primary antibody, washed and incubated with secondary antibodies, and developed with ECL Plus (GE Healthcare). The secondary antibodies were conjugated with horseradish peroxidase (1:2000; Sigma).

Chromatin immunoprecipitation assay

The chromatin immunoprecipitation (ChIP) assay was a modification of the method described by Jang *et al.* (2006). Briefly, nerves from seven post-natal Day 20 mice (*NSE-SMDF*^{+/-} mutants and wild-type littermates) were removed, chopped into small pieces and incubated in PBS/1% paraformaldehyde for 25 min at room temperature. Tissue was harvested by centrifugation (1000g for 3 min) and washed with PBS. Pellet was resuspended in 1.2 ml of buffer A (150 mM NaCl, 10%

glycerol, 0.3% Triton, 50 mM Tris-HCl pH8 and protease inhibitors), homogenized and sonicated (20 pulses of 20 s separated by 40 s on ice between each pulse) to 'high power' in the Bioruptor (Diagenode). Chromatin was clarified by centrifugation at 21 000g for 30 min at 4°C. Protein concentration in the supernatant was quantified by the bicinchoninic acid method (BCA, Pierce). An aliquot was saved as input. The volume corresponding to 60–100 µg of protein was incubated with the corresponding antibody (anti-H3K27me3 or control IgG) overnight at 4°C to form immunocomplexes. Protein A sepharose (CL-4B, GE Healthcare) was resuspended in distilled water and pelleted by centrifugation (<500g). Resin was resuspended in water with 0.5 mg/ml of bovine albumin and 0.2 mg/ml of sonicated DNA (herring sperm, Sigma). This slurry (40 µl) was added to the immunocomplex and incubated for 1 h at 4°C. Immune complexes were centrifuged (500g, 3 min) and washed twice with 1 ml of 'low salt buffer' (0.1% SDS, 1% TritonTM X-100, 2 mM EDTA, 20 mM Tris pH 8.1, 150 mM NaCl, Complete protease inhibitors, Roche). Then washed once with 1 ml of 'high salt buffer' (the same as the low but with 500 mM NaCl) and washed three times with 1 ml of LiCl buffer (0.25 M LiCl, 1% IGEPAL, 1% sodium deoxycholate, 1 mM EDTA, 10 mM Tris pH 8.1, protease inhibitors). Chromatin from immunocomplexes and input was eluted with 300 µl of 1% SDS, 0.1 M NaHCO₃, 200 mM NaCl and incubated at 65°C for 6 h (to break the DNA–protein complexes). DNA was purified using a column purification kit (GE healthcare) and submitted to SYBR[®] green quantitative PCR with the indicated primers.

Microarray analysis

Total RNA was extracted from the sciatic nerves of three matched *NSE-SMDF*^{+/-} mice and three wild-types from two different littermates. The RNA from each mouse was hybridized to GeneChip[®] Mouse Gene 1.0 ST arrays according to the manufacturer's protocol (Affymetrix). The microarray data were then analysed using GeneSpring GX 11 (Agilent Technologies, Inc). Robust Multichip Average algorithm was used for data normalization. Values show fold increase. *P*-value for each gene is shown. Complete microarray data are available on request.

Results

Schwann cell proliferation is halted in neurofibromas from adult *NSE-SMDF*^{+/-} mutant mice

We have previously shown that overexpression of the SMDF neuregulin isoform [in the *NSE-SMDF*^{+/-} mice] induces tumour development in peripheral nerves. Intriguingly, after an initial period of growth (from post-natal Days 5 to 14) Schwann cell proliferation stops in the nerves of these mice. Consequently, cellularity remains increased (about three times) but stable during the whole life of the mutant animals. We initially reasoned that proliferation was halted because of a decrease in the expression of the transgene in adult animals, however, the transgene is clearly expressed in adult animals (Supplementary Fig. 1A–C), ruling out this possibility. Then, we looked for a putative downregulation of neuregulin receptors in the mutant mice but as shown in Supplementary Fig. 1D, erbB2 and erbB3, the unique erbB

receptors in Schwann cells, are normally expressed in mutant nerves. In fact, we consistently observed an increase in the expression of erbB3 in the sciatic nerves of the *NSE-SMDF^{+/-}* mice. We then explored, at different ages, the activation status of the ERK signalling pathway, which is pivotal for neuregulin-induced Schwann cell proliferation (Birchmeier and Nave, 2008). To this end we determined the phosphorylation status of ERK1/2. As shown in Supplementary Fig. 1E, the ERK signalling pathway remains activated even when proliferation in the mutant nerves has halted (Supplementary Fig. 1F). Neuregulin promotes cell proliferation by inducing cyclin D1, a positive regulator of the G1/S transition (Kim *et al.*, 2000; Atanasoski *et al.*, 2001; Yang *et al.*, 2008). Therefore, the possibility existed that the proliferation arrest was the consequence of a failure to express this pivotal gene. Surprisingly, we found that cyclin D1 was not downregulated, but notably increased in the adult transgenic nerves (Supplementary Fig. 1G). Taken together, our data show that, despite neuregulin signalling remaining hyperactivated in the *NSE-SMDF^{+/-}* transgenic nerves, Schwann cell proliferation stops after post-natal Day 14.

Proliferation of Schwann cells is restricted by the activation of the replicative senescence programme in the *NSE-SMDF^{+/-}* neurofibromas

It has been established that over-activation of intracellular signalling pathways by oncogenes is necessary, but not sufficient, for cancer development (Collado *et al.*, 2007; Collado and Serrano, 2010; Kuilman *et al.*, 2010). Tumour overgrowth is prevented when cells detect an aberrant situation and activate a genetic programme (Oncogene Induced Senescence) that blocks the cell cycle. This programme is primarily mediated by the Arf/p53 and p16Ink4a/Rb pathways (Matheu *et al.*, 2008; Gorgoulis and Halazonetis, 2010). The establishment of oncogene induced senescence depends on ERK activation downstream of RAS and RAF. As outlined previously, in *NSE-SMDF^{+/-}* nerves Schwann cell proliferation is halted after post-natal Day 14 despite the persistence of ERK pathway activation. To test if this is mediated by the activation of the oncogene induced senescence programme, we looked for the expression of p19Arf in transgenic nerves. As is shown in Fig. 1A, a clear nucleolar expression of p19Arf was detected in post-natal Day 20 and 150 mutant nerves. In contrast, practically no expression could be detected in the PNS of wild-type littermates. This result was confirmed by western blot (Fig. 1B). Interestingly, p19Arf was exclusively expressed by the non-myelinating Schwann cells, as demonstrated by the almost complete absence of co-localization with *Krox-20* (Fig. 1C). The *Ink4a/Arf* locus encodes for both p19Arf (p14Arf in humans) and p16Ink4a. Although working through different pathways, both proteins are known to activate the senescence programme. As shown (Fig. 1D), p16Ink4a expression is also increased in mutant nerves and co-localizes with p19Arf, suggesting that the p16Ink4a/Rb pathway contributes to control Schwann cell over-proliferation in the neurofibromas developed by the *NSE-SMDF^{+/-}* mice. The absence of p19Arf expression in some p16Ink4a positive cells is

probably consequence of the p53 capacity to block the former transcript through a previously described feedback loop, that has no effect on p16Ink4a (Gil and Peters, 2006). To obtain further insight we measured the expression levels of p19Arf and p16Ink4a messenger RNAs at different ages by quantitative PCR. As is shown in Fig. 1E and F, both transcripts were clearly increased in transgenic nerves from post-natal Days 20 to 720.

To obtain a more comprehensive view we performed high throughput gene expression analysis of the mutant nerves using Affymetrix Genechip Mouse Gene 1.0ST Array. Sciatic nerves of post-natal Day 20 *NSE-SMDF^{+/-}* mice and wild-type littermates were removed, and total RNA extracted. RNA from three animals per genotype was separately hybridized to the chip. To validate the array approach we first looked for myelination markers. In agreement with what we found previously (Gomez-Sanchez *et al.*, 2009), most messenger RNAs for myelin proteins (like CNPase, MBP or MAG) were downregulated in the mutant nerves. A similar result was obtained for cholesterol biosynthetic enzymes. This is a consequence of the increased number of non-myelinating Schwann cells that over-populate mutant nerves and is not generated by expansion of the peri/epineural compartment (Gomez-Sanchez *et al.*, 2009). In support of this, we did not observe an increase in markers for this compartment (such as Resistin, Lpl or Acpr30) in the microarray data. Thus far, these results confirm our previous findings and validate the microarray approach for our subsequent analysis.

Next we analysed the expression of genes involved in oncogene induced senescence. As shown (Table 2), not only *Ink4a/Arf* but also *Ink4b* (p15) is upregulated in mutant nerves, suggesting that both loci collaborate in the establishment of the senescence programme. Interestingly, it has been shown that the expression of three genes (*p15Ink4b*, *p16Ink4a* and *p19Arf*) is highly coordinated in other systems (Gil and Peters, 2006). We also found increased levels of *p53* messenger RNA and, interestingly, *Wnt16* messenger RNA, a recently described new marker of cellular senescence (Binet *et al.*, 2009). In contrast cell cycle inhibitors like *p27^{kip1}* and (intriguingly) *p21^{cip}* were downregulated.

Histone demethylase *Jmjd3* contributes to the activation of the *Ink4a/Arf* locus in neurofibroma Schwann cells

It has recently been shown that *Jmjd3* epigenetically controls the expression of the *Ink4a/Arf* locus after oncogenic activation of RAS in primary fibroblasts (Agger *et al.*, 2009; Agherbi *et al.*, 2009; Barradas *et al.*, 2009). To establish if a similar mechanism mediates activation of the *Ink4a/Arf* locus in the *NSE-SMDF^{+/-}* mice, we checked the expression of *Jmjd3* in mutant nerves. First we performed immunofluorescence analysis with a polyclonal anti-*Jmjd3* antibody. As shown (Fig. 2A), *Jmjd3* immunoreactivity was significantly increased in mutant nerves. Measuring messenger RNA expression levels for this gene by quantitative PCR confirmed this result (Fig. 2B). The increase was specific, as demonstrated by the unchanged expression of the related demethylase *Utx* (Fig. 2B and data from the microarray analysis in Table 2). Secondly, we explored the activation/repression status of the *Ink4a/Arf* locus by ^{+/-}ChIP. Using methylation-sensitive specific antibodies,

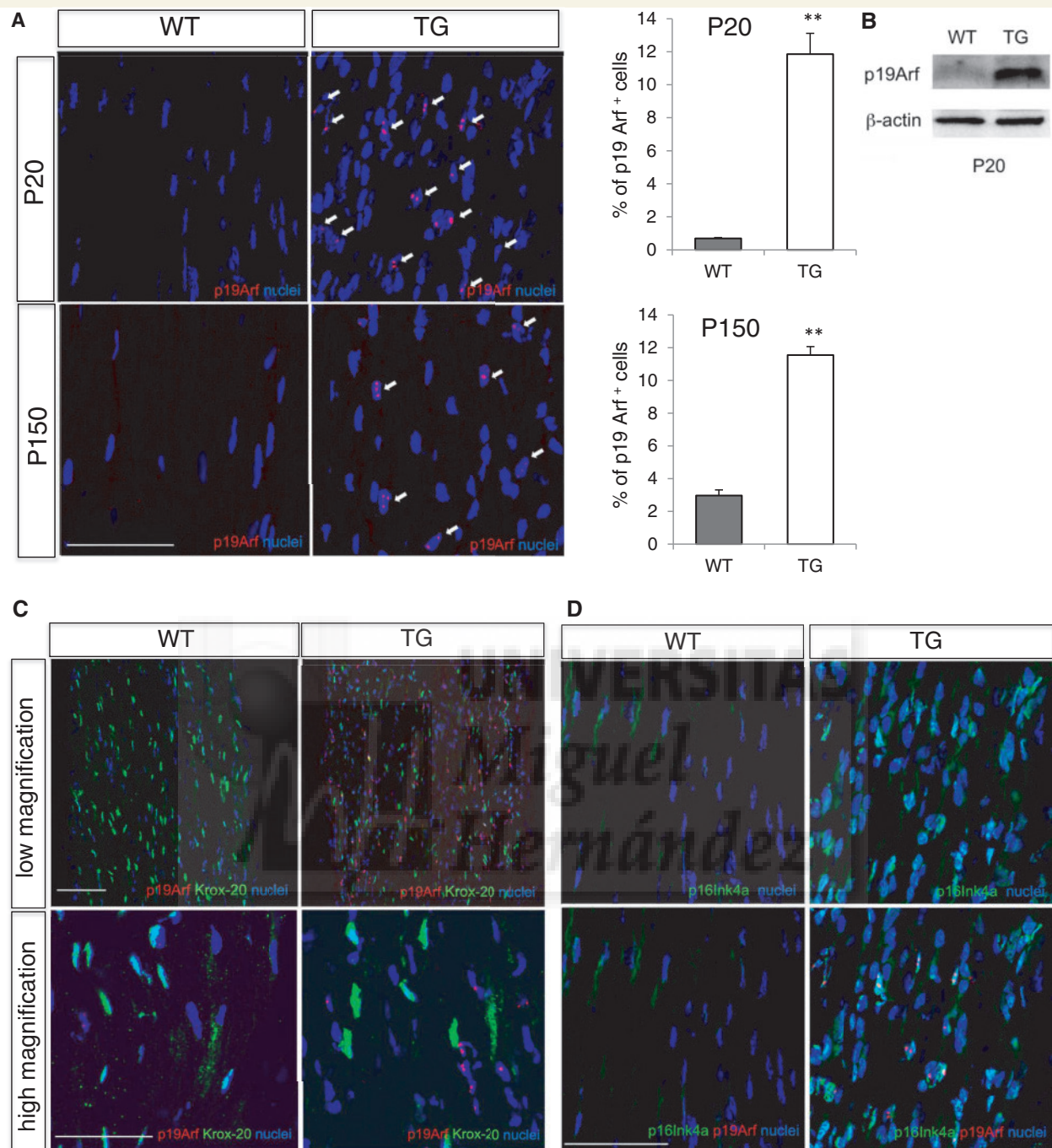


Figure 1 *Ink4a/Arf* locus products are expressed in the peripheral nerves of the *NSE-SMDF*^{+/-} mice. (A) p19Arf is highly expressed in the neurofibromas developed by the mutant mice (TG) but barely in the nerves of wild-type (WT) littermates. Longitudinal sections of mutant and wild-type nerves (P20 and P150) were incubated with anti-p19Arf rat monoclonal antibody. A clear nucleolar labelling (red) was observed in many of the neurofibroma cells under the confocal microscope. In contrast, p19Arf was barely detected in wild-type nerves. Quantification shows that the number of p19Arf⁺ cells increases slightly in wild-type (as expected) and remains high in transgenics with age (three mice per condition were used; a mean of 2752 ± 650 cells per mice were counted; *t*-test, ***P* < 0.001). (B) p19Arf upregulation was confirmed by western blotting. Protein extracts of wild-type and transgenic sciatic nerves were submitted to SDS-PAGE and blotted with the anti-p19Arf antibody. β-actin was used as loading control. This experiment was repeated twice. A representative western blot is shown. (C) Only cells that do not enter the myelinating programme (i.e. those that are negative for Krox-20) become senescent (positive for p19Arf), as supported by the practically absence of co-localization between Krox-20 and p19Arf expression. (D) The other product of the *Ink4a/Arf* locus (p16Ink4a) is also upregulated in transgenic nerves. A high degree of co-localization between p16Ink4a and p19Arf was observed (*bottom*) suggesting a coordinated expression of both products (see text). These experiments were repeated three times. More than three sections per sample were analysed with similar results. A typical image is shown. Scale bars = 50 μm.

(continued)

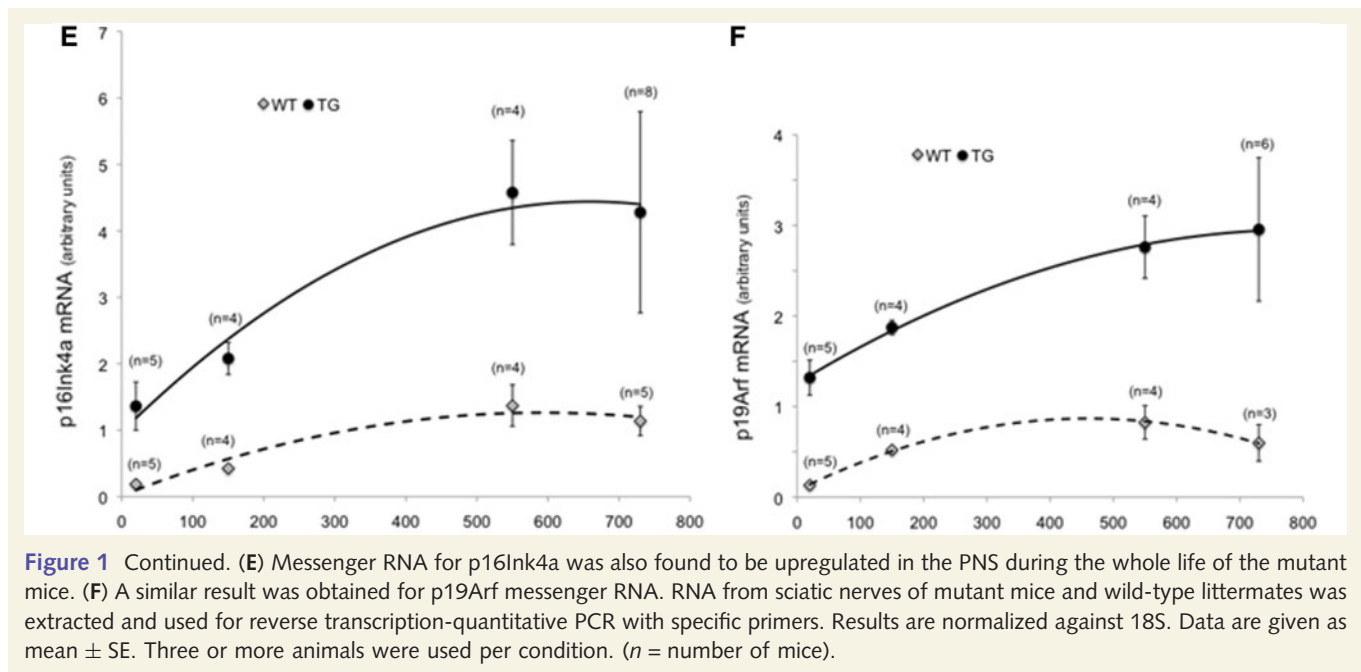


Figure 1 Continued. (E) Messenger RNA for p16Ink4a was also found to be upregulated in the PNS during the whole life of the mutant mice. (F) A similar result was obtained for p19Arf messenger RNA. RNA from sciatic nerves of mutant mice and wild-type littermates was extracted and used for reverse transcription-quantitative PCR with specific primers. Results are normalized against 18S. Data are given as mean \pm SE. Three or more animals were used per condition. (n = number of mice).

Table 2 Gene expression analysis of post-natal Day 20 NSE-SMDF^{+/-} sciatic nerves and wild-type littermates

Gene	Fold change	P-value
<i>Ink4a/Arf</i>	+1.80	2.50×10^{-4}
<i>P15 (Cdkn2b)</i>	+3.59	9.22×10^{-5}
<i>Trp53</i>	+1.51	0.006
<i>Wnt16</i>	+8.36	1.02×10^{-4}
<i>p21^{cip}</i>	-1.52	0.01
<i>p27^{cip}</i>	-1.43	7.9×10^{-4}
<i>Jmjd3</i>	+1.91	5.41×10^{-4}
<i>Utx</i>	+1.08	0.67
<i>c-Fos</i>	+2.11	0.014
<i>Sox2</i>	+6.27	4.09×10^{-7}
<i>Notch 1</i>	+2.72	6.69×10^{-5}
<i>Id2</i>	+2.07	3.20×10^{-4}
<i>Krox24</i>	+2.73	1.51×10^{-4}
<i>Egr3</i>	+2.52	3.84×10^{-4}
<i>Tenascin C</i>	+9.01	2.16×10^{-5}

Data obtained from the microarray analysis.

we immunoprecipitated H3K27me3 and performed quantitative PCR with specific primers for different promoter regions of the *Ink4a/Arf* locus (Barradas et al., 2009). Our data show that there is less H3K27me3 bound to the promoters of *p19Arf* and *p16Ink4a* in transgenic than in wild-type nerves (Fig. 2C), suggesting that they are transcriptionally active. Indeed, when we enforced the expression of *Jmjd3* in cultured rat Schwann cells (by transfecting the pCMV-*Jmjd3* vector) the expression of *p19Arf* was induced. Taken together, our data suggest that the activation of the senescence programme in neurofibroma is mediated by the recruitment of *Jmjd3* on *Ink4a/Arf* promoter regions and its de-repression by the demethylation of the H3K27me3.

Oncogene-induced senescence in human plexiform neurofibromas

NF1 patients develop plexiform neurofibromas, nerve enlargements caused by mixed cell tumours that although initially benign, can degenerate (10%) to form malignant peripheral nerve sheath tumours (Cichowski et al., 1999; Evans et al., 2002; McClatchey, 2007). To determine whether the oncogene-induced senescence programme is also activated in human neurofibromas we collected samples from human NF1-associated plexiform neurofibromas and explored the expression of senescence markers. As is shown in Fig. 3, *p14Arf* (the human homologue for *p19Arf*) is highly expressed in the human plexiform neurofibromas analysed, but not in normal peripheral nerves. A similar result was observed for *p16Ink4a*, suggesting that as in mice, malignant proliferation of Schwann cells in human plexiform neurofibroma is prevented by the activation of the senescence programme, mediated by expression of the *Ink4a/Arf* locus. We observed overexpression of this locus in 6 of 6 human NF1 plexiform neurofibromas analysed (Fig. 3 and Supplementary Fig. 2).

Malignant progression of neurofibromas is associated with the loss of p19Arf expression

We have previously shown that despite the development of neurofibromas, most NSE-SMDF^{+/-} mice show a normal external phenotype and life expectancy (Gomez-Sanchez et al., 2009). Nevertheless, ~15% of them develop neurological deficits (starting at 8 months), which are associated with the local growth of some nerve roots and/or dorsal root ganglia. In the histopathological analysis of these tumours (Fig. 4A) we observed high proliferation of atypical fusiform and round cells in short

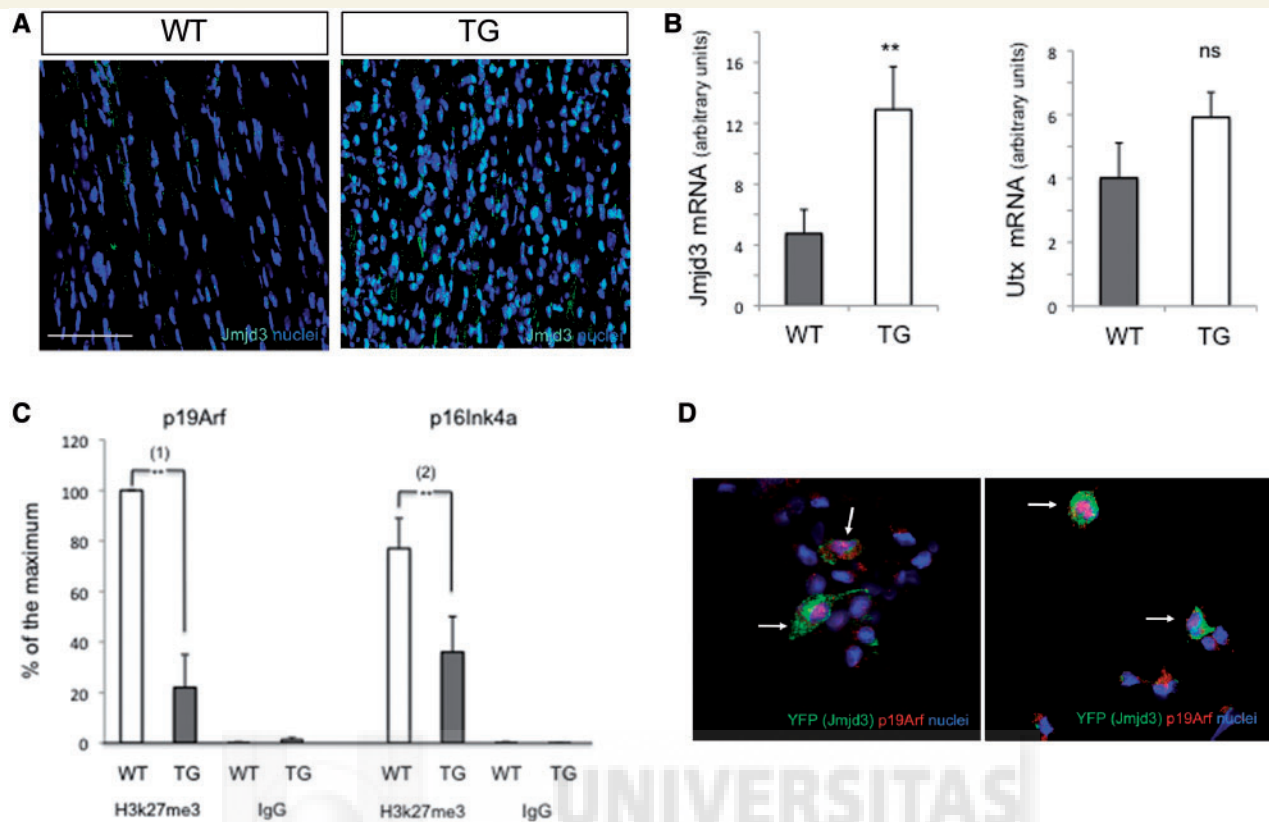


Figure 2 Chromatin modification by the Jmjd3 demethylase contributes to the activation of the *Ink4a/Arf* locus in neurofibromas. (A) Many cells in transgenic (TG) nerves express Jmjd3, whereas this protein was found to be barely detectable in wild-type (WT) post-natal Day 20 nerves. Longitudinal sections of P20 *NSE-SMDF*^{+/-} and wild-type sciatic nerves were incubated with a polyclonal anti-Jmjd3 antibody (green) and nuclei counterstained with Hoechst (blue). Representative confocal images of a typical experiment ($n = 3$) are shown. Scale bar = 50 μ m. (B) Total RNA from the sciatic nerves of post-natal Day 20 transgenic and wild-type littermates was used to perform reverse transcription quantitative PCR with specific primers for Jmjd3. Results were normalized against 18S ribosomal RNA. As shown, messenger RNA for Jmjd3 was increased 2.74-fold in transgenic nerves. The increase was specific for Jmjd3, as the messenger RNA levels of Utx, a demethylase of the same family, remained unchanged (results are given as mean \pm SE; $n = 8$ for Jmjd3, and $n = 3$ for Utx; ** P -value = 0.025; t -test). (C) ChIP shows that there is less H3K27me3 bound to the promoters of p19Arf and p16Ink4a in transgenic nerves than in wild-type littermates. Sciatic nerves from seven mice were crosslinked with paraformaldehyde and immunoprecipitated with the anti-H3K27me3 polyclonal antibody or a non-specific IgG (ChIP grade). Quantitative PCR was performed with specific primers for promoter regions in the *Ink4a/Arf* locus. Results were normalized against the maximum amount of immunoprecipitated promoter and expressed as a percentage. Data are given as mean \pm SE. Three independent experiments were performed ($n = 3$); Paired t -test; (1) P -value = 0.01; (2) P -value = 0.03. (D) Enforced expression of Jmjd3 upregulates p19Arf in Schwann cells. Rat Schwann cells were transfected with the pCMV-Jmjd3 expression vector and incubated in SATO medium for 48 h ($n = 3$). The fluorescent reporter pEYFP was co-transfected to facilitate the detection of the Jmjd3 over-expressing cells. About 40% of the pCMV-Jmjd3 expressing cells (green) were p19Arf positive (red), whereas this gene was expressed in <3% of non-transfected cells.

fascicles and focal whorled arrangement, as well as pleomorphic nuclei with high mitotic rate and focal necrosis, all of them consistent with the histology of human malignant peripheral nerve sheath tumours. To discover if this local growth is produced by resumption of Schwann cell proliferation in these neurofibromas, we explored the level of phospho-histone H3, a marker of cell proliferation, and compared it with levels in neurofibromas where proliferation was halted. As is shown in Fig. 4B, the phospho-histone H3 labelling is dramatically increased, suggesting an augmented proliferation rate in these tumours due to re-entry into the cell cycle of some previously arrested Schwann cells. We reasoned that transformation of these non-malignant neurofibromas

into malignant tumours could be related to the loss of the capacity of some cells to enter (or to stay) the senescence programme. To explore this point, we determined the messenger RNA expression levels for *p19Arf* and *p16Ink4a* in 10 highly proliferative tumours developed by the *NSE-SMDF*^{+/-} mice between post-natal Days 240 and 720. As shown in Fig. 4C, seven of these tumours showed a reduced expression of *p19Arf*, suggesting that their malignant transformation is mediated by loss of the oncogene-induced senescence programme. In contrast, we found high variability in levels of *p16Ink4a* expression (Fig. 4D), implying that the loss of the senescence programme is mainly a consequence of a failure in signalling mediated by p19Arf. To verify this hypothesis,

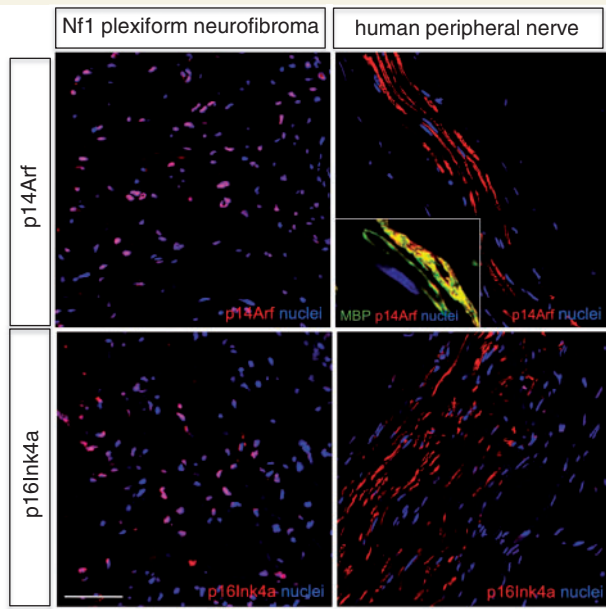


Figure 3 *Ink4a/Arf*-locus products are expressed in human plexiform neurofibromas. (A) Human NF1 plexiform neurofibromas express p14Arf (the human homologue for p19Arf), whereas it is barely detectable in the nuclei of Schwann cells of nerves obtained from biopsies of healthy subjects. (B) p16Ink4a is also abundantly expressed in human plexiform neurofibromas but it can be detected (although less frequently) in the Schwann cell nuclei of normal nerves. We did notice non-nuclear staining for p14Arf and p16Ink4a in healthy human nerves, which co-localizes with MBP (*inset*). This is probably due to non-specific binding of the antibodies to the lipid rich myelin in the formalin fixed paraffin embedded tissues (Supplementary Fig. 2H). Scale bar = 50 μ m.

we decreased the capacity to activate the senescence programme through the p19Arf/p53 pathway by obtaining *NSE-SMDF*^{+/-}; *p53*^{+/-} double heterozygotes. Strikingly, the Kaplan-Meier survival curve (Fig. 5A) demonstrated that elimination of a single copy of *p53* increases up to 100% the incidence (and decreases significantly the age) of malignant tumour development. As in the case of the *NSE-SMDF*^{+/-} simple heterozygotes, most tumours developed on nerve roots and dorsal root ganglia, but, as shown in Fig. 5B, some highly proliferative tumours also developed on sciatic nerve neurofibromas, and could be distinguished easily by the increased proliferation rate (pH3). When analysed by transmission electron microscopy they showed aberrant structures including huge deposits of extracellular collagen and dissociated Schwann cells (Fig. 5C), resembling malignant peripheral nerve sheath tumours.

Ink4a/Arf locus is induced in Schwann cells during Wallerian degeneration

After nerve injury, the myelinating Schwann cells of the distal stump de-differentiate in a process dependent on the transcription factor c-Jun (Parkinson *et al.*, 2008). If the growing axons of the

proximal segment can reach the distal stump, Schwann cells will differentiate and remyelinate generating a functional peripheral nerve. However, if the axons cannot enter the distal stump, Schwann cells will not differentiate but will remain in a non-proliferative state that can last up to 2 months (Scherer *et al.*, 1994; Shy *et al.*, 1996). The cause of proliferation arrest in the distal stumps is unknown. It could be explained by both the washing out of some mitogens and/or by the induction of some mechanism that actively blocks proliferation. To check whether, as in neurofibroma, the *Ink4a/Arf*-mediated replicative senescence contributes to halting Schwann cell proliferation after nerve injury, we performed anti-p19Arf immunofluorescence studies of the distal stump of transected nerves. As shown in Fig. 6A, in the Schwann cells of the distal stump p19Arf is expressed from the fourth to the 24th day post-injury. p19Arf-positive cells were identified as non-myelinating Schwann cells as they express S100 β but fail to express Krox-20 (Fig. 5B). To unambiguously identify the p19Arf immunoreactivity, we performed transection experiments in *Ink4a/Arf* knock-out mice. As shown in Fig. 6C, no nucleolar labelling could be observed in the distal stumps of *Ink4a/Arf*^{-/-} mice, confirming the specificity of the immunolabelling in the wild-types. Interestingly Jmjd3 was also upregulated soon after injury (Fig. 6D), suggesting that histone H3K27 demethylation also contributes to de-repressing this locus in the distal stumps of transected nerves. As expected, cell proliferation (evaluated with anti-phospho histone H3 antibody) is very low after 24 days (Fig. 6E).

Schwann cells are highly plastic and can de-differentiate and re-differentiate multiple times *in vivo* (Monje *et al.*, 2010). To determine if they can also revert the senescence programme we induced nerve injury by crushing the sciatic nerve with forceps. This strategy produces total axotomy, but the epineuria remains intact, allowing proximal segment axons to grow into the distal stump facilitating rapid nerve repair. We found that p19Arf is upregulated in crushed nerves (Fig. 6F), but remarkably, as soon as the re-entry of axons induces the differentiation programme in Schwann cells, the expression of p19Arf is downregulated (Fig. 6G). Thus far, our data suggest that the *Ink4a/Arf*-mediated senescence programme in the injured PNS is reversible, and can be switched off when Schwann cells re-enter the myelination programme.

Ink4a/Arf-mediated senescence contributes to growth arrest during Wallerian degeneration

To investigate the role of the *Ink4a/Arf* locus in the control of cell proliferation after PNS injury, we performed sciatic nerve transections in *Ink4a/Arf*^{-/-} mice. Four and 12 days after injury proliferation rate was calculated by estimating the number of Ki67-positive cells in relation to the number of total cells in defined areas of the distal stumps. As a control, we performed the same experiment in wild-type littermates. As is shown in Fig. 7A, we found a significantly increased proliferation rate in the distal stumps of mutant mice. This increased proliferation was still observed up to 12 days post injury, when it had reached ~30%. Thus far, our data suggest

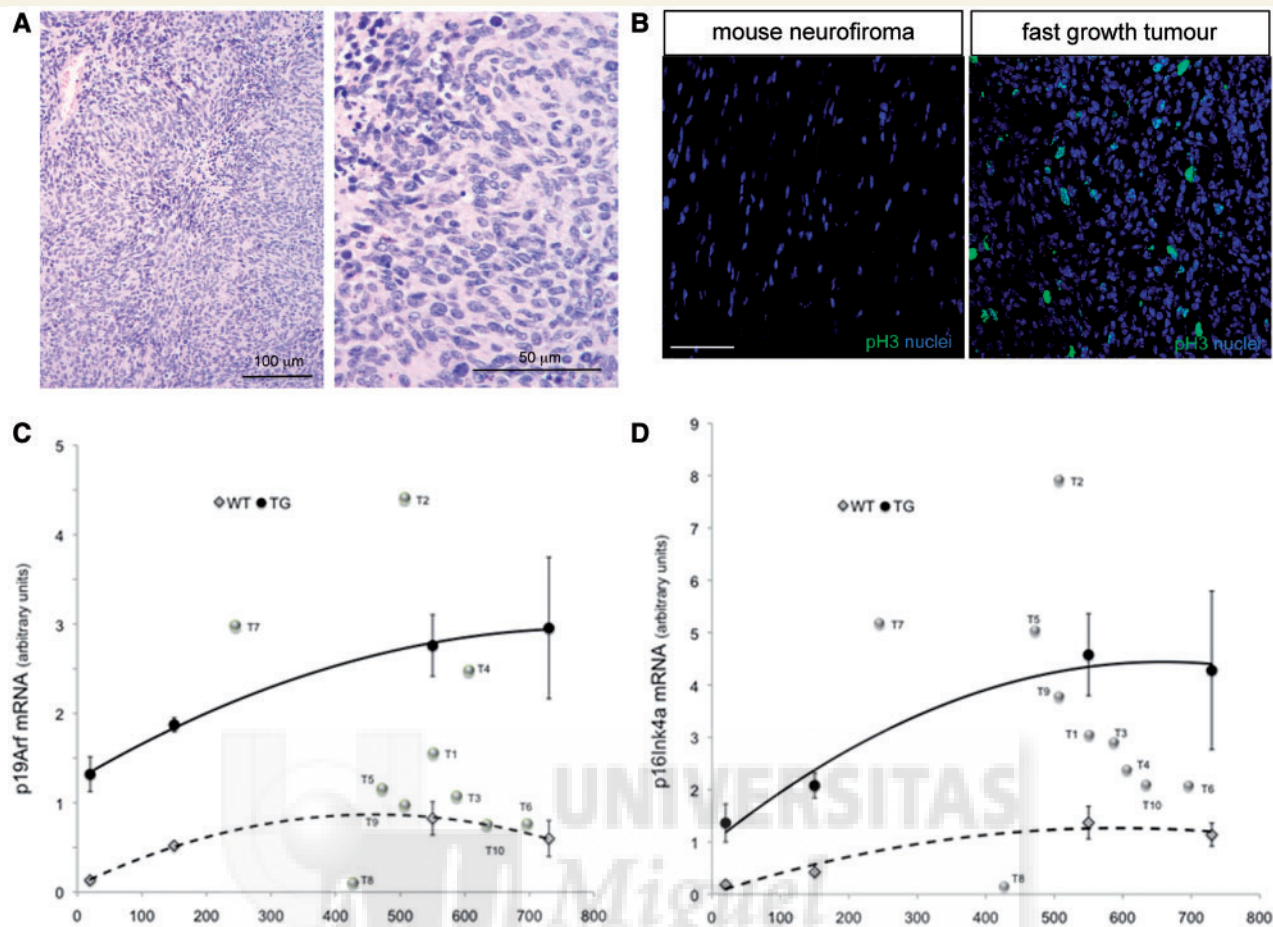


Figure 4 Loss of the senescence programme induces malignant transformation of neurofibromas. (A) Histopathological aspect of fast-growth tumours developed by ~15% of the *NSE-SMDF*^{+/-} mice. *Left*: Proliferation of atypical fusiform and round cells, in short fascicles and focal whorled arrangement. *Right*: Pleomorphic nuclei with high mitotic rate and focal necrosis, all consistent with malignant peripheral nerve sheath tumour. (B) Proliferation rate is notably increased in the malignant tumours developed in the PNS by the *NSE-SMDF*^{+/-} mice, as demonstrated by anti-phospho-histone H3 staining. Sections of fast growing tumours and *NSE-SMDF*^{+/-} sciatic nerves were incubated with anti-phospho-histone H3 antibody (green) and nuclei counterstained with Hoechst (blue). As is shown, many cells were positive for phospho-histone H3 in the tumours but not in neurofibromas. The experiment was repeated three times with similar results. A representative experiment is shown. Scale bars = 50 μ m. (C) Total RNA was obtained from 10 fast-growing tumours developed by the *NSE-SMDF*^{+/-} mice and the messenger RNA for *p19Arf* quantified by reverse transcription quantitative PCR. Results were normalized against 18S ribosomal RNA. *p19Arf* messenger RNA was plotted against the levels of wild-types and transgenics. As is shown, in seven of these tumours *p19Arf* messenger RNA was downregulated to the levels of wild-type nerves. (D) By contrast the variability in expression levels of *p16Ink4a* messenger RNA in the tumours is high, and there is no clear downregulation.

that the gene expression products of the *Ink4a/Arf* locus contribute to the proliferation arrest in the distal stumps of transected nerves. As we have shown previously, the stabilization of p53 by p19Arf is needed to block Schwann cell proliferation in the neurofibromas developed by the *NSE-SMDF*^{+/-} mice. To determine the contribution of the p19Arf/p53 pathway to Wallerian degeneration growth arrest, we performed nerve transection experiments in *p53* knock out mice. As shown in Fig. 7B, proliferation rate after injury was found increased in the *p53*^{-/-} nerves, suggesting that, as in neurofibromas, the stabilization of p53 by p19Arf contributes to the prevention of over-proliferation during the initial steps of peripheral nerve regeneration.

Discussion

Control of Schwann cell numbers in the PNS is a tightly regulated process that fits the number of glial cells to the axon length, guaranteeing adequate myelination and nerve conduction velocity (Sherman and Brophy, 2005). To this aim, axons produce signalling molecules that critically control the proliferation of the Schwann cell lineage during development (Salzer and Bunge, 1980; Salzer *et al.*, 1980). One of these axon-derived signals is thought to be a product of the *NRG1* gene (Jessen and Mirsky, 2005). We have recently shown that axonal over expression of the type III- β neuregulin 1 induces Schwann cell hyper-proliferation and nerve enlargement

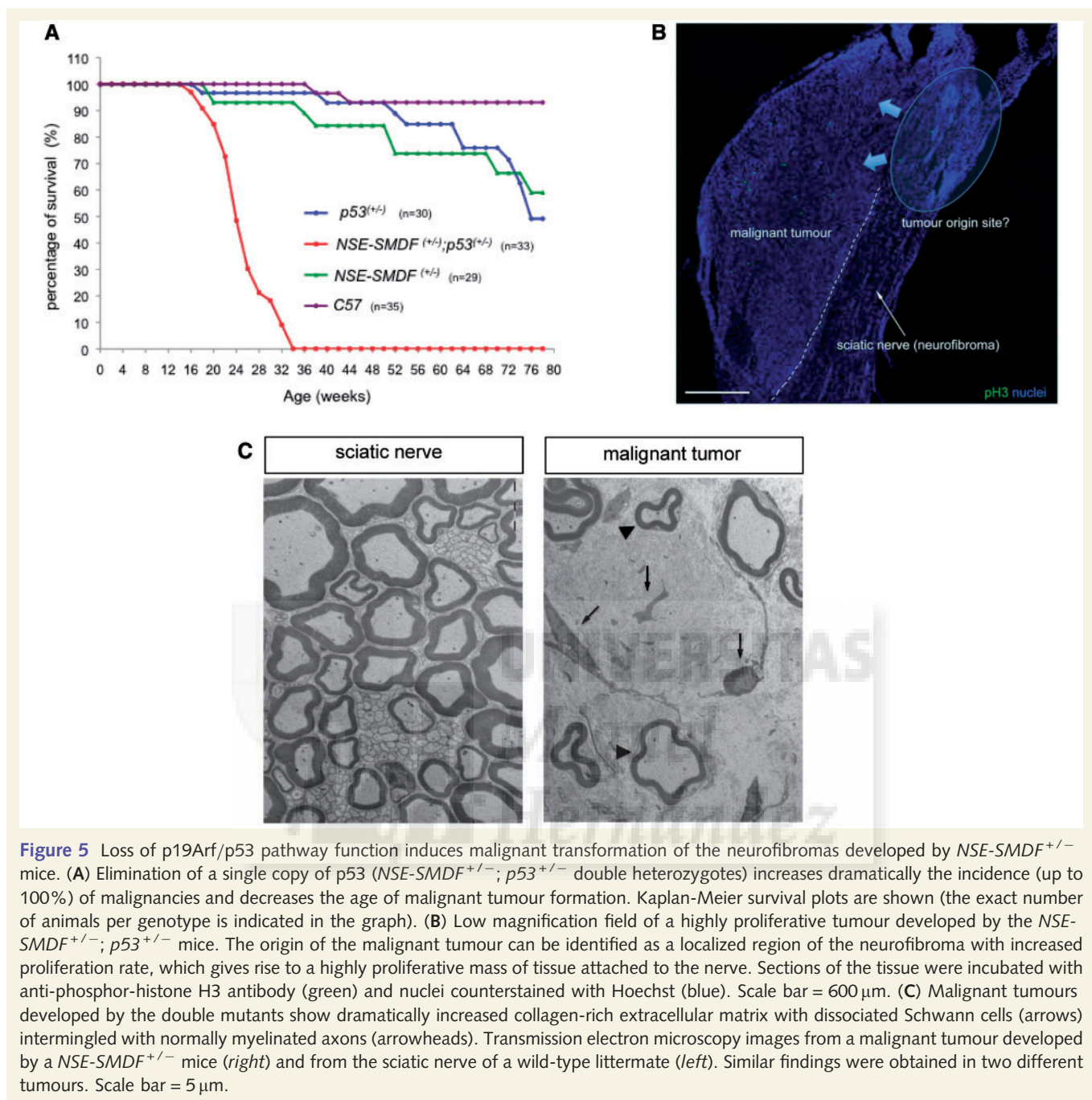


Figure 5 Loss of p19Arf/p53 pathway function induces malignant transformation of the neurofibromas developed by *NSE-SMDF*^{+/-} mice. **(A)** Elimination of a single copy of p53 (*NSE-SMDF*^{+/-}; *p53*^{+/-} double heterozygotes) increases dramatically the incidence (up to 100%) of malignancies and decreases the age of malignant tumour formation. Kaplan-Meier survival plots are shown (the exact number of animals per genotype is indicated in the graph). **(B)** Low magnification field of a highly proliferative tumour developed by the *NSE-SMDF*^{+/-}; *p53*^{+/-} mice. The origin of the malignant tumour can be identified as a localized region of the neurofibroma with increased proliferation rate, which gives rise to a highly proliferative mass of tissue attached to the nerve. Sections of the tissue were incubated with anti-phosphor-histone H3 antibody (green) and nuclei counterstained with Hoechst (blue). Scale bar = 600 μ m. **(C)** Malignant tumours developed by the double mutants show dramatically increased collagen-rich extracellular matrix with dissociated Schwann cells (arrows) intermingled with normally myelinated axons (arrowheads). Transmission electron microscopy images from a malignant tumour developed by a *NSE-SMDF*^{+/-} mice (*right*) and from the sciatic nerve of a wild-type littermate (*left*). Similar findings were obtained in two different tumours. Scale bar = 5 μ m.

(Gomez-Sanchez *et al.*, 2009). Surprisingly, after an initial period of active cell proliferation, nerve growth stops with the tissue acquiring most of the macroscopic and histological traits of neurofibromas. Interestingly, the growth of plexiform neurofibromas in *NF1* patients is also limited, despite the persistence of the tumorigenic stimulus (Harrisingh *et al.*, 2004; McClatchey, 2007; Carroll and Ratner, 2008). Our data suggest that the stop in the growth of both types of neurofibromas is a consequence of induction of the *Ink4a/Arf* locus which activates the oncogene-induced senescence programme. But, how is the *Ink4a/Arf* locus induced? In physiological conditions this locus is silenced by the trimethylation of the Lys27 on histone H3, a modification imposed by the polycomb group (PcG)

proteins (Bracken *et al.*, 2007). It has been shown that in RAS transformed fibroblasts induction the *Ink4a/Arf* locus is mediated by the demethylase *Jmjd3* (Agger *et al.*, 2009; Agherbi *et al.*, 2009; Barradas *et al.*, 2009). The activity of *Jmjd3* removes the methyl groups on the K27 of histone H3, reverting the silencing effects of the PcG proteins. Remarkably, we found increased levels of *Jmjd3* in mice neurofibromas. Using ChIP assay we show evidence that this demethylase is recruited to the *p19Arf* and *p16Ink4a* promoters, where it removes the trimethyl groups of the lysine 27 in histone H3 (Fig. 2C) de-repressing this locus. One question that remains is how *Jmjd3* itself is induced. Interestingly there is a binding site for AP-1 in the promoter of *Jmjd3* (Ameyar-Zazoua *et al.*, 2005).

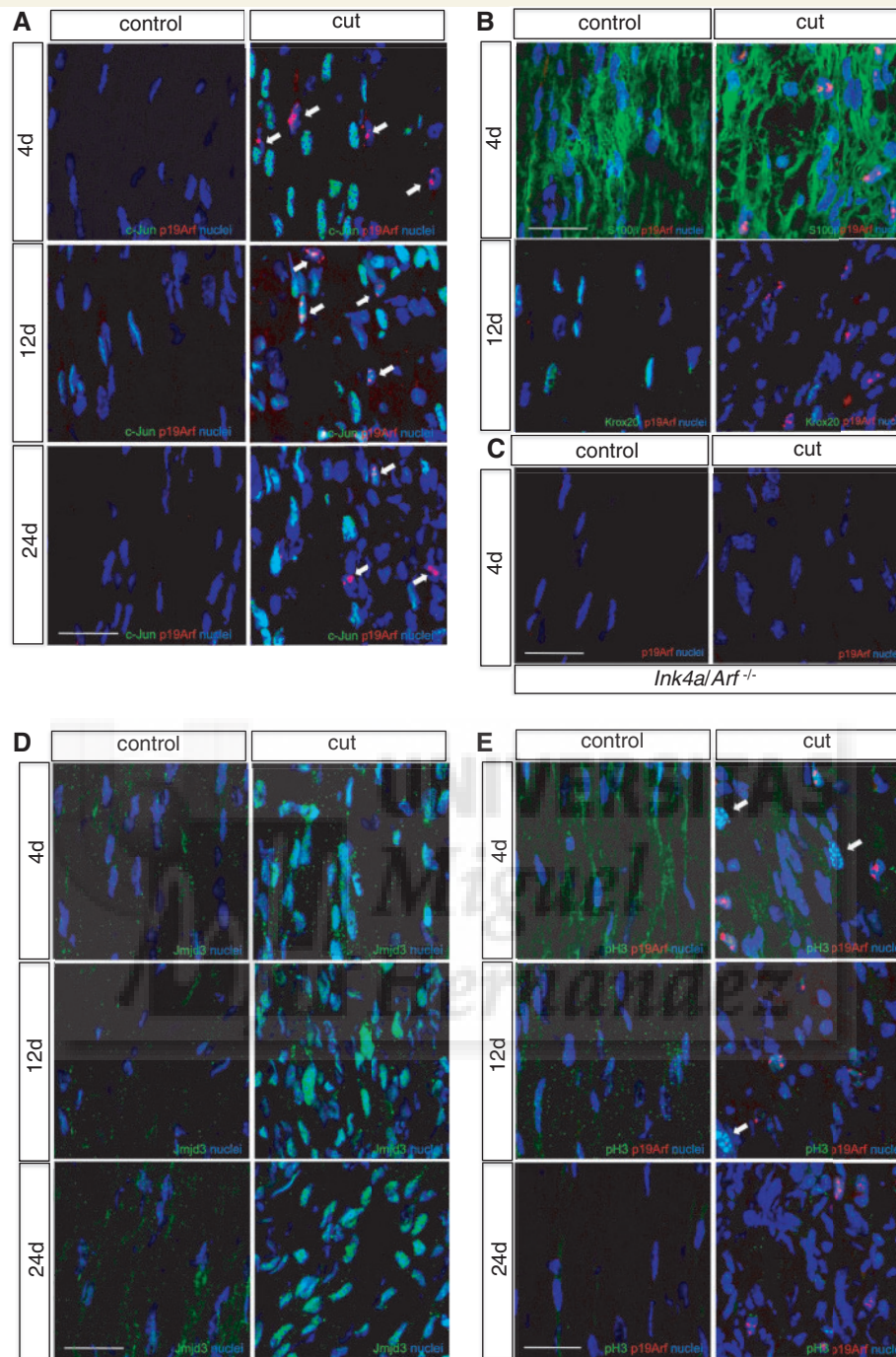


Figure 6 Nerve injury induces the expression of the *Ink4a/Arf* locus in Schwann cells. (A) After complete sciatic nerve transection, expression of p19Arf (arrows) is induced in the distal stump. Expression of this protein is maintained up to 24 days post-injury. The re-expression of c-Jun denotes the presence of de-differentiated Schwann cells in the injured nerve segment. (B) p19Arf is only expressed by non-myelin forming Schwann cells as demonstrated by its co-localization with S100 β and the absence of colocalization with Krox2. (C) The specificity of the nucleolar p19Arf labelling was demonstrated by the absence of any staining in the injured nerves of the *Ink4a/Arf*^{-/-} mice. (D) *Jmjd3* is also upregulated suggesting that epigenetic mechanisms activate the senescence programme after injury. (E) As expected, cell proliferation (phospho-histone H3 immunoreactivity) decreases with time in the distal stump. (F) p19Arf expression is also induced in crushed (but not transected) nerves. At 12 days post-crush, regrowing axons trigger the re-expression of Krox-20 and subsequently the downregulation of c-jun. Despite this, c-Jun and p19Arf can be detected in Schwann cells. (G) By Day 24 post-crush levels of c-Jun were almost undetectable and levels of p19Arf were found to be reduced to those present in non-injured nerves. Longitudinal sections of the distal stump of transected or crushed sciatic nerves (and the contralateral non-injured nerves) from adult wild-type mice were incubated with the indicated antibodies and nuclei counterstained with Hoechst. Three or more animals were used per condition. A representative image is shown. Scale bars = 50 μ m.

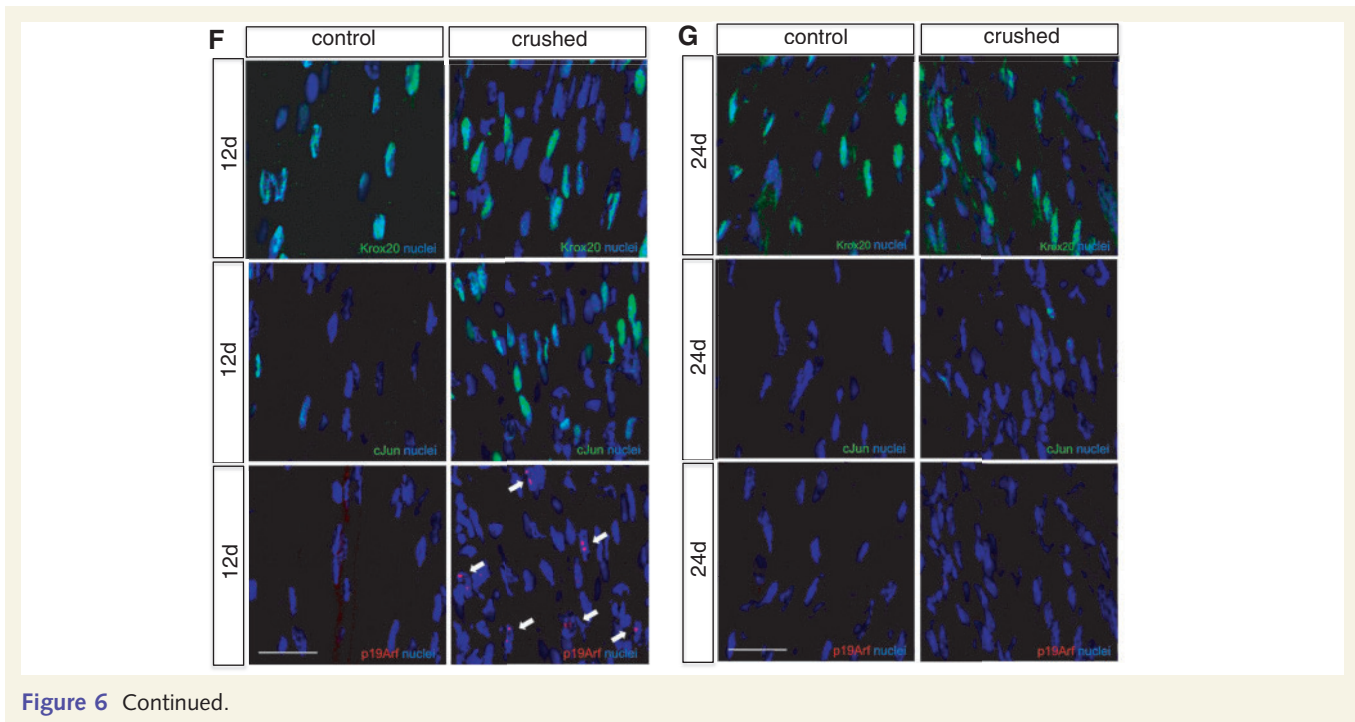


Figure 6 Continued.

We have found increased c-Jun expression in both, human and mouse neurofibromas (Supplementary Fig. 2 and 3). We also found upregulated c-Fos, the main c-Jun partner (Table 2). Therefore, it is possible that the c-Jun/c-Fos dimer stimulates *Jmjd3* expression. Functional AP-1 binding sites have also been described in the *p14Arf* promoter (Ameyar-Zazoua et al., 2005). It is thus possible that the activity of *Jmjd3* makes the *Arf* promoter accessible to the AP-1 complex which subsequently promotes *Arf* expression. We found other genes involved in the establishment of replicative senescence also upregulated in mouse neurofibromas. One of them *p15Ink4b* (Table 2) is located next to the *Ink4a/Arf* locus and their expression is usually coordinated (Gil and Peters, 2006). We also observed a slight upregulation of p53, a downstream effector of p19Arf. Surprisingly, messenger RNA for p21^{cip} is decreased, which could seem to contradict the proposed model. However, it has been shown that *p21^{cip}* fibroblasts can enter the senescence programme (Pantoja and Serrano, 1999). Moreover, the role of *p21^{cip}* in the biology of Schwann cells is more complex than being a purely inhibitory molecule for the cell cycle (Atanasoski et al., 2006). Another senescence gene that is remarkably upregulated is *Wnt16* (Table 2). Notably, this gene is overexpressed and secreted from cells undergoing oncogene-induced senescence, both *in vitro* and in the *in vivo* murine model of KRasV12-induced senescence (Binet et al., 2009).

It has been shown that a negative feedback signalling network contributes to the oncogene-induced senescence in human fibroblasts with decreased neurofibromin expression (Courtois-Cox et al., 2006). This is mediated by the inhibition of the Ras/PI3K pathway through the Sprouty family of proteins, and can impact on the senescence machinery through HDM2 and FOXO. Although we found no changes in *Hdm2* and *Foxo* gene expression, sprouty homolog 4 was found upregulated in the mouse

neurofibromas (data from the microarray analysis). Therefore the possibility exists that this mechanism contributes to block cell cycle in mouse neurofibroma Schwann cells. In summary, our results suggest that a complex array of mechanisms leading to senescence is activated in response to tumorigenic stimuli in the PNS.

The malignant peripheral nerve sheath tumours risk in NF1 is ~10% during life time (Evans et al., 2002). Akin to human NF1 patients, ~15% of peripheral nerve tumours developed by the *NSE-SMDF^{+/-}* mice progress to malignancy. Here we show that 70% of these malignant tumours have a decreased expression of p19Arf. By contrast, p16Ink4a expression is quite variable and appears to be normal (or even increased) in most. These data suggest that the p19Arf/p53 pathway plays a more relevant role in maintaining the senescence programme in neurofibromas. In support of this, we found that elimination of a single copy of *p53* increases dramatically the incidence of malignancies (up to 100%) and decreases the age of tumour initiation (Fig. 5A). These fast growing tumours are histologically similar to the malignant peripheral nerve sheath tumours developed by some human NF1 patients (Fig. 4A).

In agreement with our results with the *NSE-SMDF^{+/-}* mice, it has been shown by others that *Nf1^{+/-}*; *p53^{+/-}* heterozygotes develop soft tissue sarcomas, including malignant peripheral nerve sheath tumours (Vogel et al., 1999). Moreover, the inactivation of *p14Arf* and *p16Ink4a* has been associated with a bad prognosis in human malignant peripheral nerve sheath tumours (Endo et al., 2011). Taken together, these data support the view that a failure in the establishment of the senescence programme in plexiform neurofibromas underlies their transformation into highly aggressive malignant tumours.

In addition to tumorigenesis, differentiated Schwann cells also re-enter cell cycle during Wallerian degeneration. Thus, after injury

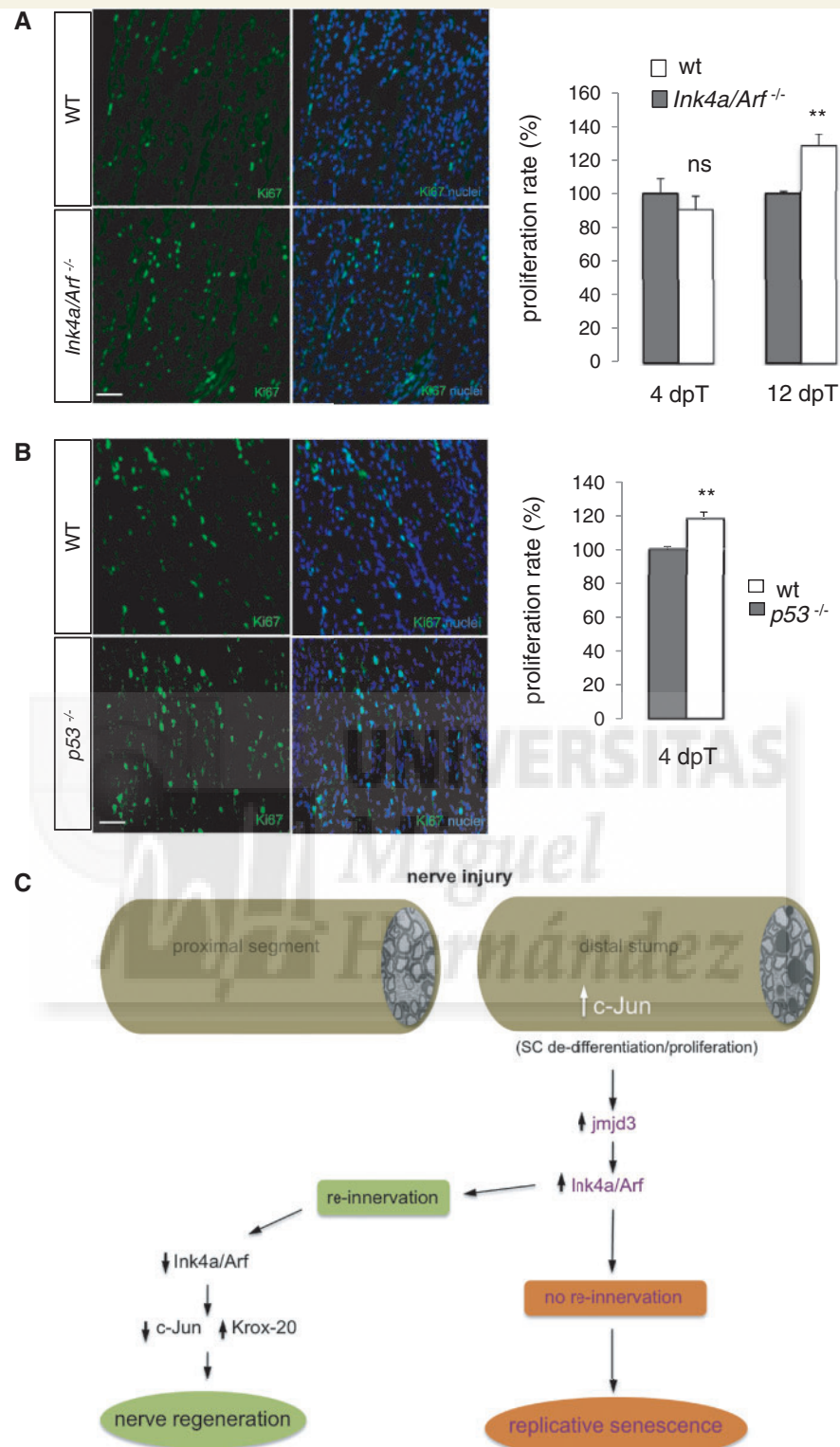


Figure 7 *Ink4a/Arf* locus contributes to proliferation arrest in injured nerves. (A) Cell proliferation is increased in the injured nerves of *Ink4a/Arf*^{-/-} mice. The number of Ki-67-positive cells was counted in the distal stumps of *Ink4a/Arf*^{-/-} and wild-type littermates. Proliferation rate was calculated by dividing the number of Ki-67-positive cells by the total nuclei. As is shown, the density of proliferating cells was significantly increased in the *Ink4a/Arf*^{-/-} mice ($n = 3$; ** P -value = 0.016). (B) Proliferation rate was also increased in the injured nerves of *p53*^{-/-} mice ($n = 3$; ** P -value = 0.012). (C) Graphical summary: the senescence programme contributes to controlling the proliferation of Schwann cells in the distal stump of injured nerves. If the re-growing axons can reach the distal stump, c-Jun is downregulated and Krox-20 upregulated, inducing Schwann cells to go into the myelination programme. In contrast, when the axons are prevented from entering the distal stump, the *Ink4a/Arf* locus remains activated maintaining Schwann cells in the replicative senescence programme. dpT = days post-transaction; ns = no significant.

factors are released that induce Schwann cell de-differentiation and proliferation (Guertin *et al.*, 2005). It has been elegantly shown that this process is controlled by the re-expression of the transcription factor *c-Jun* in the Schwann cell (Parkinson *et al.*, 2008; Arthur-Farraj *et al.*, 2012). Later, contact of Schwann cells with regrowing axons downregulates *c-Jun* and upregulates *Krox-20*, instructing them to myelinate and regenerate a full-blown and functional nerve. However, if the regrowing axons cannot reach the distal segment (as happens in some complete nerve transections), *c-Jun* expression remains high for long periods of time. Intriguingly, despite this, Schwann cell proliferation stops after few days (Scherer *et al.*, 1994; Shy *et al.*, 1996). Here we show that this stop in proliferation is associated with *p19Arf* upregulation. Interestingly we also observed strong immunoreactivity for *Jmjd3* in these nerves, suggesting that this demethylase de-represses the *Ink4a/Arf* locus in the distal stumps of injured nerves. By using genetically modified mice we show that *Ink4a/Arf* loss of function increases the cell proliferation rate in distal stumps, proving that replicative senescence contributes to the arrest of proliferation after injury. We found a similar effect in the distal stumps of *p53* knock-out mice suggesting that as in neurofibromas, the *p19Arf/p53* pathway mediates this arrest. However, in this case the *p16Ink4a/Rb* pathway is also involved, as shown by the increased proliferation of Schwann cells in the injured nerves of the *p16Ink4a* knock-out mice (Atanasoski *et al.*, 2006). Proliferation arrest eventually occurs in the *Ink4a/Arf*^{-/-} and *p53*^{-/-} injured nerves, suggesting that other pathways (potentially involving *p15Ink4b* and/or *Wnt16*) may also contribute to block proliferation.

In summary, our data support the tenet that a physiological response is activated to control Schwann cell overproliferation after nerve injury. But, why is the control of Schwann cell proliferation biologically important in the distal stumps of injured nerves? Schwann cell plasticity is central for nerve regeneration (Jessen and Mirsky, 2005). To this end, the fully differentiated myelinating Schwann cells completely de-differentiate to an immature-like stage after injury. These immature-like cells are sensitive to mitogens and proliferate in response to factors like neuregulins or TGF- β (Ridley *et al.*, 1989; Levi *et al.*, 1995). It has been shown that they can also synthesize and release neuregulins and other trophic factors, which hypothetically can stimulate autocrine proliferation (Carroll *et al.*, 1997; Rosenbaum *et al.*, 1997). Also, in addition to this, soluble neuregulins are present in the serum (Shibuya *et al.*, 2010) and can theoretically activate *erbB* receptors on Schwann cells, as the blood nerve barrier is broken in injured nerves. Therefore the plasticity of the Schwann cell lineage is a double-edged sword. To guarantee re-innervation it is needed to generate de-differentiated Schwann cells, which are highly sensitive to mitogens and oncogenic stimuli, and exposes the organism to a dangerous situation. The risk is particularly high if axons cannot finally reach the distal stumps and Schwann cells have to remain de-differentiated for long periods of time. Interestingly, we also observed that the expression of *p19Arf* disappears when the contact with axons induces Schwann cell re-differentiation in regenerating nerves (Fig. 6G). Although we cannot rule out that some *p19Arf* expressing cells could be cleared by phagocytosis, most of them probably re-differentiate to

myelinating Schwann cells, in what could be another example of the remarkable Schwann cell lineage plasticity. Experiments to unambiguously address this point are currently ongoing in our laboratory.

Our data suggest that senescence is a general mechanism for the control of Schwann cell proliferation. An emerging idea proposes that some types of tumours arise when oncogenic stimuli activate persistently the repair programme of a tissue (Dvorak, 1986; Beachy *et al.*, 2004). Thus tumour growth may represent the continuous activity of an unregulated state of tissue repair that fails to come back to the quiescence that normally follows regeneration. In the PNS, it has been reported that nerve injury fosters neurofibroma development (Riccardi, 1981; Parrinello and Lloyd, 2009; Napoli *et al.*, 2012) suggesting a link between nerve regeneration and tumorigenesis. Our microarray analysis shows that many genes that are re-expressed after nerve injury by Schwann cells (*Sox2*, *Notch1*, *Id2*, *Krox-24*, *Egr3* and *Tnc*) (Fruttiger *et al.*, 1995; Jessen and Mirsky, 2008) are also highly expressed during neurofibroma development (Table 2). Importantly, we show (Supplementary Fig. 2 and 3) that *c-jun*, a master gene that drives Schwann cell de-differentiation during Wallerian degeneration (Parkinson *et al.*, 2008; Arthur-Farraj *et al.*, 2012) is highly expressed in human and mice neurofibromas. This suggests that the same programme that drives Schwann cell de-differentiation and proliferation after injury is activated by oncogenic stimuli to induce tumours in the PNS. We also show that a common mechanism, mediated by the epigenetic induction of the *Ink4a/Arf* locus, is used to avoid Schwann cell over-proliferation after injury and after oncogenic challenge. Together our results substantiate the idea of a link between nerve regeneration and tumour development, and support the concept that peripheral nerve tumours can be produced by the misactivation of persistent state of repair.

Acknowledgements

We thank Dr Daniel Wilton (University College London) for insightful comments on the manuscript. We also thank Dr F.J. Vera and Dr Federico Gomis (Hospital La Fe, Valencia, Spain) for human neurofibroma samples and non-pathologic peripheral nerve biopsies. We are in debt with Luis M. Valor for his help with microarray data analysis. We thank Consuelo Martinez-Moratalla, Pedro Morenilla-Ayala and Virginia Martin-Arranz for technical assistance.

Funding

This work has been funded by grants SAF2008-04106 (Spanish Ministerio de Ciencia e Innovación), PI012/164 (Instituto de Salud Carlos III) and PROMETEO 2008/134 (Conselleria Educació Generalitat Valenciana) to H.C.

Supplementary material

Supplementary material is available at *Brain* online.

References

- Agger K, Cloos PA, Christensen J, Pasini D, Rose S, Rappsilber J, et al. UTX and JMJD3 are histone H3K27 demethylases involved in HOX gene regulation and development. *Nature* 2007; 449: 731–4.
- Agger K, Cloos PA, Rudkjaer L, Williams K, Andersen G, Christensen J, et al. The H3K27me3 demethylase JMJD3 contributes to the activation of the INK4A-ARF locus in response to oncogene- and stress-induced senescence. *Genes Dev* 2009; 23: 1171–6.
- Agherbi H, Gausmann-Wenger A, Verthuy C, Chasson L, Serrano M, Djabali M. Polycomb mediated epigenetic silencing and replication timing at the INK4a/ARF locus during senescence. *PLoS One* 2009; 4: e5622.
- Ameyar-Zazoua M, Wisniewska MB, Bakiri L, Wagner EF, Yaniv M, Weitzman JB. AP-1 dimers regulate transcription of the p14/p19ARF tumor suppressor gene. *Oncogene* 2005; 24: 2298–306.
- Arthur-Farraj PJ, Latouche M, Wilton DK, Quintes S, Chabrol E, Banerjee A, et al. c-Jun reprograms Schwann cells of injured nerves to generate a repair cell essential for regeneration. *Neuron* 2012; 75: 633–47.
- Atanoski S, Boller D, De Ventura L, Koegel H, Boentert M, Young P, et al. Cell cycle inhibitors p21 and p16 are required for the regulation of Schwann cell proliferation. *Glia* 2006; 53: 147–57.
- Atanoski S, Shumas S, Dickson C, Scherer SS, Suter U. Differential cyclin D1 requirements of proliferating Schwann cells during development and after injury. *Mol Cell Neurosci* 2001; 18: 581–92.
- Barradas M, Anderton E, Acosta JC, Li S, Banito A, Rodriguez-Niedenfuhr M, et al. Histone demethylase JMJD3 contributes to epigenetic control of INK4a/ARF by oncogenic RAS. *Genes Dev* 2009; 23: 1177–82.
- Beachy PA, Karhadkar SS, Berman DM. Tissue repair and stem cell renewal in carcinogenesis. *Nature* 2004; 432: 324–31.
- Binet R, Ythier D, Robles AI, Collado M, Larrieu D, Fonti C, et al. WNT16B is a new marker of cellular senescence that regulates p53 activity and the phosphoinositide 3-kinase/AKT pathway. *Cancer Res* 2009; 69: 9183–91.
- Birchmeier C, Nave KA. Neuregulin-1, a key axonal signal that drives Schwann cell growth and differentiation. *Glia* 2008; 56: 1491–7.
- Bracken AP, Kleine-Kohlbrecher D, Dietrich N, Pasini D, Gargiulo G, Beekman C, et al. The Polycomb group proteins bind throughout the INK4A-ARF locus and are disassociated in senescent cells. *Genes Dev* 2007; 21: 525–30.
- Brockes JP, Fields KL, Raff MC. Studies on cultured rat Schwann cells. I. Establishment of purified populations from cultures of peripheral nerve. *Brain Res* 1979; 165: 105–18.
- Carroll SL, Ratner N. How does the Schwann cell lineage form tumors in NF1? *Glia* 2008; 56: 1590–605.
- Carroll SL, Miller ML, Frohnert PW, Kim SS, Corbett JA. Expression of neuregulins and their putative receptors, ErbB2 and ErbB3, is induced during Wallerian degeneration. *J Neurosci* 1997; 17: 1642–59.
- Cichowski K, Shih TS, Schmitt E, Santiago S, Reilly K, McLaughlin ME, et al. Mouse models of tumor development in neurofibromatosis type 1. *Science* 1999; 286: 2172–6.
- Collado M, Serrano M. Senescence in tumours: evidence from mice and humans. *Nat Rev Cancer* 2010; 10: 51–7.
- Collado M, Blasco MA, Serrano M. Cellular senescence in cancer and aging. *Cell* 2007; 130: 223–33.
- Courtis-Cox S, Genter Williams SM, Reczek EE, Johnson BW, McGillicuddy LT, Johannessen CM, et al. A negative feedback signaling network underlies oncogene-induced senescence. *Cancer Cell* 2006; 10: 459–72.
- Dvorak HF. Tumors: wounds that do not heal. Similarities between tumor stroma generation and wound healing. *N Engl J Med* 1986; 315: 1650–9.
- Endo M, Kobayashi C, Setsu N, Takahashi Y, Kohashi K, Yamamoto H, et al. Prognostic significance of p14ARF, p15INK4b, and p16INK4a inactivation in malignant peripheral nerve sheath tumors. *Clin Cancer Res* 2011; 17: 3771–82.
- Evans DG, Baser ME, McCaughran J, Sharif S, Howard E, Moran A. Malignant peripheral nerve sheath tumours in neurofibromatosis 1. *J Med Genet* 2002; 39: 311–4.
- Fruttiger M, Schachner M, Martini R. Tenascin-C expression during wallerian degeneration in C57BL/Wjds mice: possible implications for axonal regeneration. *J Neurocytol* 1995; 24: 1–14.
- Gil J, Peters G. Regulation of the INK4b-ARF-INK4a tumour suppressor locus: all for one or one for all. *Nat Rev Mol Cell Biol* 2006; 7: 667–77.
- Gomez-Sanchez JA, Lopez de Armentia M, Lujan R, Kessar N, Richardson WD, Cabedo H. Sustained axon-glia signaling induces Schwann cell hyperproliferation, Remak bundle myelination, and tumorigenesis. *J Neurosci* 2009; 29: 11304–15.
- Gorgoulis VG, Halazonetis TD. Oncogene-induced senescence: the bright and dark side of the response. *Curr Opin Cell Biol* 2010; 22: 816–27.
- Guertin AD, Zhang DP, Mak KS, Alberta JA, Kim HA. Microanatomy of axon/glia signaling during Wallerian degeneration. *J Neurosci* 2005; 25: 3478–87.
- Harrisingh MC, Perez-Nadales E, Parkinson DB, Malcolm DS, Mudge AW, Lloyd AC. The Ras/Raf/ERK signalling pathway drives Schwann cell dedifferentiation. *EMBO J* 2004; 23: 3061–71.
- Jang SW, LeBlanc SE, Roopra A, Wrabetz L, Svaren J. In vivo detection of Egr2 binding to target genes during peripheral nerve myelination. *J Neurochem* 2006; 98: 1678–87.
- Jessen KR, Mirsky R. The origin and development of glial cells in peripheral nerves. *Nat Rev Neurosci* 2005; 6: 671–82.
- Jessen KR, Mirsky R. Negative regulation of myelination: relevance for development, injury, and demyelinating disease. *Glia* 2008; 56: 1552–65.
- Kim HA, Pomeroy SL, Whoriskey W, Pawlitzky I, Benowitz LI, Sicinski P, et al. A developmentally regulated switch directs regenerative growth of Schwann cells through cyclin D1. *Neuron* 2000; 26: 405–16.
- Kuilman T, Michaloglou C, Mooi WJ, Peepers DS. The essence of senescence. *Genes Dev* 2010; 24: 2463–79.
- Le N, Nagarajan R, Wang JY, Araki T, Schmidt RE, Milbrandt J. Analysis of congenital hypomyelinating Egr2Lo/Lo nerves identifies Sox2 as an inhibitor of Schwann cell differentiation and myelination. *Proc Natl Acad Sci USA* 2005; 102: 2596–601.
- Levi AD, Bunge RP, Lofgren JA, Meima L, Hefti F, Nikolics K, et al. The influence of heregulins on human Schwann cell proliferation. *J Neurosci* 1995; 15: 1329–40.
- Matheu A, Maraver A, Serrano M. The Arf/p53 pathway in cancer and aging. *Cancer Res* 2008; 68: 6031–4.
- McClatchey AI. Neurofibromatosis. *Annu Rev Pathol* 2007; 2: 191–216.
- Monje PV, Soto J, Bacallao K, Wood PM. Schwann cell dedifferentiation is independent of mitogenic signaling and uncoupled to proliferation: role of cAMP and JNK in the maintenance of the differentiated state. *J Biol Chem* 2010; 285: 31024–36.
- Napoli I, Noon LA, Ribeiro S, Kerai AP, Parrinello S, Rosenberg LH, et al. A central role for the erk-signaling pathway in controlling schwann cell plasticity and peripheral nerve regeneration in vivo. *Neuron* 2012; 73: 729–42.
- Pantoja C, Serrano M. Murine fibroblasts lacking p21 undergo senescence and are resistant to transformation by oncogenic Ras. *Oncogene* 1999; 18: 4974–82.
- Parkinson DB, Bhaskaran A, Arthur-Farraj P, Noon LA, Woodhoo A, Lloyd AC, et al. c-Jun is a negative regulator of myelination. *J Cell Biol* 2008; 181: 625–37.
- Parrinello S, Lloyd AC. Neurofibroma development in NF1—insights into tumour initiation. *Trends Cell Biol* 2009; 19: 395–403.
- Riccardi VM. Cutaneous manifestation of neurofibromatosis: cellular interaction, pigmentation, and mast cells. *Birth Defects Orig Artic Ser* 1981; 17: 129–45.
- Ridley AJ, Davis JB, Stroobant P, Land H. Transforming growth factors-beta 1 and beta 2 are mitogens for rat Schwann cells. *J Cell Biol* 1989; 109(6 Pt 2): 3419–3424.
- Rosenbaum C, Karyala S, Marchionni MA, Kim HA, Krasnoselsky AL, Happel B, et al. Schwann cells express NDF and SMDF/n-ARIA mRNAs, secrete neuregulin, and show constitutive activation of

- erbB3 receptors: evidence for a neuregulin autocrine loop. *Exp Neurol* 1997; 148: 604–15.
- Salzer JL, Bunge RP. Studies of Schwann cell proliferation. I. An analysis in tissue culture of proliferation during development, Wallerian degeneration, and direct injury. *J Cell Biol* 1980; 84: 739–52.
- Salzer JL, Bunge RP, Glaser L. Studies of Schwann cell proliferation. III. Evidence for the surface localization of the neurite mitogen. *J Cell Biol* 1980; 84: 767–78.
- Scherer SS, Wang DY, Kuhn R, Lemke G, Wrabetz L, Kamholz J. Axons regulate Schwann cell expression of the POU transcription factor SCIP. *J Neurosci* 1994; 14: 1930–42.
- Sherman DL, Brophy PJ. Mechanisms of axon ensheathment and myelin growth. *Nat Rev Neurosci* 2005; 6: 683–90.
- Shibuya M, Komi E, Wang R, Kato T, Watanabe Y, Sakai M, et al. Measurement and comparison of serum neuregulin 1 immunoreactivity in control subjects and patients with schizophrenia: an influence of its genetic polymorphism. *J Neural Transm* 2010; 117: 887–95.
- Shy ME, Shi Y, Wrabetz L, Kamholz J, Scherer SS. Axon-Schwann cell interactions regulate the expression of c-jun in Schwann cells. *J Neurosci Res* 1996; 43: 511–25.
- Vogel KS, Klesse LJ, Velasco-Miguel S, Meyers K, Rushing EJ, Parada LF. Mouse tumor model for neurofibromatosis type 1. *Science* 1999; 286: 2176–9.
- Yang C, Klein EA, Assoian RK, Kazanietz MG. Heregulin beta1 promotes breast cancer cell proliferation through Rac/ERK-dependent induction of cyclin D1 and p21Cip1. *Biochem J* 2008; 410: 167–75.

